Interaction of perilipin amphipathic helices with lipid droplets

Manuel Giménez Andrés

université PARIS-SACLAY

Interaction of perilipin amphipathic helices with lipid droplets

Thèse de doctorat de l'université Paris-Saclay

École doctorale n° 577, Structure et dynamique des systèmes vivants (SDSV)
Spécialité de doctorat : Sciences de la vie et de la santé
Unité de recherche : Institut Jacques Monod
Référent : Faculté des sciences d'Orsay

Thèse présentée et soutenue à Paris, 28 Septembre 2020, par

Manuel GIMENEZ ANDRES

Composition du Jury

Thierry CHARDOT DR, INRAE, Institut Jean-Pierre Bourgin	Président
Romain GAUTIER HDR, Enseignant-Chercheur, Université Côte d'Azur	Rapporteur & Examinateur
Monika OBERER Professeur associé, University of Graz	Rapporteur & Examinatrice
Véronique ALBANESE CR, CNRS, Institut Jacques Monod	Examinatrice
Abdou Rachid THIAM DR, École normale supérieure d'Ulm	Examinateur
Alenka Čopič CR, CNRS, Institut Jacques Monod	Directrice de thèse

Thèse de doctorat

NNT : 2020UPASL006

Acknowledgements

First, I would like to thank my thesis director, Alenka Čopič, for trusting me with this project that made me grow professionally and personally. I thank you sincerely for always being very willing and available to discuss any results and ideas, and also for showing your passion for science. Moreover, thank you for offering me many opportunities to complete my training as a scientist. For all these reasons: najlepša hvala.

I would also like to thank other people involved in this project. Sandra Antoine-Bally, it was a pleasure to work with you, as well as with Jaka Snoj. I am also very grateful to Bruno Antonny, for collaborating in this project sharing your ideas and protocols, and for allowing me to go to your laboratory to show me new techniques. I am thankful to Tadej Emeršič and Jure Derganc for collaborating in this project contributing with a biophysics point of view, for introducing to me the microfluidics systems, and for your hospitality.

I also want to express my gratitude to the jury members, Thierry Chardot, Romain Gautier, Monika Oberer, Véronique Albanèse and Abdou Rachid Thiam for spending their time in judging and discussing with me my thesis work. Thanks also to Luc Busset for the discussions during my thesis committees.

Thanks to all the Membrane dynamics and intracellular trafficking group members among these years, especially to Cathy Jackson, Jean-Marc Verbavatz, Laurence Walch, Mélina Heuzé, Juan Martín d'Ambrosio, Hugo Siegfried and Emilie Pellier. Thanks to Nicolas Joly, Xavier Baudoin and Vincent Contremoulins for their help to resolve technical issues. I also thank the doctoral school “Structure et Dynamique des Systèmes Vivants”.

I want to thank the people that I had the good luck to meet in the Institut Jacques Monod during these years. Quiero agradecer también a la gente excepcional que he conocido durante mi estancia en la Cité Universitaire de Paris. Habéis sido un gran apoyo y habéis hecho que mi estancia en París sea un momento increíble, inolvidable y muy enriquecedor en mi vida. Sois muchos y sabéis quienes sois, siempre podréis contar conmigo. Asi mismo, quiero agradecer a los amigos que ya conocía antes de iniciar el doctorado.

Para finalizar, no puedo dejar pasar la oportunidad de agradecer otra vez a mi familia, en especial a mis padres y a mi hermana, todo el apoyo recibido. Aunque sea en la distancia, recibo siempre vuestro apoyo y cariño como si estuviera en Alcañiz. Me siento increíblemente afortunado de teneros y poder contar con vosotros siempre.

INDEX

List of abbreviations

aa: Amino acid

ACAT: Acyl-CoA:Cholesterol acyltransferase

AH: Amphipathic helix

ALPS: Amphipathic lipid packing sensor

ApoB: Apolipoprotein B

ApoLp-III: Apoliphorin-III

ATGL: Adipose triglyceride lipase

BSA: Bovine serum albumin

CCT1: CTP:phosphocholine cytidyltransferase

CD: circular dichroism

CIDE: cell death-inducing DFF45-like effector

DGAT: Acyl-CoA: Diacylglycerol acyltransferase enzymes

DLS: Dynamic light scattering

EPR: Electron paramagnetic resonance

ER: Endoplasmic reticulum

Fig.: Figure

GFP: Green fluorescent protein

HSL: Hormone-sensitive lipase

LD: Lipid droplet

Lyso-PC: Lyso-phosphatidylcholine

Lyso-PL: Lyso-phospholipid

MD: Molecular dynamics

NBD: Nitrobenzoxadiazole

NMR: Nuclear magnetic resonance

PAGE: Polyacrylamide gel electrophoresis

PC: Phosphatidylcholine

PE: Phosphatidylethanolamine

PI: Phosphatidylinositol

PKA: Protein kinase A

PL: Phospholipid

Plin1: Perilipin 1

Plin2: Perilipin 2

Plin3: Perilipin 3

Plin4: Perilipin 4

Plin5: Perilipin 5

Plins: Perilipins

PS: Phosphatidylserine

SDS: Sodium dodecyl sulfate

STE: Sterol esters

TAG: Triacylglycerol

VLDL: Very low-density lipoproteins

INTRODUCTION

Chapter 1: Lipid droplets

1.1 General aspects of LDs

Organisms need to store energy in order to survive in the fluctuating conditions of their environment. Energy can be stored in energy-rich molecules or electrochemical gradients across membranes. The two main molecules to store energy in animals are glycogen and triacylglycerols (TAG). Glycogen is a polymer of glucose that is stored in the cytosol. Glycogen is hydrated, and its storage retains a lot of water needing a lot of space. On the other hand, TAG are very hydrophobic and separate from water, needing less space. Moreover, TAG are highly reduced molecules available for oxidation and therefore energy-dense. TAG and other neutral lipids are stored in lipid droplets (LDs; also named lipid particles, lipid bodies, fat bodies or oil bodies). LDs are present in many organisms: bacteria, archaea and eukaryotes (Murphy 2011). LDs were first described in 1890 by Richard Altmann in frog liver cells (Altmann 1890). For a long time, they were considered inert energy deposits inside the cell, until the 1990s when some of their regulation was discovered (Greenberg et al. 1991; Walther and Farese 2012).

1.2 LD structure and lipid composition

1.2.1 LD structure

LDs have a spherical structure, which is optimal for a minimal exposure of the surface to the aqueous cytosol environment and the number of hydrophobic molecules that an LD stores. In the center of the sphere, there are the neutral lipids like TAG and sterol esters (STE) that are very hydrophobic, lacking charged and polar groups. On their surface, LDs have a monolayer of amphipathic lipids as shown by the thin layer observed in cryo-electron microscopy images (Tauchi-Sato et al. 2002). Therefore, the LD structure is a hydrophobic core surrounded by a monolayer of amphipathic molecules (Fig. 1-1). The most abundant amphipathic molecules are phospholipids (PLs), but diacylglycerol (DAG) and cholesterol are also present. Proteins are

also embedded in that monolayer. In this subchapter, I will discuss the lipid composition of LDs.

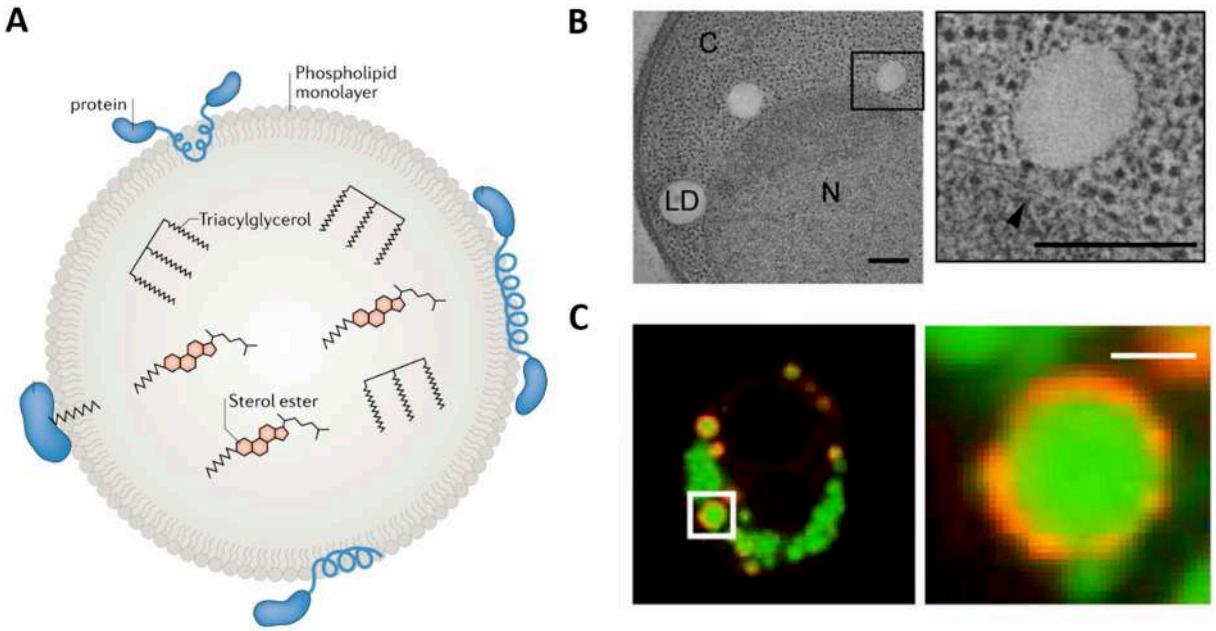

Fig 1-1. LD structure. A. Schematic representation of the structure of an LD**.** Figure modified from (Olzmann and Carvalho 2018). **B.** LDs imaged by transmission electron microscopy. Figure taken from (Grippa et al. 2015). Scale bar: 200 nm. C stands for cytoplasm and N for nucleus. **C.** LDs imaged by light microscopy. The hydrophobic core was labelled with a hydrophobic dye, shown in green, and the surface was labelled by immunofluorescence the LD surface protein GPAT4, shown in red. Scale bar: 1 μm. Figure taken from (Wilfling et al. 2015).

1.2.2 Majority of neutral lipids: TAG and STE

TAG are molecules composed of glycerol with three fatty acids linked by ester bonds. Fatty acid length and unsaturation level can vary, resulting in different species of TAG. They are synthesized in mammals by acyl-CoA:diacylglycerol acyltransferase enzymes (DGAT) DGAT1 and DGAT2, using as substrates DAG and acyl CoA (Cases et al. 2001). Although DGAT1 and DGAT2 have the same catalytic activity, they have distinct protein sequences and differ in their cellular, biochemical and physiological functions. The endoplasmic reticulum (ER) protein DGAT1 esterifies into TAG the excess of fatty acids present in the ER. Otherwise, free fatty acids would accumulate, causing lipotoxicity. In contrast, DGAT2 localizes to LDs and the ER and is related to de novo lipogenesis (Kuerschner et al. 2008; Wurie et al. 2012). In yeast, the DGAT enzyme Dga1p also catalyzes the acylation step from DAG to TAG. Furthermore, Lro1p can also catalyze TAG formation using DAG and the acyl chain from a PL, mainly

phosphatidylcholine (PC) or phosphatidylethanolamine (PE). Finally, a little amount of TAG in yeast cells can be generated by the catalytic activity of Are1p and Are2p (Sorger and Daum 2002; Czabany et al. 2007).

STE are composed of a sterol molecule bound to a fatty acid by an ester bond. STE can differ in their sterol molecule depending on the organism. STE also varies depending on the length and unsaturation level of the fatty acid. Intracellular STE are synthesized by the acyl-CoA:Cholesterol acyltransferase (ACAT) enzymes, ACAT1 and ACAT2 in mammals (Goldstein et al. 1974; Luo et al. 2019). ACATs are ER transmembrane proteins. Both enzymes have sequence homology in their c-terminus part, and both are allosterically activated by excess cholesterol. In humans, ACAT1 has ubiquitous expression, whereas ACAT2 is expressed in enterocytes and hepatocytes (Wang et al. 2017; Luo et al. 2019). In *S. cerevisiae*, there are two enzymes with homologous sequences to ACAT enzymes, Are1p and Are2p. They localize to the ER (Zweytick et al. 2000).

Depending on the organism and cell type, the relative concentrations of the two main neutral lipids can vary. LDs in adipocytes contain mainly TAG. In contrast, testicular Leydig cells contain LDs with comparable quantities of TAG and STE. Adrenal cortex LDs also contain more STE than other cell types (Wang et al. 2015b; Yu et al. 2018). Cholesterol is used in these tissues as a substrate for steroid hormones biosynthesis, such as testosterone (Wang et al. 2015b). Moreover, LD composition can change depending on environmental factors, such as the carbon source (Athenstaedt et al. 2006) or temperature. For instance, in *S. cerevisiae*, the quantity of TAG increases when cells are grown at low temperatures, whereas ergosterol quantity does not vary much. Likewise, TAG quantity increases in the stationary phase when nutrients get depleted (Klose et al. 2012).

1.2.3 Other neutral lipids

Besides TAG and STE, other neutral lipids can be found in LDs in smaller quantities. This depends on the cell type and metabolism. Examples of minor neutral lipids are acylceramides, retinol esters, squalene, neutral ether lipids, wax oils, vitamin E and long-chain polyprenols.

Ether lipids are a group of glycerolipids in which one of the lipids is bound to glycerol by an ether bond instead of an ester bond. They have signaling functions and structural roles. A

study using mass spectrometry and nuclear magnetic resonance (NMR) spectroscopy quantified the ether lipids present in LDs to represent 10-20% of all neutral lipids in Chinese hamster ovary cells. The same study found that other cell types like white adipose tissue do not contain any detectable ether lipids, according to thin-layer chromatography (Bartz et al. 2007). The enzyme fatty acyl-CoA reductase 1 produces fatty alcohols necessary for the formation of ether lipids. This peroxisomal protein has been shown to localize also to LDs (Exner et al. 2019).

Acylceramides are produced at the ER-LD interface by the enzyme DGAT2, which forms a complex with the ceramide synthase and the fatty acyl-CoA synthase ACSL5. They can be found in the hepatic cells of mice fed a high-fat diet. The lack of DGAT2 results in a higher level of ceramides and ceramide-mediated apoptosis (Senkal et al. 2017). In *S. cerevisiae*, Dga1p (DGAT2 ortholog) and Lro1p are able to produce acylceramides (Voynova et al. 2012). Retinyl esters are formed by lecithin:retinol acyltransferase using retinol and PC as substrates (Golczak et al. 2012). Retinyl esters are precursors of vitamin A and accumulate in LDs, for instance in hepatic stellate cells. The amphipathic helix (AH) in the N-terminal part of lecithin:retinol acyltransferase interacts with retinol esters (Molenaar et al. 2019). The isoprenoid squalene is an intermediate molecule of sterol biosynthesis and can also be stored in LDs (Spanova et al. 2010). Another kind of neutral lipids are wax esters. They are produced by wax ester synthase using acyl-CoA and acyl-CoA-derived fatty alcohol as substrates (Lardizabal et al. 2000). Wax esters can be found in plant LDs (Parker and Murphy 1981). Polyprenols are isoprenoid lipids. Long-chain polyprenols can be stored in LDs. During spore wall formation in yeast, polyprenols are stored in LDs (Hoffman et al. 2017).

1.2.4 Distribution of neutral lipids inside an LD

How these various neutral lipids are organized within the LD core have different possibilities. The first option will be to have an amorphous LD core and all the neutral lipids mixed. Moreover, some studies have suggested that phase transitions occur within the neutral lipid core of LDs. Studies on yeast that used differential scanning calorimetry and small x-ray scattering suggested that TAG and squalene formed the fluid inner core of LDs whereas STE was in layers surrounding that core (Fig. 1-2 A) (Czabany et al. 2008). A study on HeLa cells with cryo-electron microscopy found LDs to be amorphous under normal conditions.

However, under certain conditions that lead to TAG consumption (e.g. mitotic arrest, starvation) ordered layers of a few nm, likely formed by STE, could be observed (Fig. 1-2 B) (Mahamid et al. 2019). These studies show that phase transitions can occur under physiological conditions in LDs, affecting the distribution and availability of neutral lipids.

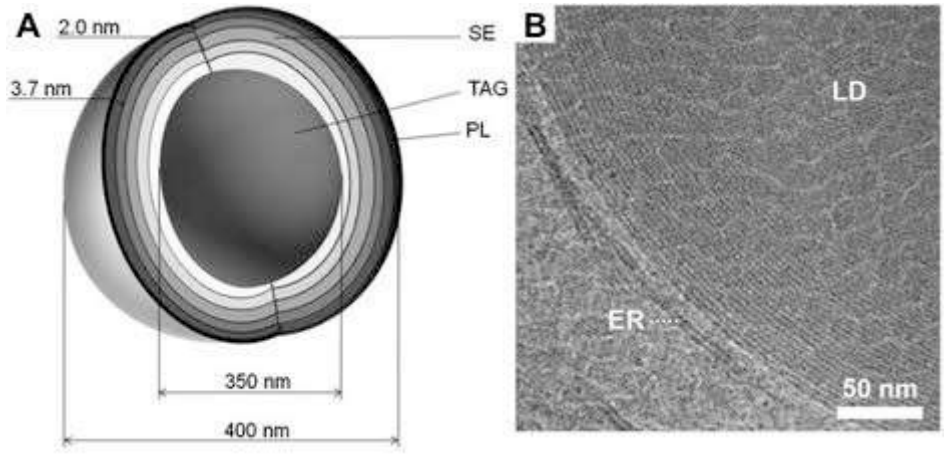

Fig 1-2 Phase transition inside an LD core. A. Diagram of a yeast LD proposing the separation of neutral lipids into phases (Czabany et al. 2008). **B.** Organized layers were observed in LDs from HeLa cells by cryo-electron microscopy (Mahamid et al. 2019).

Separation could also occur between TAG species depending on their acyl chain length and unsaturation level. Broadband coherent anti-Stokes Raman spectroscopy is a technique sensitive to vibrational signatures of molecules. When applied to differentiated 3T3-L1 adipocytes, it showed that saturated TAGs were located in the outer parts of LDs and that they were relatively more abundant on big LDs (Paul et al. 2019).

Besides separation of neutral lipids within one LD, different LDs within the same cells could also contain different neutral lipids. A study using bodipy-based fluorescent probes found populations of TAG and STE-rich LDs within the same cell in several different cell types (mice adrenocortical cells, mice liver cells, and Chinese hamster ovary cells among others) (Hsieh et al. 2012). However, a study on hepatic cells using Raman scattering microscopy did not find different populations of LDs containing different neutral lipids (Fu et al. 2014). Therefore, it is not clear if different LDs with distinct neutral lipid composition co-exist within cells. More studies combining several techniques will be necessary to resolve this question.

1.2.5 PLs

PLs protect the neutral lipid core from the hydrophilic cytosolic environment, stabilizing the LD. PLs represent a minor quantity of molecules in the LDs. For instance, PLs only represent 1-2% in weight of LDs in Chinese hamster ovary cells (Bartz et al. 2007). The fraction of PLs in LDs varies depending on their size. Assuming a density of 0.95 g/ml and a molecular weight of 885 g/mol for triolein, and that the LD would be covered by a monolayer of PC of 2.5 nm in thickness, Penno and coauthors arrive to the following equation: $\frac{TG}{PC} = 0.215\ nm^{-3} \cdot a \cdot \frac{(r-2.5)^3}{r^2}$ (Penno et al. 2013). a is the surface area per PC molecule. One PL molecule was measured to occupy 0.78 nm^2 in the PL monolayer on LDs when the PLs are well-packed (Chorlay and Thiam 2020). Applying this equation, one LD of 300 nm in diameter would have 4.2 mol% of PLs, whereas one LD of 100 μm would have 0.01 mol% of PLs. The difference in PL fractions between LDs of different sizes shows that if an LD is expanding or shrinking its PL content will need to be adjusted. This could happen either by local synthesis or consumption of PLs, by lipid transfer through membrane contact sites, via direct contact between the ER bilayer and the LD monolayer, or by LD fusion or fission. Vesicular transport pathways are excluded from contributing to the remodelling process of the LD monolayer due to biophysical constraints. Here I will explain in more detail the synthesis pathways of PL that are relevant for LDs. Some of the other mechanisms will be discussed later.

The first way of synthesizing PLs is the Lands cycle, which uses lyso-phospholipids (lyso-PLs). Lyso-PLs are generated from PLs by phospholipase A2 (PLA2), which removes the sn-2 fatty acid (Fig. 1-3). The half time of the release of lyso-phosphatidylcholine (lyso-PC) from a membrane is around 20ms (Massey et al. 1997). Therefore, lyso-PC can escape from membranes spontaneously and with no additional enzymatic activity. LD-localized lyso-PL acyltransferases, such as LPCAT, can re-acylate the PL (Moessinger et al. 2011). This re-acylation would explain the different fatty acid composition of the PLs in the LD monolayer compared to the ER membrane (Tauchi-Sato et al. 2002).

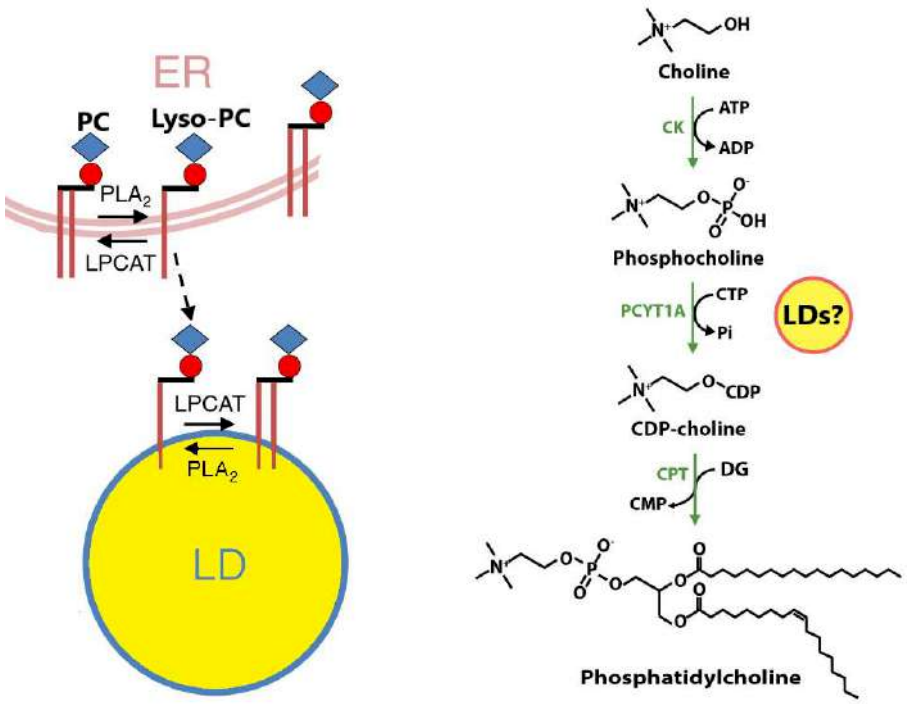

Fig 1-3. PLs synthesis pathways and LDs. Left panel: Lands cycle operating between the ER and LDs. Adapted from (Penno et al. 2013). Right panel: Kennedy pathway for synthesis of PC. Adapted from (Payne et al. 2014). See text for details.

The other pathway to synthesize PLs that is important for LDs is the Kennedy pathway, which synthesizes PC (Fig. 1-3). The rate-limiting step is catalyzed by the enzyme CTP:phosphocholine cytidyltransferase (CCT1 or PCYT1A), which generates cytidine-diphosphocholine. CDP-choline:diacylglycerol phosphocholine transferase (CPT) catalyzes the next step to obtain PC from cytidine-diphosphocoline and DAG (Payne et al. 2014). CCT1 was observed on LDs when it was transiently expressed in drosophila cells (Krahmer et al. 2011). However, another study using immunostaining of mice tissues did not find LD localization of endogenous CCT1 (Haider et al. 2018). Moreover, the subsequent PC-synthesis step occurs on the ER (Moessinger et al. 2011). Therefore, even if the formation of cytidine-diphosphocholine occurs on LDs, intracellular transport of PC needs to take place to carry PC from the ER to LDs.

Lipidomics analysis of the PLs present in purified LDs suggested increased quantities of PC, PE, and their respective lyso-PLs, and lower levels of phosphatidylserine (PS), sphingomyelin and phosphatidic acid in LDs compared with total membranes (Bartz et al. 2007).

1.3 LD proteome

1.3.1 Identification of LD proteins

Proteins present on LDs mediate their metabolism and other functions. LD proteome can be identified by purifying LDs using density gradients (Brasaemle and Wolins 2016), followed by techniques to analyze all associated proteins, such as mass spectrometry. Of note, one issue of this technique is the contamination by proteins from other cellular compartments in the buoyant fraction after centrifugation (Brasaemle et al. 2004). In order to avoid contaminations and identify bona fide LD proteins, the Olzmann group added a step of proximity labelling of LD-bound proteins to the previous protocol and apply it in human liver and bone cancer-derived cells (Bersuker et al. 2017). Proteins related to the metabolism of TAG, STE, PLs and sugars, membrane-organization, vesicular trafficking, cytoskeleton, protein processing, autophagy and transcription have been identified on LDs (Bersuker et al. 2017).

1.3.2 Protein motifs that target LDs

The hydrophobic core of LDs is devoid of proteins because this is an energetically unfavourable environment for hydrophilic protein domains. Therefore, LD proteins are located on the LD surface (Thiam et al. 2013b; Pataki et al. 2018). Proteins can interact with the LD surface via the following motifs (Fig. 1-4):

- Amphipathic helices (AHs). These are secondary helical structures, in which the amino acids (aa) are segregated in two distinct faces: one hydrophobic and one polar. Proteins containing AHs target LDs from the cytoplasm. Perilipins (Plins), acyl-CoA synthetase 3, CCT1 or cell death-inducing DFF45-like effector (CIDE) A, and other proteins use this motif to target LDs (Bersuker and Olzmann 2017; Giménez-Andrés et al. 2018). AHs are explained in detail in Chapter 3.

- Hydrophobic hairpin loops: these aa segments are embedded in the PL monolayer and are flanked by regions exposed to the cytosol. In the middle of the hydrophobic region, there is in some cases a proline required for LD localization (Abell et al. 1997). Proteins with this motif are inserted in the ER either co-translationally by the signal recognition particle and Sec61 or post-translationally by Pex19 and Pex3. These proteins

translocate from the ER to LDs during LD biogenesis or later via ER-LD bridges (Kory et al. 2016; Bersuker and Olzmann 2017). Some proteins that use this motif are DGAT2 (Stone et al. 2006), GPAT4 (Wilfling et al. 2013) and plant oleosins (Abell et al. 1997).

- Lipid modifications. Lipid conjugations as palmitoylation, prenylation or myristoylation, can mediate targeting to membranes, as well as to LDs. Palmitoylation is reversible, therefore the interaction of these proteins can be regulated (Bersuker and Olzmann 2017).

- Peripheral association via another protein. These are proteins that localize to LDs by interacting with proteins already present in LDs. Hormone-sensitive lipase (HSL) interacts with phosphorylated N-terminus of Perilipin 1 (Plin1) (Egan et al. 1992). This is also the case for histones H2A and H2B in Drosophila embryos, where they interact with the LD protein Jabba (Li et al. 2012).

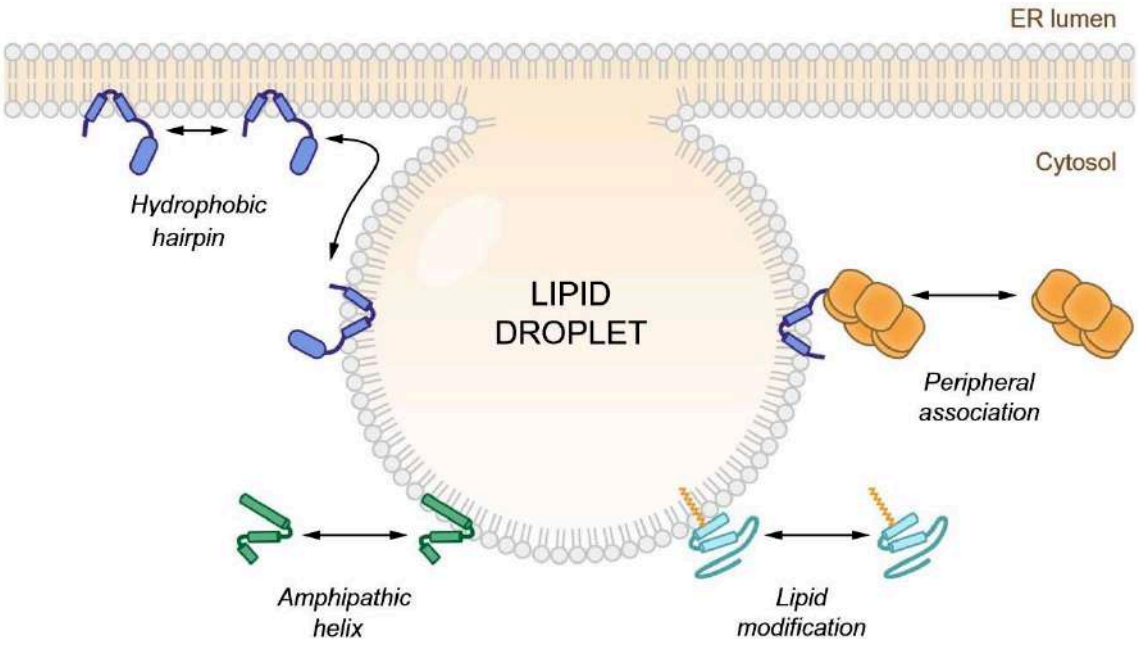

Fig. 1-4. **Motifs for protein localization to LDs.** Proteins localizing to LDs can use these four motifs: hydrophobic hairpins, AHs, lipid modifications or peripheral association via another protein. Adapted from (Bersuker and Olzmann 2017).

An intriguing case is the enzyme implicated in ether lipid formation fatty acyl-CoA reductase (FAR1). It localizes to peroxisomes and ER using one transmembrane domain and one AH.

However, it also localizes to LDs, where it has been suggested that the transmembrane domain acquires another structure compatible with LDs, like an AH or a hydrophobic hairpin (Exner et al. 2019).

1.3.3 Removal and degradation of LD proteins

Removal of proteins from LDs can occur by degrading them with several pathways. Proteins can be degraded by the ubiquitination-proteasome system (Xu et al. 2006). In the case of proteins with hydrophobic embedded domains, the ER-associated protein degradation (ERAD) machinery is necessary. ERAD substrates are ubiquitylated, extracted from the membrane and degraded by the cytosolic proteasome (Ruggiano et al. 2016; Olzmann and Carvalho 2018). The last system is chaperone-mediated autophagy, where specific proteins are identified by HSC70 and introduced in the lysosome for their degradation by LAMP2A (Kaushik and Cuervo 2015).

LDs have limited space on their surface, especially when they are small or shrinking because of energy consumption. Limited surface availability leads to molecular crowding effects, and some proteins with less affinity for LDs will fall off during shrinking. For instance, CCT1 heterologously expressed is displaced during LD shrinkage, whereas GPAT4 remains on them (Kory et al. 2015).

1.4 LD dynamics

LDs are very dynamic organelles that adapt to different metabolic conditions.

1.4.1 LD biogenesis

De novo formation of LDs occurs in the ER (Jacquier et al. 2011; Choudhary et al. 2015). Neutral lipids can be synthesized either in the ER or in LDs, but predominantly in the ER. The main model of LD biogenesis can be divided into four steps (Fig. 1-5) (Walther et al. 2017):

- Step 1: Neutral lipid synthesis within the ER (see Chapter 1.2).
- Step 2: Formation of an oil lens between the ER PLs leaflets. Newly formed neutral lipids accumulate in the ER bilayer forming an oil lens between the two leaflets (Thiam and Forêt 2016; Walther et al. 2017). The protein FIT2 could participate in the

nucleation by interacting with TAG (Gross et al. 2011). This process was proposed to occur in microdomains of the tubular ER. There, Acyl-CoA synthetase 3 (ACSL3) localize early and it is required for efficient LD nucleation and lipid storage (Kassan et al. 2013).

- Step 3: Budding and nascent LD formation. When there is a certain quantity of neutral lipids within the ER bilayer, the lens becomes unstable. This lens buds from the ER when there is an asymmetry between the surface tension of the two PL leaflets (Chorlay and Thiam 2018). This asymmetry can be due to an excess of PLs or more proteins embedded in one leaflet (Chorlay et al. 2019). Moreover, some lipids promote LD budding, such as triolein, lyso-PC and phosphatidylinositol (PI) (M'barek et al. 2017). LD budding is orchestrated by seipin, an ER protein that determines the sites of LD formation (Wang et al. 2018). Even though its structure has been resolved (Sui et al. 2018), many open questions remain about how seipin and its partner proteins promote LD budding. FIT2 could also promote LD budding (Choudhary et al. 2015).

- Step 4: LD growth and expansion. Some budded LDs continue to acquire more neutral lipids. Many proteins localize to the LD surface during this step. For instance, DGAT2 relocates from the ER to the LD surface, promoting LD growth (Wilfling et al. 2013). Which LDs are selected in the subpopulation that keeps growing is influenced by the small GTPase ARF1 and the COPI coatomer protein complex (Wilfling et al. 2014).

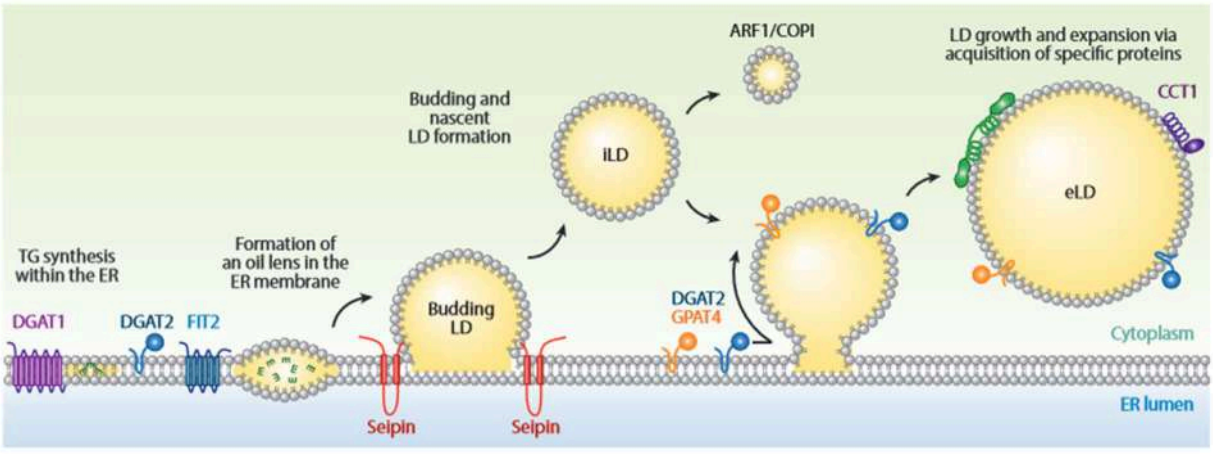

Fig. 1-5. Steps of the *de novo* LD formation and budding from the ER. (Walther et al. 2017). See text for details.

1.4.2 LD fusion and fission

LDs can fuse (Guo et al. 2008; Sun et al. 2013). LD fusion could occur by coalescence of unstable LDs or be mediated by proteins at LD-LD contact sites (Fig. 1-6) (Gluchowski et al. 2017). Coalescence of very unstable LDs in vivo would have very fast dynamics, and it so far has not been directly observed in cells.

Fusion by diffusion in LD-LD contact sites is regulated by the CIDE family of proteins. A member of the family, CIDEA, greatly enhances LD size when ectopically expressed in preadipocytes and favours cellular lipid accumulation (Puri et al. 2008). Neutral lipids are transferred from the smaller LD to the larger one (Gao et al. 2017b).

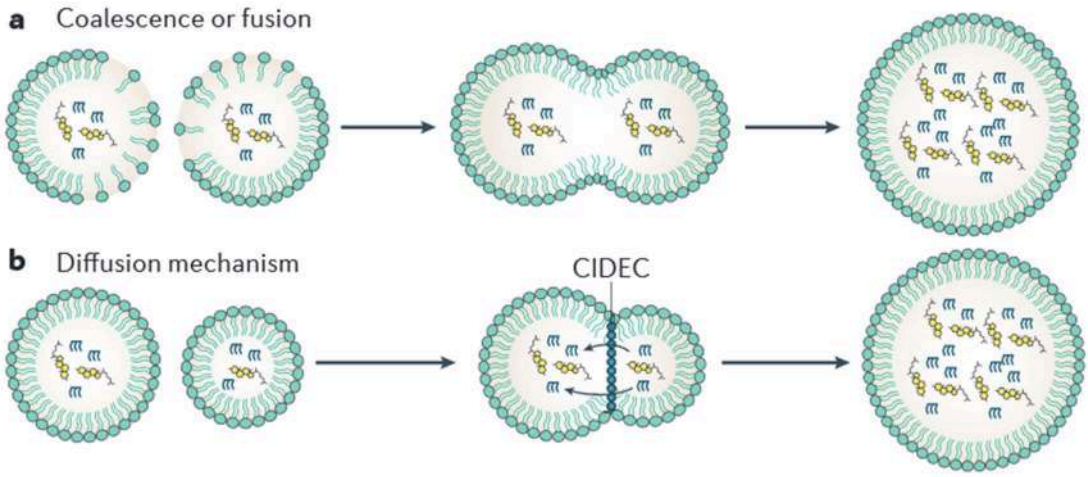

Fig. 1-6. Fusion of LDs. A. Coalescence of LDs due to their instability. **B.** LD-LD contact site where a CIDE protein is mediating LD fusion via lipid diffusion (Gluchowski et al. 2017).

LDs can also produce small LDs by budding. This occurs with the help of ARF1 and the coat protein complex I (COPI). ARF1 and COPI bud vesicles from bilayers for intracellular trafficking. This complex also buds small LDs (around 60 nm) from a bigger LD in vivo and *in vitro*. This results in a lower phospholipid density on the LD, which recruits some key enzymes (Soni et al. 2009; Thiam et al. 2013a; Wilfling et al. 2014). The destiny of the small budded LDs has not been addressed yet.

1.4.3 LD consumption

Neutral lipids stored on LDs are broken down to obtain energy and membrane compounds.

- 1.4.3.1 Lipolysis

Cytoplasmic lipases release free fatty acids from TAG in LDs. Three main lipases are present in the cytoplasm: adipose triglyceride lipase (ATGL, or PNPLA2), HSL and monoacylglycerol lipase (Zechner et al. 2017). ATGL catalyzes the 1st step of lipolysis by hydrolyzing fatty acids in sn-2 or sn-1 position of TAG (Fig. 1-7 A). It has a narrow substrate specificity, having a 10-fold higher affinity for TAG than for DAG (Zimmermann et al. 2004). It requires interaction with ABHD5, also named CGI-58, for its full activation and it is inhibited when it is in contact with G0S2 or hypoxia-inducible lipid droplet associated protein (Das et al. 2018; Kulminskaya and Oberer 2019). ATGL is found in most tissues, having its highest expression in white and brown adipose tissue. Its deletion in mice produces a moderate obese phenotype and its overexpression results in a lean phenotype (Ruggles et al. 2013). In yeasts, the lipases Tgl3p, Tgl4p and Tgl5p are homologous to ATGL and catalyze the same reaction step (Czabany et al. 2007).

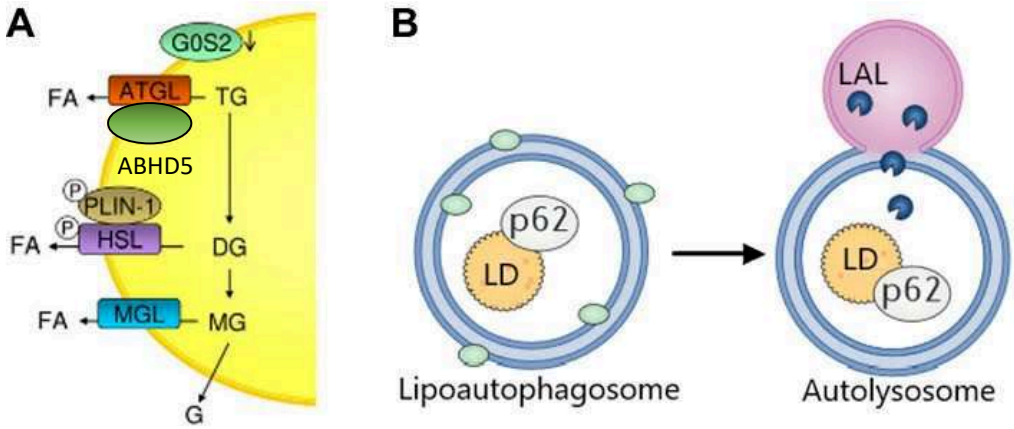

Fig. 1-7. Two pathways for LD consumption. **A.** Lipolysis pathway. See text for details. Adapted from (Zechner et al. 2012). **B.** A lipophagy step where an autophagosome with LDs inside due to the recognition cargo p62 and is fused with lysosomes containing the enzyme lysosomal acid lipase (LAL) resulting in an autolysosome. Adapted from (Zechner et al. 2017).

HSL mediates the second step of lipolysis, releasing one fatty acid and monoacylglycerol. HSL has a broad substrate specificity, being able to hydrolyze TAG, DAG, monoacylglycerol, STE and retinyl esters (Holm et al. 2000). HSL is expressed mainly in adipose tissue, but also in skeletal muscle, pancreas and macrophages. Phosphorylation by protein kinase A (PKA) promotes HSL localization to LDs and improves its catalytical activity. Knocking out HSL in mice

results in increased DAG accumulation in adipose tissue (Ruggles et al. 2013). The last step of neutral lipolysis is catalyzed by monoacylglycerol lipase. It cleaves the last fatty acid from monoacylglycerol. The enzyme is cytoplasmic and does not act on LDs (Zechner et al. 2017).

- 1.4.3.2 Sterol esters hydrolysis.

STE are hydrolyzed to free fatty acid and a sterol by the neutral cholesteryl ester hydrolase that localizes to the ER (Ruggles et al. 2013). They can also be hydrolyzed by HSL (Fredrikson et al. 1981). In yeasts, they are degraded by Yeh2p on the plasma membrane and by Yeh1p and Tgl1p on LDs (Köffel et al. 2005).

- 1.4.3.3 Lipophagy

Breakdown of TAG and STE does not occur only on LDs. During autophagy, cytoplasmic components are sequestered into a de novo formed double-membrane structure called autophagosome that then deliver their cargo to lysosomes for their degradation. When autophagosomes sequester LDs selectively, the process is called lipophagy (Fig. 1-7 B) (Schulze et al. 2017). Lipid degradation is carried out by the lysosomal acid lipase that has broad specificity and acts at an optimal pH of 4.5 – 5 (Zechner et al. 2017). It was suggested that catabolism of big LDs was carried by lipolysis whereas degradation of small LDs was fulfilled by lipophagy (Schott et al. 2019). Therefore, the proposed model would be that TAG on big LDs would be degraded by lipolysis until they have a small size and can be consumed by lipophagy.

1.5 LD size

LD size depends on the balance between neutral lipid synthesis and degradation, and by the fusion and fission processes. LD size varies depending on the organism, environmental conditions and cell type. Size of mature LDs ranges over three orders of magnitude in their diameter: from hundreds of nm to more than 100 μm (Suzuki et al. 2011). This means that the difference in volume between the smallest and the biggest mature LD is $1x10^9$ times.

White adipocytes often contain only one LD that occupies the majority of their cell volume, reaching even more than 100 μm in diameter. Their shape is more polyhedral than spherical due to its definition by the cell periphery and contacts with other cells (Chen and Farese 2002).

The family of proteins CIDE mediates in the transfer of neutral lipids between LDs for obtaining a large unilocular LD in human adipocytes (Gong et al. 2011).

LDs in human non-adipose cells are completely spherical and their size is usually ≤ 1 μm and rarely exceeds 10 μm (Suzuki et al. 2011). For instance, in HeLa cells, the size of LDs is typically 1 μm, and in oleic acid treatment is around 1.75 μm (Smirnova et al. 2006). In yeast *Saccharomyces cerevisiae* in stationary phase the LD size can be around 450 nm (Czabany et al. 2008).

Neutral lipids and PLs influence LD size. The lack of PLs like PC in the LD monolayer results in LDs with large size because they tend to fuse to reduce the surface to volume ratio and stabilize themselves (Guo et al. 2008; Krahmer et al. 2011). During LD budding, some PLs reduce more the surface tension in the ER leaflets than others, resulting in more numerous and smaller LDs. Lyso-PC, PI, saturated PLs and poly-unsaturated fatty acids have this effect in a biochemical reconstituted system (M'barek et al. 2017). In mammary glands, it was suggested that cells grown with oleic acid in the media contained larger LDs than cells grown with palmitic acid (Cohen et al. 2015).

Proteins regulate LDs and influence their size. Two examples are seipin and the yeast protein Pet10p (or Pln1p). Seipin deletion results in many nascent LDs and one large LD that accumulates the big majority of neutral lipids within the cell (Wang et al. 2016). Pet10p deletion in yeast leads to larger LDs when cells are grown in oleic acid media (Gao et al. 2017a)

Chapter 2: Biophysics of lipid droplets

2.1 Emulsions and surface tension

Emulsions are heterogeneous systems in which two immiscible liquids are in contact being one dispersed in the other. From a physical point of view, LDs can be considered like the dispersed phase of a direct emulsion or oil-in-water emulsion. The continuous phase is the aqueous cytosol of cells (Thiam et al. 2013b). One way of characterizing emulsions is by the size of their droplets. This can be measured using dynamic light scattering (DLS). DLS measures the hydrodynamic diameter and size distribution of the particles in a suspension based on their diffusion coefficient obtained from the light scattering intensity fluctuations during time (Stetefeld et al. 2016). DLS measures the size of the whole population giving a distribution of sizes and its measuring range goes from 0.1 nm to 10 μm.

Molecules of water interact through hydrogen bonds. In contrast, neutral lipids do not provide or accept hydrogen bonds. The lack of cohesive interactions between the two components of the emulsion generates surface tension. Surface tension (γ), or interfacial tension, is the force per unit area that is required to increase the surface area of a liquid due to intermolecular forces. The units of surface tension are millinewtons per meter (mN/m) (Thiam et al. 2013b). High surface tension results in an unstable emulsion that will tend to fuse to reduce the volume to surface ratio and the surface tension. There are several techniques to measure surface tension. One of them consists in measuring the pressure required to flatten a meniscus into a plane surface in a capillary tube (Nevin et al. 1951). With this method, surface tension at 25 °C between water and the TAG triolein (3 oleic acids, 18:1n-9) was measured to be 14.61 mN/m, 13.16 mN/m between water and trilinolein (3 linoleic acids, 18:2n-6), and 20.16 mN/m between water and tripelargonin or trinonanoin (3 nonanoic acids, 9:0) (Benerito et al. 1954). These results suggest that depending on the chemical composition of the neutral lipid, the surface tension changes. Of note, these values should be taken cautiously and only for comparison between the different TAGs, because the surface tension of triolein was measured afterwards to be around 32 - 35 mN/m (Daubert and Danner 1989, Mitsche et al. 2010).

Another method for measuring surface tension is using the oil-drop tensiometer. The droplet is subjected to different pressures (P) and the droplet radius (R) is measured. The surface tension can be obtained using the Young-Laplace equation: $\gamma\left(\frac{1}{R1}+\frac{1}{R2}\right)=\Delta P \equiv \Delta P0-\Delta\rho gz$ (Stauffer 1965).

2.2 Surfactants

Surfactants are amphipathic molecules that are situated at the interphase and reduce the surface tension, producing a more stable emulsion (Thiam et al. 2013b). Surface pressure is used to describe surfactants. Surface pressure (Π) is defined as the difference between the energies required to maintain various lipid/water interfaces and correlates with the density of amphipathic molecules at lipid surfaces (Meyers et al. 2015). When the surface tension of a droplet is reduced and it is more stable, the surface pressure increases. PLs act as surfactants thanks to their hydrophilic head, charged in some cases, and their two hydrophobic acyl chains. The effect of PLs on oil droplets is studied with oil droplet tensiometry. For instance, the surface tension of triolein alone went from 32 mN /m to 20 mN/m after 4h in the presence of egg PC. Therefore, surface pressure was 12 mN/m (Mitsche et al. 2010).

Another technique to measure surface tension on neutral LDs with PLs is the aspiration by micropipette of micron size droplets. Droplets in the range of 1 μm – 35 μm are formed by vortexing neutral lipids, buffer and PLs for 1h. Afterwards, droplets are introduced in a micromanipulation device, where the micropipette will completely aspire the droplet (Delacotte et al. 2014). Surface tension is calculated with the diameter sizes of the droplet and the pipette, and by the pressure need to aspirate the droplet (Yeung et al. 2000). Moreover, PL density can be obtained from this method if a fraction of fluorescent PLs are added. Therefore, both surface tension and surfactant density can be obtained by using a fluorescent microscope (Delacotte et al. 2014).

Another technique to explore further the physical properties of monolayers of PLs in neutral LDs are molecular dynamic (MD) simulations. These computer simulations analyze the physical movement of atoms and molecules, and therefore can be used to study the properties of certain systems. An MD study found that at similar concentration of phospholipids (66 Å per lipid) in a bilayer and a monolayer on TAG gave the same surface

tension, ~ 0 mN/m (Bacle et al. 2017). But if that concentration diminished by 10%, the surface tension of the LD monolayer increased to 12.5 mN/m. Moreover, the formation of packing defects, or hydrophobic cavities because there are no PLs covering them, increased nonlinearly for surface tensions higher than 10 mN/m, likely due to interdigitation of acyl chains from TAGs and PLs (Bacle et al. 2017). Another study agreed with the previous one showing that when TAGs are added to a bilayer, the surface area per one PL molecule increased due to the mixing of TAG and PLs acyl chains (Prévost et al. 2018). MD simulations can give insights into many membrane processes. However, their results should be compared with experimental data. PL area was measured in *in vitro* assays determining that the area per PC molecule in the monolayer is around 78 Å, whereas in a bilayer it varies between 69 and 74 Å (Chorlay and Thiam 2020).

Other surfactants present in LDs are lyso-PLs and fatty acids. DAG can also decrease surface tension at low concentrations and in the presence of PLs to avoid membrane deformation (Mirheydari et al. 2017). Sterols such as cholesterol have also a small amphipathic character, with a bulky hydrophobic part and a small hydroxyl group. The potential contribution of cholesterol to lower the surface tension has not been measured yet. Fatty acids, lyso-PLs, DAG and sterols are the products of reactions occurring on the LD surface. Therefore, their impact on surface tension if they accumulate is relevant for LD homeostasis.

2.3 Proteins acting as surfactants

Some proteins also have an amphipathic character with regions enriched in hydrophobic aa and other polar aa. Proteins embedded in the interface of neutral lipids and water can reduce the surface tension, acting as surfactants (McClements and Gumus 2016). Many proteins can interact with the oil surface non-specifically. These proteins normally lose their native structure, achieving another conformation with lower energy for their interaction with oil. This is the case for many proteins used to make emulsions in pharmaceutical or alimentary industry. Some examples are beta-lactoglobulin, albumin and whey protein isolate (Tabibiazar et al. 2015; Ali et al. 2016).

2.3.1 Apolipoproteins as proteins interacting with neutral lipids

Lipoproteins are particles formed by specific proteins and lipids, mainly TAG, STE, cholesterol and PLs. They are present in the blood, where they transport these lipids around the organism. There are different types of lipoproteins, depending on their lipid and protein composition, that fulfil distinct functions. Their size ranges between 10nm and 1000nm (Pan and Segrest 2016). Their neutral hydrophobic core makes them similar to LDs in structure and in biophysical properties (Small et al. 2008).

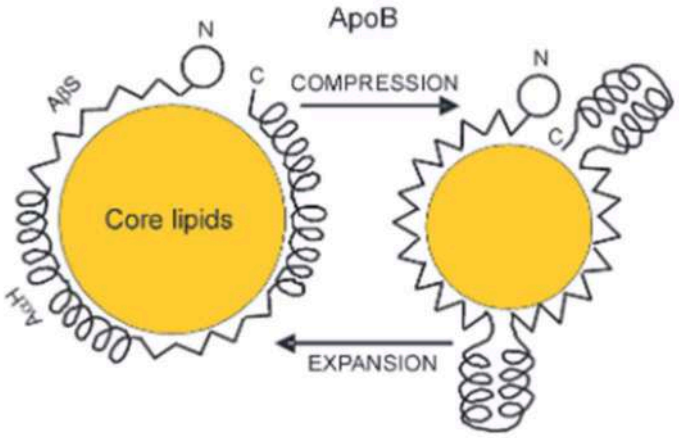

Fig. 2-1. ApoB has two modes of interaction with lipoproteins. At low surface pressure, ApoB AHs are interacting with the lipids in the lipoprotein. When the surface pressure rises, ApoB AHs desorb from the lipid surface. ApoB therefore acts as a buffer for surface pressure (Wang et al. 2006).

Apolipoprotein B (ApoB) is present in chylomicrons, very low-density lipoproteins (VLDL) and low-density lipoproteins. Chylomicrons transport TAGs from enterocytes to peripheral tissues in the fed state and have a truncated version of ApoB. VLDLs have full length ApoB and are formed in the liver from where they are released in the fasting state (Sirwi and Hussain 2018). ApoB reduces surface tension of triolein/water interfaces measured by the oil drop tensiometer. Furthermore, drop compression and expansion lead to determine that the maximal surface pressure resisted by ApoB without partially detaching from the interface was 13 mN/m (Wang et al. 2006). Another study from the same group aimed to study the structural motifs of ApoB involved in this interaction. The N-terminal part of ApoB contains an alpha helical region, formed by 17 predicted AHs, and two amphipathic beta-strands. When the alpha helical domain is adsorbed at the oil-water interface, it forms a viscoelastic surface.

ApoB helices could be ejected or remodelled depending on the surface tension. However, the two amphipathic beta-strands form an elastic film and are irreversibly anchored to the lipid surface (Mitsche et al. 2014). Therefore, the amphipathic beta-strands are always interacting with the oil surface whereas the interaction of ApoB AHs depends on the surface pressure (Fig. 2-1). ApoB is a very good example of a protein that can interact very stably or transiently with neutral lipids.

Apoliphorin-III (ApoLp-III) is an exchangeable apolipoprotein present in insects that contains a helix bundle formed by five alpha helices. The surface pressure when the ApoLP-III is added to triolein is 20 mN/m. A monolayer of PC in triolein has a surface pressure of 7.5 mN/m. When ApoLP-III and PC were added together the surface pressure was similar to protein alone. However, when PE or DAG were present in combination with PC, surface pressure was higher than with only protein (Mirheydari et al. 2017). This study suggests that the combination of certain proteins and some lipids increases the surface tension, while the combination with other lipids does not have any effect.

Apolipoprotein A I (ApoA-I) is an exchangeable apolipoprotein. Two ApoA-I chains form a ring around the lipid core in high-density lipoprotein particles. The two chains stabilize via lateral interactions between their charged residues. ApoA has been studied in neutral lipid-PLs-Protein-water interface. The C-terminal part of ApoA-I has a desorption pressure of 25.8 mN/m. Of note, when ApoA-I detaches from the lipid surface, it removes PLs, reducing the surface pressure by having fewer proteins and less PLs (Mitsche and Small 2011).

2.4 LD surface tension and stability

LDs contain many surfactants on their surface: various kinds of PLs, different proteins, fatty acids, DAG. The surface tension of purified LDs has been measured. By microaspiration technique, the surface tension of purified LDs was ~3 – 4 mN/m for mammalian LDs, and around 2 mN/m for Drosophila cells (M'barek et al. 2017). When the concentrations of surfactants in the neutral lipid surface is low, the emulsion will be thermodynamically unstable because there is too much hydrophobic surface exposed to the aqueous environment. When this happens, there are several ways of decreasing instability. The first one is LD fusion or coalescence. Another way is by Ostwald ripening, where molecules from smaller droplets are

transferred to larger droplets through the continuous phase. If LDs have a continuous monolayer with the ER bilayer, neutral lipids could travel from one LD to another inside the ER bilayer, where they are soluble. Ostwald ripening was demonstrated in biochemical reconstitutions using membrane-embedded droplets (Thiam et al. 2013b; Salo et al. 2019). In vivo, proteins can regulate the ripening process, for instance, the seipin complex counteracts the ripening process (Salo et al. 2019).

Chapter 3: Amphipathic helices

Amphipathic helices (AHs) are protein sequences that fold into helical structures with their aa segregated in two well differentiated faces: one hydrophobic and one polar. They are present in many proteins and were first identified in apolipoproteins (Segrest et al. 1974). By adopting a parallel orientation to the membrane plane, AHs can interact with membranes inserting their hydrophobic residues between fatty acyl-chains while polar residues face lipid polar heads (Fig. 3-1) (Jao et al. 2008; Giménez-Andrés et al. 2018).

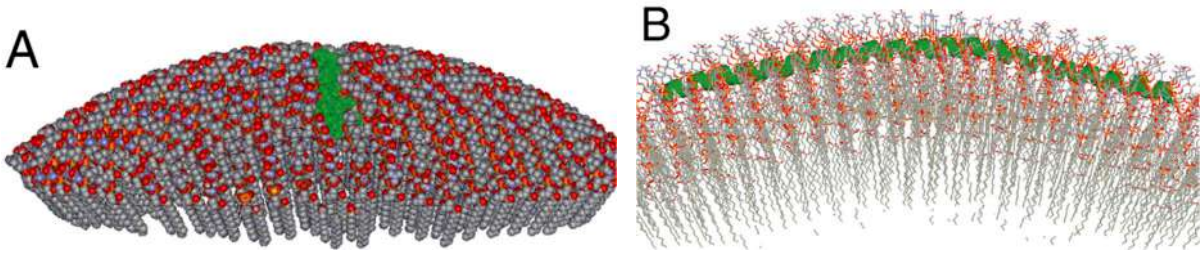

Fig. 3-1. Interaction of an AH with membranes. **A.** Frontal view of alpha-synuclein AH (green) interacting with a curved membrane. **B.** Lateral view of the positioning of alpha-synuclein in a membrane. The helical axis is positioned just below the level of the phosphate groups of PLs. Adapted from (Jao et al. 2008).

3.1 Helicity of aa and types of helices

Some aa are more prone to form a helix than others. For instance: alanine, leucine, arginine and lysine have high helix propensity while glycine, proline and aspartic acid have less helix propensity (Pace and Scholtz 1998). Proline is a helix breaker due to its limited lateral angle positions and its inability to form hydrogen bonds that stabilize the internal structure of a helix (Rey et al. 2010). Aa helicity has been largely studied in helices of globular proteins, where many crystallized protein structures are available. For transmembrane helices or AHs that interact with membranes, this information is much more limited. Many AHs are unfolded when they are not interacting with membranes (Bigay et al. 2005; Giménez-Andrés et al. 2018). There are four different thermodynamic states for AHs depending on their folding and partitioning to the interface (Fig. 3-2). The interaction of hydrophobic residues with the lipid surface promotes the helix formation (Strandberg et al. 2018).

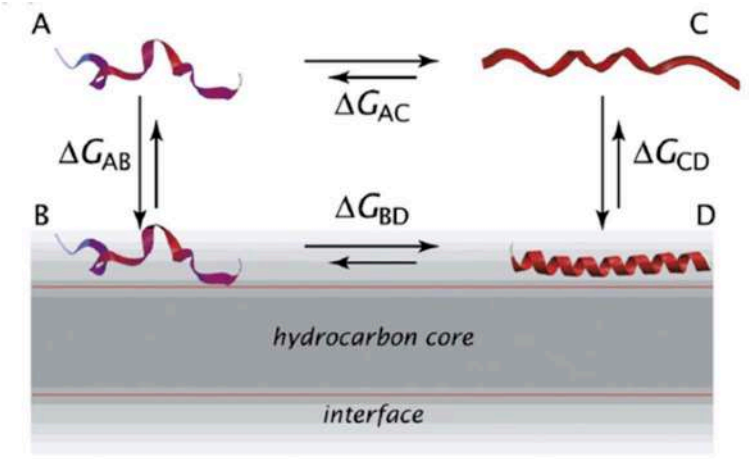

Fig. 3-2. Thermodynamic states of an AH. **A.** Unfolded protein in an aqueous environment, **B.** Unfolded protein on the interface, **C.** Partially folded protein in the cytosol, **D.** fully folded on the membrane interface. The most abundant states are A and D. Figure from (Fernández-Vidal et al. 2007).

AHs that interact with membranes have been shown to form alpha helices (most common form), or 3-11 helices. Alpha helices have 3.6 aa per turn or 18 aa for 5 turns. 3-11 helices have 3.67 aa per turn or 11 aa for 3 turns. Some examples of AHs adopting an alpha helix are the amphipathic lipid packing sensor (ALPS) motif (Drin et al. 2007) and Opi1p (Hofbauer et al. 2018). 3-11 helices are used to interact with membranes by synucleins (Jao et al. 2008) and are predicted to be present in Plins.

3.2 AH properties

Several parameters can be used to characterize AHs. AH hydrophobicity is calculated as the average of the hydrophobic residues of a helix. aa hydrophobicity is measured from its partitioning into polar-apolar phases, like octanol/water (Fauchère and Pliska 1983). However, taking into account only hydrophobicity could lead to misidentification of some structures such as hydrophobic hairpins. The hydrophobic moment combines the hydrophobicity of each residue with its position in the helix by vector summing their hydrophobicities. The hydrophobic moment influences the binding to lipid surfaces more than only hydrophobicity (Fernández-Vidal et al. 2007). AHs that localize to polar-hydrophobic interfaces like membranes can be distinguished from other helices because of their relatively small hydrophobicity but a large hydrophobic moment (Eisenberg et al. 1982). Net charge also influences AH behaviour, for example, by mediating in the interaction with negatively charge

PLs in the membrane (Pranke et al. 2011). The structure of the backbone surrounding the helices can influence their targeting (Doucet et al. 2015).

3.3 Identification of AHs

AHs can be identified using several techniques. The bioinformatic tool HeliQuest can plot the aa sequence as an AH and calculate its hydrophobic moment (Gautier et al. 2008). A useful experimental technique is circular dichroism (CD) spectroscopy. Left-handed and right-handed circularly polarized light is absorbed differentially by the purified protein depending on their secondary structure. CD gives global structural information, where the helical content is given by minima peaks at 222 nm and at 208 nm (Greenfield 2006). It does not distinguish AH from other helices by itself. However, AH can be strongly suggested by this method if a protein is unfolded in solution and folded in the presence of liposomes (Drin et al. 2007). Moreover, CD spectra of mutants with reduced amphipathic character can be performed.

Liposomes are useful models for testing protein-membrane interactions, such as the interaction between AHs and bilayers. Apart from using liposomes in CD, they can be incubated with a purified protein to test its interaction with membranes. If the protein is conjugated with a fluorescent probe like nitrobenzoxadiazole (NBD), which changes its fluorescence depending on the environment, the interaction can be followed with a fluorimeter (Drin et al. 2007, Pranke et al. 2011). Otherwise, the mixture of protein and liposomes can be analyzed by a sucrose gradient in a flotation assay to separate the bound protein from the unbound (Bigay et al. 2005). Of note, these two methods do not confirm whether the structure that interacts with membranes is a helix.

Deeper structural analysis of the helices can be performed with NMR (Herbert et al. 2012) and electron paramagnetic resonance (EPR) (Jao et al. 2008). NMR is usually performed on detergent micelles, which can break the helix due to their small size, whereas EPR can be done in liposomes (Jao et al. 2008). However, EPR is time-consuming as it requires that many of protein aa be mutated to cysteine one at a time to spin-label them. Structure of the 11-mer repeats of alpha-synuclein was characterized by EPR and shown to form a 3-11 helix, where each of its aa occupies 1.5 Å along the helical axis (Jao et al. 2008).

Another technique to identify AHs is to determine the exposure of different aa positions by mutating them to cysteine and adding methoxy polyethylene glycol maleimide to react with them. AHs signature with this method will be a periodic pattern of alternating exposed and buried residues (Pataki et al. 2018). Finally, cryo-electron microscopy can also reveal AHs, as in the case of the ER protein seipin (Sui et al. 2018).

3.4 AHs functions

AHs can localize selectively to one kind of membrane within the cell. For instance, the ALPS motif, a common type of AH (Fig. 3-3 A), interacts with curved membranes of the early secretory pathway (Drin et al. 2007).

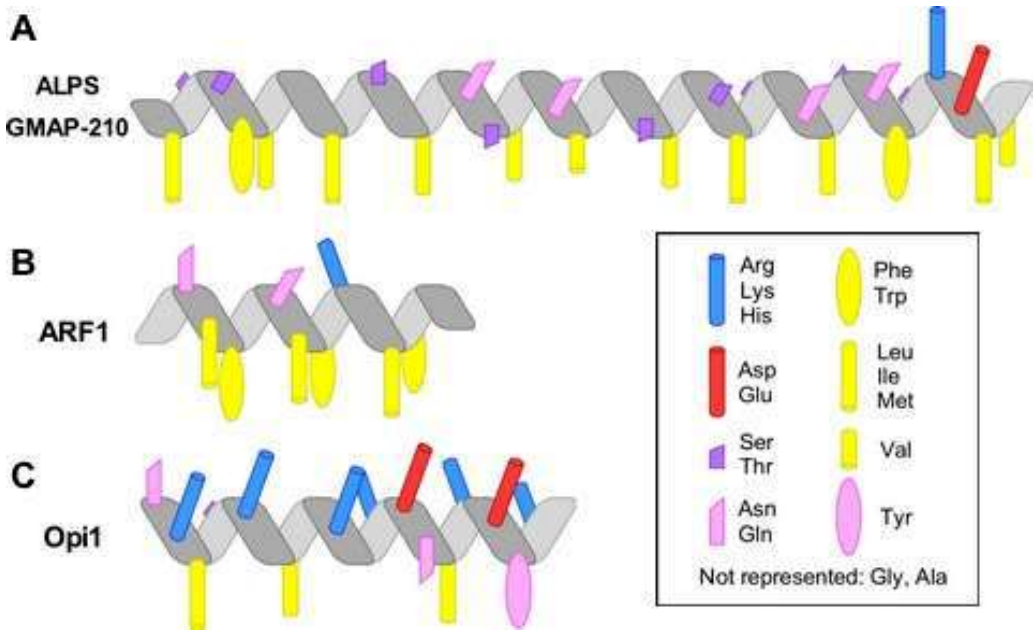

Fig. 3-3. Examples of AHs. Diagrams show lateral views of some AHs. **A.** ALPS motif of GMAP 210. **B.** N-terminal AH of ARF1. **C.** AH of Opi1p. Adapted from (Giménez-Andrés et al. 2018, Annex I).

AHs are also implicated in the intracellular trafficking of vesicles. ARF1 is a small G protein that is myristoylated and contains a small AH of 14 aa (Giménez-Andrés et al. 2018). Its AH is very hydrophobic and has a very little charge (Fig. 3-3 B). When the AH is buried in the protein, it interacts transiently with membrane surfaces due to the myristoylation. However, when the AH is exposed due to an exchange of GDP for GTP, it interacts stably with many different

membranes (Antonny et al. 1997). Its cellular localization is controlled by other proteins that regulate the exchange of GDP for GTP or its GTPase activity.

Opi1p is a yeast protein that interacts with the ER using two motifs, an AH and two phenylalanines in an acidic track, which interacts with the ER protein Scs2p (Loewen et al. 2004, Hofbauer et al. 2018). Its AH is small and contains many positive charges, one per turn (Fig. 3-3 C). These positive residues interact stereospecifically with the phosphatidic acid present in the ER, regulating Opi1p ER localization (Hofbauer et al. 2018). When there is no phosphatidic acid, Opi1p translocates to the nucleus and repress some genes involved in membrane biogenesis (Loewen et al. 2004).

3.5 Targeting of AHs to LDs

Many proteins use AHs to target LDs (Giménez-Andrés et al. 2018). CCT1 is an enzyme in the biosynthetic pathway of PC. It contains an AH that interacts with membranes and targets LDs when it is expressed heterogeneously in cells (Prévost et al. 2018). Its AH has big hydrophobic residues, like phenylalanines and tryptophans. Charged residues are also abundant. Plins are a family of non-enzymatic proteins that localize to LDs. Plins are explained more in-depth in chapter 4. A comparison of the characteristics of LD-localized AHs shows that different AHs can target LDs. This question is addressed in Chapter 6.

Chapter 4: Perilipins

Perilipins (Plins) are a family of proteins that target and regulate LDs in a non-enzymatic manner. The name 'perilipin' means 'surrounding lipid' in Greek (Kimmel et al. 2010). Plins were initially identified by their affinity for LDs and the presence of a 'PAT' domain. Five Plins have been identified in mammals (Bickel et al. 2009).

Perilipin 1 (Plin1) was first described in the early 1990s by a study looking for phosphorylation substrates of PKA and was found to localize to LDs (Greenberg et al. 1991). Perilipin 2 (Plin2), also called adipophilin or adipose differentiation-related protein (ADRP) was the next member described on LDs (Brasaemle et al. 1997). Perilipin 3 (Plin3), also named Tail-interacting protein of 47 kDa (TIP47), was initially misidentified as a cargo selection for mannose phosphate receptors. Afterwards, it was also described on LDs (Wolins et al. 2000; Bulankina et al. 2009). Perilipin 4 (Plin4), or S3-12, was identified during a screening of secreted and cell surface proteins in 3T3-L1 adipocytes (Scherer et al. 1998). It associates with small LDs in cultured 3T3-L1 (Wolins et al. 2003). Plin5, also named OXPAT, MLDP or Lsdp5, targets LDs and regulates LD-mitochondria contact sites (Wolins et al. 2006b; Wang et al. 2011b).

4.1 Plins protein structure

Plins are composed of three main regions: PAT region, 11-mer region and the C-terminal region. The PAT (perilipin, ADRP and TIP47) domain is defined by about 100 aa at the N-terminal end of Plin1 and was identified by homology in other members of the family (Lu et al. 2001). There is no structure proposed for this domain. The PAT domain is not responsible for Plin LD targeting (McManaman et al. 2003). The PAT domain of Plin2 (1 – 89 aa) prevents localization of Plin3 to LDs occupied by Plin2 (Orlicky et al. 2008). Plin4 is the only Plin member that does not have a clear PAT sequence.

Plins have a region composed of repeated sequences of 11 aa (11-mer) after the PAT sequence. This region targets LDs in Plin2 and Plin3 (Targett-Adams et al. 2003; Bulankina et al. 2009). It is predicted to form a 3-11 helix (Bussell and Eliezer 2003). 11-mer repeats of Plin1 has been confirmed to form an AH that localizes to LDs (Rowe et al. 2016). Plin4 belongs to the Plin family because the sequence homology of these repeats with other members. Of

note, the 11-mer repeat sequence of Plin4 is exceptional in terms of its length and repetitiveness at the level of three 11-mer repeats. Human Plin4 has about 950 aa of predicted AH, 10 times longer than the other Plins (Fig. 4-1).

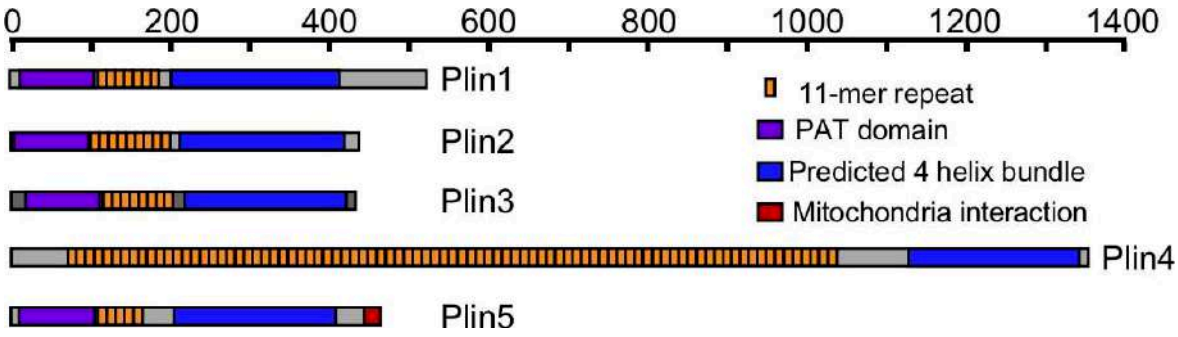

Fig. 4-1. Diagram of sequences of mammalian perilipins. 11-mer repeats are marked in orange, predicted C-terminal part in blue and PAT domain in purple. Plin5 also contains a mitochondrial interaction motif. Adapted from (Čopič et al. 2018).

The C-terminal domain can also target LDs in Plin1, Plin2 and Plin3 (Nakamura and Fujimoto 2003; Ajjaji et al. 2019). The C-terminal domain of Plin3 was purified and crystallized in its soluble form. It has an alpha/beta domain and a four-helix bundle containing a hydrophobic cleft. The four-helix bundle is composed of AHs that might disrupt their protein-protein interaction and interact with the lipid surface (Hickenbottom et al. 2004). The same structure was proposed for Plin1 and Plin2 by homology. This c-terminal domain was suggested to provide different stabilization of Plins in LDs (Ajjaji et al. 2019).

4.2 Plins tissue expression

Plin expression in different tissues is regulated by the transcription factors peroxisome proliferator-activated receptors (PPARs) (Rodriguez and Kersten 2017). Plin1 has 4 splicing variants. Plin1 A (full length) is specifically expressed in adipocytes (Fig. 4-2), whereas variant with a shorter c-terminal part is expressed in steroidogenic cells (Kimmel and Sztalryd 2016). Plin2 has a more ubiquitous expression. Plin3 is widely expressed among tissues (Fig. 4-2). Plin4 is expressed mainly in adipocytes, but also in heart and skeletal muscle (Wolins et al. 2003). Perilipin 5 (Plin5) is expressed in highly oxidative tissues that use fatty acids for energy, such as heart, muscle, liver and brown adipose tissue (Fig. 4-2).

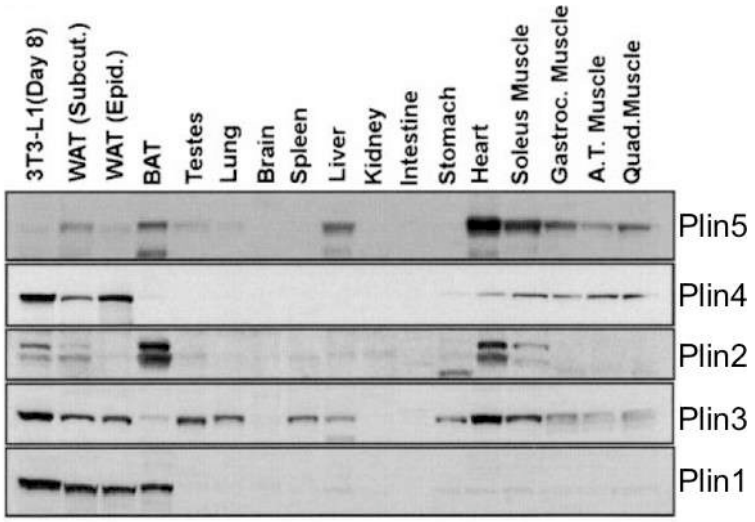

Fig. 4-2. Expression of Plins in different tissues checked by Western-Blot. Adapted from (Wolins et al. 2006b)**.**

4.3 Distribution and dynamics of Plins on LDs

Plins have been classified depending on their observed intracellular localization: constitutive if they were exclusively localized to LDs (Plin1 and Plin2); or exchangeable if they were also observed in the cytosol or at the PM (Plin3, Plin4 or Plin5) (Bickel et al. 2009). However, this classification depends on whether proteins are degraded when they are not on LDs. When Plin1 is not in contact with LDs, it is degraded by lysosomal protein degradation machinery (Xu et al. 2006). Likewise, when Plin2 is not on LDs, it cannot be found in the cytosol due to proteasomal degradation (Gross et al. 2006).

Immunostaining and light microscopy showed that Plin1 did not cover the totality of the giant LD surface in 3T3-L1 adipocytes. It was unevenly dispersed on the LD surface, which included some patches devoid of Plin1 (Blanchette-Mackie et al. 1995). Super-resolution microscopy showed micrometre-sized Plin1 patches on LD surface of adipocytes (Fig. 4-3) (Hansen et al. 2017).

Plin1-LD interaction resists alkaline carbonate solution incubation (Garcia et al. 2002). These results suggest the strong interaction of Plin1 with LDs. Plin3 and Plin2 have faster dynamics than Plin1 on LDs as measured by fluorescence recovery after photobleaching (Ajjaji et al. 2019).

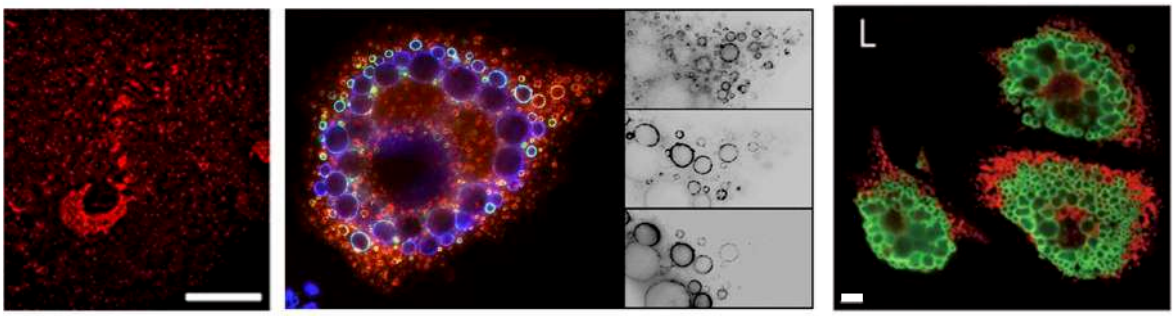

Fig. 4-3. Plins target to different LD pools in 3T3-L1 differentiated adipocytes. Left panel shows a super-resolution image of Plin1 on LD surface in primary adipocytes. Scale bar: 10 μm. Image from (Hansen et al. 2017). Middle panel shows an image of immunofluorescence of Plin 3 (red), Plin2 (green) and Plin1 (blue), revealing their distribution in a cultured 3T3-L1 adipocyte (Wolins et al. 2006a). Right panel shows Plin4 (red) and Plin1 (green) distribution. Scale bar: 10 μm. Image from (Wolins et al. 2003).

Immunofluorescence showed that Plin3 and Plin4 are localized on the small LDs in cultured 3T3-L1 adipocytes. Plin2 is bound to intermediate LDs, whereas Plin1 is present on the surface of big LDs (Fig. 4-3) (Wolins et al. 2003, 2006a). Different association of Plins with LDs is also found in hepatocytes undergoing abnormal lipid accumulation (Straub et al. 2008).

4.4 Regulation of lipolysis by Plins

Even though Plins do not have enzymatic functions, they play a key role in the regulation of lipolysis. Plin1 is a well characterized inhibitor or promotor of lipolysis in adipocytes depending on its phosphorylation state. Under basal conditions, Plin1 is not phosphorylated and is found on the surface of LDs, whereas the lipases HSL and ATGL are cytosolic (Fig. 4-4). Moreover, the C-terminal domain of Plin1 interacts with the ATGL activator ABHD5, sequestering it (Sztalryd and Brasaemle 2017).

Under lipolytic stimulation conditions, cyclic adenosine monophosphate levels increase activating cAMP-dependent PKA. PKA phosphorylates Plin1, ABHD5, ATGL and HSL. ABHD5 is liberated from Plin1 and interacts with phosphorylated ATGL that localizes to LDs. Phosphorylated HSL interacts with phosphorylated Plin1 and it is recruited to LD surface (Fig. 4-4) (Sztalryd et al. 2003; Sztalryd and Brasaemle 2017).

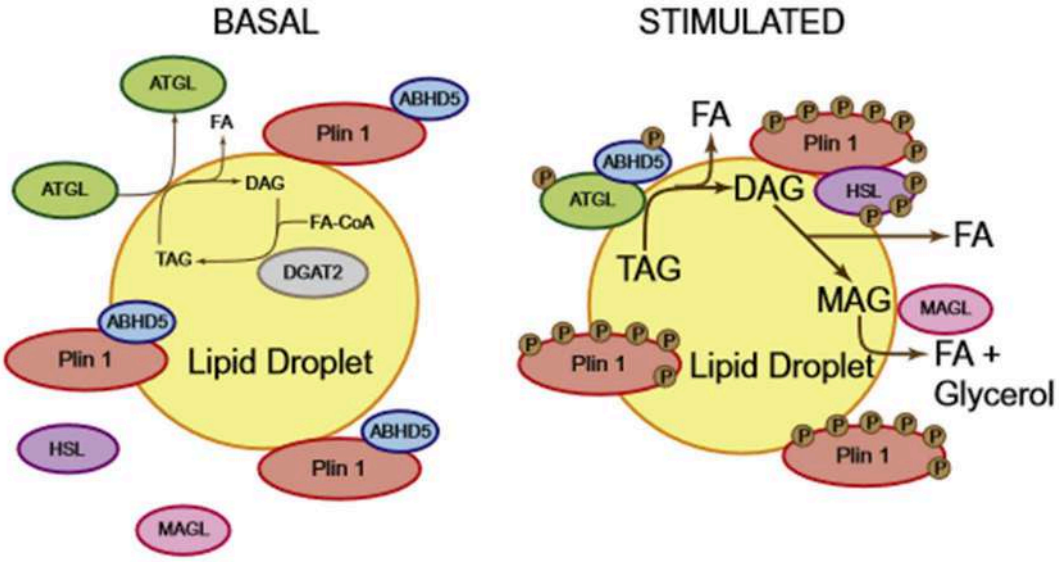

Fig. 4-4. Plin1 regulates lipolysis under non-induced lipolytic conditions (basal) and stimulated conditions (Sztalryd and Brasaemle 2017).

Plin5 also regulates lipolysis in oxidative tissues. Under basal conditions, Plin5 on LDs interacts via its N-terminal part with HSL, sequestering it. Plin5 also interacts via its C-terminal part with either ABHD5 or ATGL, preventing their interaction (Wang et al. 2011a). PKA also phosphorylates Plin5, which increases lipolysis by unknown mechanisms. Phosphorylation may disrupt the interaction of Plin5 with ATGL and ABHD5, allowing them to interact and hydrolyze TAG (Sztalryd and Brasaemle 2017).

Plin2 attenuates basal lipolysis only moderately, it is not phosphorylated by PKA and does not interact with lipases (Sztalryd et al. 2003; Sztalryd and Brasaemle 2017). Overexpression of Plin2 reduces the access of ATGL to LDs, resulting in an attenuation of lipolysis (Listenberger et al. 2007).

4.5 Plins outside mammals

Plin orthologues have been found in non-mammalian species (Miura et al. 2002; Granneman et al. 2017). Pet10p is a protein from the unicellular eukaryote *Saccharomyces cerevisiae* that has sequence homology to the PAT domain in Plins. Pet10p is very abundant on the surface of LDs (Gao et al. 2017a). The mechanism of Pet10p targeting to LDs is not clear; its sequence does not contain a repetitive region nor a good candidate AH, in contrast to mammalian Plins.

The multicellular eukaryote *Drosophila melanogaster* has also been shown to express two Plin-related proteins: lipid storage droplet 1 (Lsd1 or Plin1) and lipid storage droplet 2 (Lsd2 or Plin2). These two proteins localize to LDs in mice and drosophila cells (Miura et al. 2002). Drosophila can survive without these two proteins, but their fat storage homeostasis is impaired (Beller et al. 2010).

Other animals closer to humans, like teleost fish, also have orthologous of Plins. Plin1, Plin2 and Plin5 orthologues were found as well as Perilipin 6. Perilipin 6 is expressed in their skin where it localizes to the surface of droplets containing hydrophobic carotenoids. Its deletion impairs accumulation of carotenoids (Granneman et al. 2017).

4.7 Yeast as a tool to study LDs and Plins

The yeast *Saccharomyces cerevisiae*, hereafter termed simply yeast, is a model organism for biological studies of eukaryotes. Yeasts have rapid growth, they are easy for replica plating and mutant isolation, they have a well-defined genetic system, and a versatile DNA transformation system (Sherman 2002). These characteristics have made it possible to develop many tools and apply several techniques that gain a lot of information about yeast processes and general biology. There are available yeast collections in which one gene at a time has been deleted or fused with a reporter gene (Giaever and Nislow 2014), and the sub-cellular localization of many of its proteins are known (Huh et al. 2003). Thanks to all these tools and resources, yeast lipid metabolism has been very well described (Klug and Daum 2014).

Yeasts accumulate LDs when cells enter the stationary phase or deal with environmental stresses (Wang 2015a). TAG synthesis can depend greatly on the environment, for instance, on growth temperature or the carbon source (Klose et al. 2012). The most abundant TAG species in yeasts are the only formed by palmitoleic acid or either palmitic and palmitoleic acids, or palmitoleic and oleic acids (Ejsing et al. 2009). Increased amount of LDs can be obtained if yeasts are grown in a media containing oleic acid. LD size also increases if the yeast strain is *pet10Δ* (Gao et al. 2017a). Moreover, yeast grown in oleic acid contain more TAG, less STE, and more unsaturation in their lipid species. Interestingly, there are changes in the LD proteome depending if yeasts are grown in oleic acid or in glucose (Grillitsch et al. 2011).

There are available yeast strains that contain only either TAG or STE. The ΔTAG strain (*dga1Δ lro1Δ)* contains mainly STE as neutral lipids and has a reduced number of LDs (Sorger and Daum 2002). The ΔSTE strain (*are1Δ are2Δ*) contain only TAG and its LD number is not affected (Sandager et al. 2002). The deletion of the four proteins involved in neutral lipid synthesis (ΔLDs or *dga1Δ lro1Δ are1Δ are2Δ* strain) results in a strain named quadrupole mutant that is viable and has no growth defects despite lacking neutral lipids and LDs (Sandager et al. 2002). An inducible LDs strain was made by regulating the expression of Dga1p and Are2p upon galactose addition in the *lro1Δ* and *are1Δ* background (Becuwe et al. 2018).

Full length Plin1, Plin2 and Plin3 have being expressed in budding yeast. They target yeast LDs, confirming that the LD targeting mechanism is highly conserved (Jacquier et al. 2013, Rowe et al. 2016). The 11-mer repeats regions of Plin1, Plin2 and Plin3 were confirmed to target LDs by expressing WT and mutated N-terminal parts of Plins in yeast and checking their localization with light microscopy (Rowe et al. 2016).

Chapter 5: Lipid droplets and diseases

Excessive or insufficient lipid storage is associated with many pathological conditions. These include obesity, fatty liver disease, insulin resistance, atherosclerosis, infectious diseases, cancer development and neurodegenerative diseases (Fig. 5-1) (Yu and Li 2017). In this chapter, I am going to focus mainly on the lack or excess of lipid accumulation in adipocytes, and the role of LDs in cancer development.

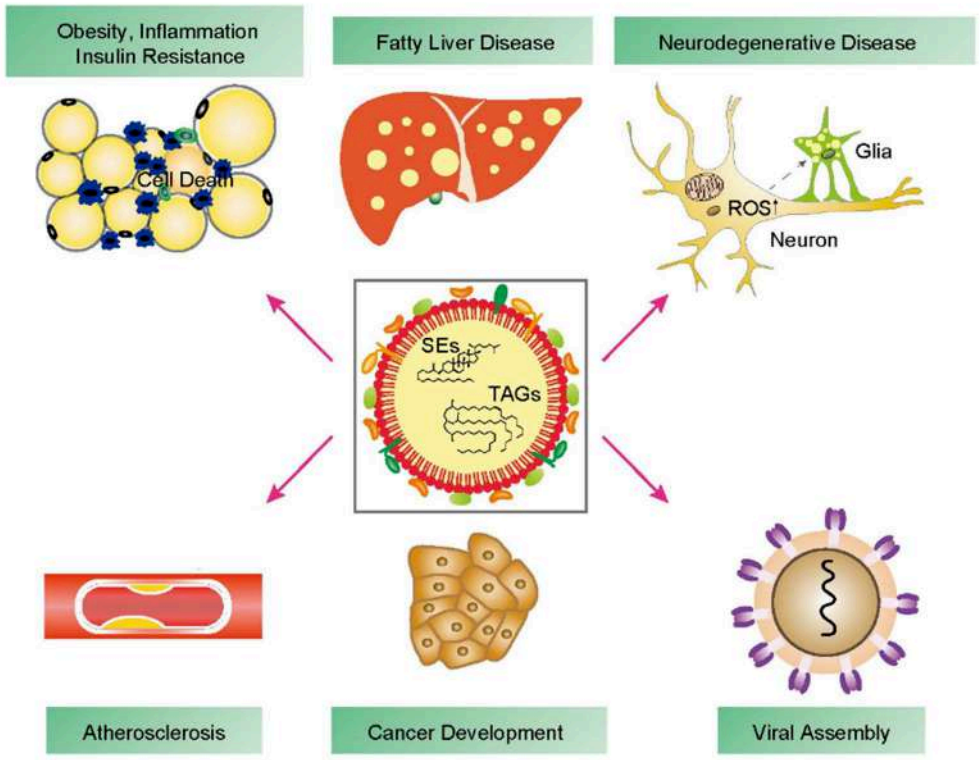

Fig. 5-1. Diseases related with LDs. LDs are related with obesity, fatty liver disease, neurodegenerative diseases, atherosclerosis, cancer development and infectious diseases. For instance, during obesity, an excess of neutral lipids are stored on adipocytes, leading to hypoxia, inflammation and insulin resistance. The excess of neutral lipids are accumulated also in other tissues, as in the liver. Figure from (Yu and Li 2017).

5.1 Lipodystrophies and obesity

Excessive fat accumulation leads to obesity, which is increasingly prevalent in today's society. It is associated with many pathologies, such as insulin resistance and cardiovascular disease (Rydén and Arner 2017). Both genetic and environmental factors, such as diet and lifestyle, contribute to the development of obesity (Krahmer et al. 2013). The excess of fat

accumulation in adipose tissue can be achieved either by increasing the adipocyte mass, hypertrophy; or their number, hyperplasia (Rutkowski et al. 2015). Hypertrophic adipocytes have impaired cellular function, resulting in inflammation and impaired hormonal response (Fig. 5-2) (Stenkula and Erlanson-Albertsson 2018). Adipocyte size has been proposed as a potential biomarker for cardiometabolic alterations and diseases (Laforest et al. 2015). When the storage capacity of adipose tissue is near its saturation, there is an overflow of excess lipids into the plasma and ectopic LD accumulation in muscle, liver or heart (Gross and Silver 2014).

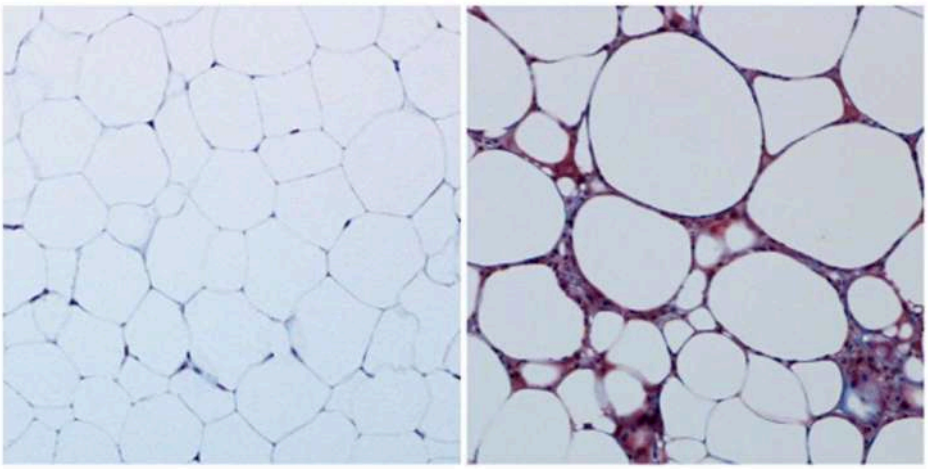

Fig. 5-2. Histological differences between healthy and unhealthy adipose tissue. Mice subcutaneous adipose tissue in a healthy state (left) or in an unhealthy state due to high-fat diet resulting in adipocyte hypertrophy (right). In healthy adipose tissue, there is a sparse extracellular matrix. In unhealthy adipose tissue, there is a denser and more fibrous extracellular matrix due to hypoxia and inflammation (Rutkowski et al. 2015).

Lipodystrophies are conditions where there is a loss of body fat. Reduced triglyceride storage results in adipocyte lipotoxicity, mitochondrial dysfunction and increased oxidative stress (Vigouroux et al. 2011). Lipodystrophies are commonly associated with insulin resistance, hepatic steatosis and hypertension. They can be due to mutations in genes encoding proteins related with LDs biology. Some examples are seipin gene (BSCL2), Plin1 and CIDEC (Krahmer et al. 2013).

5.2 Cancer

Low vascularization of tumor tissues causes adverse conditions such as oxidative stress and nutrient shortage. To survive, cancer cells have to adapt by reprogramming their metabolism (Schulze and Harris 2012). Lipid metabolic pathways are highly affected by this reprogramming. For instance, cancer cells display increased uptake and production of lipids and obtain more energy from fatty acid oxidation (Cheng et al. 2018). In hepatocellular carcinoma, which represents the second most frequent cause of cancer-related death worldwide, researchers have identified large differences in the metabolism of fatty acids (Nakagawa et al. 2018). LDs protect cells against lipotoxicity by controlling the levels of free fatty acids, cholesterol and ceramides (Chitraju et al. 2019). Many types of cancer cells, including breast, liver, lung and pancreatic, display an increase in their LD content, suggesting that increased production or stability of LDs is advantageous for the propagation of neoplastic cells. High LD content is in fact considered a hallmark of aggressive carcinomas (Koizume and Miyagi 2016). Therefore, LDs present a promising yet largely unexplored target for cancer treatment (Liu et al. 2017). Moreover, LDs perform various functions during cells stress, such as maintenance of redox homeostasis and production of lipid mediators (Henne et al. 2018), and can thus make cancer cells more resistant to treatment (Cotte et al. 2018). Importantly, altered expression of several Plins is associated with various types of cancer, including hepatocellular carcinoma and lung adenocarcinoma (Zhang et al. 2018).

RESULTS

Chapter 6: Plin4 contains a large AH that targets LDs in yeast and interacts with neutral lipids *in vitro*.

The results shown in this chapter are my contribution to the paper titled "A giant amphipathic helix from a perilipin that is adapted for coating lipid droplets" published in the journal Nature Communications in 2018 (Čopič et al. 2018). The whole publication is on the Annex II of this manuscript.

LDs store energy and membrane compounds in the form of neutral lipids and a monolayer of PLs and proteins. Depending on the density of the PLs in the monolayer, the surface tension of the LD can change (Thiam et al. 2013b). LDs have proteins on their surfaces that mediate and regulate their functions (Kory et al. 2016; Bersuker and Olzmann 2017). Some proteins use AHs to target LDs. What are the features of these AHs to target LDs is not known. Likewise, which are the properties of LD surface to be selectively targeted is poorly understood.

Plins are a family of proteins containing AHs that target LDs. Plin4, a member of the Plin family, contains the largest predicted AH. It is made of repeats of 33 aa called 33-mer (Scherer et al. 1998; Bussell and Eliezer 2003). Plin4 has been found endogenously on LDs in 3T3-L1 adipocytes (Wolins et al. 2003, 2005, 2006a). However, its physiological role is not clear (Chen et al. 2013). In this paper, we addressed how AHs can target LDs selectively using the AH of Plin4 as a model. Moreover, we wondered what the function of this long AH in Plin4 is.

6.1 Plin4 AH length influences LD targeting

The 33-mer repeat region of Plin4 is exceptional in terms of its length, with 33-mer repeated 29 times in humans, about 960 aa in total (Fig. 6-1 A). This region is 10 times longer in Plin4 than in the other members of the mammalian Plin family. This region could fold into a 3-11 helix, resulting in an AH (Fig. 6-1 B). This AH has little hydrophobic character because of the lack of big aromatic residues and the presence of some polar aa, as threonines, in the hydrophobic face. The alignment of each of the 29 33-mer of Plin4 and the Weblogo shows

that the repeats are very well conserved (Fig. 6-1 C). Therefore, the chemistry of the putative AH will be constant along it.

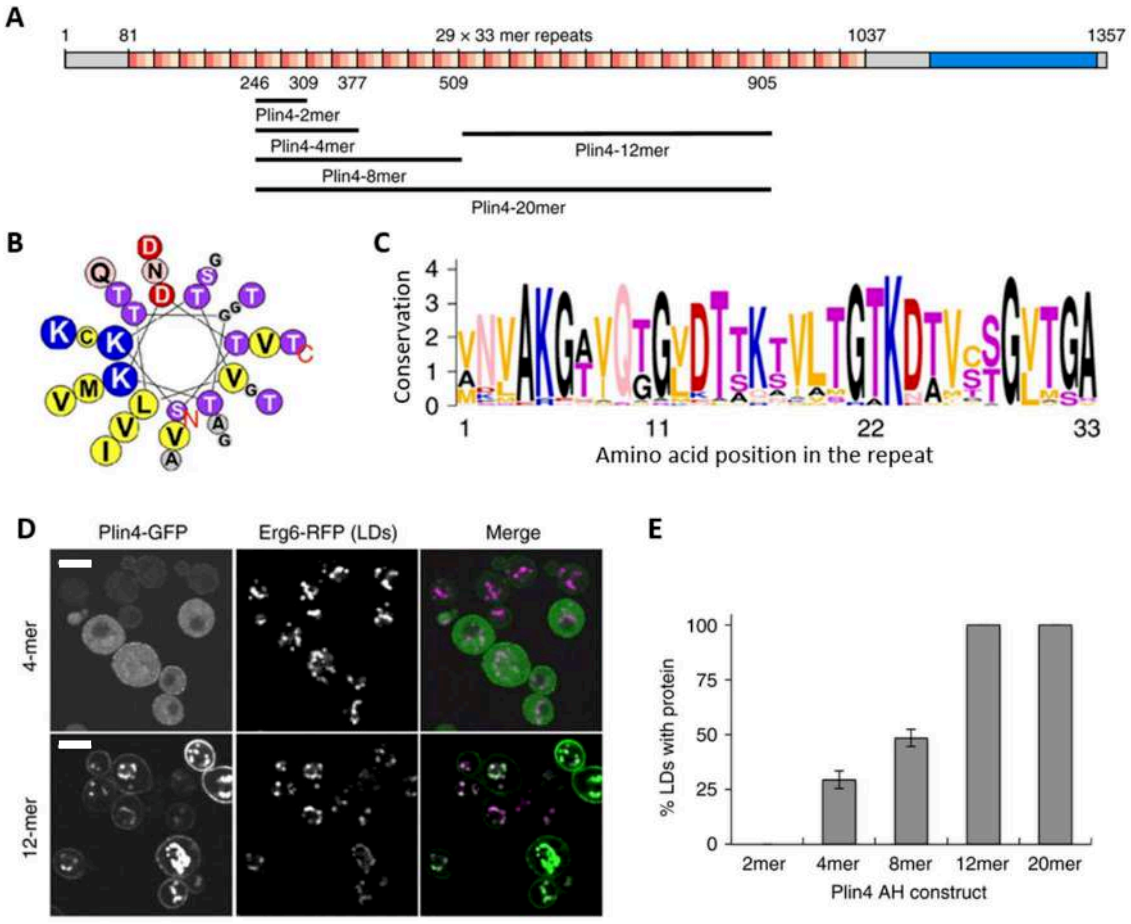

Fig. 6-1. Plin4 contains a long region of 33-mer repeats that localizes to LDs. A. Schematic representation of human Plin4. Fractions of the AH cloned are marked under it. 33-mer repeats are marked in orange. The homology region with the 4-helix bundle crystalized in Plin3 is marked in blue. **B**. Helical wheel plot of one 33-mer repeat from Plin4, plotted as a 3–11 helix. **C**. Weblogo generated from an alignment of each of the 29 33-mer repeats from human Plin4 sequence. **D**. Localization of Plin4 4-mer and Plin4 12-mer GFP fusions in yeast. LDs are marked with Erg6-RFP. Scale bar: 5 µm. **E**. Targeting of Plin4 AH to LDs improves increasing the AH length in HeLa cells (results obtained by Cesar La Torre Garay, Institut Jacques Monod). Figure adapted from (Čopič et al. 2018).

The 33mer region may mediate the localization of Plin4 to LDs. To address this possibility, I expressed different fragments of Plin4 (Fig. 6-1 A) fused to green fluorescent protein (GFP) in yeast. A fragment of four 33-mer, 132 aa in total called hereafter Plin4 4-mer, is cytosolic in yeast. A longer fragment of twelve 33-mer, 396 aa called hereafter Plin4 12-mer, localizes to LDs (Fig. 6-1 D). In HeLa cells, some Plin4 constructs target LDs. The targeting increases with

the length of the construct (Fig. 6-1 E, results obtained by Cesar La Torre Garay, Institut Jacques Monod). Longer Plin4 constructs interact better owing to a more extensive interaction surface. Furthermore, the same sequence is targeted to LDs in such evolutionarily distant organisms as yeast and humans. This suggest that targeting of Plin4 to LDs is direct and non-protein mediated, as shown previously for other Plins (Jacquier et al. 2013; Rowe et al. 2016).

In addition, Plin4 12-mer also localizes at the periphery of yeast cells. This is in accordance with the net positive charge of this amphipathic sequence (Fig. 6-1 B) which could be interacting electrostatically with the negatively charged plasma membrane (Yeung et al. 2008). Plin4 was firstly identified in a screening of secreted and surface proteins during adipocyte differentiation (Scherer et al. 1998).

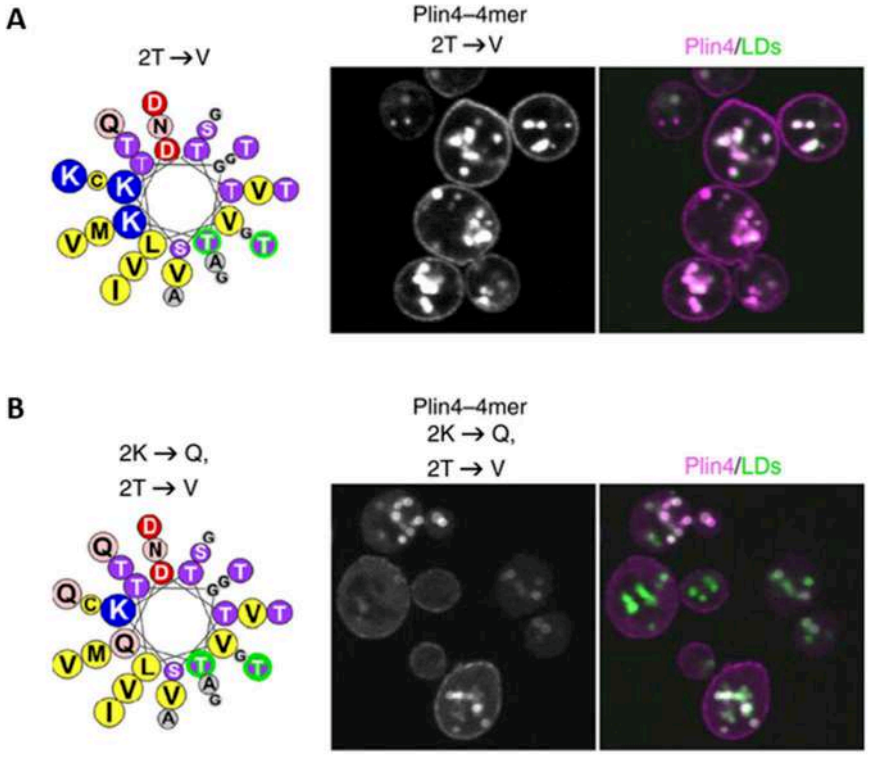

Fig. 6-2. Hydrophobicity and net charge influence the targeting of Plin4 AH. A. Hydrophobicity can compensate short length in Plin4 targeting LDs. Left part: helical wheel of the more hydrophobic mutant (2T-V). The two threonines mutated to valines are signaled in green. Right part: localization of 2T-V mutant in yeasts. **B.** Positive charge is not fundamental for targeting LDs. Left part: helical wheel of the net negative charge mutant because the change of two lysines to glutamines (2K-Q). Right panel: localization in yeast of 2K-Q mutant. LDs were marked with Erg6-RFP. Figure adapted from (Čopič et al. 2018).

The putative AH of Plin4 has low hydrophobicity (Fig. 6-1 B). In order to see how hydrophobicity affects Plin4 AH targeting, we designed a mutant in which two threonines present in the apolar face were mutated to valines (2T-V) per 33-mer repeat. Four 33-mer repeats of the 2T-V mutant localized to LDs in yeast (Fig. 6-2 A). Thus, increased hydrophobicity in the apolar face can compensate for a shorter length of Plin4 AH. In HeLa cells, increased hydrophobicity improved localization to LDs as well. However, its targeting was unspecific as it was also localizing to other membranes, like the ER (Annex II, results obtained by Cesar La Torre Garay and Sandra Antoine-Bally, Institut Jacques Monod). This suggests that low hydrophobicity is tuned in the long AH of Plin4 in order to detect specifically LDs.

Charge of AHs can determine to which membranes they bind. For instance, alpha synuclein, which also has a poorly hydrophobic face, requires its positive residues to bind to negatively charged vesicles (Pranke et al. 2011). To test the effect of net positive charge in Plin4 AH on LD binding, we mutated two lysines to glutamines (2K-Q) per 33-mer, resulting in an AH with negative net charge of -1. This mutation is gentle and should not perturb the helicity of Plin4 AH (Pace and Scholtz 1998). 2K-Q mutation joint to 2T-V localizes to LDs in yeast (Fig. 6-2 B). Hence, positive charge is not essential for LD targeting: a negatively charged AH can also localize to the LD surface. This excludes the large contribution from electrostatic interactions in the binding of AHs to LDs. In contrast, the 2K-Q mutation largely prevented localization of the AH to the negatively charged plasma membrane, where electrostatic interactions are important for protein targeting

6.2 Plin4 AH can be efficiently purified and fluorescently labelled

To better characterize the interaction of Plin4 with LDs, we decided to purify two Plin4 AH constructs, Plin4 4-mer and Plin4 12-mer, and perform *in vitro* or biochemical reconstitution assays, where the conditions can be highly controlled. Plin4 4-mer and Plin4 12-mer synthetic genes were cloned in a bacterial expression plasmid without any tag for their purification (Čopič et al. 2018) (Karine Eudes, Institut Jacques Monod). We adapted the protocols for purifying these Plin4 fragments from the protocol of alpha-synuclein AH purification (Der-Sarkissian et al. 2003) with the help of Bruno Antonny (IPMC, Sophia Antipolis). Plin4 purification protocol includes two main steps: boiling to precipitate most of proteins but Plin4

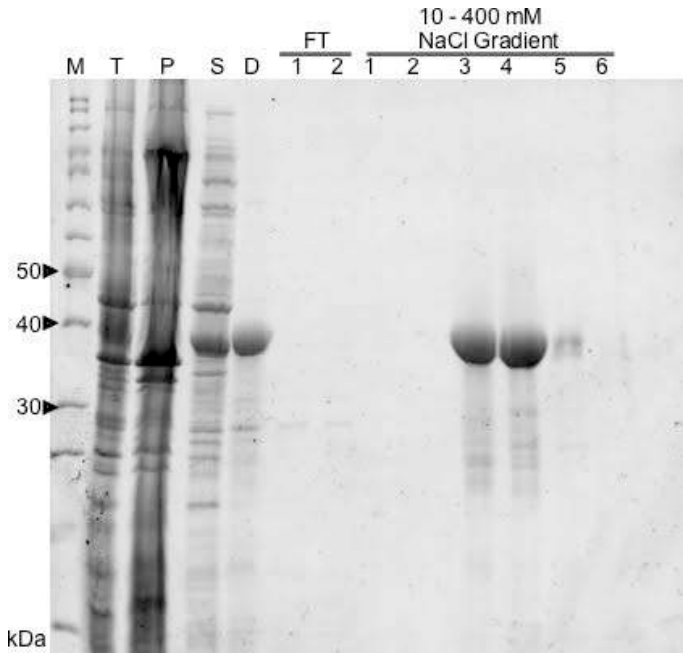

Fig. 6-3. Plin4 12-mer is efficiently purified. Plin4 12-mer purification, analyze by polyacrylamide gel electrophoresis (PAGE). Fractions 3 and 4 show Plin4 12-mer purified with high purity and efficiency. M: marker, T: total fraction, P: precipitated fraction after centrifugation, S: supernatant after centrifugation, D: fraction after boiling and dialysis steps, FT: flow-through. Gel stained with Sypro Orange.

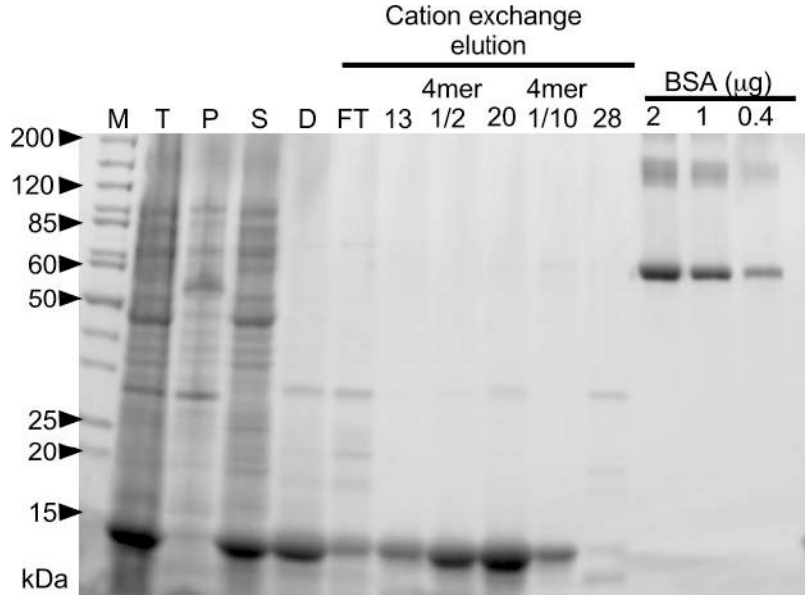

Fig. 6-4. Plin4 4-mer efficient purification and quantification. Fractions labelled as 4-mer and 20 show the Plin4 4-mer purified with high purity. Fractions labelled as 4-mer are the fractions with higher concentration of Plin4 4-mer (14, 15, 16, 17, 18 and 19) pooled and the number under it shows its dilution. BSA samples make a standard curve to quantify 4-mer dilutions and fraction 20. Fractions are run in a tris-tricine acrylamide bis-acrylamide gel. M: marker, T: total fraction, P: precipitated fraction after centrifugation, S: supernatant after centrifugation, D: fraction after boiling and dialysis steps, FT: flow-through. Gel stained with Sypro Orange.

and a cation exchange chromatography. Using this protocol, I obtained efficient purifications of Plin4 12-mer and Plin4 4-mer (Fig. 6-3, Fig. 6-4). Plin4 AH is devoid of aromatic residues, which are commonly used for protein quantification due to their absorbance of UV light at 280 nm or their interaction with Coomassie blue in Bradford assay. Therefore, I needed other techniques to measure Plin4 AH concentration reliably. In order to quantify the concentration of the purified protein, I used bovine serum albumin (BSA) standards of known concentration with the purified proteins in protein electrophoresis (Fig. 6-4). I stained the gels with Sypro Orange, which interacts with the sodium dodecyl sulfate (SDS) bound to the protein to make it migrate in the gel. As one molecule of SDS interacts with around two aa, the quantification does not depend on the presence or absence of certain aa. However, this method relies on the image quantification of the stained gel. I measured protein concentration additionally quantifying the concentration of cysteines using the method of Ellman (Ellman 1959).

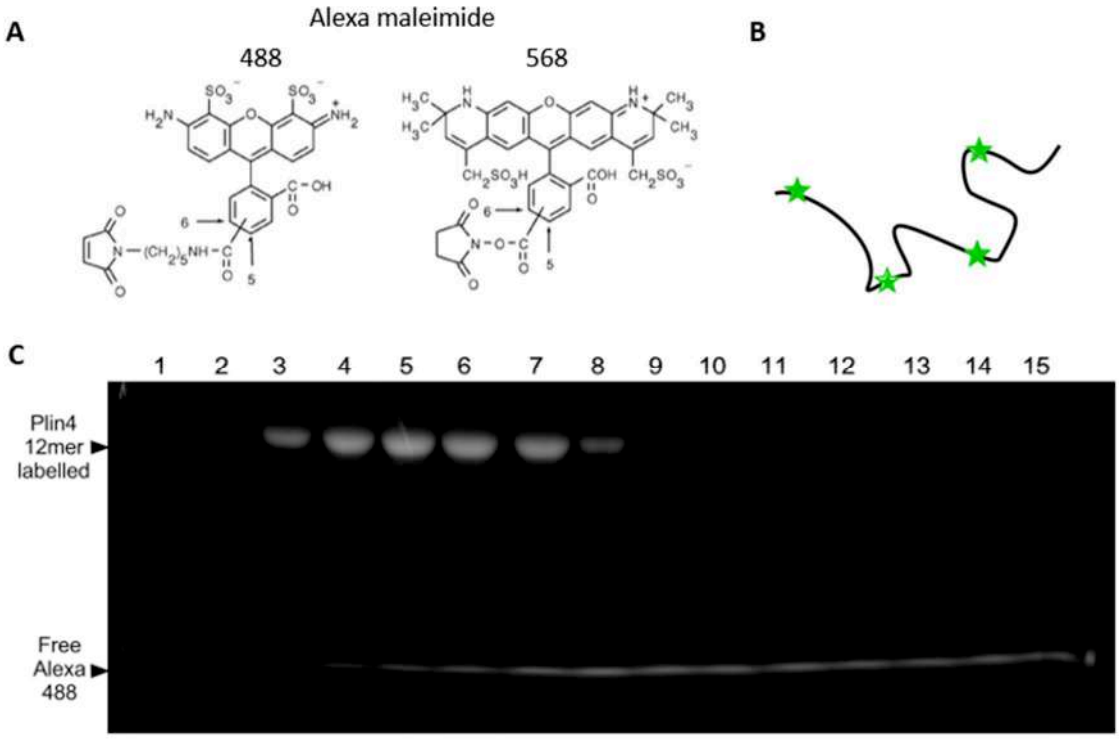

Fig. 6-5. Plin4 12-mer labelling with Alexa. A. Structures of Alexa maleimides 488 and 568 fluorescent probes. **B.** Diagram of unstructured Plin4 12-mer labelled with Alexa 488 in its 4 cysteine (Čopič et al. 2018). **C.** Fluorescence emission in the protein electrophoresis gen run after protein incubation with Alexa 488. Fractions 3 to 8 show Plin4 12-mer labelled with Alexa 488. Fractions from 7 to 15 shows free unreacted Alexa 488.

To be able to visualize the protein with light microscopy, I labelled some protein fractions with fluorophores using endogenous cysteines in Plin4. Plin4 4-mer and Plin4 12-mer were labelled in their endogenous cysteines with Alexa maleimide probes (Invitrogen), either A488 (green) or A568 (red) (Fig. 6-5 A, B). The labelling protocol was efficient and very little free Alexa dye is present in the labelled protein samples (Fig. 6-5 C).

6.3 Plin4 AH folds into a helix in contact with lipids

Plin4 33-mer repeat region could form an AH, as suggested by the aa sequence. Furthermore, the 11-mer repeat region present in Plin1 has been shown to form a helix in the presence of N,N-dimethyldodecylamine N-oxide (Rowe et al. 2016). To test whether Plin4 33-mer repeat region can from a helix, we performed CD spectroscopy with purified Plin4 12-mer (396 aa fragment) of Plin4 20-mer. Results showed that the proteins were unstructured in solution.

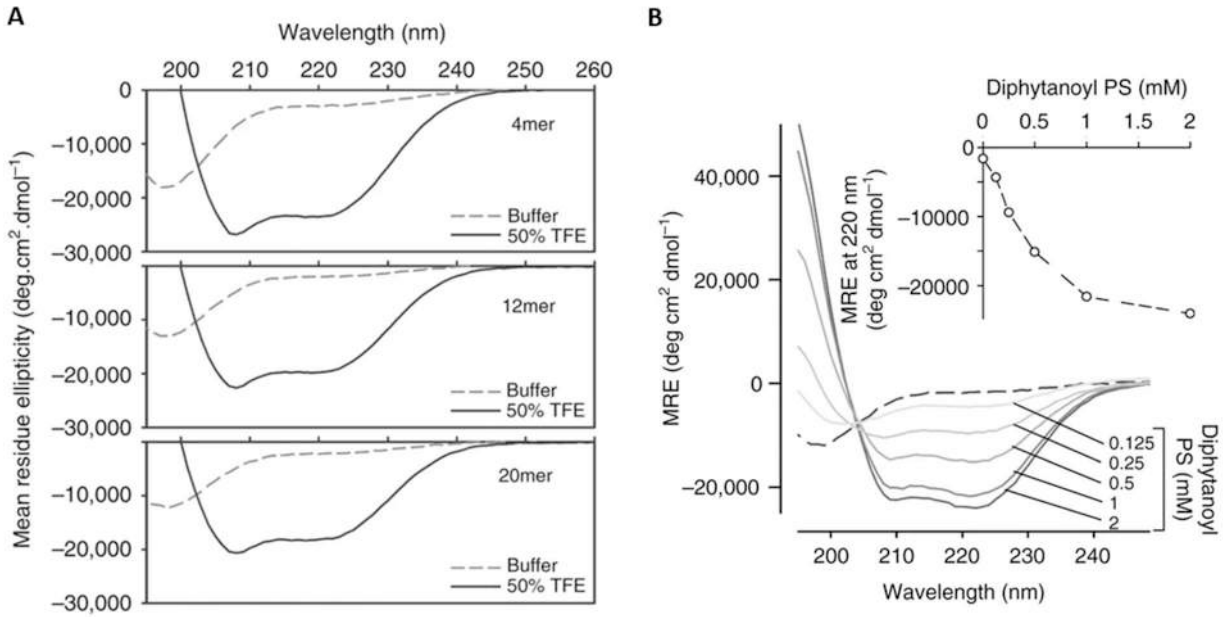

Fig. 6-6. Plin4 constructs have helical conformation. A. CD spectra of different lengths of Plin4 AH either in the buffer, where the protein is unstructured; or in 50% trifluoroethanol (TFE), where it has helical conformation. **B**. CD spectra of Plin4 20-mer showing helical conformation with increasing amounts of diphytanoyl PS liposomes. On the upper left there is the CD signal depending on the number of liposomes present. Experiment performed with Bruno Antonny in his lab at Université Côte d'Azur, CNRS, IPMC. Figure adapted from (Čopič et al. 2018).

However, in the presence of the organic compound trifluoroethanol that promotes secondary structure, they displayed a highly helical conformation as shown by the spectral peaks at 208 and 222 nm (Fig. 6-6 A). The protein also has helical conformation in the presence of diphytanoyl PS liposomes, which expose many packing defects or hydrophobic cavities being permissive for AH binding (Fig. 6-6 B). Hence, these results suggest that Plin4 AH is unstructured in the cytosol and folds into a helix when it interacts with the lipid surface of LDs. Other, much shorter, AHs have been demonstrated to fold in contact with bilayers (Drin and Antonny 2010).

6.4 Plin4 AH is able to interact directly with neutral lipids, forming oil particles

Hydrophobic cavities from the membrane that are exposed to the cytosol are named lipid packing defects. They have been described as an important factor for some AHs to interact with lipid surfaces (Bigay et al. 2005; Drin et al. 2007). At the extreme end, an LD completely devoid of a PL monolayer and consisting only of neutral lipids, will have its acyl chain exposed over the whole surface. Thus, it could be pictured as a lipid surface with infinite lipid packing defects. We, therefore, asked if Plin4 AH was capable of interacting with neutral lipids in the absence of any PLs. To test this, I mixed a drop of the TAG triolein with purified Plin4 12-mer at increasing protein concentrations. The protein concentration was up to a protein-to-lipid molar ratio 1:2000. After vigorous vortexing, the suspensions became turbid, suggesting that the oil was emulsified into smaller droplets that dispersed the light (Fig. 6-7 A). The suspension observed by negative staining in electron microscopy showed numerous spherical droplets with a diameter ranging concentrated between 50 to 250 nm (Fig. 6-7 B, assay done by Sophia Pagnotta, electron microscopy facility Université Côte d'Azur, CNRS, IPMC). DLS measurements confirmed the presence of particles between 100 and 1000 nm. This range did not vary depending on the length of Plin4 AH (Fig. 6-7 C, D).

The vortexing step was used to disrupt the oil droplets so Plin4 AH can bind to the oil surface. The vortexing step could have the undesired effect of denaturalizing the protein or affecting its properties to interact with lipid surfaces. In order to test this possibility, Marco Manni (Université Côte d'Azur, CNRS, IPMC) checked the binding to diphytanoyl PS liposomes with or without prior vortexing of the protein. The protein interacted with liposomes to the same

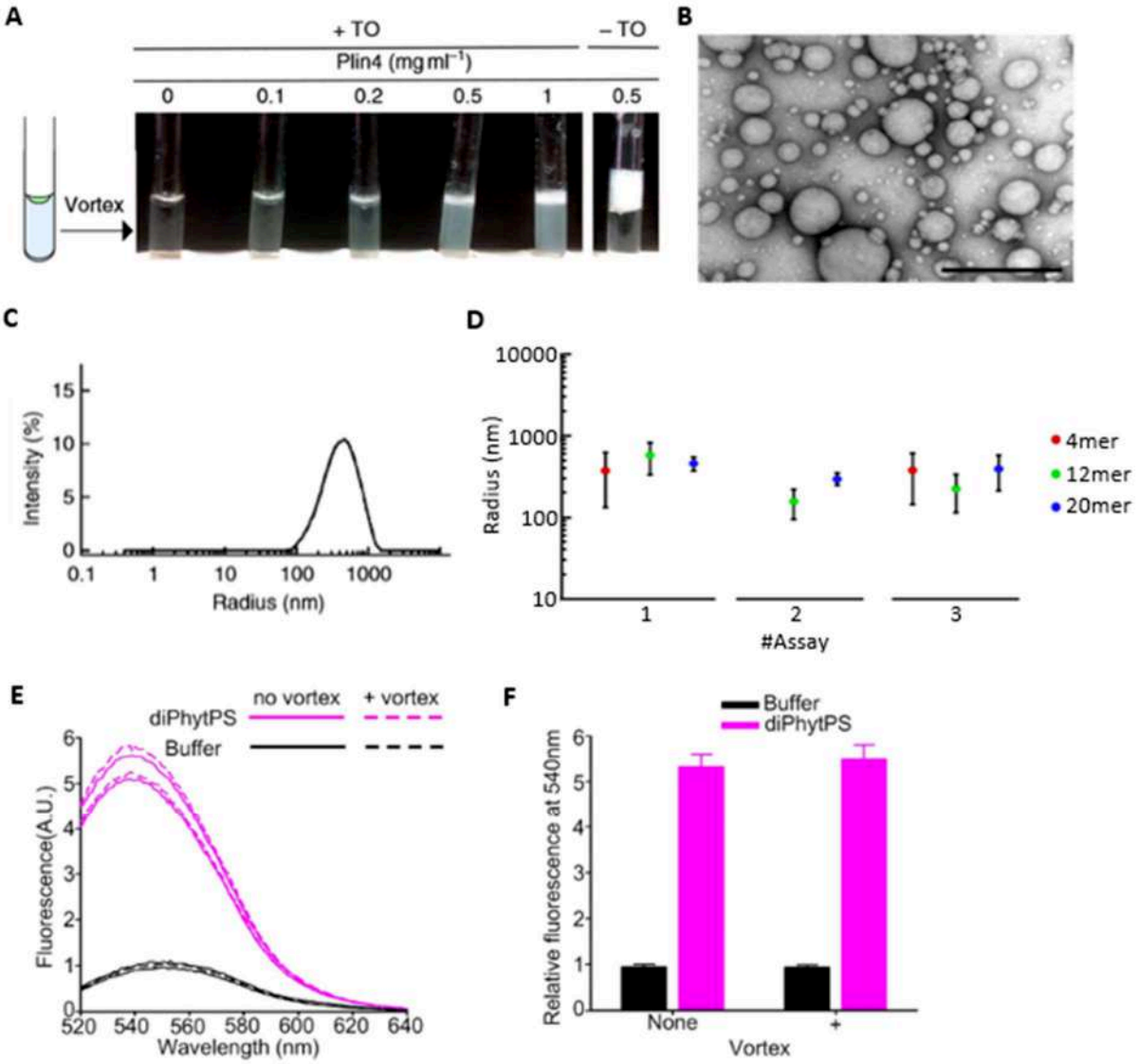

Fig. 6-7. Plin4 interacts directly with neutral lipids *in vitro*, forming oil droplets. **A.** Images of tubes in which a drop of triolein (10 µl) was vigorously mixed with a solution (190 µl) of increasing concentration of Plin4 12-mer. **B.** Representative image of the Plin4-oil emulsion by negative staining electron microscopy. Scale bar: 0.5 µm. Image taken by Sophia Pagnotta, electron microscopy facility Université Côte d'Azur, CNRS, IPMC. **C.** Size distribution obtained by DLS measurement of an aliquot withdrawn from the middle of the oil emulsion obtained with 0.5 mg/ml Plin4 12-mer. D**.** Comparison of size distribution between different lengths of Plin4 AH, Plin4 4-mer, Plin4 12-mer and Plin4 20-mer. Three independent experiments are shown. Dots represent maxima peak and vertical bars represent polydispersity. **E, F**. Vortexing does not affect Plin4 interaction with lipids. **E.** Fluorescence emission of Plin4 12-mer labelled with NBD in vortex and not vortexed conditions in contact with Diphytanoyl liposomes and only buffer. Done by Marco Manni, Université Côte d'Azur, CNRS, IPMC. **F.** Comparison of the maximum of fluorescence with or without vortex. Done by Marco Manni, Université Côte d'Azur, CNRS, IPMC. Figure adapted from (Čopič et al. 2018).

extent in both cases (Fig. 6-7 E, F). These results show that Plin4 is able to interact with neutral lipids forming small particles.

The emulsion could also be observed by light microscopy using a mixture between fluorescently labelled and non labelled Plin4 12-mer and oil labelled with Bodipy. Whereas most particles were below the resolution of the microscope, I could visualize larger oil droplets, which showed uniform staining with fluorescent protein (Fig. 6-8). This confirms that these oil particles have oil in the centre and Plin4 12-mer surrounding it.

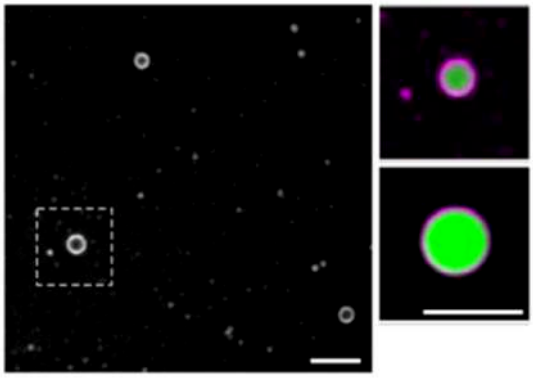

Fig. 6-8. Light microscopy images confirm that oil is in the core and Plin4 12-mer is directly surrounding it in the emulsion droplets. Images of unlabeled Plin4 12-mer (0.3 mg/ml) mixed with Plin4 12-mer-Alexa568 at a ratio 20:1 (magenta), and vortexed with oil stained with Bodipy (green). Left panel shows a confocal image of the fluorescent signal of Plin4. Right panels show zoom-ins of droplets. Scale bars: 5 µm. Figure adapted from (Čopič et al. 2018).

Many protein emulsifiers interact with neutral lipids essentially by denaturing themselves (Small et al. 2009; McClements and Gumus 2016). In contrast, apolipoproteins have been shown to interact with neutral lipids via AHs or β-sheets (Pan and Segrest 2016). Given the uniform fluorescent signal of Plin4 12-mer that we observed around oil droplets (Fig. 6-7 B, Fig. 6-8), we hypothesize that Plin4 AH also folds into a secondary structure in contact with oil, likely a helix, as it does with diphytanoyl liposomes (Fig. 6-6). Due to high light scattering of the emulsion, testing this directly by CD spectroscopy was challenging. Instead, I tested if Plin4 displayed any resistance to proteolysis upon triolein binding, which can be an indication of folding (Bigay et al. 2005). We observed that Plin4 12-mer forming the oil emulsion was more resistant to trypsin than Plin4 in solution, suggesting an increase in secondary structure

when Plin4 is in contact with neutral lipids. Moreover, I could always observe a band of Plin4 12-mer, even after 30 min with 10 times the concentration of trypsin (Fig. 6-9 A). In order to know how much of the protein is stably interacting with neutral lipids, I did a sucrose gradient with the emulsion. The protein associated with neutral lipids is on the top after centrifugation (Fig. 6-9 B). This quantification reveals that the majority of the protein (≥90%) is not bound to oil (Fig. 6-9 C). This result agrees with the trypsinization experiment, where the majority of the protein was cleaved by trypsin.

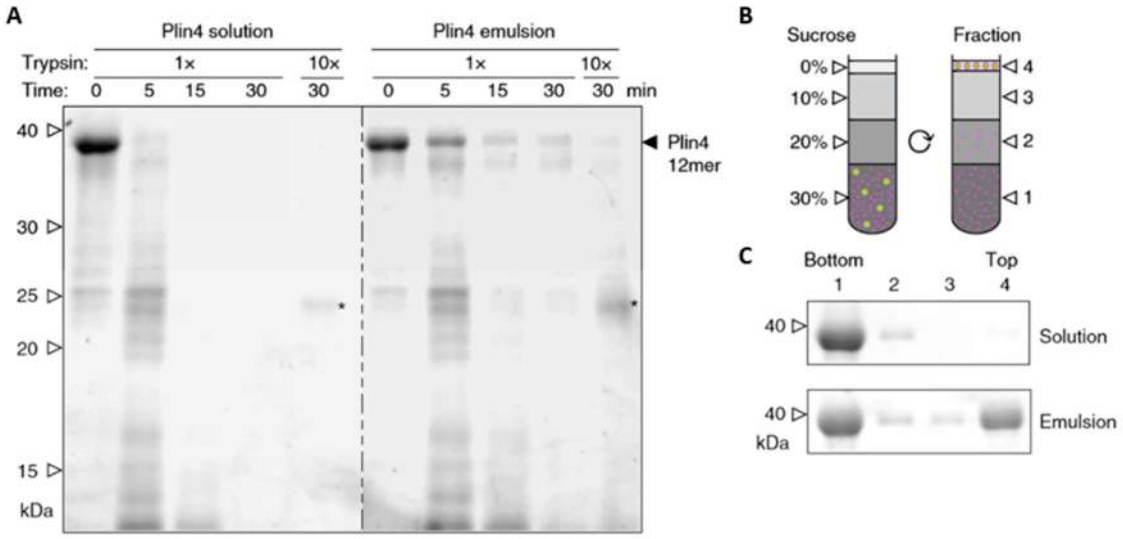

Fig. 6-9. Plin4 AH interacting with oil has secondary structure. A Plin4 in forming the oil emulsion is protected from degradation by trypsin. Plin4 12-mer (1 mg/ml) was incubated in buffer only or vortexed with triolein as in Fig. 6-7 A, then digested with 13 µg/ml (×1) or 130 µg/ml (×10) trypsin for the amount of time indicated. Samples were analyzed by SDS-PAGE with Sypro Orange staining. Five times less sample was loaded in the 0 min controls than in the other lanes. White arrowheads indicate the migration of molecular weight standards. Asterisks indicate the trypsin band. **B, C**. Plin4 12-mer (1 mg/ml) before (solution) or after (emulsion) the reaction depicted in Fig. 6-7 A was mixed with sucrose and loaded on the bottom of a sucrose gradient. After centrifugation, four fractions were collected from the bottom and equal volumes were analyzed by SDS-PAGE with Sypro Orange staining. Adapted from (Čopič et al. 2018).

One aa in a folded 3-11 helix will occupy 0.15 nm longitudinally of the backbone, based on the structure of alpha-synuclein (Jao et al. 2008). Assuming that Plin4 12-mer adopts a perfectly helical conformation in contact with oil and that its width would be 1 nm, one Plin4 12-mer molecule (396 aa) would cover the area of ~60 nm^2. If all the triolein vortexed (10×10^{-6} L) was

consumed into oil droplets of 200 nm in diameter (and volume of $3.3x10^7$ nm^3) this would give the result of a total of $3×10^{11}$ oil droplets. All of them together will have a total surface area of $1.5 × 10^{17}$ nm^2. Considering that 10% of Plin4 molecules ((0.5 mg/ml / 38000 Da) x 0.1 = 1 nmol) used in the experiment are coating the oil, this gives a total Plin4 helical area of $3.6 × 10^{16}$ nm2, in the same range as the estimated oil surface area. This calculation suggests that Plin4 12-mer is covering the whole surface of the oil droplets, as shown in the model (Fig. 6-10).

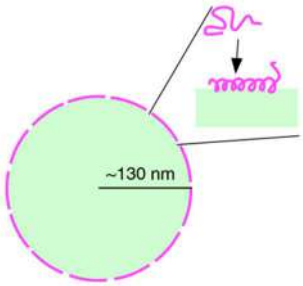

Fig. 6-10. **Model of a Plin4 12-mer-covered oil droplet**. Drawn to scale. Adapted from (Čopič et al. 2018).

These results *in vitro* show that Plin4 AH can interact and stabilize a hydrophobic core of neutral lipids *in vitro*. We hypothesized that this could also happen in cells. In order to test this possibility, Sandra Antoine-Bally cultured drosophila S2 cells with or without transfection of Plin4 12-mer. The cells were cultured with oleic acid and the expression of the enzyme CCT1, which produces PC, was knocked down. In S2 cells without Plin4 12-mer, LDs were oversized. However, the cells expressing Plin4 12-mer had normal size LDs (Čopič et al. 2018) (done by Sandra Antoine-Bally, Annex II). This result suggests that what I showed *in vitro* also happens in vivo. The function of Plin4 could be to interact with neutral lipids in vivo stabilizing LDs and avoiding their fusion when there is an excess of neutral lipids or depletion of PLs.

6.5 Conclusions

These results show that the 33-mer repeat region of Plin4 forms an AH that localizes to LDs in yeasts. Increased Plin4 AH length and hydrophobicity improve AH binding to LDs. Moreover, Plin4 AH fragments can be efficiently purified and labelled to perform highly controlled *in vitro* assays. Plin4 AH is unstructured in solution and folds into a helix when it is in contact with a membrane permissive for AH binding. Purified fragments of Plin4 AH are able to directly coat

neutral lipids making small oil droplets in the absence of any other emulsifier, even PL. Plin4 AH would completely cover those oil particles with a secondary structure.

Chapter 7: Dynamics of perilipin 4 at the surface of lipid droplets suggests a coat function

In LDs, neutral lipids are covered by a monolayer of PLs and embedded proteins. Many proteins use an AH to target LDs. The interaction between AHs and LDs is still poorly characterized. Binding of AHs to LDs could also affect LD stability and function.

Plins are a family of abundant LD proteins that use AHs to target LDs. Some Plin members, in particular Plin1, have well described functions regulating LD metabolism. Plin4 has by far the longest AH among Plins and proteins in general. This AH is made of 33-mer repeats, making the AH to have a constant repetitive distribution of residues. The function of Plin4 is not well understood. Plins are often referred as LD coats because of their high abundance on LDs.

In the previous chapter we used the Plin4 AH as a model to study how AHs target LDs. We showed how AH features like length, hydrophobicity and charge affect LD targeting. Plin4 AH seems optimized for LD binding because of its length, particular aa composition and low hydrophobicity that reduces its interaction with other membranes. We also showed that Plin4 AH is able to interact with neutral lipids directly *in vitro*. In cells with PL depletion, expression of Plin4 AH reduced LD size, suggesting that it can replace the PL monolayer.

This chapter addresses how Plin4 AH, and the AHs of other Plins, interact with LDs. We focus on the dynamics and stability of these interactions. In this way, we can understand also their function on LDs. The manuscript presented in this chapter is titled “Dynamics of perilipin 4 at the surface of lipid droplets suggests a coat function” (Gimenez-Andres, M; Emeršič, T; Antoine-Bally, S; Antonny, B; Derganc, J and Čopič, A., submitted).

In order to characterize the interaction of Plin AHs with LDs, I developed assays to evaluate the protein dynamics on oil droplets and the stability of the oil droplets formed *in vitro* using purified and fluorescently-labeled proteins. These protocols include: evaluation of the protein exchange on the surface of oil droplets and observation of the fluorescent protein recovery on the surface of oil droplets after photobleaching. I used DLS to follow the size of protein-oil droplets over time. To gain information about the adsorption of the protein interacting with neutral lipids, we collaborated with Tadej Emeršič and Jure Derganc (Institute of Biophysics,

University of Ljubljana) to develop a microfluidics device that can follow protein dynamics in real time by fluorescence microscopy. The combination of these approaches showed that Plin4 AH makes extremely stable protein-oil emulsions. Moreover, Plin4 AHs are remarkably immobile when they are bound to the neutral lipid particles at a high concentration.

To test whether the stable interaction and slow dynamics of Plin4 AH with neutral lipids is shared with other members of Plin family, I compared it with other Plin AHs. I identified the Plin AH sequences detecting the 11mer repeats with HHrepID and plotting them into helical wheels with Heliquest. AHs of other Plins are longer than most other AHs (close to 100 aa), but 10 times shorter than Plin4 AH. Only Plin5 has a somewhat shorter predicted AH (about 55 aa), and I left it out of further analysis. I evaluated the LD targeting and dynamics of Plin1 AH, Plin2 AH and Plin3 AH using budding yeast as a model system. Yeast allowed me to test these AHs in a naïve LD model. I used different strains and growth conditions that displayed different permissibility for LD binding. The AHs of Plin2 and Plin3 had similar affinities for LDs as a Plin4 AH fragment of comparable length, whereas Plin1 AH showed a bit higher affinity for LDs. Plin1 AH increased LD targeting was consistent with this AH being slightly more hydrophobic, a property that we showed to improve LD binding (Chapter 6)(Čopič et al. 2018). However, when they were compared with a longer fragment of Plin4 AH, Plin4 AH targeted better LDs than the other Plin AHs. Plin1 AH and Plin3 AH were much more dynamic on LD surface of yeasts than Plin4 AH.

In order to test these results *in vitro*, I developed a protocol to purify the AH of Plin3. Plin3 AH was also able to solubilize neutral lipids. However, the particles formed by it were less stable and Plin3 AH was quickly replaced by Plin4 AH on the particle surface, even when a short Plin4 AH fragment was used. These results confirm that Plin4 AH binds more strongly and stably to neutral lipids than the other Plin AHs, even at comparable length of AH. This result suggests that differences between Plin4 AH and Plin AHs are not only due to Plin4 AH being longer.

We hypothesized that specific features of Plin4 AH sequence were responsible for the different stabilities on neutral lipids of Plin4 AH and other Plin AHs. For instance, Plin4 AH sequence shows a strong preference for certain polar residues, lysines over arginines and aspartic acids over glutamic acids, and an asymmetrical distribution of the positive charges concentrated on one side of the polar face of the AH. Results obtained by Sandra Antoine-

Bally with different Plin4 AH mutants in HeLa cells supported the hypothesis that selection of some polar residues and their specific position in the helix are important for LD targeting by Plin4 AH. My analysis of Plin4 AH mutants with redistributed positive charge between the two sides of the AH polar face in yeast and *in vitro* confirmed the hypothesis. Therefore, we propose that polar residues and their particular distribution in Plin4 AH enable strong binding to the LD surface.

The polar residues and their distribution in the Plin4 AH could lead to a special higher-order organization on the LD surface. Lateral interactions between Plin4 molecules could stabilize them on the LD surface. Polar and charged residues can mediate the lateral interactions. This would result in a very stable protein layer surrounding the neutral lipids. Lateral interactions have been shown to occur between the two chains of ApoA-I helices when they are interacting with neutral lipids to make high density lipoproteins (Bibow et al. 2017; Melchior et al. 2017). The main difference between Plin4 AH and other Plin AHs interacting with LDs would be that once these AHs are folded and on the LD surface, Plin4 AH can interact also with other Plin4 molecules contributing to their stabilization and forming a very immobile protein layer.

The Plin4 AH protein layer could act as a stable coat, protecting LDs from instability by preventing the exposure of the neutral lipid core to the aqueous cytosol. This function will prevent LD fusion and would explain why when Plin4 AH was expressed in drosophila S2 cells in a depleted PL condition or in yeast with oversized LDs, no large LDs could be observed.

Moreover, this work shows that Plin4 AH and other Plin AHs interact in a distinct manner with LDs. We propose that AHs of other Plins (Plin1 – 3) interact with LDs as monomers, whereas Plin4 AHs polymerize on the LD surface. This model would explain why Plin4 AH can form such stable oil particles.

Dynamics of perilipin 4 at the surface of lipid droplets suggests a coat function

Manuel Giménez-Andrés[1,2], Tadej Emeršič[3], Sandra Antoine-Bally[1], Bruno Antonny[4], Jure Derganc[3,5], Alenka Čopič[1,6]

1. Institut Jacques Monod, CNRS, UMR 7592, Université de Paris, France
2. Université Paris-Saclay, 91405, Orsay, France
3. Institute of Biophysics, Faculty of Medicine, University of Ljubljana
4. Université Côte d'Azur, CNRS, IPMC, 06560 Valbonne, France
5. Chair of Microprocess Engineering and Technology – COMPETE, University of Ljubljana
6. Corresponding author: alenka.copic@ijm.fr

Abstract

Numerous proteins target lipid droplets (LDs) through amphipathic helices (AHs). It is generally assumed that AHs insert bulky hydrophobic residues in packing defects at the LD surface. However, this model does not explain the targeting of perilipins, the most abundant and specific amphipathic proteins of LDs. The gigantic Plin4 contains a highly repetitive AH that lacks bulky hydrophobic residues, and its LD targeting depends strongly on its length. We show that Plin4 forms a remarkably immobile protein layer at the surface of cellular or artificial LDs, making them stable over days. This Plin4 AH feature is not shared with the AHs of other perilipins, which display much faster dynamics on lipid surfaces. Plin4 AH stability on LDs is exquisitely sensitive to the nature and distribution of its polar residues. These results suggest that Plin4 forms stable arrangements of adjacent AHs via polar interactions, thereby behaving as an LD coat.

Introduction

Lipid droplets (LDs) are cellular organelles specialized for storage of lipids and maintenance of cellular lipid homeostasis. They are composed of a neutral lipid core that is covered by a monolayer of PLs and other amphiphilic lipids, and by proteins (Thiam et al., 2013b; Olzmann and Carvalho, 2019). LDs vary in size over four orders of magnitude, depending on organism/cell type and fasting state of a cell; in mature adipocytes, the majority of the cell can be occupied by a single LD measuring >100 µm in diameter (Lundquist et al., 2020; Stenkula and Erlanson-Albertsson, 2018). Secreted lipoprotein particles are similar to LDs in terms of their over-all composition but are much smaller, ranging from 10 to 1000 nm in diameter (Ohsaki et al., 2014).

Different types of proteins have been found to associate with LDs (Brasaemle et al., 2004; Bersuker et al., 2018; Kory et al., 2015; Pataki et al., 2018; Mejhert et al., 2020). They can be either stably embedded in the LD monolayer, coming by diffusion from the endoplasmic reticulum (ER), from which LDs emerge, or they associate with LDs peripherally from the cytosol (Ohsaki et al., 2014; Bersuker and Olzmann, 2017). Many of them are enzymes involved in lipid synthesis or hydrolysis, for example triglyceride synthases, acyltransferases, lipases and their inhibitors or activators (Wilfling et al., 2013; Zechner et al., 2017). Proteins can also regulate LDs in a non-enzymatic manner. A prominent example is the perilipins: in mammals, this is a family of five proteins that share related structural features and are abundant on LDs (Sztalryd and Brasaemle, 2017). They vary in their tissue distribution: Plin2 and Plin3 are widely expressed, whereas Plin1 and Plin4 are most highly expressed in adipocytes, and Plin5 is enriched in oxidative tissues (Wolins et al., 2006; Brasaemle et al., 2004; Wolins et al., 2003). Plin4 and Plin5 are also enriched in muscle tissues. Less closely related abundant LD proteins have been identified in many other species (Gao et al., 2017; Granneman et al., 2017; Miura et al., 2002). Whereas perilipins contain no known enzymatic motifs, a number of them, in particular Plin1, have been shown to regulate the recruitment of lipases to the LD surface (Sztalryd and Brasaemle, 2017).

Many LD-localized proteins use amphipathic helices (AHs) to directly interact with the LD lipid surface (Bersuker and Olzmann, 2017; Giménez-Andrés et al., 2018). All mammalian perilipins contain a predicted AH region in their N-terminal part, which has been shown to be important

for their LD localization (McManaman et al., 2003; Nakamura and Fujimoto, 2003; Bulankina et al., 2009; Rowe et al., 2016; Copic et al., 2018). This region is composed of 11-aa repeats that would fold into a 3-11 helix, which is slightly more extended than the classical α-helix (Bussell and Eliezer, 2003; Jao et al., 2008). Other regions, including a C-terminal region that can fold into a 4-helix bundle (Hickenbottom et al., 2004), can also contribute to LD targeting to varying extents (Targett-Adams et al., 2003; Subramanian et al., 2004; Nakamura et al., 2004; Ajjaji et al., 2019). Interestingly, both the 11-aa repeat region and the 4-helix bundle bear structural similarities with apolipoproteins, which are required for formation of lipoprotein particles (Saito et al., 2003; Melchior et al., 2017).

The 11-aa repeat AH region is by far the longest in Plin4, containing close to 1000 aa in the human protein, with repeats that are highly homologous at the 33-aa level (Copic et al., 2018; Scherer et al., 1998). The aa composition of Plin4 AH reveals a striking bias towards small hydrophobic residues, in particular V, T and A, whereas large residues such as W and F are almost entirely absent (Figure 1A). Whereas the 11-aa repeat regions of other perilipins are about 10-times shorter than that of Plin4 and the repeats are far less conserved, they are similar in terms of their over-all aa composition. We have demonstrated that the Plin4 AH region is unfolded in solution, but adopts a highly helical structure in contact with a lipid surface. The low hydrophobicity of this AH promotes specific targeting to LDs, which are permissive for the binding of many amphipathic proteins (Copic et al., 2018; Prévost et al., 2018). This is likely due to the physical properties of the LD surface, where the spreading of the PL monolayer leads to exposure of the hydrophobic core with which the hydrophobic face of an AH can interact more strongly (Bacle et al., 2017; Chorlay et al., 2019). Due to its extreme length, Plin4 in particular can cover a large LD surface and could act as a substitute for PL (Čopič et al., 2018). A recent study has identified expansion of Plin4 33-aa repeats in a family with a rare autosomal dominant progressive myopathy, underscoring the importance of studying this protein (Ruggieri et al., 2020).

Due to their high abundance on LDs, perilipins are often referred to as LD coat proteins (Sztalryd and Brasaemle, 2017). Protein coats have been well characterized on transport vesicles, for example COPI, COPII and clathrin coat. In all these cases, the coat forms in a tightly controlled manner by sequential recruitment of coat subunits on the membrane surface (Schekman and Orci, 1996; Taylor et al., 2011). Importantly, coat subunits laterally interact to

form a highly polymerized structure covering the surface of a vesicle (Faini et al., 2013). Coat polymerization is in fact the main force that generates these membrane vesicles (Saleem et al., 2015). Perilipins have not been shown to be directly involved in LD budding from the ER; LD formation may be principally driven by lipids, with proteins playing a more regulatory role (Ben M'barek et al., 2017; Chorlay et al., 2019; Santinho et al., 2020). On the other hand, COPI coat components have also been observed to bind to and influence LDs and to regulate recruitment of other LD proteins (Guo et al., 2008; Thiam et al., 2013a; Wilfling et al., 2014; Soni et al., 2009).

Here, we ask whether perilipins possess qualities traditionally associated with protein coats. We focus on the 11-aa repeat AH regions of mammalian perilipins, which directly associate with the lipid surface of LDs. We analyze the stability of perilipin AHs on the lipid surface and their ability to form an immobile structure using various cellular and biochemical approaches, as well as a novel microfluidics set-up to follow the interaction of AHs with oil over time. We show that one perilipin, Plin4, is capable of making highly stable protein-lipid structures by forming an immobile coat on the surface of pure oil using its uniquely long AH. These protein-oil droplets remain stable over the course of many days. In contrast, we show that the interaction of the AHs from other perilipins with LDs or with oil is highly dynamic. Extensive mutagenesis shows that the AH of Plin4 can form an immobile coat due to its organized structure that could enable interhelical interactions on the lipid surface.

Results

Purified Plin4 AH forms very stable protein-oil emulsions

We have previously shown that the AH of Plin4 is optimized for LD binding both by its length and particular aa composition (Copic et al., 2018). The AH sequence of human Plin4 is composed of ~29 highly homologous 33-aa repeats (Figure 1A). The efficiency of LD targeting correlated with AH length: at least four 33-aa repeats of the wild-type Plin4 AH were needed to detect some LD localization in HeLa cells (Figure 1B). Furthermore, the strong bias towards small residues is decisive for LD targeting: mutations that increased hydrophobicity (T > V) made Plin4 promiscuous for other organelles besides LDs; mutations that decreased hydrophobicity (T > S) rendered Plin4 cytosolic (Figure 1B).

The amphipathic region of Plin4 is capable of emulsifying triolein upon vigorous mechanical mixing (vortex) in aqueous buffer in the absence of any other surfactant, such as phospholipids. A similar result was obtained with a shorter Plin4 AH construct containing 4 33-aa repeats (Plin4 4mer) or a longer construct comprising 12 33-aa repeats (Plin4 12mer) (Figure 1C) (Copic et al., 2018). Electron microscopy and dynamic light scattering (DLS) revealed that emulsions of triolein and Plin4 12mer contained spherical oil particles with a large range of sizes; typically with a diameter of 50 to 500 nm (mean ≈ 200 nm), although some larger particles (diameter > 1 µm) could also be observed (Copic et al., 2018). We focused on these latter particles, whose size made them suitable for imaging by fluorescence light microscopy. For this, we performed triolein emulsification in the presence Plin4 12mer labeled with the fluorescent dye Alexa488 (Plin4 12mer-A488), mixed with unlabeled Plin4 12mer. The spherical particles displayed a homogenous fluorescent surface, which allowed us to perform dynamics measurements by fluorescence recovery after photobleaching (FRAP) (Figure 1D).

In the first FRAP protocol, we bleached an entire Plin4-oil particle. In this case, fluorescence recovery should occur by exchange between free Plin4 12mer-A488 in solution and bleached Plin4 12mer-A488 molecules bound to the lipoparticle surface. As shown in Figure 1D, we could detect no recovery within the time range of the measurement (3 min). In the second FRAP protocol, we bleached a limited area of the lipoparticles surface to follow fluorescence recovery of Plin4 12mer molecules by lateral diffusion. Again, the surface of the Plin4 12mer-coated particles showed no detectable recovery within 5 minutes after bleaching (Figure 1D). These experiments suggest that Plin4 12mer forms a very stable and immobile coat at the surface of triolein.

To gain further insight into the stability of the Plin4 12mer/triolein particles, we visualized the fluorescent emulsions over 7 days after the vortexing step. As shown in Figure 1E, the emulsions at t = 15 min, 75 min, 4 days and 7 days appeared very similar, showing numerous submicrometer particles and a few larger (> 1 µm) particles. Importantly, most if not all particles remained isolated during this long observation time, showing no obvious clustering or aggregation.

For comparison, we used a mutated form of Plin4 4mer (4T>S), in which several threonines in the hydrophobic face of the amphipathic region had been replaced by the more polar residue serine (Figure 1A). Plin4(4T>S) was purified from bacteria following the same procedure as for Plin4 4mer or Plin4 12mer. This mutant was inefficient at emulsifying olein (Figure 1C), in agreement with its inability to target LDs in HeLa cells (Figure 1B) (Copic et al., 2018). However, we could observe a few large triolein droplets formed by fluorescently-labeled Plin4(4T>S). The lipoparticles covered by Plin4(4T>S) clustered over time, suggesting that their coat was much less protective than what we observed with Plin4 12mer-oil droplets (Figure 1E).

Analysis by DLS revealed an even more remarkable stability of Plin4 12mer-oil particles over time, as we could not detect any change in particle size distribution even 28 days after emulsification by vortexing (Figure 1F). This puts Plin4 AH on par with natural emulsifiers used for technological purposes in food or pharmaceutical industry (McClements and Gumus, 2016). In contrast, the particles formed by Plin4(4T>S) were too heterogenous for analysis by DLS even at the first time-point (3h) after emulsion formation.

Following Plin4-oil interaction in real time using microfluidics

Large energies are required to disperse oil in order to form oil-protein emulsions *in vitro*; in our case, we provided this energy through vigorous vortexing. In order to further study the interaction of Plin4 AH with neutral lipids, we required a method where we could present the AH to the oil surface in a gentle manner and follow in real time the assembly of protein on the oil surface. We therefore developed a microfluidics system, in which we used a glass chip with two channels joined by a T-junction. We introduced the water-based buffer into the main channel and pure triolein into the side channel and stabilized the buffer-triolein interface 50-100 µm below the T-junction by closing the valve in the side-channel (Figure 2A). In this configuration, the buffer-triolein interface is not disturbed by the flow in the main channel, whereas the solutes from the main channel are free to diffuse to the oil surface. In terms of diffusion and hydrodynamic characteristics, this system is similar to microfluidic cavities (Osterman et al., 2016; Vrhovec et al., 2011).

We introduced Alexa-488-labeled Plin4 12mer into the main channel, and we followed the change in fluorescent signal inside the side channel and on the triolein interface over time using a confocal microscope (Figure 2B and Supplementary movies). As the protein solution in

the main channel reached the T-junction we could observe its diffusion into the side channel. After several seconds, we detected an increase in fluorescence on the oil interface, which stabilized in about 3 min at a level about 3-fold higher than the fluorescence of the solution, indicating an enrichment of Plin4 AH on the oil surface (Figure 2C). We then replaced the protein solution in the main channel with buffer to promote protein dissociation. However, the fluorescence on the interface remained constant, indicating a stable interaction between Plin4 12mer and oil. No enrichment of fluorescence on the oil interface was observed when we introduced buffer containing Alexa488 conjugated to free cysteine instead of Plin4 12mer (lower row in Figure 2B, C). These experiments confirm that Plin4 AH forms a very stable protein layer at the interface between oil and water.

We further compared the interaction Plin4 12mer with oil to that of the less hydrophobic Plin4(4T>S) mutant using the microfluidics system. The mutant assembled on the oil surface with no measurable difference in the kinetics of assembly or in the factor of enrichment compared to Plin4 12mer. However, the difference between Plin4 12mer and Plin4(4T>S) became obvious when the two proteins were used as unlabeled proteins in a 50:1 molar excess over labeled Plin4 12mer. We observed strong fluorescent signal on the oil interface in the presence of the Plin4(4T>S) mutant, but not in the presence of Plin4 12mer, indicating that the wild-type protein out-competed with Plin4(4T>S) for oil coating (Figure 2—figure supplement 1).

Comparison between the AH of Plin4 and other perilipins

So far, we focused on the interaction between the AH of Plin4 and LDs as it represents a most striking example of an LD-binding AH. We wanted to specifically compare the characteristics and LD-binding properties of Plin4 AH with the AH regions of the other human perilipins (Plin1, Plin2, Plin3), which have been shown to contribute to LD targeting (McManaman et al., 2003; Nakamura and Fujimoto, 2003; Bulankina et al., 2009; Rowe et al., 2016). The number of 11-aa repeats that we could identify in each protein ranged from 5 for Plin5 to about 8 for Plin1/2/3, compared to the 87 repeats in Plin4. In addition, the repeats are more highly conserved in Plin4, and Plin4 AH is also striking for the absence of any deletions or insertions between the repeats (Copic et al., 2018) (Figure 3A). Comparison of the aa composition of the 11-mer regions showed that they were similar in character in Plin2/3/4, with low

hydrophobicity due to a lack of large hydrophobic residues (Figure 3B). Plin1 AH is somewhat more hydrophobic and contains some aromatic residues. A more divergent character of this AH is consistent with the evolutionary divergence of Plin1 from the other perilipins (Granneman et al., 2017). The AH of Plin5 is shorter than in other perilipins and we did not consider it in further analysis.

We first expressed Plin AHs as GFP fusions in budding yeast and assessed their ability to target LDs. Budding yeast was used previously for expression of mammalian perilipins; full-length Plin1, Plin2 and Plin3, as well as their N-terminal halves, which include a region termed 'PAT domain' in addition to 11-aa repeats, targeted LDs in this system (Jacquier et al., 2013; Rowe et al., 2016; Copic et al., 2018). We expressed the AHs of Plin1, Plin2, and Plin3, and fragments of different lengths from the AH region of Plin4, containing 4, 6, or 12 33-aa repeats (132, 198 and 396 aa, respectively). In the case of Plin3, we could not observe any expression of just the AH region (aa 113-205) fused to GFP, therefore we added some additional upstream sequence (aa87-205) (Bulankina et al., 2009). We expressed these constructs under three different growth conditions that promote LD accumulation (Gao et al., 2017) : (i) wild-type cells grown to stationary phase; (ii) stationary phase cells lacking the most abundant yeast LD protein, Pet10p/Plin1p (*pet10Δ*); (iii) *pet10Δ* cells grown in oleic-acid rich medium, which promoted the formation of large LDs (*pet10Δ* + OA). In wild-type cells, Plin1 AH, but not Plin2 AH, Plin3 AH or Plin4 4mer, could be observed on LDs (Figure 3C). In contrast to Plin4 4mer, Plin4 6mer and Plin4 12mer localized to LDs, in line with our finding that increasing the AH length improves LD targeting (Copic et al., 2018). In agreement with the work of Gao et al., deletion of Pet10p/Plin1p improved LD targeting of our mammalian constructs, presumably because more LD surface was available (Kory et al., 2015). Targeting to LDs was further increased by the addition of oleic acid to stationary phase cells, which induced large LDs (Figure 3C). In addition, we observed some protein at the PM, in particular in the case of longer Plin4 AHs, consistent with observations from human cells and tissues (Scherer et al., 1998; Ruggieri et al., 2020). Based on these results, we conclude that the 11-aa repeat regions of Plin1, Plin2, Plin3, and Plin4 are all sufficient for targeting LDs. Comparison of different growth conditions (Figure 3D) allowed us to establish a ranking of LD affinities for perilipin AHs: extrapolating to its full length, Plin4 AH has the highest affinity for LDs, followed by Plin1 AH, and finally by Plin2 AH and Plin3 AH. However, correcting for length differences reveals that per unit of AH

length, Plin1 AH has a higher affinity for LDs than those of Plin2, Plin3 or Plin4. This is consistent with the higher hydrophobicity of Plin1 AH compared to other perilipin AHs; higher hydrophobicity has been shown to promote LD binding (Copic et al., 2018; Prévost et al., 2018).

Strikingly, we noticed a difference in the size of the large LDs that formed in *pet10Δ* cells grown in oleic acid-rich medium, depending on the AH expressed (Figure 3C,E): LDs were significantly larger (2.5-fold difference in projected area, which would correspond to 1.5-fold difference in diameter and a 4-fold difference in volume) when covered with Plin1, Plin2 or Plin3 AH, compared to LDs covered with Plin4 12mer (Figure 3C,E). LDs with Plin4 6mer were also somewhat bigger than those covered with Plin4 12mer. LDs with Plin4 4mer were more variable in size and appearance, preventing the use of the same quantification protocol.

We conclude that AHs from all four perilipins (Plin1 to Plin4) can by themselves target LDs and that their affinity for LDs correlates with their length and hydrophobicity. However, the AH of Plin4 could reduce the size of LDs more strongly than the AHs of other perilipins.

Stability of binding of perilipin AHs to LDs in model cellular systems

We used FRAP to assess the stability of AH binding to LDs in cells using the yeast model system. Plin1 AH-GFP could readily exchange between LD surface and the cytosol in cells grown for 24h in oleic acid medium, as reflected by a recovery half-life on the order of a few seconds (Figure 4A). The exchange of Plin3 AH-GFP was about two times faster than Plin1 AH-GFP, consistent with a lower amount of binding to LDs at steady state that we observed for this construct and with results obtained in mammalian cells with N-terminal halves of Plin1 and Plin3 (Ajjaji et al., 2019). In striking contrast, Plin4 12mer-GFP displayed almost no recovery on LDs over a period of more than 5 min (Figure 4A). We obtained similar measurements in cells grown for a shorter time, to early stationary phase, in standard growth medium (Figure 4B). However, these LDs were much smaller and more mobile, leading to a large variability in the fluorescence measurement. We also performed FRAP of Plin4 AH-GFP constructs bound to the PM in cells in exponential phase, to ensure that the poor recovery times that we observed on LDs were not due to protein aggregation in aged cells. The results that we obtained for Plin4 12mer-GFP on the PM were qualitatively similar to the results that we

obtained on LDs, showing slow and incomplete recovery of fluorescent signal after photobleaching. The recovery was faster and more complete for shorter Plin4 AH constructs (8mer and 6mer), confirming that the length of the Plin4 AH contributes to its stable binding to lipid surfaces (PM or LD) in the yeast model system (Figure 4C). However, even for the shortest Plin4 AH construct for which we could consistently observe targeting to yeast membranes, the recovery after photobleaching was still an order of magnitude slower than for Plin1 AH or Plin3 AH, suggesting that length of Plin4 AH is not the only parameter determining its stable binding to LDs.

Next, we moved to LDs in Drosophila Schneider 2 (S2) cells, which have been used to decipher several general mechanisms of LD formation (Guo et al., 2008; Krahmer et al., 2011). We previously demonstrated that expression of Plin4 12mer in S2 cells rescued the increase in size of LDs following the depletion of phosphatidylcholine (PC) (Copic et al., 2018). In these cells, the FRAP recovery curves of Plin4 12mer-GFP on LDs were variable, with a half-time covering a full range between 1 s to >100 s (Figure 4 – figure supplement 1). However, this variability was highly cell-dependent: within the same cell, the FRAP curves as assessed from different LDs were similar, suggesting that a cell-to-cell dependent variable was at play. PC depletion upon CCTα knocked-down had a small effect, but this was not the main driver of cell-to-cell variability. The level of protein expression was also not very predictive of recovery rate. In contrast, we observed a strong correlation between the rate of FRAP recovery and the intensity of the Plin4 fluorescent signal on LDs. This observation suggests that Plin4 AH density at the LD surface influences its dynamics, a feature reminiscent of protein coat. At low membrane coverage level, coat subunits diffuse and exchange quickly; at high membrane coverage level, their polymerization by side-side interaction prevents lateral mobility and fast turnover (Saleem et al., 2015; Sorre et al., 2012).

Comparison of proteolipid droplets formed with Plin4 AH or Plin3 AH

To study in more detail the difference between Plin4 and other perilipin AHs binding to LDs, we used our *in vitro* assays to compare the behavior of purified Plin4 AH fragments with that of Plin3 AH. We chose Plin3 AH because it displayed a similar steady-state distribution in yeast as the slightly longer Plin4 4mer, however, it showed a rapid exchange between LDs and the cytosol and it did not decrease LD size in oleic acid media. Mixing purified Plin3 AH with oil

resulted in a highly turbid suspension, similar to the suspensions obtained with Plin4 4mer or Plin4 12mer (Figure 5A and Figure 5 – figure supplement 1). By DLS, Plin4 4mer-oil droplets behaved like Plin4 12mer oil droplets (see Figure 1G) (Copic et al., 2018), displaying a particle size profile with a single peak that did not change over the course of 14 days after droplet formation (Figure 5B, left panel). In contrast, the droplets produced by Plin3 AH were more heterogenous in size already 3h after droplet formation. Thereafter, we observed a spreading of the peaks until the samples became too complex for DLS analysis (14 days after formation in the experiment shown in Figure 5B, right panel). Note that such complexity is generally due to the presence of particles of variable sizes, suggesting that Plin3 AH-oil particles were undergoing fusion over time due to less stable coating by Plin3 AH.

Centrifugation of AH-oil suspensions on sucrose gradients revealed a smaller fraction of total Plin3 AH protein associated with the oil fraction (top of the gradients) than was the case for Plin4 4mer or Plin4 12mer, even though we used the same protein to oil mass ratio in all cases (Figure 5C, D). This could be either because less Plin3 AH was bound to the oil droplets or because Plin3 AH bound to oil less strongly and dissociated during centrifugation. To distinguish between these possibilities, we performed competition experiments in which we first formed protein-oil droplets by mixing oil with a high concentration of unlabeled purified AH constructs (Plin4 12mer, Plin4 4mer or Plin3 AH). Then, we gently added to these suspensions Alexa488-labeled Plin4 12mer at an excess mass ratio of 20:1 compared to unlabeled protein, and we monitored the fluorescence of the suspensions over time using confocal microscopy (Figure 5E). When we combined unlabeled and labeled Plin4 12mer, we observed no incorporation of fluorescent Plin4 12mer into the preformed Plin4 12mer-oil particles over a period of 24 h, unless we vortexed the suspension (Figure 5E,F; top panel). This result is consistent with the lack of Plin4 12mer dissociation from oil, as determined by FRAP or by the microfluidics assay (Figure 1D and Figure 2B). In contrast, we observed some incorporation of fluorescent Plin4 12mer into Plin4 4mer-oil particles after 3 or 24 hours of incubation, suggesting that Plin4 4mer was bound to oil somewhat less stably than the 3-times longer Plin4 12mer (Figure 5E, F; middle panel). Strikingly, when we pre-formed AH-oil particles using Plin3 AH, Plin4 12mer readily incorporated into these particles, reaching close to maximal particle fluorescence already 10 min after Plin4 12mer addition (Figure 5E, F; bottom panel). We also observed clustering of Plin3 AH-formed oil particles, especially after

24 hours of incubation. Together, these experiments suggest that like Plin4 AH, Plin3 AH can function as an emulsifier to form protein-oil particles. However, Plin3 binding to oil is much less stable and the Plin3-oil particles cluster or fuse over time. The stability of Plin4-oil particles is promoted by the length of the Plin4 AH. However, Plin4 4mer, which is less than 1.5-times longer than Plin3 AH (in contrast to Plin4 12mer, which is 4.5-times longer), also produced much more stable oil droplets. We conclude that the difference in the stability of Plin4-oil and Plin3-oil droplets is not only due to the length of Plin4 AH, but also to differences in the sequences of the two AHs.

The nature and distribution of aa in the polar face of Plin4 AH is critical for LD targeting

We asked how the aa sequence of the Plin4 AH enabled this helix to form an immobile coat on lipid surfaces. The Plin4 AH sequence displays a remarkable repetitiveness (Figure 3A). We noticed that some polar residues, (e.g. N and Q), were extremely conserved among all repeats of Plin4 AH (Figure 6A). In addition, the Plin4 AH sequence shows a remarkable preference for lysine over arginine (22-fold) and for aspartic over glutamic acid (18-fold), which is less pronounced (K/R) or absent (D/E) in other perilipin AHs (Figure 3B). These considerations prompted us to construct mutants of Plin4 4mer in which we introduced in every 33-mer repeat modest mutations (e.g. N>Q, D>E, or K>R) that should not modify the folding and overall physical chemistry of the helix, including its charge and hydrophobic moment.

We first focused on the two conserved amide residues: an asparagine present in 25 out of 29 repeats of human Plin4, and a glutamine seven residues apart, conserved in all repeats (Figure 6A). The $N[x]_6Q$ sequence was replaced by $N[x]_6N$ (NN), $Q[x]_6Q$ (QQ) or $Q[x]_6N$ (QN) in the context of the Pin4 4mer construct. Strikingly, these three mutations almost eliminated the targeting of Plin4 4mer to LDs in HeLa cells (Figure 6C). Next, we considered the charged residues. Replacing all 8 aspartates with glutamates within the Plin4 4mer (2D>E) led to a small decrease in AH targeting to LDs in HeLa cells, whereas replacing the 12 lysine residues with arginine (3K>R) almost abolished AH targeting to LDs (Figure 6B, C). These substitutions did not affect the overall charge of the AH, only slightly changed its hydrophobicity and would even increase its helical propensity in the case of K>R substitution (Pace and Scholtz, 1998). Their effect on Plin4 AH targeting therefore suggested that a precise interaction between charged and/or polar residues could be important for LD binding.

We also noted an unusual distribution of charged residues throughout the Plin4 AH sequence, with positive ones always lying on one side of the helix close to the apolar/polar interface (Figure 6D). To test whether charged residues in Plin4 AH could mediate interhelical interaction to stabilize the helices bound to the LD surface, we prepared a mutant of Plin4 12mer, in which we reorganized the distribution of charges in the polar face of all 33-mer repeats without changing their overall composition (Figure 6D). This more symmetric Plin4 12mer AH mutant, termed charge-swap (csw), was similar to a 4-mer mutant that we tested previously and which did not localize to LDs when expressed in HeLa cells (Copic et al., 2018). We observed some localization of the longer csw 12mer-GFP mutant to LDs in HeLa cells, which was significantly reduced compared to Plin4 12mer-GFP (Figure 6E). When we compared the localization of these two constructs in the yeast model, we observed a difference in their distribution between LDs and the PM, with csw 12mer showing a lower ratio of LD-to-PM signal compared to Plin4 12mer (Figure 6F). This preference for the PM is consistent with the distribution of positive charges in csw 12mer, which is more optimal for mediating electrostatic interactions with the negative surface of the PM, compared to Plin4 12mer. Remarkably, when we performed FRAP of Plin4 12mer-GFP and csw 12mer-GFP bound to the PM in exponentially-growing cells, we observed a faster recovery of the csw construct compared to WT (Figure 6G). The observation that even though the csw mutant partitioned more strongly to the PM, its binding to the PM was more dynamic than in the case of Plin4 12mer, was suggestive of two separate kinetic steps: initial binding of individual helices followed by their assembly into a more stable lattice. We could not perform a similar comparison of binding to LDs due to their mobility. However, we noted a small shift towards bigger LDs in LDs surrounded by csw 12mer, compared to Plin4 12mer (Figure 6 – figure supplement 1). Together, these results suggest that reorganization of charged residues in the Plin4 AH decreased the stability of helices bound to the LD surface.

We purified csw 12mer following the same purification procedure as for Plin4 AHs, and we tested the interaction of this mutant with oil. Like Plin4 AH, csw 12mer could produce oil droplets in our vortexing assay (Figure 7A). However, when we added Alexa488-labeled Plin4 12mer to preformed csw-12mer-oil droplets, we observed a significant incorporation of Alexa-488 fluorescent signal into the droplets (Figure 7B, C), in contrast to the lack of exchange observed between non-fluorescent and fluorescent Plin4 12mer (Figure 5E, F). We conclude

that the particular amino-acid distribution in the polar face of the Plin4 AH enables the formation of a highly stable structure on a neutral lipid surface (Figure 7D).

Discussion

Perilipins are among the most abundant proteins in the LD proteomes (Brasaemle et al., 2004; Sztalryd and Brasaemle, 2017). Whereas their importance for LD metabolism has been known for a long time, notably for the recruitment of lipases and their inhibitors, this does not explain their abundance on the LD surface. The role of Plin4, by far the largest of perilipins, has been particularly puzzling. Plin4 is a mammalian-specific protein and is highly expressed in adipocytes (Wolins et al., 2003). Its deletion in a mouse model has so far not revealed any strong phenotypes (Chen et al., 2013). However, the striking features of Plin4 AH in terms of its length, repetitiveness and particular aa composition, suggest a strong selection for a specific function of Plin4 in mammalian metabolism. The present work shows that the interaction of Plin4 AH with LDs *in vitro* and in cellular model systems is remarkably stable. The slow lateral diffusion and the very slow dissociation of Plin4 AH molecules at the LD surface as assessed by FRAP, by microfluidics, or by exchange assays, are reminiscent of the behavior of vesicular coat components that polymerize on a membrane surface via lateral interactions (Saleem et al., 2015; Sorre et al., 2012).

We previously showed that the extreme length and the low hydrophobicity of Plin4 AH contributed to the specificity of its LD targeting (Copic et al., 2018). Large residues such as F (n = 2) or W (n = 0) are rare or absent in the Plin4 AH sequence (aa 81-1037), whereas three small hydrophobic residues, V (n = 144), T(n = 204) and A (n = 103), are extremely abundant (Figure 3B). Mutations that slightly increased hydrophobicity (T > V) made Plin4 promiscuous for other organelles besides LDs, whereas mutations that slightly decreased hydrophobicity (T > S) made Plin4 cytosolic. We now show that the Plin4(4T>S) mutant is also unable to emulsify oil *in vitro* although it binds to an exposed oil surface in microfluidics experiments. Thus, the hydrophobicity of Plin4 AH appears just at the threshold of promoting LD binding. Our experiments in the yeast model (Figure 3C-E) show that this is also the case for other perilipin AHs, consistent with their overall similar chemistries. A slight exception is the AH of Plin1, which contains some aromatic residues and partitions to LDs better than other AHs (Rowe et al., 2016; Ajjaji et al., 2019). Overall, the hydrophobicity of perilipins appears at best modest

and generally extremely low. As such, these proteins challenge a recent model for AH-LD interaction in which the main driving force is the intercalation of bulky hydrophobic residues within lipid packing defects at the LD surface (Prévost et al., 2018). This model derives from binding experiments and cellular observations performed with AHs that are much smaller than those of perilipins and bind not only to LDs but also other organelles (e.g. ALPS motif, CCTα, ARF1). As such, this model does not account for the particular chemistry of Plin AHs, which are the most abundant and specific AHs of LDs.

Surprising as it may seem, the polar face of Plin4 AH makes a very large contribution to LD targeting. The consistency in the distribution of charged residues along the length of the Plin4 AH, combined with a strong preference for K over R and D over E suggested that polar and charged residues play an important role in Plin4 AH. All conserved mutations that we tested, including N>Q, Q>N, K>R and D>E, decreased Plin4 AH LD targeting, with the first three mutations causing an almost complete dissociation. Furthermore, merely changing the distribution of these residues in the polar face also led to a reduction in LD targeting and in stability of binding to triolein droplets *in vitro*. We thus propose that binding of Plin4 AH is controlled by the numerous electrostatic/hydrogen interactions that its polar side chains can engage in along its gigantic length. These features speak in favor of a 'coat' model: numerous Plin4 molecules held together by side-side interactions would form a network at the LD surface. A prediction of this model is that Plin4 should be immobilized at the LD surface and, thereby, should exhibit very limited dynamics. This was confirmed by our experiments, which revealed a drastic difference in the behavior Plin4 AH compared to other perilipin AHs in cells and *in vitro*.

The coat model of Plin4 is reminiscent of the interactions that apolipoproteins engage in to form secreted lipoprotein particles (Phillips, 2013). In particular, ApoA1, for which most structural information is available, forms a ring around the lipid core in low density lipoprotein particles, stabilizing itself via interactions between specific charged residues in two adjacent molecules (Bibow et al., 2017; Pourmousa et al., 2018; Melchior et al., 2017). 26 intermolecular salt-bridges connect two antiparallel rings of ApoA1, which is about 200 aa long. The abundance of positively (3) and negatively (2) charged residues in each 33-aa repeat of Plin4 is compatible with the formation of a similar large network of intra or intermolecular interactions in the Plin4 coat. Interestingly, this model does not impose a strict geometry on

the protein network organization. The large number of glycine residues in Plin4 AH (5 G per 33-aa repeat) could enable the formation of various turns, resulting in a spaghetti-like layer rather than a geometrically well-defined assembly.

The observation that perilipins decorate different LDs in the same cell type supports our model of a higher-order perilipin organization on the LD surface (Hsieh et al., 2012; Wolins et al., 2005). The network of electrostatic interactions between perilipin AHs should be strongly dependent on their exact sequences, making the formation of hybrid coats between different perilipins less likely than homogenous perilipin coats. However, what drives the sequential coating of LDs by different perilipins remains quite mysterious. In addition to their repetitive AH regions, other segments of Plin1, Plin2 and Plin3 have been implicated in binding to LDs, in particular the C-terminal 4-helix bundle (Subramanian et al., 2004; Mirheydari et al., 2016; Ajjaji et al., 2019), but this has not been the case for Plin4 (Copic et al., 2018). In contrast to the behavior of their AHs, the association of full-length Plin1 and Plin2 with LDs can be very stable (Targett-Adams et al., 2003; Soni et al., 2009; Pataki et al., 2018; Ajjaji et al., 2019), and the COPI machinery has been implicated in the recruitment of Plin2 to LDs by an unknown mechanism (Nakamura et al., 2004; Soni et al., 2009).

Whereas vesicular coats uniformly cover the surface of a vesicle, following their assembly that enabled vesicle budding, this is unlikely to be the case for perilipin coats. Non-uniform distribution of Plin1 on LD surface has been observed in cultured adipocytes (Blanchette-Mackie et al., 1995; Hansen et al., 2017); these can be explained by the coating model, where patches of polymerized perilipin coat might coexist with other LD regions decorated by other proteins. More generally, the molecular arrangements of Plin4 molecules or other perilipins on LDs is a considerable challenge for the future. In the case of apolipoproteins, a consensual model for their organization is just starting to emerge despite decades of intense investigations on these proteins.

Materials and Methods

Sequence analysis

The 11-aa repeats of perilipins were identified using HHrepID tool from the MPI Bioinformatics

Toolkit server (Biegert and Söding, 2008; Zimmermann et al., 2018). The amphipathic character of these sequences was analysed using HeliQuest (Gautier et al., 2008). Helical wheels were plotted as complete 3–11 helices; the presentation of helices was chosen such as to maximize their hydrophobic moment, as calculated by Heliquest, and inclusion of identified 11-aa repeats, excluding helix-breaking proline (Pace and Scholtz, 1998) from the middle of the helices. The amino acid conservation of the 33-aa repeats of Plin4 was represented using Weblogo (Crooks et al., 2004).

Plasmid DNA construction

All plasmids used in this study are listed in Supplementary table 1. DNAs encoding AHs of human Plin1, Plin2 and Plin3 were PCR-amplified from the corresponding cDNAs that had been cloned into pGREG576 plasmids (gift from R. Schneiter, U. of Fribourg) (Jacquier et al., 2013). DNA for Plin4 6mer and Plin4 8mer was amplified from plasmid pCLG26, and DNA for Plin4 4mer mutant 4T>S was amplified from plasmids pSB49 (Copic et al., 2018). Plin4 4mer mutants (2D>E, 3K>3, NN, QN and QQ), and Plin4 12mer mutant csw 12mer were constructed using synthetic double-stranded DNA fragments (Supplementary table 2). All 4mer mutants were exact 4× repeats of a 33-aa sequence, based on the parental sequence of human Plin4 fragment aa246-278. The protein sequence for csw 12mer was designed by manually adjusting 33-aa helical wheels of the parental Plin4 12mer sequence using HeliQuest to increase the symmetry of charged residue distribution in the polar side of the helix while minimizing changes in the hydrophobic moment. DNA sequences were optimized for synthesis using the algorithm on the Eurofins website (https://www.eurofinsgenomics.eu). Supplementary table 2 also lists all protein sequences used in this study. For expression of proteins in *E. coli*, PCR-amplified DNA fragments were inserted into pET21b (Novagen) without adding a tag using *NheI* and *XhoI* restriction sites, which were introduced by PCR. For expression of Plin3 AH, an additional sequence 'MASC' was introduced upstream of the AH. For expression of GFP fusion proteins in *S. cerevisiae*, PCR-amplified DNA fragments were inserted into pRS416-derived (URA3 and AmpR markers) CEN plasmid pRHT140 containing ADH1 promoter and GFP for C-terminal tagging (gift from S. Leon, IJM). For expression of mCherry fusion proteins, GFP-encoding fragment in this vector was replaced with mCherry using *KpnI* and *BamHI* restriction sites to generate plasmid pMGA4. All AH DNA fragments were cloned into these plasmids using *NheI* and *BamHI* restriction sites that were introduced

by PCR. The sequence of the multiple cloning site introduces a linker peptide in the resulting fusion protein between the AH and GFP, 'PLDPPGLQEF', and linker peptide 'VKDPDIKLID' between the AH and mCherry. Plasmids for expression of mCherry fusion proteins in HeLa cells were constructed by subcloning synthetic genes for Plin4 mutants into pmCherry-N1 (Invitrogen) using *BamHI* and *XhoI* restriction sites. All plasmids were verified by sequencing.

Protein purification

All proteins were purified from *E. coli* without a tag. Plin4 12mer and Plin4 4mer were purified as previously described (Copic et al., 2018). Plin3 AH (aa103 to 205), Plin4 4T>S and csw 12mer were purified following a similar protocol, with some modifications in the case of Plin 3 AH, as outlined below. *E. coli* cells BL21DE3 transformed with expression plasmids were grown to O.D. ≈ 0.6 at 37°C from a liquid preculture and induced with 1 mM IPTG for 1 h at 37 °C. Cells from 0.25 l cultures were collected by centrifugation and frozen. The bacterial pellets were thawed in lysis buffer (50 mM Tris-HCl pH 7.5, 150 mM NaCl, 1 mM DTT, supplemented with 0.1 mM PMSF, and Complete protease inhibitor cocktail (Roche)). Cells were broken by sonication. The lysate was centrifuged at 100,000 × g for 30 min at 4°C in a 70.1Ti Rotor (40,000 rpm; Beckman). The supernatant in centrifuge tubes was immersed in boiling water (95°C) for 30 min. The resulting cloudy suspension was centrifuged at 100,000 × g for 15 min at 4°C to remove precipitated material. The supernatant was dialyzed against 20 mM Tris-HCl pH 7.5, 10 mM NaCl, 1 mM DTT (2 x 30 min using 1 l of buffer) at 4 °C using Spectra/Por membranes with a cut-off of 6000 Da (Spectrum labs) and then centrifuged again at 100,000 × g for 30 min at 4 °C. Plin4 4T>S and csw 12mer were then further purified in a single step by cation exchange chromatography on a 20 ml Hiprep S HP column (GE Healthcare), as described for Plin4 AHs (Copic et al., 2018). In contrast to Plin4 AH, Plin3 AH has a net negative charge at neutral pH (pI = 4.65). Therefore, Plin3 AH was purified by anion exchange chromatography on a 20 ml Hiprep Q HP column (GE Healthcare). It was eluted with a salt gradient from 10 mM to 400mM NaCl (3 column volumes) in 20 mM Tris-HCl pH 7.5, 1 mM DTT at a flow rate of 2 ml/min using an Akta purifier system (GE Healthcare), eluting at approximately 100 mM NaCl. After analysis of the chromatography fractions by protein electrophoresis, the protein pools were divided in small aliquots and stored at –80°C.

Protein electrophoresis and determination of protein concentration

Standard Glycine SDS-PAGE was used for the analysis of Plin4 12mer and csw 12mer (Mw ~ 40 kDa) using homemade 13% acrylamide bis-acrylamide gels. Tricine SDS-PAGE (Schägger and Jagow, 1987) was used for proteins with lower molecular weight, i.e. Plin4 4mer, Plin4 4T>S, or Plin3 AH (9 – 15 kDa). For that we either used TruPAGE commercial gels (Sigma) and homemade Tris-MOPS buffer (60 mM Trizma, 30 mM 4-Morpholinepropanesulfonic acid (MOPS), 0.1% w/v SDS), or, for better resolution, homemade 16.5% acrylamide-polyacrylamide (29:1) gels run with tricine buffer (100 mM Tris-HCl pH 8 – 8.5, 0.1 M Tricine, 0.1% SDS) in the cathode and 200 mM Tris HCl pH 8.9 in the anode chamber. Gels were rinsed in 7.5% acetic acid, stained with Sypro Orange (Life Technologies) and visualized with a MP imaging system (Bio-Rad) using the Alexa 488 settings. Because all perilipin AH purified constructs lack aromatic residues, preventing protein quantification by UV spectroscopy or by Coomassie Blue, protein concentration was routinely determined by densitometry of Sypro-Orange stained gels against a calibration curve with protein standards (Sigma) using ImageJ. Quantification by gel electrophoresis was verified by Ellman´s reaction method as previously described (Copic et al., 2018).

Protein labelling with fluorescent probes

Purified AHs were covalently labeled via cysteines using Alexa C5 maleimide probes (either 488 or 568; Thermofisher). Plin4 12mer, Plin4 4mer and Plin4 4T>S and csw 12mer were labeled on endogenous cysteines present in their AHs; they all contain 4 cysteines in total. Plin3 AH is devoid of cysteines, therefore a single cysteine was introduced at its N-terminus. To remove DTT, 1 ml of protein solution at concentration 0.7 mg/ml (18 µM of Plin4 12mer and csw 12mer, 50 µM of Plin4 4mer and Plin4 4T>S) was exchanged into labelling buffer (20 mM Tris-HCl pH 7.5, 100 mM NaCl) using size exclusion NAP10 columns (GE Healthcare). Protein-containing fractions were identified by protein electrophoresis and pooled. Protein solutions were incubated for 5 minutes at 4 °C with Alexa C5 maleimide probes at an equimolar ratio to their total number of cysteines (1 ml reaction volume). The reactions were stopped by the addition of DTT to 10 mM final concentration and loaded on NAP10 columns to separate the labeled protein from the excess of fluorescent probe. Fractions were analyzed by protein electrophoresis. Fluorescence in the gel was directly visualized on ChemiDoc MP

imaging system (Bio-Rad) either with Alexa 488 or Sypro Ruby (for Alexa 568) settings. Fractions with labeled protein were pooled, aliquoted and stored at -80°C. The same protocol was used for labelling of free cysteine, but without NAP10 purification steps.

We used FRAP assays on protein-oil emulsions (see below) with different ratios of labeled to unlabeled proteins to verify that the fluorescent label did not change the behavior of the protein. This was not the case for labeled Plin3 AH, thus we only used this protein in unlabeled form in our biochemical assays.

Preparation of protein-oil emulsions

Proteins were diluted to 0.5 mg/ml in freshly degassed HKM buffer (50 mM Hepes-KOH pH 7.2, 120 mM K-acetate, 1 mM $MgCl_2$) supplemented after degassing with 1 mM DTT. 190 µl of each solution were pipetted into a 600 µl glass tube, and a 10 µl drop of triolein (>99% purify, T7140 Sigma) was added to the top. In some cases, emulsions were prepared to have a final volume of 100 µl and the drop of triolein was 5 µl. They were vortexed manually at a fixed angle of ~30° for three cycles of 30 s on 30 s off at 25 °C under argon atmosphere. Images of resulting emulsions were taken with a compact camera. For analysis by fluorescent microscopy, emulsions were prepared using a mixture of fluorescent and unlabeled protein at a mass ratio 1:20.

Dynamic Light Scattering (DLS)

Measurements of the mean hydrodynamic radius of the Plin4-oil droplets by dynamic light scattering were performed on a sample taken from the middle of the tube, avoiding any unreacted oil that remained at the top of the emulsion, at least 3 h after vortexing to prevent the interference of gas bubbles with the measurement. Subsequent samples at later time points were removed in the same manner without any additional mixing. Emulsion samples were diluted 100-fold in freshly degassed HKM buffer with 1mM DTT. Measurements were performed on a Zetasizer Nano ZS machine (Malvern) at 25°C, and data were processed using the CONTIN method.

Observation of protein-oil interaction using microfluidics

Microfluidic experiments were performed in a glass microfluidic chip with a T-junction

geometry purchased from Dolomite (part # 3000086 and 3000024). All channels had a rounded cross-section with a 100 µm height and a 110 µm width. Prior to the measurements, the channel walls were wetted with 100 µl of freshly degassed HKM buffer supplemented with 1 mM DTT. The flows were driven and precisely controlled using a piezoelectric pressure control system (OB1 MK3, Elveflow), with typically applied pressures below 300 mbar. After wetting, the main and side inlet channels were filled with buffer and triolein (Sigma), respectively. Injection of oil in the side inlet channel was gently stopped with a manual valve (MV201, LabSmith) before the oil reached the junction (when the meniscus was approximately 400 µm from the junction). In this way, the flow in the main inlet channel could be stopped without significantly affecting the meniscus of oil, and the inlet vial with buffer could be exchanged by a vial with fluorescent protein solution (0.1 mg/ml in HKM buffer, mixed at a ratio 10 : 1 for unlabeled vs Alexa488-labeled protein). The sample volume in the vial was approximately 400 µl. The flow in the main inlet channel was then resumed and the diffusion of the protein from the main inlet channel into the side channel and its adsorption onto oil meniscus was monitored by time-lapse confocal microscopy for up to 30 min at a rate of 1 frame every 3 seconds (ECLIPSE TE2000-E, Plan Fluor 40x objective, EZC1 software, Nikon). Finally, the flow in the main inlet channel was stopped again, the inlet vial exchanged by a vial with buffer, and the main inlet channel was rinsed while monitoring the diffusion of the protein from the side channel. For competition experiments between Plin4 12mer and 4T>S mutant, proteins were mixed at a mass ratio 50:1 for unlabeled to labeled protein, Plin4 12mer: Plin4 12mer-Alex488 or 4T>S: Plin4 12mer-Alex488, with a total protein concentration of 0.1 mg/ml. All experiments were conducted at room temperature. Between experiments, glass chips were regenerated by copious washing with 3% SDS at 50°C, followed by distilled water, 3% TFD4 at 50°C, distilled water and finally dried by air. Image analysis was performed with ImageJ/Fiji (Schindelin et al., 2012) and Matlab.

Separation of Plin4-oil emulsion on sucrose gradients

Emulsions were prepared as specified in a final volume of 300 µl including 15 µl of triolein and 0.5 mg/ml of protein. Next, 240 µl of 60% w/v solution of sucrose in HKM buffer with 1 mM DTT was mixed with 240 µl of emulsion, avoiding any oil. 450 µl of this suspension was loaded on the bottom of a centrifuge tube and overlaid with a step sucrose gradient consisting of 300 µl 20%, 300 µl 10% and 100 µl 0% sucrose in HKM buffer with 1mM DTT. The samples were

centrifuged at 50,000 rpm (214,000 × g) in a Beckman swing-out rotor (TLS 55) for 80 min at 8°C. Four fractions were carefully collected from the bottom with a Hamilton syringe, having the following volumes: 450 µl, 300 µl, 300 µl, and 100 µl, respectively. Equal volumes of all fractions were analyzed by protein electrophoresis.

Yeast growth and media

Yeast strains used were: BY4742 MATα *his3Δ1 leu2Δ0 lys2Δ0 ura3Δ0 (Euroscarf)*, BY4742 *ERG6-mRFP::KanMX6 (Jackson lab collection)*, BY4742 *pet10Δ::KANMX4 (Euroscarf)*, and BY4741 MATa *his3Δ1 leu2Δ0 met15Δ0 ura3Δ0 PET10-GFP::HisMX* (Huh et al., 2003). Yeast were transformed by standard lithium acetate/polyethylene glycol procedure. Yeast cells expressing different AH constructs were grown in synthetic complete medium lacking uracil (SC-Ura, 6.7 g/l yeast nitrogen base, amino acid supplement without uracil, 2% glucose). To induce LDs, yeast cells either grown in SC-Ura for 24h at 30°C (stationary phase) or for 24h in SC-Ura, followed by 24h incubation in oleic acid (OA) medium (0.67% yeast nitrogen base without amino acids, 0.1 % yeast extract, 0.1 % (v/v) oleate, 0.25 % (v/v) Tween 40, amino acid supplement lacking uracil). For imaging of LDs in early stationary phase, yeast cells were inoculated from a preculture and grown at 30°C in SC-Ura to a final OD_{600}=1-2.

Cell culture and transfection

HeLa cells were grown in Dulbecco's modified Eagle's medium (DMEM) supplemented with 4.5 g/l glucose (Life technologies), 10% fetal bovine serum (FBS, Life technology) and 1% Penicillin/Streptomycin antibiotics (Life technologies). For protein expression, subconfluent cells were transfected with Lipofectamine 2000 (Invitrogen) in Optimem medium (Life technologies) for 6 h, followed by 16 h in standard growth medium before the cells were fixed and prepared for imaging.

Drosophila S2 cells (ThermoFisher) were cultured in Schneider's Drosophila medium (Invitrogen) supplemented with 10% FBS and 1% Penicillin/Streptomycin at 25°C. For generating stably-transfected cells, cells were incubated with plasmid DNA and TransIT-Insect Reagent (Mirus), followed by selection with 2 µg/ml puromycin (Life technologies) for 2 weeks. Protein expression from the metal-inducible promoter was induced for 48 h with the addition of 100 µM Cu-sulfate to the medium. LDs were induced with 1 mM oleic acid (Sigma)

in complex with fatty-acid free BSA (Sigma) for 24 h. RNAi depletion against CCT1 was performed as described (Copic et al., 2018).

Fluorescent microscopy

For imaging of purified protein-oil emulsions, emulsions prepared with fluorescent protein were gently mixed in the glass tube before 1.5 µl of emulsion was withdrawn with a long 200 µl tip and placed on untreated glass slides (Thermo Scientific). A coverslip was carefully placed on top without applying any pressure.

Yeast cells were harvested by centrifugation, washed, placed on a glass slide and covered with a coverslip. For some experiments, LDs were stained with 1 µg/ml Bodipy 493/503 (Life Technologies) or with Autodot blue dye (Clinisciences) diluted 1000-fol for 30 min at room temp, after which the cells were washed twice and imaged. Drosophila S2 cells were imaged on glass slides in the same way as yeast cells.

Transfected HeLa cells were fixed with 3.2% paraformaldehyde (Sigma) in PBS for 30 min at room temp. After washing three times with PBS, cells were stained with Bodipy 493/503 at 1 µg/ml for 30 min at room temperature and washed three times with PBS. Cells were mounted on coverslips with Prolong (Life technologies).

Images of emulsions, yeast and S2 cells were acquired at room temperature with an Axio Observer Z1 (Zeiss) microscope, equipped with an oil immersion plan-Apochromat 100x/1.4 objective, an sCMOS PRIME 95 (Photometrics) camera, and a spinning-disk confocal system CSU-X1 (Yokogawa) driven by MetaMorph software (Molecular Devices). GFP-tagged or Alex488-labeled proteins and mCherry-tagged or Alex568-labeled proteins were visualized with a GFP Filter 535AF45 and an RFP Filter 590DF35, respectively. When imaging emulsions, images were acquired in 10 to 15 z-sections of 0.2 µm were taken. For imaging HeLa cells and quantification of LD-to-PM signal ratio in yeast, we used an LSM 780 confocal microscope (Zeiss) with a x63/1.4 oil objective and a PMT GaAsP camera, driven by ZEN software. Images were processed with ImageJ and prepared for figures with Canvas Draw (canvas X).

Fluorescence recovery after photobleaching (FRAP)

FRAP assays *in vitro* were performed on freshly-prepared fluorescent emulsions with Alex488-labeled proteins on glass slides using the CSU-X1 spinning disc microscope and 100x objective, bleaching laser with a wavelength of 473 nm and iLas software controlled by Metamorph. Several circular areas of 25 x 25 pixels were bleached in each field (828 x 960 pixels), either on oil particles or in surrounding solution. The following FRAP time-course was used: 6 images pre-bleach, then bleach followed by 10 s of 1 image/s, 60 s of 1 image/10 s, and finally 600 s of 1 image/30 s (or until the loss of focus). Fluorescence of the bleached area at each time point was normalized to the average fluorescence before bleaching. Data was processed using Excel.

For FRAP assays in yeast cells, a circular area of 15 x 15 pixels in a cell expressing a GFP-fusion protein was bleached, either on the LDs or on the plasma membrane. 5 images were taken before bleaching, followed by a post-bleach time-course: 15 s of 1 image/s, 60 s of 1 image/5 s, and ~200 s of 1 image/20 s. Background fluorescence outside the cell was subtracted from the bleached area and the signal was normalized to the whole cell signal for each time-point. Data was processed with Excel and plotted using SigmaPlot (Systat Software).

FRAP assays in Drosophila S2 cells expressing Plin4 12mer-GFP were performed as for yeast, except that 3 circular areas of 15 x 15 pixels containing isolated LDs were selected per cell. The following FRAP time-course was used: 5 images pre-bleach, then bleach, followed by 30 s of 1 image/s, 60 s of 1 image/5 s, and finally ~200 s of 1 image/20 s. Data was analyzed in Excel and plotted using SigmaPlot. To obtain the half-time of recovery, average curves from the 3 FRAP measurements from the same cell were fitted with an exponential-rise equation.

Protein exchange assay on protein-oil emulsions

Emulsions were prepared as described using unlabeled protein at 0.5 mg/ml and checked by microscopy using CSU-X1 spinning disc microscope (time 0). Then, fluorescent Plin4 12mer-Alexa488 was gently added to the suspension to a final concentration of 0.025 mg/ml (20 : 1, unlabeled protein : labeled Plin4 12mer). Samples from the emulsions were withdrawn at indicated time-points without mixing and imaged on glass slides. The re-vortex sample was prepared after 2h of incubation by withdrawing 20 µl of the emulsion and vortexing it in a

fresh 600 μl glass tube in the same manner as for initial emulsion preparation. Samples were imaged in 10 z-sections of 0.5 μm in randomly-selected fields of 76 μm x 101 μm. The z-section containing the highest number of small droplets was selected for analysis.

Image analysis

Images were analyzed using ImageJ/Fiji (Schindelin et al., 2012). To quantify the number of droplets in protein-oil emulsions, the number of particles in a randomly-selected area in a single z-section was counted using 'find maxima' in the fluorescent channel with noise tolerance set to 100. Larger clusters were counted manually. For quantification in the exchange assay, the noise tolerance was set to 150. To quantify the number of yeast cells with protein signal on LDs, cells were counted manually after applying the same brightness/contrast settings to all images. To quantify the ratio of LD to PM protein signal (mCherry fusions), Pet10p-GFP LD marker was used to select the regions of interest (ROIs) corresponding to LDs and the total mCherry fluorescence in the ROIs was recorded. For the quantification of PM fluorescence, images were converted to binary to select the whole yeast perimeter. Them, a band of 5 pixels was applied to include all of PM signal. After background subtraction, the total LD signal per cell was divided by the total PM signal.

LD size in yeast cells grown in oleic-acid medium was measured using the fluorescent protein. Isolated LDs were fitted manually with a perfect circle and the size of each circular area was recorder. Data were analyzed in Excel and plotted with KaleidaGraph (Synergy software).
To determine the fraction of LDs in HeLa cells that were positive for transfected fluorescent protein, a single z-section that contained the most LDs in a cell was first selected. All LDs in the selected cell section were identified in the green (Bodipy dye) channel using the 'Analyze particle' plug-in. LDs positive for fluorescent protein were then identified by determining a threshold value for the red fluorescent signal (mCherry-protein fusion), 1.4x above average cellular fluorescence, and counting all LDs with fluorescence above this threshold. This number was divided by the total LD number to calculate the fraction of LDs in one cell section positive for protein. Data was processed in Microsoft Excel and plotted using SigmaPlot.

Acknowledgments

We thank C. La Torre Garay, Marko, V. Countremoulins and N. Joly for technical help, and R. Schneiter and S. Léon for plasmids. We acknowledge the IJM ImagoSeine facility, member of IBiSA and the France-BioImaging infrastructure (ANR-10-INBS-04), and L. Bousset, V. Albanèse, J.M. D'Ambrosio, R. Gautier, J. Snoj, N. Mejhert, C. Jackson and Jackson-Verbavatz team for helpful discussions and comments on the manuscript. This work was supported by the CNRS, including a CNRS PICS grant, the Slovenian Research Agency (research core funding No. P1-0055), and PhD fellowships from the French "Ministère de l'Education National, de l'Enseignement Supérieur de la Recherche" and Fondation ARC pour la recherche sur le cancer (DOC20190509052) to M.G.-A.

Author Contributions

- Manuel Giménez-Andrés: Conceptualization, Data curation, Formal analysis, Investigation, Methodology, Writing—review and editing
- Tadej Emeršič: Conceptualization, Data curation, Formal analysis, Investigation, Methodology
- Sandra Antoine-Bally: Data curation, Formal analysis, Investigation, Methodology
- Bruno Antonny: Conceptualization, Formal analysis, Writing—review and editing
- Jure Derganc: Supervision, Conceptualization, Formal analysis, Methodology, Writing—review and editing
- Alenka Čopič: Supervision, Conceptualization, Data curation, Formal analysis, Investigation, Methodology, Writing—original draft, Funding acquisition

Competing Interests

The authors have no competing interests to declare.

References

Ajjaji, D., K. Ben M'barek, M.L. Mimmack, C. England, H. Herscovitz, L. Dong, R.G. Kay, S. Patel, V. Saudek, D.M. Small, D.B. Savage, and A.R. Thiam. 2019. Dual binding motifs underpin the hierarchical association of perilipins1-3 with lipid droplets. *Mol Biol Cell*. 30:703–716. doi:10.1091/mbc.E18-08-0534.

Bacle, A., R. Gautier, C.L. Jackson, P.F.J. Fuchs, and S. Vanni. 2017. Interdigitation between Triglycerides and Lipids Modulates Surface Properties of Lipid Droplets. *Biophys J*. 112:1417–1430. doi:10.1016/j.bpj.2017.02.032.

Ben M'barek, K., D. Ajjaji, A. Chorlay, S. Vanni, L. Forêt, and A.R. Thiam. 2017. ER Membrane Phospholipids and Surface Tension Control Cellular Lipid Droplet Formation. *Dev Cell*. 1–31. doi:10.1016/j.devcel.2017.05.012.

Bersuker, K., and J.A. Olzmann. 2017. Establishing the lipid droplet proteome_ Mechanisms of lipid droplet protein targeting and degradation. *BBA - Mol Cell Biol Lipids*. 1862:1166–1177. doi:10.1016/j.bbalip.2017.06.006.

Bersuker, K., C.W.H. Peterson, M. To, S.J. Sahl, V. Savikhin, E.A. Grossman, D.K. Nomura, and J.A. Olzmann. 2018. A Proximity Labeling Strategy Provides Insights into the Composition and Dynamics of Lipid Droplet Proteomes. *Dev Cell*. 44:97–112.e7. doi:10.1016/j.devcel.2017.11.020.

Bibow, S., Y. Polyhach, C. Eichmann, C.N. Chi, J. Kowal, S. Albiez, R.A. McLeod, H. Stahlberg, G. Jeschke, P. Güntert, and R. Riek. 2017. Solution structure of discoidal high-density lipoprotein particles with a shortened apolipoprotein A-I. *Nat Struct Mol Biol*. 24:187–193. doi:10.1038/nsmb.3345.

Biegert, A., and J. Söding. 2008. De novo identification of highly diverged protein repeats by probabilistic consistency. *Bioinformatics*. 24:807–814. doi:10.1093/bioinformatics/btn039.

Blanchette-Mackie, E.J., N.K. Dwyer, T. Barber, R.A. Coxey, T. Takeda, C.M. Rondinone, J.L. Theodorakis, A.S. Greenberg, and C. Londos. 1995. Perilipin is located on the surface layer of intracellular lipid droplets in adipocytes. *J Lipid Res*. 36:1211–1226.

Brasaemle, D.L., G. Dolios, L. Shapiro, and R. Wang. 2004. Proteomic analysis of proteins associated with lipid droplets of basal and lipolytically stimulated 3T3-L1 adipocytes. *J Biol Chem*. 279:46835–46842. doi:10.1074/jbc.M409340200.

Bulankina, A.V., A. Deggerich, D. Wenzel, K. Mutenda, J.G. Wittmann, M.G. Rudolph, K.N. Burger, and S. Honing. 2009. TIP47 functions in the biogenesis of lipid droplets. *J Cell Biol*. 185:641–655. doi:10.1074/jbc.M402264200.

Bussell, R., Jr, and D. Eliezer. 2003. A Structural and Functional Role for 11-mer Repeats in α-Synuclein and Other Exchangeable Lipid Binding Proteins. *J Mol Biol*. 329:763–778. doi:10.1016/S0022-2836(03)00520-5.

Chen, W., B. Chang, X. Wu, L. Li, M. Sleeman, and L. Chan. 2013. Inactivation of Plin4 downregulates Plin5 and reduces cardiac lipid accumulation in mice. *Am J Physiol Endocrinol Metab.* 304:E770–9. doi:10.1152/ajpendo.00523.2012.

Chorlay, A., L. Monticelli, J.V. Ferreira, K. Ben M'barek, D. Ajjaji, S. Wang, E. Johnson, R. Beck, M. Omrane, M. Beller, P. Carvalho, and A.R. Thiam. 2019. Membrane Asymmetry Imposes

Directionality on Lipid Droplet Emergence from the ER. *Dev Cell*. 1–26. doi:10.1016/j.devcel.2019.05.003.

Copic, A., S. Antoine-Bally, M. Giménez-Andrés, C. La Torre Garay, B. Antonny, M.M. Manni, S. Pagnotta, J. Guihot, and C.L. Jackson. 2018. A giant amphipathic helix from a perilipin that is adapted for coating lipid droplets. *Nat Commun*. 9:1332. doi:10.1038/s41467-018-03717-8.

Crooks, G.E., G. Hon, J.-M. Chandonia, and S.E. Brenner. 2004. WebLogo: a sequence logo generator. *Genome Res.* 14:1188–1190. doi:10.1101/gr.849004.

Faini, M., R. Beck, F.T. Wieland, and J.A.G. Briggs. 2013. Vesicle coats: structure, function, and general principles of assembly. *Trends Cell Biol*. 1–10. doi:10.1016/j.tcb.2013.01.005.

Gao, Q., D.D. Binns, L.N. Kinch, N.V. Grishin, N. Ortiz, X. Chen, and J.M. Goodman. 2017. Pet10p is a yeast perilipin that stabilizes lipid droplets and promotes their assembly. *J Cell Biol*. 181:jcb.201610013–23. doi:10.1083/jcb.201610013.

Gautier, R., D. Douguet, B. Antonny, and G. Drin. 2008. HELIQUEST: a web server to screen sequences with specific -helical properties. *Bioinformatics*. 24:2101–2102. doi:10.1093/bioinformatics/btn392.

Giménez-Andrés, M., A. Copic, and B. Antonny. 2018. The Many Faces of Amphipathic Helices. *Biomolecules*. 8:45. doi:10.3390/biom8030045.

Granneman, J.G., V.A. Kimler, H. Zhang, X. Ye, X. Luo, J.H. Postlethwait, and R. Thummel. 2017. Lipid droplet biology and evolution illuminated by the characterization of a novel perilipin in teleost fish. *Elife*. 6:799. doi:10.7554/eLife.21771.

Guo, Y., T.C. Walther, M. Rao, N. Stuurman, G. Goshima, K. Terayama, J.S. Wong, R.D. Vale, P. Walter, and R.V. Farese. 2008. Functional genomic screen reveals genes involved in lipid-droplet formation and utilization. *Nature*. 453:657–661. doi:10.1038/nature06928.

Hansen, J.S., S.M. x000E9, H.A. Jones, O.G.X. ransson, and K. Lindkvist-Petersson. 2017. Visualization of lipid directed dynamics of perilipin 1 in human primary adipocytes. *Sci Rep*. 1–14. doi:10.1038/s41598-017-15059-4.

Hickenbottom, S.J., A.R. Kimmel, C. Londos, and J.H. Hurley. 2004. Structure of a lipid droplet protein; the PAT family member TIP47. *Structure*. 12:1199–1207. doi:10.1016/j.str.2004.04.021.

Hsieh, K., Y.K. Lee, C. Londos, B.M. Raaka, K.T. Dalen, and A.R. Kimmel. 2012. Perilipin family members preferentially sequester to either triacylglycerol-specific or cholesteryl-ester-specific intracellular lipid storage droplets. *J Cell Sci*. 125:4067–4076. doi:10.1242/jcs.104943.

Huh, W.-K., J.V. Falvo, L.C. Gerke, A.S. Carroll, R.W. Howson, J.S. Weissman, and E.K. O'Shea. 2003. Global analysis of protein localization in budding yeast. *Nature*. 425:686–691. doi:10.1038/nature02026.

Jacquier, N., S. Mishra, V. Choudhary, and R. Schneiter. 2013. Expression of oleosin and perilipins in yeast promotes formation of lipid droplets from the endoplasmic reticulum. *J Cell Sci*. 126:5198–5209. doi:10.1242/jcs.131896.

Jao, C.C., B.G. Hegde, J. Chen, I.S. Haworth, and R. Langen. 2008. Structure of membrane-bound alpha-synuclein from site-directed spin labeling and computational refinement. *Proc Natl Acad Sci USA*. 105:19666–19671. doi:10.1073/pnas.0807826105.

Kory, N., A.R. Thiam, R.V. Farese Jr, and T.C. Walther. 2015. Protein Crowding Is a Determinant of Lipid Droplet Protein Composition. *Dev Cell*. 34:351–363. doi:10.1016/j.devcel.2015.06.007.

Krahmer, N., Y. Guo, F. Wilfling, M. Hilger, S. Lingrell, K. Heger, H.W. Newman, M. Schmidt-Supprian, D.E. Vance, M. Mann, R.V.F. Jr, and T.C. Walther. 2011. Phosphatidylcholine Synthesis for Lipid Droplet Expansion Is Mediated by Localized Activation of CTP:Phosphocholine Cytidylyltransferase. *Cell Metab*. 14:504–515. doi:10.1016/j.cmet.2011.07.013.

Lord, S.J., K.B. Velle, R.D. Mullins, and L.K. Fritz-Laylin. 2020. SuperPlots: Communicating reproducibility and variability in cell biology. *J Cell Biol*. 219:94–10. doi:10.1083/jcb.202001064.

Lundquist, P.K., K.-K. Shivaiah, and R. Espinoza-Corral. 2020. Lipid droplets throughout the evolutionary tree. *Prog Lipid Res*. 78:101029. doi:10.1016/j.plipres.2020.101029.

McClements, D.J., and C.E. Gumus. 2016. Natural emulsifiers — Biosurfactants, phospholipids, biopolymers, and colloidal particles: Molecular and physicochemical basis of functional performance. *Adv Colloid Interface Sci*. 234:3–26. doi:10.1016/j.cis.2016.03.002.

McManaman, J.L., W. Zabaronick, J. Schaack, and D.J. Orlicky. 2003. Lipid droplet targeting domains of adipophilin. *J Lipid Res*. 44:668–673. doi:10.1194/jlr.C200021-JLR200.

Mejhert, N., L. Kuruvilla, K.R. Gabriel, S.D. Elliott, M.-A. Guie, H. Wang, Z.W. Lai, E.A. Lane, R. Christiano, N.N. Danial, R.V. Farese Jr, and T.C. Walther. 2020. Partitioning of MLX-Family Transcription Factors to Lipid Droplets Regulates Metabolic Gene Expression. *Mol Cell*. 77:1251–1264.e9. doi:10.1016/j.molcel.2020.01.014.

Melchior, J.T., R.G. Walker, A.L. Cooke, J. Morris, M. Castleberry, T.B. Thompson, M.K. Jones, H.D. Song, K.-A. Rye, M.N. Oda, M.G. Sorci-Thomas, M.J. Thomas, J.W. Heinecke, X. Mei, D. Atkinson, J.P. Segrest, S. Lund-Katz, M.C. Phillips, and W.S. Davidson. 2017. A consensus model of human apolipoprotein A-I in its monomeric and lipid-free state. *Nat Struct Mol Biol*. 24:1093–1099. doi:10.1038/nsmb.3501.

Mirheydari, M., S.S. Rathnayake, H. Frederick, T. Arhar, E.K. Mann, S. Cocklin, and E.E. Kooijman. 2016. Insertion of perilipin 3 into a glycero(phospho)lipid monolayer depends on lipid headgroup and acyl chain species. *J Lipid Res*. 57:1465–1476. doi:10.1194/jlr.M068205.

Miura, S., J.-W. Gan, J. Brzostowski, M.J. Parisi, C.J. Schultz, C. Londos, B. Oliver, and A.R. Kimmel. 2002. Functional Conservation for Lipid Storage Droplet Association among Perilipin, ADRP, and TIP47 (PAT)-related Proteins in Mammals, Drosophila, and Dictyostelium. *J Biol Chem*. 277:32253–32257. doi:10.1074/jbc.M204410200.

Nakamura, N., and T. Fujimoto. 2003. Adipose differentiation-related protein has two independent domains for targeting to lipid droplets. *Biochem Biophys Res Commun*. 306:333–338. doi:10.1016/S0006-291X(03)00979-3.

Nakamura, N., T. Akashi, T. Taneda, H. Kogo, A. Kikuchi, and T. Fujimoto. 2004. ADRP is dissociated from lipid droplets by ARF1-dependent mechanism. *Biochem Biophys Res Commun*. 322:957–965. doi:10.1016/j.bbrc.2004.08.010.

Ohsaki, Y., M. Suzuki, and T. Fujimoto. 2014. Open Questions in Lipid Droplet Biology. *Chemistry & Biology*. 21:86–96. doi:10.1016/j.chembiol.2013.08.009.

Olzmann, J.A., and P. Carvalho. 2019. Dynamics and functions of lipid droplets. *Nat Rev Mol Cell Biol*. 1–19. doi:10.1038/s41580-018-0085-z.

Osterman, N., J. Derganc, and D. Svenšek. 2016. Formation of vortices in long microcavities at low Reynolds number. *Microfluidics and Nanofluidics*. 20:33.

Pace, C.N., and J.M. Scholtz. 1998. A helix propensity scale based on experimental studies of peptides and proteins. *Biophys j*. 75:422–427.

Pataki, C.I., J. Rodrigues, L. Zhang, J. Qian, B. Efron, T. Hastie, J.E. Elias, M. Levitt, and R.R. Kopito. 2018. Proteomic analysis of monolayer-integrated proteins on lipid droplets identifies amphipathic interfacial α-helical membrane anchors. *Proc Natl Acad Sci USA*. 115:E8172–E8180. doi:10.1073/pnas.1807981115.

Phillips, M.C. 2013. New insights into the determination of HDL structure by apolipoproteins: Thematic Review Series: High Density Lipoprotein Structure, Function, and Metabolism. *J Lipid Res*. 54:2034–2048. doi:10.1194/jlr.R034025.

Pourmousa, M., H.D. Song, Y. He, J.W. Heinecke, J.P. Segrest, and R.W. Pastor. 2018. Tertiary structure of apolipoprotein A-I in nascent high-density lipoproteins. *Proc Natl Acad Sci USA*. 115:5163–5168. doi:10.1073/pnas.1721181115.

Prévost, C., M.E. Sharp, N. Kory, Q. Lin, G.A. Voth, R.V. Farese, and T.C. Walther. 2018. Mechanism and Determinants of Amphipathic Helix-Containing Protein Targeting to Lipid Droplets. *Dev Cell*. 44:73–86.e4. doi:10.1016/j.devcel.2017.12.011.

Rowe, E.R., M.L. Mimmack, A.D. Barbosa, A. Haider, I. Isaac, M.M. Ouberai, A.R. Thiam, S. Patel, V. Saudek, S. Siniossoglou, and D.B. Savage. 2016. Conserved Amphipathic Helices Mediate Lipid Droplet Targeting of Perilipins 1–3. *J Biol Chem*. 291:6664–6678. doi:10.1074/jbc.M115.691048.

Ruggieri, A., S. Naumenko, M.A. Smith, E. Iannibelli, F. Blasevich, C. Bragato, S. Gibertini, K. Barton, M. Vorgerd, K. Marcus, P. Wang, L. Maggi, R. Mantegazza, J.J. Dowling, R.A. Kley, M. Mora, and B.A. Minassian. 2020. Multiomic elucidation of a coding 99-mer repeat-expansion skeletal muscle disease. *Acta Neuropathologica*. 1–5. doi:10.1007/s00401-020-02164-4.

Saito, H., P. Dhanasekaran, D. Nguyen, P. Holvoet, S. Lund-Katz, and M.C. Phillips. 2003. Domain Structure and Lipid Interaction in Human Apolipoproteins A-I and E, a General Model. *J Biol Chem*. 278:23227–23232. doi:10.1074/jbc.M303365200.

Saleem, M., S. Morlot, A. Hohendahl, J. Manzi, M. Lenz, and A. Roux. 2015. A balance between membrane elasticity and polymerization energy sets the shape of spherical clathrin coats. *Nat Commun*. 6:6249. doi:10.1038/ncomms7249.

Santinho, A., V.T. Salo, A. Chorlay, S. Li, X. Zhou, M. Omrane, E. Ikonen, and A.R. Thiam. 2020. Membrane Curvature Catalyzes Lipid Droplet Assembly. *Curr Biol*. 1–21. doi:10.1016/j.cub.2020.04.066.

Schägger, H., and G. von Jagow. 1987. Tricine-sodium dodecyl sulfate-polyacrylamide gel electrophoresis for the separation of proteins in the range from 1 to 100 kDa. *Anal Biochem*. 166:368–379.

Schekman, R., and L. Orci. 1996. Coat proteins and vesicle budding. *Science*. 271:1526–1533.

Scherer, P.E., P.E. Bickel, M. Kotler, and H.F. Lodish. 1998. Cloning of cell-specific secreted and surface proteins by subtractive antibody screening. *Nat Biotechnol.* 16:581–586. doi:10.1038/nbt0698-581.

Schindelin, J., I. Arganda-Carreras, E. Frise, V. Kaynig, M. Longair, T. Pietzsch, S. Preibisch, C. Rueden, S. Saalfeld, B. Schmid, J.-Y. Tinevez, D.J. White, V. Hartenstein, K. Eliceiri, P. Tomancak, and A. Cardona. 2012. Fiji: an open-source platform for biological-image analysis. *Nat Meth*. 9:676–682. doi:10.1038/nmeth.2019.

Soni, K.G., G.A. Mardones, R. Sougrat, E. Smirnova, C.L. Jackson, and J.S. Bonifacino. 2009. Coatomer-dependent protein delivery to lipid droplets. *J Cell Sci*. 122:1834–1841. doi:10.1242/jcs.045849.

Sorre, B., A. Callan-Jones, J. Manzi, B. Goud, J. Prost, P. Bassereau, and A. Roux. 2012. Nature of curvature coupling of amphiphysin with membranes depends on its bound density. *Proc Natl Acad Sci USA*. 109:173–178. doi:10.1073/pnas.1103594108.

Stenkula, K.G., and C. Erlanson-Albertsson. 2018. Adipose cell size: importance in health and disease. *Am J Physiol Regul Integr Comp Physiol*. 315:R284–R295. doi:10.1152/ajpregu.00257.2017.

Subramanian, V., A. Garcia, A. Sekowski, and D.L. Brasaemle. 2004. Hydrophobic sequences target and anchor perilipin A to lipid droplets. *J Lipid Res*. 45:1983–1991. doi:10.1194/jlr.M400291-JLR200.

Sztalryd, C., and D.L. Brasaemle. 2017. The perilipin family of lipid droplet proteins: Gatekeepers of intracellular lipolysis. *BBA - Mol Cell Biol Lipids*. 1862:1221–1232. doi:10.1016/j.bbalip.2017.07.009.

Targett-Adams, P., D. Chambers, S. Gledhill, R.G. Hope, J.F. Coy, A. Girod, and J. McLauchlan. 2003. Live Cell Analysis and Targeting of the Lipid Droplet-binding Adipocyte Differentiation-related Protein. *J Biol Chem*. 278:15998–16007. doi:10.1074/jbc.M211289200.

Taylor, M.J., D. Perrais, and C.J. Merrifield. 2011. A High Precision Survey of the Molecular Dynamics of Mammalian Clathrin-Mediated Endocytosis. *PLoS Biol*. 9:e1000604. doi:10.1371/journal.pbio.1000604.s013.

Thiam, A.R., B. Antonny, J. Wang, J. Delacotte, F. Wilfling, T.C. Walther, R. Beck, J.E. Rothman, and F. Pincet. 2013a. COPI buds 60-nm lipid droplets from reconstituted water-phospholipid-triacylglyceride interfaces, suggesting a tension clamp function. *Proc Natl Acad Sci USA*. 110:13244–13249. doi:10.1073/pnas.1307685110.

Thiam, A.R., R.V. Farese Jr, and T.C. Walther. 2013b. The biophysics and cell biology of lipid droplets. *Nat Rev Mol Cell Biol*. 14:775–786. doi:10.1038/nrm3699.

Vrhovec, S., M. Mally, B. Kavčič, and J. Derganc. 2011. A microfluidic diffusion chamber for reversible environmental changes around flaccid lipid vesicles. *Lab Chip*. 11:4200–4206. doi:10.1039/c1lc20531e.

Wilfling, F., A.R. Thiam, M.-J. Olarte, J. Wang, R. Beck, T.J. Gould, E.S. Allgeyer, F. Pincet, J. Bewersdorf, R.V. Farese, and T.C. Walther. 2014. Arf1/COPI machinery acts directly on lipid

droplets and enables their connection to the ER for protein targeting. *Elife*. 3:e01607. doi:10.7554/eLife.01607.

Wilfling, F., H. Wang, J.T. Haas, N. Krahmer, T.J. Gould, A. Uchida, J.-X. Cheng, M. Graham, R. Christiano, F. Fröhlich, X. Liu, K.K. Buhman, R.A. Coleman, J. Bewersdorf, R.V. Farese, and T.C. Walther. 2013. Triacylglycerol synthesis enzymes mediate lipid droplet growth by relocalizing from the ER to lipid droplets. *Dev Cell*. 24:384–399. doi:10.1016/j.devcel.2013.01.013.

Wolins, N.E., B.K. Quaynor, J.R. Skinner, A. Tzekov, M.A. Croce, M.C. Gropler, V. Varma, A. Yao-Borengasser, N. Rasouli, P.A. Kern, B.N. Finck, and P.E. Bickel. 2006. OXPAT/PAT-1 Is a PPAR-Induced Lipid Droplet Protein That Promotes Fatty Acid Utilization. *Diabetes*. 55:3418–3428. doi:10.2337/db06-0399.

Wolins, N.E., B.K. Quaynor, J.R. Skinner, M.J. Schoenfish, A. Tzekov, and P.E. Bickel. 2005. S3-12, Adipophilin, and TIP47 package lipid in adipocytes. *J Biol Chem*. 280:19146–19155. doi:10.1074/jbc.M500978200.

Wolins, N.E., J.R. Skinner, M.J. Schoenfish, A. Tzekov, K.G. Bensch, and P.E. Bickel. 2003. Adipocyte protein S3-12 coats nascent lipid droplets. *J Biol Chem*. 278:37713–37721. doi:10.1074/jbc.M304025200.

Zechner, R., F. Madeo, and D. Kratky. 2017. Cytosolic lipolysis and lipophagy: two sides of the same coin. *Nat Rev Mol Cell Biol*. 18:671–684. doi:10.1038/nrm.2017.76.

Figure 1

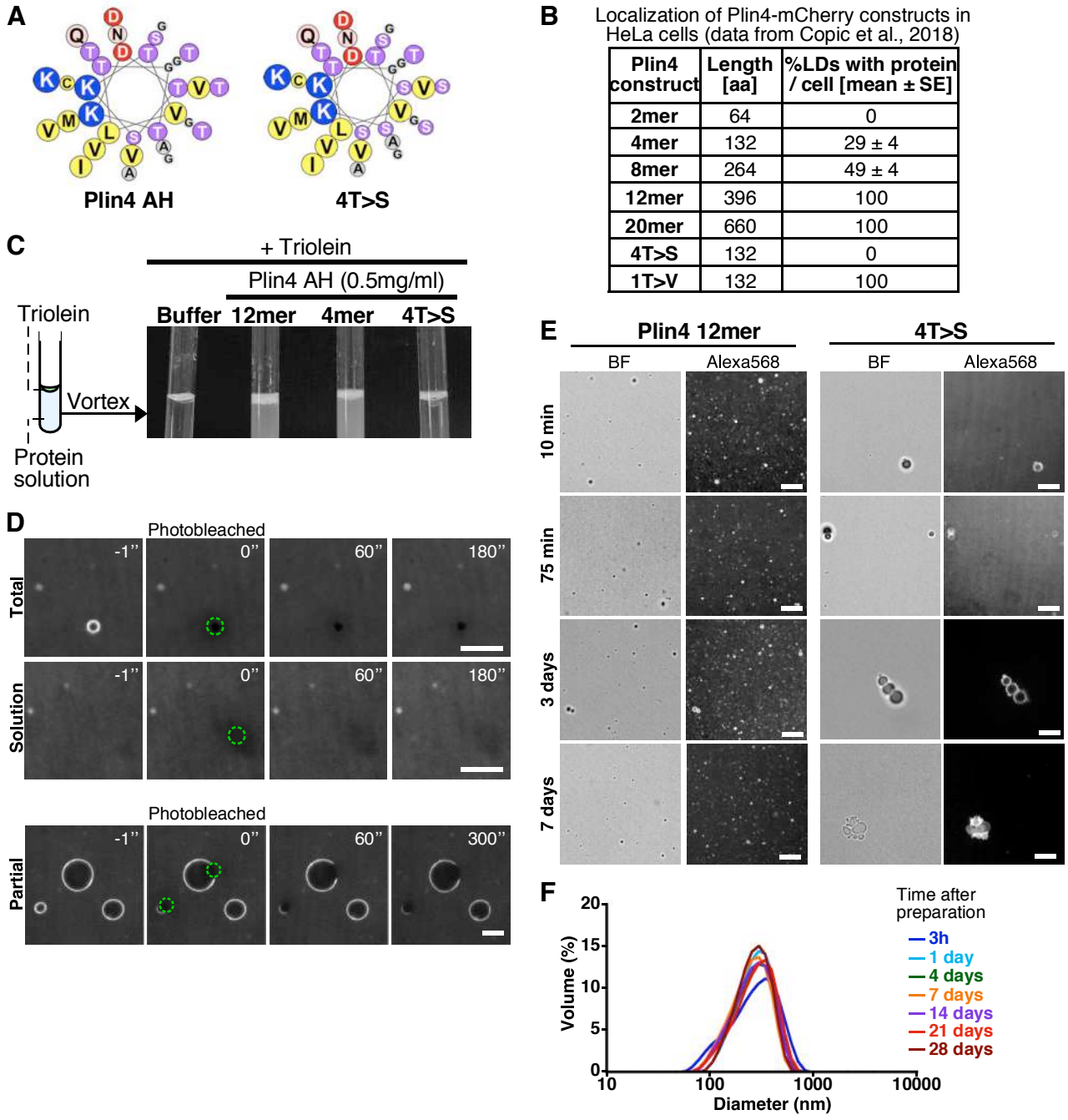

Plin4 construct	Length [aa]	%LDs with protein / cell [mean ± SE]
2mer	64	0
4mer	132	29 ± 4
8mer	264	49 ± 4
12mer	396	100
20mer	660	100
4T>S	132	0
1T>V	132	100

Figure 1: Plin4 AH forms very stable oil particles. A: Helical wheel representations of Plin4 and Plin4 4T>S AHs. **B**. Summary of LD localization of Plin4 AH and mutants (Copic et al., 2018). **C.** A 10 μl drop of triolein was added to 190 l of HK buffer containing the indicated proteins (Plin4 12mer, Plin4 4mer or 4T>S, all at 0.5 mg/ml). After vigorous vortexing, the samples were photographed. **D**. Dynamics of Plin4 12mer interaction with oil as assessed by FRAP (Fluorescence recovery after photobleaching) assays. An emulsion of triolein with unlabeled Plin4 12mer (0.5 mg/ml) and Alexa488-labeled Plin4 (0.025 mg/ml) 12mer was prepared as in C and visualized by fluorescence microscopy. FRAP was performed on large droplets, which were entirely bleached (top row), or in the bulk as a control (middle row). The lower row shows a FRAP experiment performed on a limited region of the surface of the droplet. **E.** Light microscopy images of Plin4 12mer and 4T>S emulsions at different time points after preparation by vortexing, showing the stability of the particles in the emulsions over several days. **F.** Size distribution as assessed by dynamic light scattering (DLS) of the particles present in a Plin4 12mer/triolein emulsion from 3 hours to 28 days after the vortexing reaction. Scale bars: 5 μm.

Figure 2

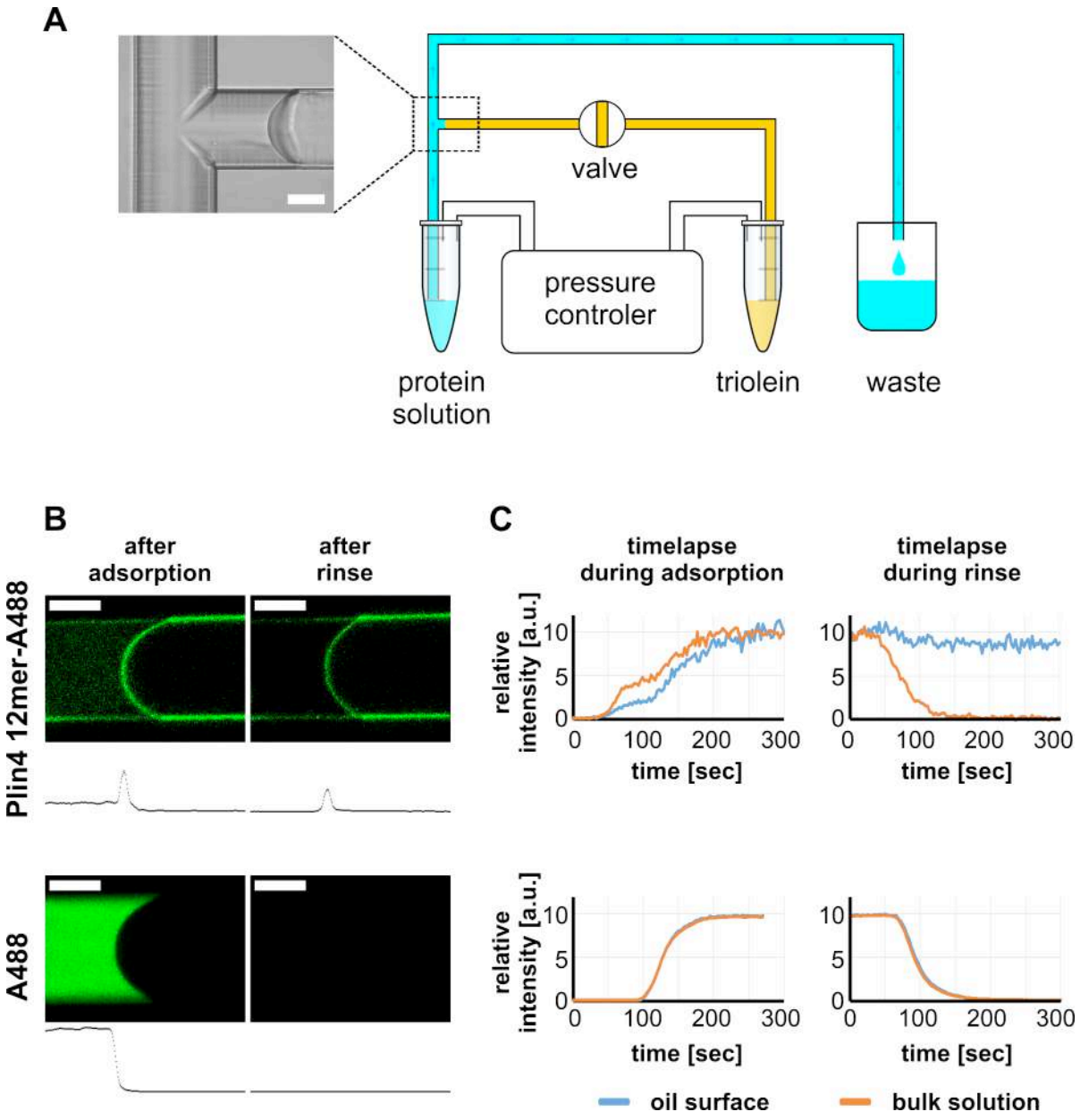

Figure 2. Real-time monitoring of protein–oil interaction in a microfluidic system shows irreversible adsorption of Plin4 12mer-A488 on triolein. A. Scheme of the microfluidics experimental set-up. **B.** Top row: confocal images of the triolein-buffer interface as formed in the microfluidic system after adsorption of Alexa488-labeled Plin4 12mer on the triolein surface and after rinsing with buffer. Bottom row: control experiment with the free fluorophore Alexa488. The intensity profile along the channel center is shown below each confocal image. The protein adsorbs irreversibly at the oil surface, whereas Alexa488 conjugated to free cysteine (A488) does not. See also supplementary movies 1-4. **C.** Time course of the signal of Alexa488-labeled Plin4 12mer or of free Alexa-488 in the side channel as quantified from the experiment shown in B.

Figure 3

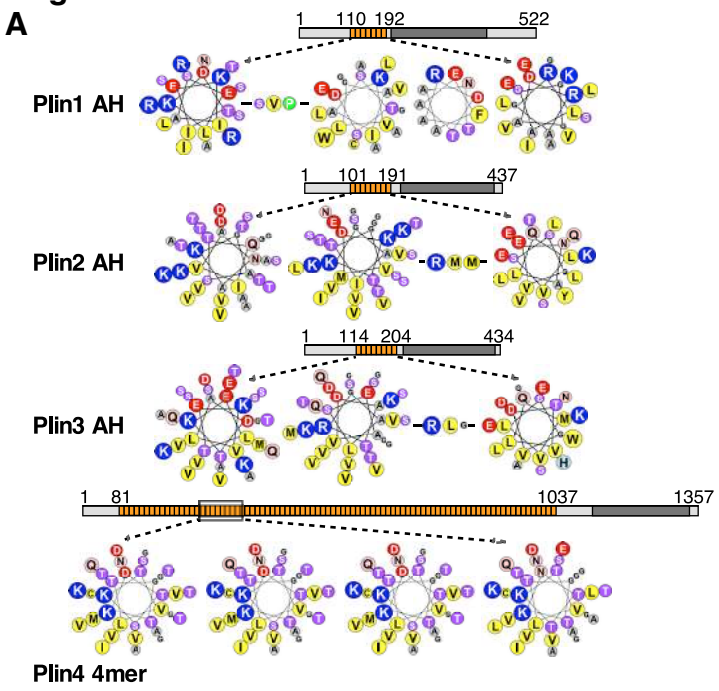

B

aa	Plin1	Plin2	Plin3	Plin4	Plin5	Av. vert
Trp + Phe	2.4	0	1.1	0.2	3.6	5.3
Leu + Ile	18.1	9.9	7.7	6.7	8.9	11.4
Val	6	15.4	16.5	15.0	23.3	6.8
Gly	8.4	9.9	9.9	15.6	3.6	7.4
Ala	18.1	9.9	8.8	10.8	7.1	7.4
Thr	6	14.3	8.8	21.3	5.4	6.2
Ser	10.8	12.1	13.2	5.4	14.3	8.1
Asn + Gln	2.4	6.6	6.6	6.5	0	10.2
Lys	4.8	8.8	7.7	8.8	5.4	7.2
Arg	7.2	1.1	2.2	0.4	8.9	4.2
Glu	7.2	4.4	6.6	0.3	8.9	3.7
Asp	4.8	3.3	6.6	5.3	7.1	5.9
AH length (aa)	83	91	91	957	56	

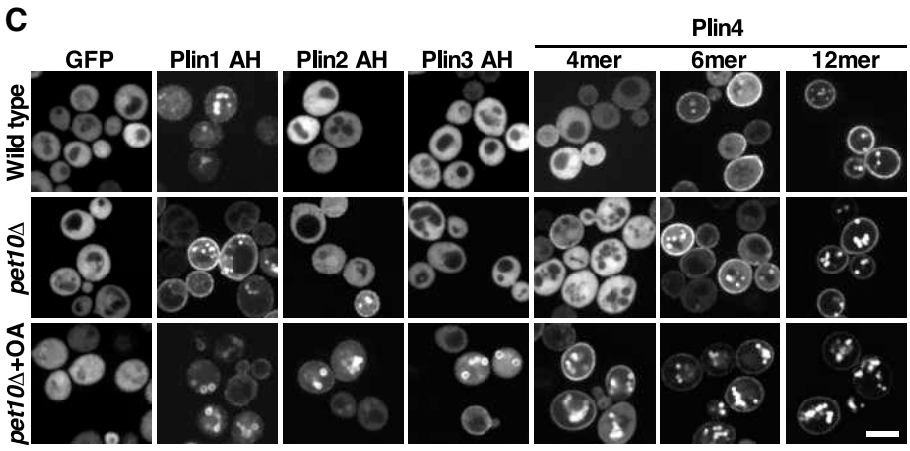

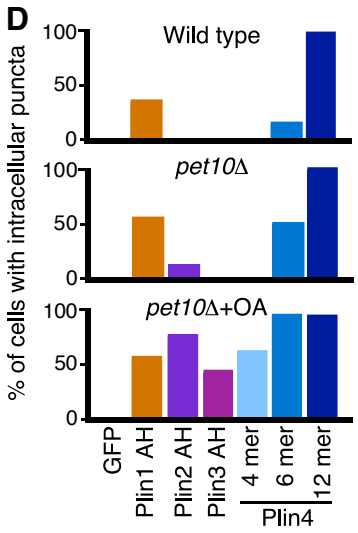

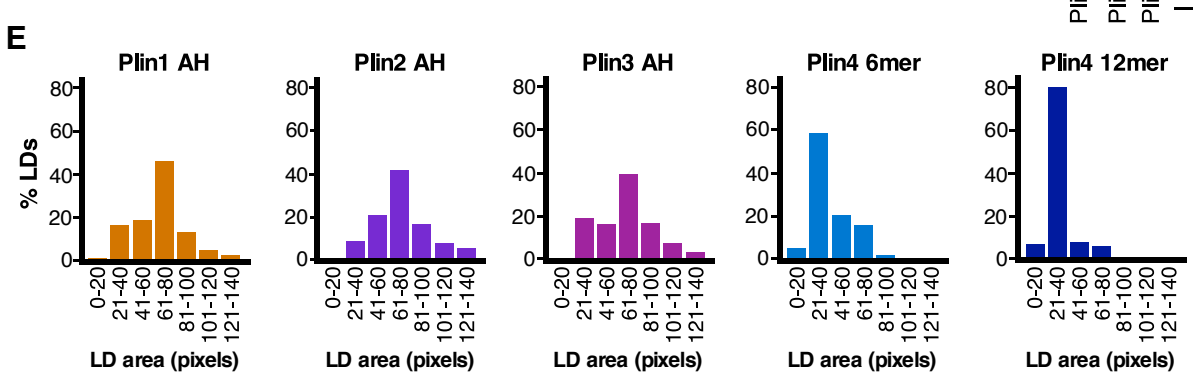

Figure 3. Comparison of the LD binding properties of the AH of Plin1, 2, 3 and 4 in yeast. A. Helical wheel representation of the AHs of Plin1 (aa 110-189 aa), Plin2 (aa 101-191 aa), Plin3 (aa 114-204) and Plin4 (aa 246-377, corresponding to the Plin4 4mer construct). In the case of Plin1, Plin2 and Plin3, the predicted AH regions are interspersed by short aa linkers, which are also indicated. Diagrams above the helical wheels show the full-length proteins, with AH regions shown in orange and the 4-helix bundle in dark grey. **B**. AA composition of the AH of Plin1, 2, 3 and 4 (in %) in comparison with the average aa composition of vertebrate proteins (av. vert). The blue and red backgrounds indicate lower or higher % as compared to vertebrate values, respectively. **C**. Localization of GFP fusions with the AH region of Plin1, Plin2, Plin3 or Plin4 in *S. cerevisiae* cells. The experiment was performed with wild-type yeast cells (upper row) or with *pet10Δ* cells (medium row) grown for 24h to stationary phase, or with *pet10Δ* cells grown to stationary phase and then transferred for 24h to oleic acid (OA) medium (lower row). **D**. Bar plots of the percentage of yeast cells showing intracellular puncta for the different proteins expressed. 60 cells per each condition were counted in one of at least two representative experiments. **E**. Quantification of the size distribution of fluorescent LDs (labeled with GFP-fusion proteins) in *pet10Δ* + OA cells. The plots show representative measurements from two independent experiments, where the following number of LDs was counted: Plin1 AH, 136; Plin2 AH, 143; Plin3 AH, 133; Plin4 6mer, 148; Plin4 12mer, 159. Pixel size: 0.091 μm x 0.091 μm.

Figure 4

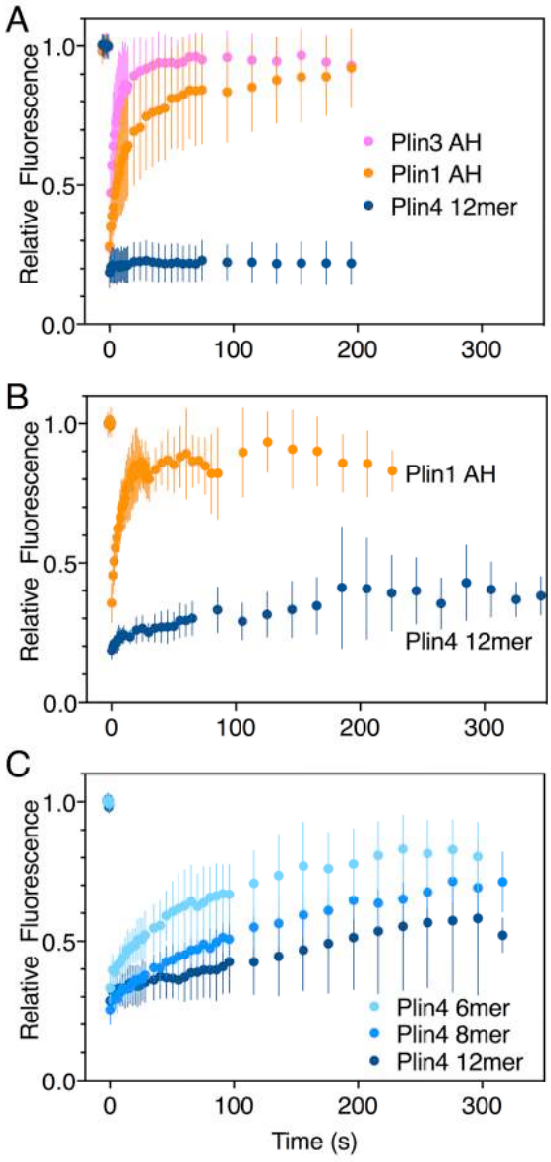

Figure 4. Dynamics of Plin 1, Plin 3, and Plin 4 AHs on LDs or at the plasma membrane in yeast as assessed by FRAP measurement. The AH region of Plin 1, Plin 3 or Plin4 was expressed as a GFP fusion in *S. cerevisiae* cells. FRAP was performed on LDs or the PM covered with the indicated Plin construct. The graphs show the mean ± SD of the fluorescence recovery curves from n FRAP measurements on different LDs or different regions of the PM. **A.** Plin1 AH-GFP (n=29), Plin3 AH-GFP (n=36) or Plin4 12mer-GFP (n=24) on LDs in *pet10*Δ + OA (growth for 48h, large LDs). **B.** Plin1 AH-GFP (n=11) or Plin4 12mer-GFP (n=5) on LDs in the yeast strain *pet10*Δ in early stationary cells (small LDs). **C.** Plin4 6mer-GFP (green; n=12), Plin4 8mer-GFP (red; n=7), Plin4 12mer-GFP (blue; n=7) at the PM in exponentially-growing wild-type cells.

Figure 5

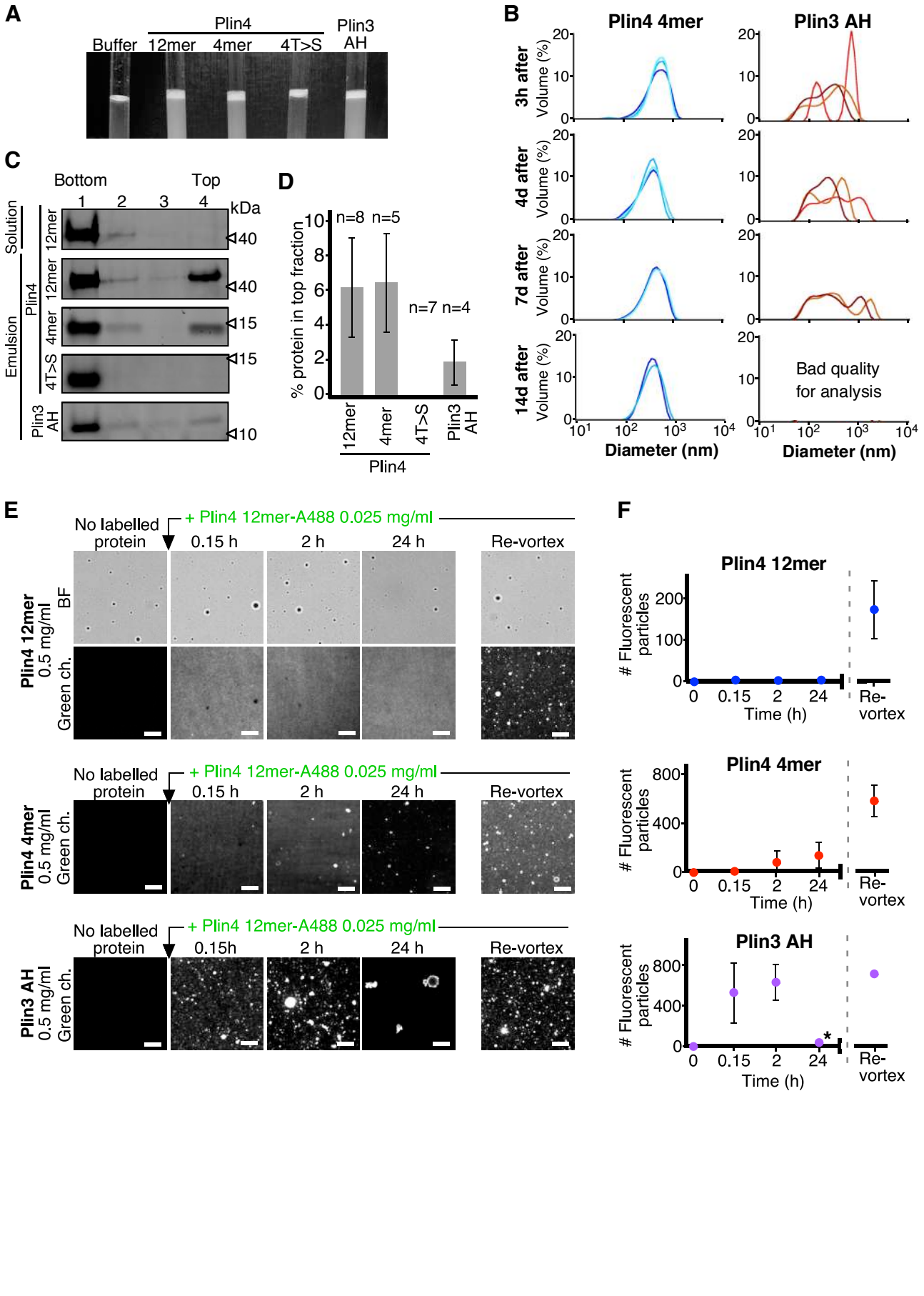
A
Plin4
Buffer
12mer
4mer
4T>S
Plin3 AH
B
Plin4 4mer
Plin3 AH
3h after
4d after
7d after
14d after
Volume (%)
Bad quality for analysis
Diameter (nm)
C
Bottom
Top
1
2
3
4
kDa
Solution
Emulsion
Plin4
12mer
4mer
4T>S
Plin3 AH
40
40
15
15
10
D
% protein in top fraction
n=8
n=5
n=7
n=4
12mer
4mer
4T>S
Plin3 AH
Plin4
E
No labelled protein
+ Plin4 12mer-A488 0.025 mg/ml
0.15 h
0.15h
2 h
24 h
Re-vortex
Plin4 12mer 0.5 mg/ml
Plin4 4mer 0.5 mg/ml
Plin3 AH 0.5 mg/ml
BF
Green ch.
F
Plin4 12mer
Plin4 4mer
Plin3 AH
Fluorescent particles
Time (h)
Re-vortex

Figure 5. Plin3 AH interacts much less strongly with oil than Plin4 AH. A. Turbidity assays with 0.5 mg/ml protein solutions of Plin4 12 mer, Plin4 4mer, Plin4 4mer mutant [4T>S], or Plin3 AH after vigorous vortexing with triolein (15 µl for 285 µl of protein solution). **B.** Size distribution of the droplets in triolein emulsions formed with Plin4 4mer or Plin3 AH at various times after vortexing was determined by DLS. Particle size is shown by volume weighted distributions. Each curve represents one measurement. **C.** Protein/oil emulsions or protein solutions of the indicated variants of Plin4 or Plin3 AH were mixed with sucrose and loaded on the bottom of a sucrose step gradient. After centrifugation, four fractions were collected from the bottom and equal volumes were analysed by protein gels with Sypro Orange staining. **D.** Quantification of the experiment shown in C showing the mean ± SD of protein at the top fraction of the sucrose gradient. The number of repeats for each experiment is indicated above the bar graphs. **E.** Protein exchange assay in LD emulsions. Top panel: a Plin4 12mer (0.5 mg/ml) / triolein emulsion was prepared by vortexing. Thereafter, 0.025 mg/ml Alexa-488-labeled Plin4-12 mer was gently added. The emulsion was imaged at the indicated time points by light microscopy in bright field (BF) to see all particles and by fluorescence to detect the coverage of the particles by Alexa-488-labeled Plin4 12 mer. Finally, the suspension was vortexed again to promote maximum incorporation of Alexa488-labeled Plin4 12mer in the emulsion. The middle and lower rows show similar experiments performed with Plin4 4mer and Plin3 AH emulsions, respectively. Scale bars: 5 µm. **F.** Quantification of the experiments shown in E. The number of fluorescent particles (mean ± SD) was determined from four separate fields (73 x 100 µm) in the same experiment. The graphs are representative of at least two independent experiments. Time on the x-axis is plotted using logarithmic scale. Asterisks indicates clustering of particles, which resulted a in low total number of fluorescent puncta, as seen in the image.

Figure 6

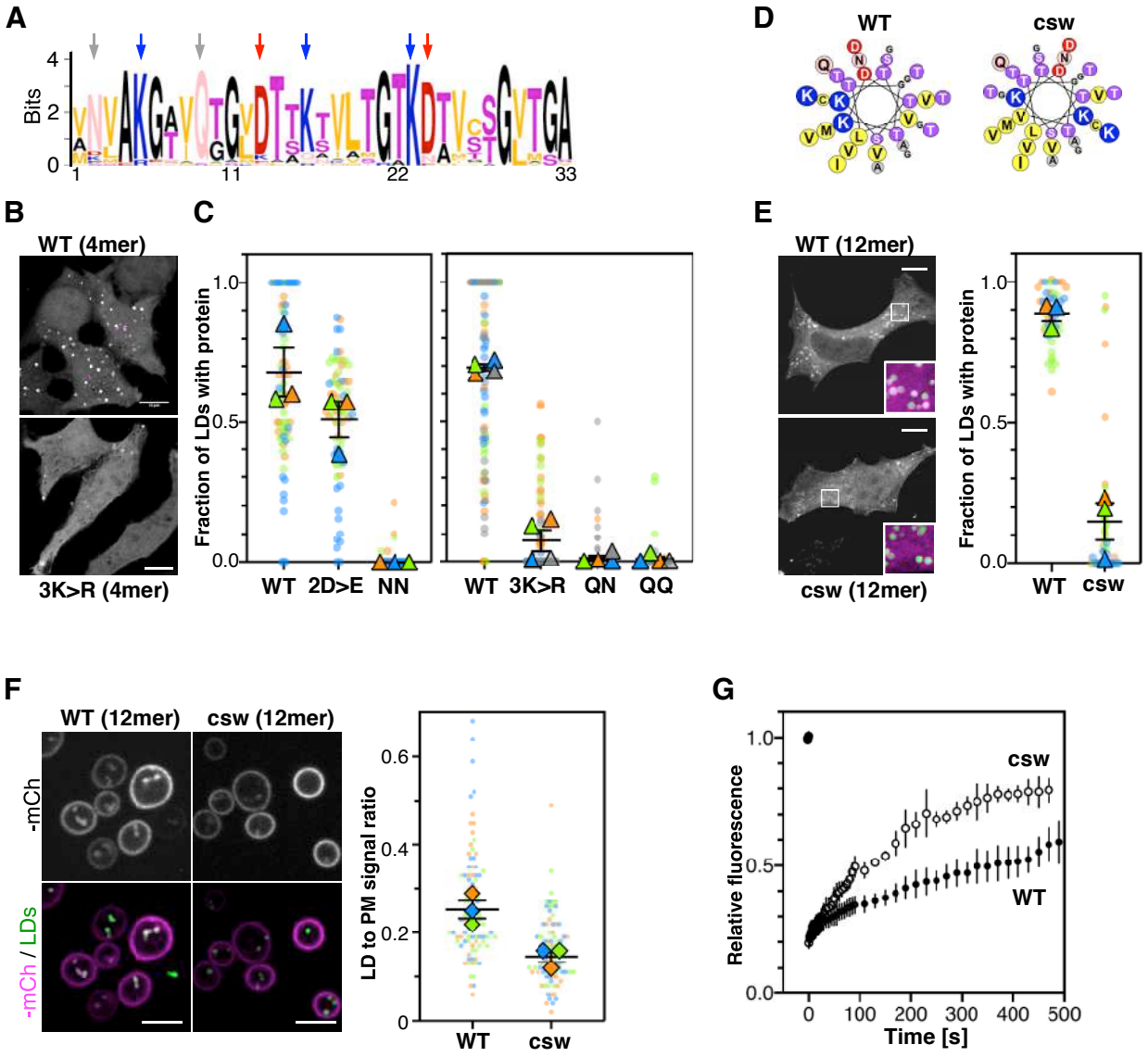

Figure 6.The nature and the distribution of charged residues in the polar face of Plin4 AH contribute is key for specific and stable coating of LDs in cells. A. Weblogo plot of the AH region of human Plin4 as determined by aligning its 29 33-mer repeats. The vertical arrows indicate the mutated aa: the NQ pair (grey), which was mutated into NN, QQ or QN; the three K (blue), which were mutated into R, and the two D (red), which were mutated into E. **B**. Co-localization of GFP-fusion of Plin4 4mer wild-type and 3K>R (in white) with LDs (purple) in HeLa cells. **C**. Quantification of the percentage of LDs stained with the indicated protein per cell. These “SuperPlots” (Lord et al., 2020) show all data fom 3 to 4 independent experiments, each with a different color; each light dot represents one cell, whereas each triangle shows the mean from one experiment. The black bars show the mean ± SE of the 3 or 4 independent experiments. **D**. Helical wheels of Plin4 WT and csw mutant. Mutations were introduced to redistribute positive and negative residues in a symmetrical manner while keeping the number and nature of these residues constant. **E.** Localization of Plin4 12mer wild-type or csw mutant in HeLa cells. The insets show extended views with the protein in purple and LDs in green (stained with Bodipy). The ‘super’ plots on the right were built as in C and show the mean ± SE of the percentage of LDs positive for the indicated protein per HeLa cell as determined from 3 independent experiments. **F**. Light microscopy images of mCherry fusions of Plin4 12mer wild-type or csw mutant in yeast. Top: mCherry fluorescence (mCh); bottom co-localization of mCherry (purple) with LDs stained with bodipy (green). The relative fluorescence signal of mCherry fusions of Plin4 12mer wild-type or csw mutant on LDs and at the PM in *PET10-GFP* yeast strain was used to build the SuperPlots shown on the right. Data are from three independent experiments, with n ≥ 25 for each condition in each assay. **G**. Fluorescence recovery curves of GFP fusions of Plin4 12mer wild-type or and csw mutant at the PM of late exponential phase yeast cells.

Figure 7

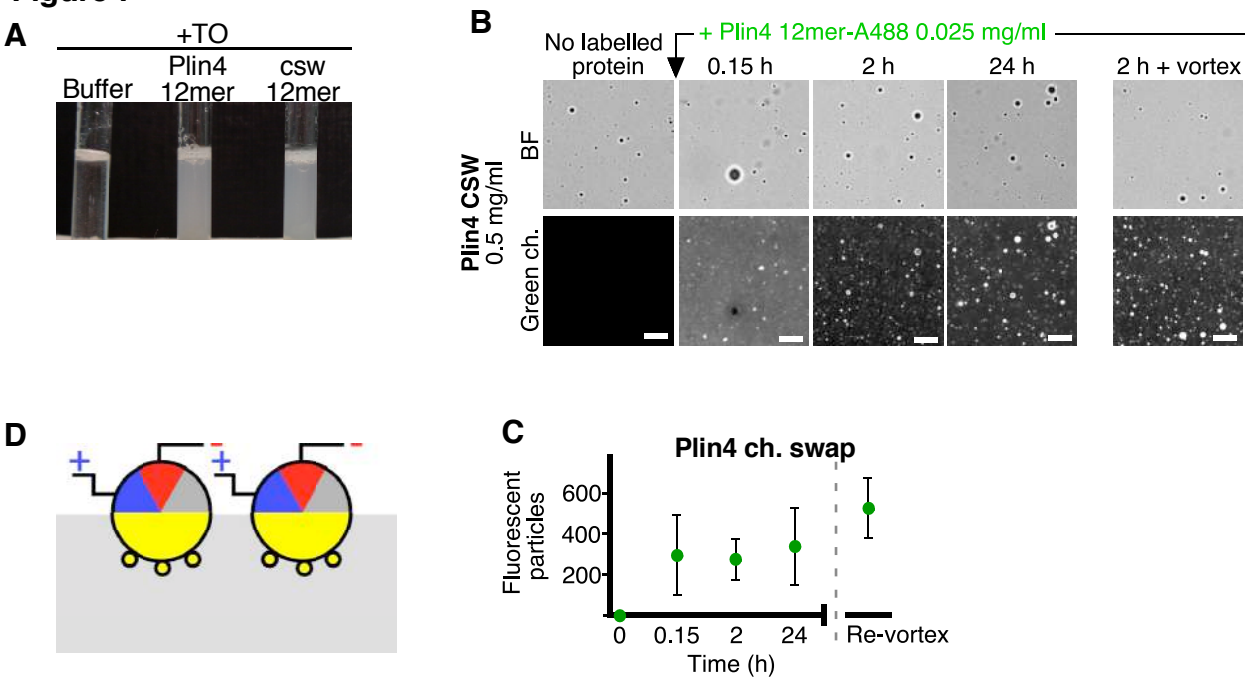

Figure 7. The distribution of charged residues in the polar face of Plin4 AH is key for stable coating of triolein *in vitro*. A. 15 μl triolein was added to 285 μl of HK buffer containing Plin4 12mer wild-type or the csw mutant (0.5 mg/ml each). After vigorous vortexing, the samples were photographed. **B**. A triolein emulsion was prepared with Plin4 12mer or csw 12mer mutant (0.5 mg/ml protein). At the indicated time, fluorescent Plin4 12mer-Alexa488 (0.025 mg/ml) was gently added. The emulsions were imaged by light microscopy in the bright field mode (BF) to see all particles and by fluorescence to detect the incorporation of Plin4 12mer-Alexa488 into the proteolipid particles. At the end of the experiment, the suspension was vortexed again to promote maximum incorporation of Plin4 12mer-Alexa488 in the emulsion. **C**. Quantification of the experiment shown in B. **D**. Model of how positive and negative charges could self-stabilize different Plin4 AHs at the surface of triolein.

Chapter 8: Additional results

8.1 Plin4 AH does not show a preference for STE in the yeast model.

TAG and STE quantities in LDs vary depending on cell type and environmental factors. Yeast grown at low temperatures like 15 °C have more TAG than the ones grown at 30 – 37 °C. Moreover, when the concentration of yeast is higher in the culture and there are fewer nutrients, yeasts also contain more TAG (Klose et al. 2012). In multicellular organisms, the level of TAG and STE can vary depending on the cell type. Testicular Leydig cells and adrenocortical cells have more content than other cell types of STE because of their production of sterol hormones (Wang et al. 2015b; Yu et al. 2018). It has also been suggested using Bodipy based fluorophore probes that TAG-rich and STE-rich LD pools coexist in some cell types as adrenocortical cells (Hsieh et al. 2012). However, this is not clear using Raman based spectroscopy (Fu et al. 2014).

Plin4 AH is able to interact with neutral lipids and coat them as we have demonstrated (Čopič et al. 2018) (Chapter 6, 7). It was proposed that Plin4 preferentially localizes to LDs containing STE in adrenocortical cells (Hsieh et al. 2012). I aimed to study if Plin4 AH interacts with a higher affinity with one kind of neutral lipid than the other. If this was the case, it would suggest that the composition of the neutral lipid core could influence whether LDs are coated and stabilized by Plin4.

8.1.1 Plin4 AH targets LDs in both ΔSTE and ΔTAG strains

Lipid metabolism in yeast has been thoroughly studied (Czabany et al. 2007; Klug and Daum 2014), which provided available mutants of yeast lipid metabolism, such as yeast devoid of TAG, devoid of STE or both of them (Zweytick et al. 2000; Sorger and Daum 2002; Sorger et al. 2004). These strains can be used to study Plin4 AH targeting depending on the kind of neutral lipid.

First, I checked the LD content in these strains in stationary phase using the neutral lipid marker Bodipy 493/503. Bodipy signal was brighter and more abundant in WT and ΔSTE (*are1Δ, are2Δ*) cells compared to ΔTAG (*dga1Δ, lro1Δ*) cells (Fig. 8-1 A). This result suggests that ΔTAG cells have a lower LD content, which is supported by bright-field images showing

fewer LDs. However, some of the difference could also be due to Bodipy having a lower affinity for STE than for TAG.

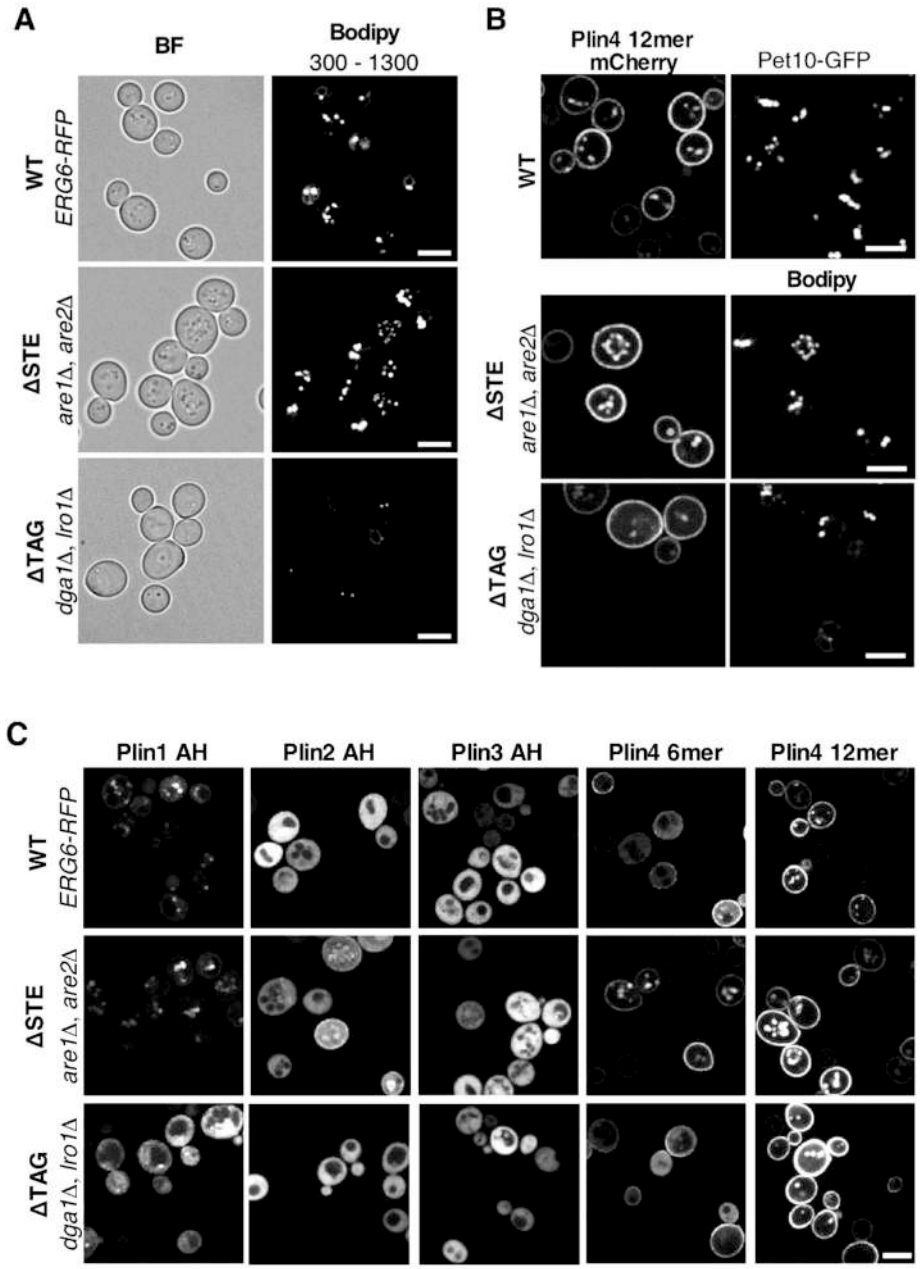

Fig. 8-1. **LD targeting of AHs in ΔSTE and ΔTAG yeast strains. A.** Representative light microscopy images of WT, ΔSTE and ΔTAG yeast strains stained with Bodipy reveal a lower content of neutral lipids in ΔTAG than in ΔSTE cells. All fluorescence images are adjusted to the same intensity levels (300 – 1300). **B**. Plin4 12mer-mCherry targets LDs in WT, ΔSTE and ΔTAG yeast. LDs are marked with the LD marker Pet10-GFP or with Bodipy. **C**. Plin AHs expressed as GFP fusions in yeast reveal a differential targeting capacity to LDs in ΔTAG yeast. Scale bars: 5 μm.

Plin4 12mer fused to mCherry expressed in these yeast strains could target LDs under conditions ΔSTE and ΔTAG condition (Fig. 8-1 B). I also analyzed the targeting of AHs from Plin1, Plin2, Plin3 and Plin4 fused to GFP in these strains (Fig. 8-1 C). All the AHs were able to target LDs in the ΔSTE strain, even the constructs with cytosolic localization in WT yeast, although the signal on LDs was often weak. However, only AHs with high affinity for LDs, Plin1 AH and Plin4 12mer, showed any localization to LDs in the ΔTAG strain. These results suggest that neutral lipid composition can affect AH targeting to LDs. In general, AHs seem to prefer LDs enriched in TAG (Chorlay and Thiam 2020). There are also fewer LDs in yeast with only STE and no TAG. Moreover, the presence of STE mixture with TAG also reduces LD targeting, as can be observed by the comparison between WT condition and ΔSTE in Plin2 AH and Plin3 AH. STE ordered layers can form due to phase transition (Czabany et al. 2008; Mahamid et al. 2019) and might be affecting LD targeting by some AHs.

8.1.2 Plin4 AH expression does not affect to yeast viability and growth

Heterologous expression of Plin4 AH in yeast could affect cell viability and growth. By sequestering Plin4 AH from the cytosol, LDs could have a protective role when this large heterologous protein is expressed. In order to test this, I prepared serial dilutions of Plin 12mer expressing strains (WT or neutral lipid synthesis mutants) and tested their growth at

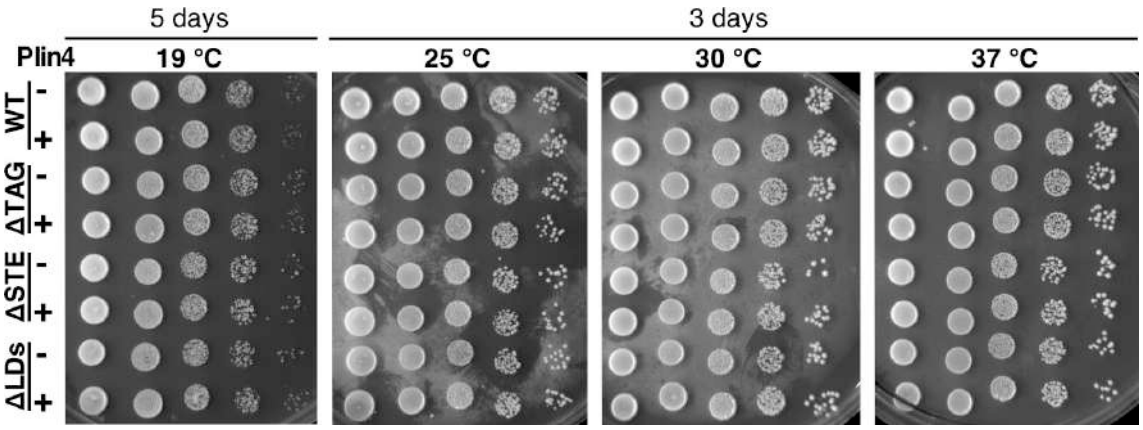

Fig. 8-2. Growth assays in yeast show non-detrimental effect neither in neutral lipid pathways mutations or in Plin4 12mer expression. Images of yeast colonies inoculated at different dilutions and grown at different temperatures in synthetic media plates.

different temperatures. There was no difference in growth between strains expressing Plin4 12mer or not under any condition tested (Fig. 8-2). This shows that Plin4 12mer expression does not affect yeast viability, even when there is only one of the neutral lipids or none.

8.1.3 Testing the interaction of Plin4 AH with different neutral lipids *in vitro*

In order to complement the results obtained in yeast, we wanted to test the interaction of Plin4 AH with different neutral lipids: triolein (3 oleic acids, 18:1 Δ9), a mixture of triolein and the cholesteryl oleate (3:1, triolein:cholesteryl oleate), Trilinoleate (3 linoleic acids, 18:2 Δ9, 12) and trinonaoate or tripelargonin (3 nonanoic acids, 9:0) (all purchased from Sigma). We could not use pure cholesteryl oleate because it is not liquid at the temperature at which these reactions are done, 25 °C. Vortexing of buffer with these neutral lipids resulted in high turbidity in them but in triolein (Fig. 8-3). This indicated that some contaminant molecules were present in these oils acting as surfactants and solubilizing these neutral lipids, as we confirmed by lipidomics analysis using mass spectrometry (Mass spectrometry platform, IPMC, CNRS). In order to extract information from this assay, these oils should have been purer in order to exclusively test the capacity of Plin4 12mer to stabilize and coat these neutral lipids.

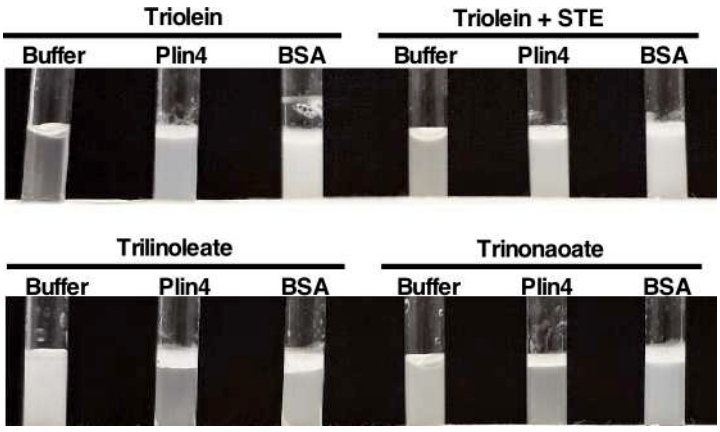

Fig. 8-3. Protein-oil emulsions varying the neutral lipid. 10 µl of the indicated neutral lipid were vortexed with 190 µl of either Buffer, 0.5 mg/ml Plin4 or 0.5 mg/ml BSA.

8.1.4 Conclusion

In yeast, Plin4 12mer and Plin1 AH do not show neutral lipid preference. Expression of Plin4 12mer is not detrimental for yeasts even in the absence of LDs.

8.2 Plin4 AH aa sequence is conserved in mammals, whereas the number of repeats varies

We have shown previously that increased length improved targeting of Plin4 AH to LDs. Moreover, the polar face plays a crucial role (Chapter 6, 7) (Čopič et al. 2018). Interestingly, an increase number of Plin4 33mer repeats, 40 instead of 29, originates a rare autosomal dominant progressive myopathy in humans because of protein aggregation (Ruggieri et al. 2020).

In these results we aimed to know how many Plin4 33mer repeats do other mammals have in other to observe if their number is conserved. Moreover, we also wondered if Plin4 repeats aa sequence is conserved among mammals.

8.2.1 Plin4 AH conservation among mammals

To address these questions, I checked the aa sequence of the AH from Plin4 orthologues from different mammalian species. Plin4 aa sequences from 16 species belonging to 15 families covering the whole mammalian tree (Bininda-Emonds et al. 2007) were obtained from Uniprot. I identified the number of 33mer repeats using HHrepID (Biegert and Söding 2008; Zimmermann et al. 2018). Results are shown in Table 8-1. The number of Plin4 33mer repeats varies from species to species. The AH regions varied in length from 736 aa and 22 repeats in *Tupaia chinensis* to 1919 aa and 58 repeats in the bat *Myotis davidii*. Most species had between 27 and 31 repeats. In all cases, the 33mer repeat region, and therefore the predicted AH, occupied the majority of the Plin4 sequence. In many of the species (8), there were no insertion or deletions between the repeats.

In order to analyze the conservation of the aa sequence of the 33mer repeats, repeats from each species were aligned and the alignments were plotted with Weblogo. All sequences had very good conservation within their repeats; conservation was lowest in platypus, which is the most distant mammal (Fig. 8-4). The best conservation was in Plin4 from the bat *Myotis brandtii*, with little variations among its 47 repeats. In chapter 7, we showed that charged aa (lysines and aspartic acid) and polar aa (glutamine) were important for LD targeting and coating of Plin4. These aa were very well conserved among the analyzed species, which highlights their importance for Plin4 function. Glycines, alanines, threonines and some hydrophobic residues were also highly conserved. Conservation of repeats was also good between species.

Table 8-1: Plin4 AH length analysis in different species of the mammalian family.

Species		Length of Plin4 AH		Start (aa)[1]	End (aa)[1]	Helix perturbations[2]	Total Plin4 length (aa)
Scientific name	Uniprot entry code	aa	# repeats				
Ornithorhynchus anatinus	F7FVK1	**932**	**28**	14	946	90 + aa in 590	1227
Monodelphis domestica	F7DNE7	**1096**	**33**	20	1116	-	1339
Loxodonta africana	G3UDZ0	**1051**	**32**	106	1157	-	1415
Myotis brandtii	S7MI15	**1544**	**47**	115	1659	-	1957
Myotis davidii	L5MGD7	**1919**	**58**	107	2026	-	2319
Felis catus	M3W5M0	**971**	**29**	82	1053	1 + in 632	1336
Canis lupus familiaris	J9JHP1	**1169**	**35**	104	1273	-	1588
Ailuropoda melanoleuca	G1L582	**949**	**29**	80	1029	2 + in 560 1 + in 939	1343
Sus scrofa	F1S7K4	**978**	**30**	107	1085	7 Δ in 1080 (at the end)	1425
Bos taurus	F1MNM7	**883**	**27**	78	961	1 Δ in 230	1260
Tupaia chinensis	L8Y4I8	**736**	**22**	21	757	2 Δ in 194	1210
Callithrix jacchus	F7GWD9	**926**	**28**	20	946	-	1200
Homo sapiens	Q96Q06	**952**	**29**	80	1032	-	1357
Macaca mulatta	F7FM35	**899**	**27**	20	919	-	1206
Ictidomys tridecemlineatus	I3MUC2	**819**	**25**	107	926	12 Δ in 310 4 + in 734	1291
Mus musculus	O88492	**1022**	**31**	105	1127	11 Δ in 1075 (1 turn)	1403

Notes: [1] Start and end of the AH in the aa sequence of Plin4.

[2] Insertions (+) or deletions (Δ) of aa between individual 33mer repeats. The position and number of inserted or deleted aa are indicated.

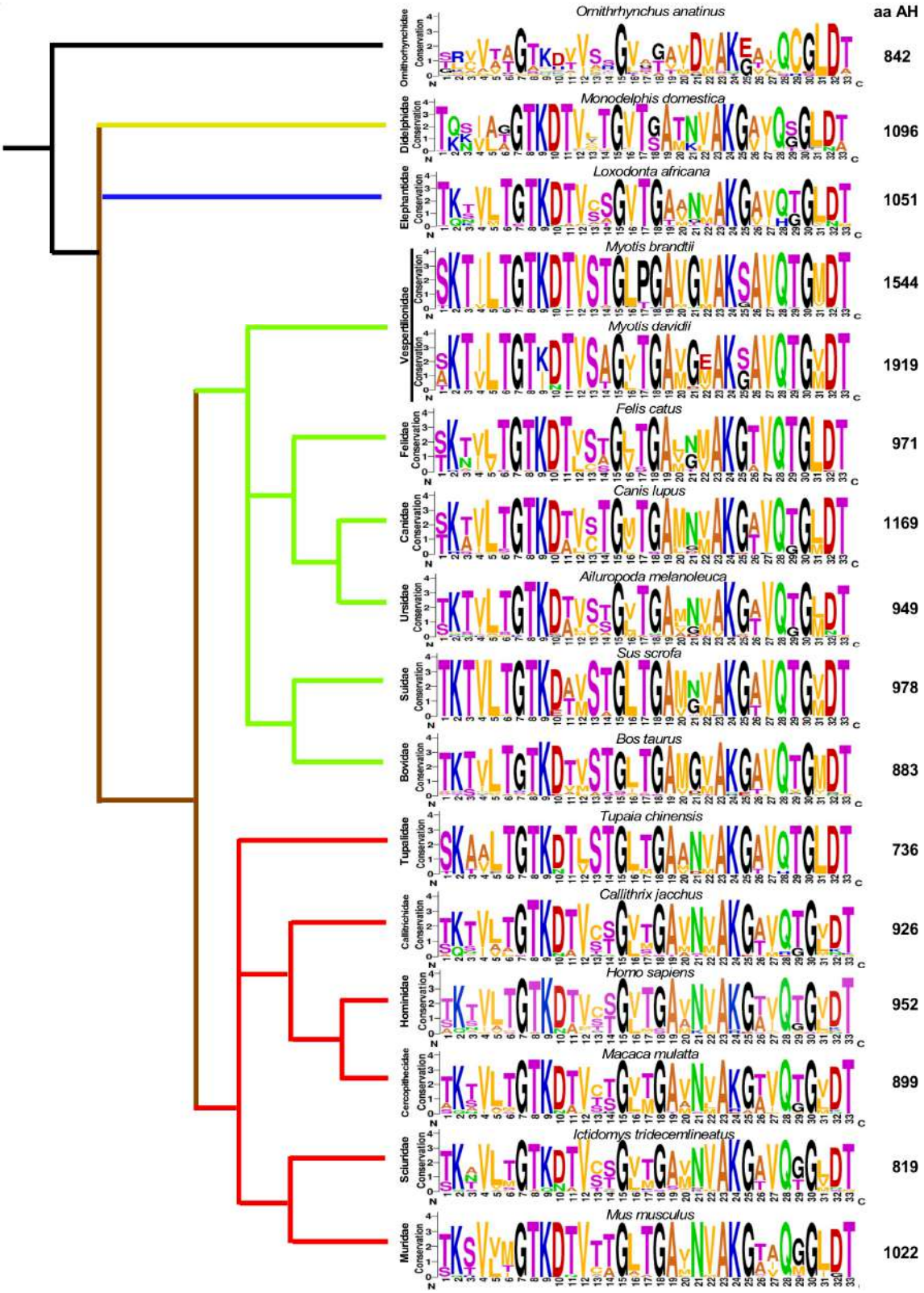

Fig. 8-4. Analysis of Plin4 33mer repeats in different mammals. Weblogos obtained from the alignments of the repeats of the same species are shown. The evolutionary tree on the left shows the evolutionary distance between the analyzed mammalian families (Bininda-Emonds et al. 2007). Major clades are coloured as follows: yellow for Xenarthra, blue for Afrotheria, green for Laurasiatheria, and red for Euarchontoglires.

One of those variations is having either an asparagine or a glycine in position 21 of the repeats that appears in the major lineage Laurasiatheria (Fig. 8-4, green lines of the evolutionary tree). Asparagine in position 21 also contributed to Plin4 AH localization to LDs in HeLa cells (Chapter 7, data obtained by Sandra Antoine-Bally, Institut Jacques Monod).

8.2.2 *Myotis brandtii* Plin4 sequence

The bat *M. brandtii* has a proline in the position 17 of its repeats whereas the rest of analyzed sequences have a threonine. Prolines are normally excluded from helices because they promote helix kinks due to incapability to make hydrogen bonds (Rey et al. 2010). The Uniprot sequence obtained for this species was not curated and an error during sequencing cannot be excluded. Apart from the presence of proline and absence of asparagine, we were interested in this sequence because it is the most repetitive of all sequences that we analyzed, and also very long. Therefore, we decided to express AHs derived from the *M. brandtii* sequence in yeast to observe their localization. Three sequences derived from bats were expressed in yeast, 12 repeats of the *M. brandtii* wild-type sequence (M24bT 12mer) and 6 and 12 repeats with proline changed to threonine (M25bT 6mer and M25bT 12mer, respectively) (Fig. 8-5 A, B). In contrast to Plin4 12mer, none of these constructs were able to target LDs in WT yeast. However, under more permissive conditions, M25bT 6mer and M25bT 12mer could localize to LDs. On the other hand, M24bP was not able to target LDs under any condition. These results show how prolines can affect AH targeting to LDs, likely by interfering with AH folding. Moreover, M25bT 12mer also displayed a lower affinity for LDs compared to human Plin4 12mer. Agreeing with results in chapter 7, this could be due to the lack of asparagine in its polar face. It is likely that the low affinity of *Myotis brandtii* Plin4 for LDs is overcome by its large length.

8.2.3 Conclusion

The number of 33mer repeats in Plin4 orthologues varies from species to species, ranging from 22 to 58 repeats. Plin4 AH sequences are conserved among mammals with very few changes. *M. brandtii* and *M. davidii* have very long and repetitive Plin4 AHs. 1 proline every 33 aa is enough to prevent Plin4 AH binding to LDs.

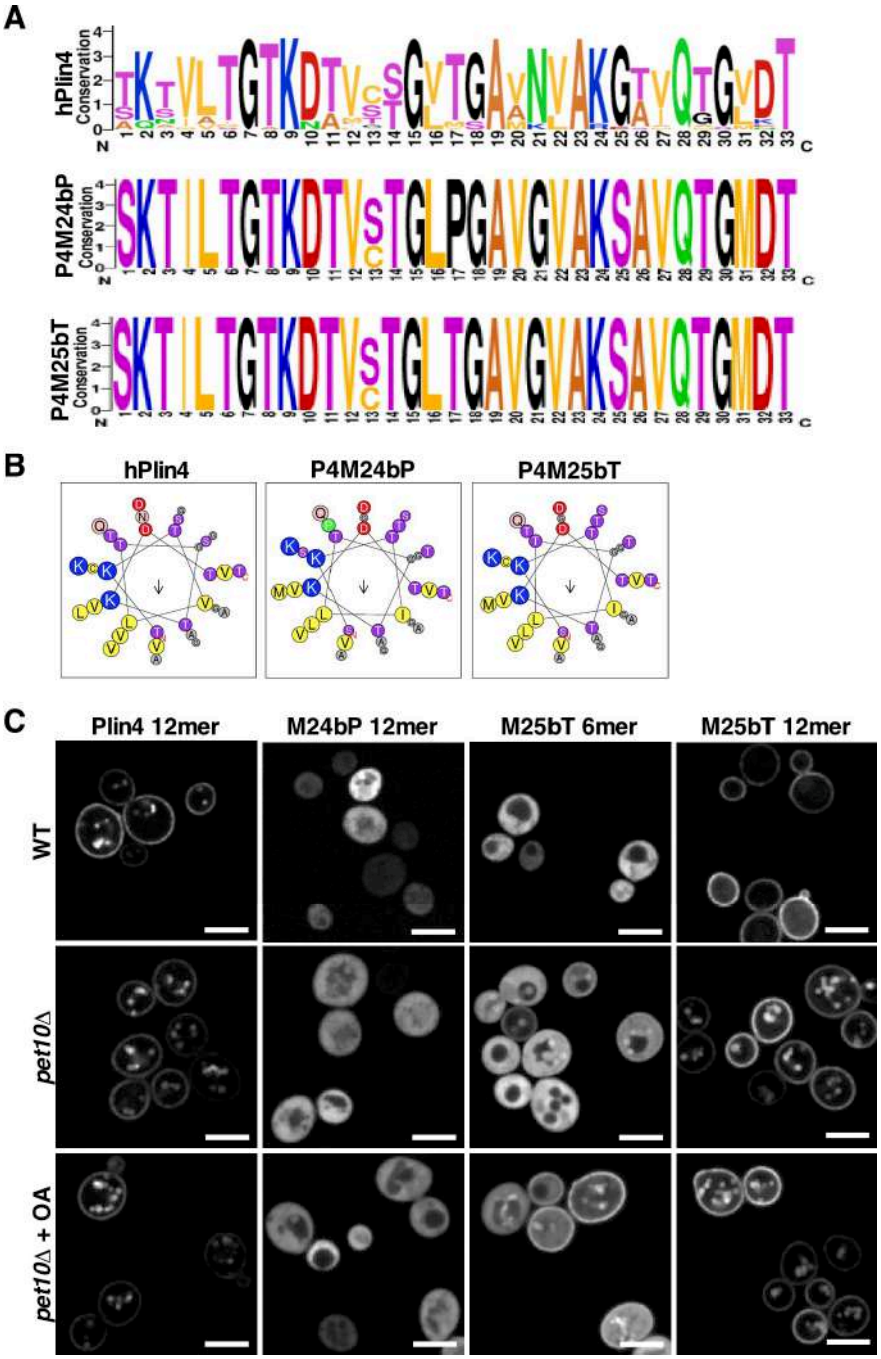

Fig. 8-5. Expression of Plin4 12mer bat sequence in yeast. A. Weblogos showing the comparison between human Plin4 repeats (hPlin4), the sequence from *Myotis brandtii* (P4M24bP) and sequence from *Myotis brandtii* without the proline (P4M25bT). **B**. Helical wheels of sequences expressed in yeast. **C**. Localization of these constructs fused to mCherry in yeasts with different permissibility for LD targeting (see Chapter 7). Scale bars: 5 µm. Yeast imaging done with M2 student Jaka Snoj (Institut Jacques Monod).

8.3 Plin4 AH does not have an observable effect on newly formed LDs in yeast

Plin3, Plin4 and Plin5 have been proposed to target nascent LDs (Wolins et al. 2003, 2005, 2006a). Some authors have also proposed that Plin AHs could promote LD formation (Robenek et al. 2006; Jacquier et al. 2013). We aimed to address this question using Plin4 AH and the yeast model.

To test if Plin4 has an effect on the formation of LDs in yeast, we needed to use yeast in exponential phase, where LDs are scarce and small. The drug 2-Deoxyglucose (2-DG) inhibits glycolysis in cells and causes ER stress (Defenouillère et al. 2019). S. Léon (Institut Jacques Monod) also observed an increase in LD content after addition of 0.2% of 2-DG to yeast media. We confirmed this using Bodipy to mark LDs (Fig. 8-6 A). 2-DG led to an increase in LD content in yeast, with the largest effect observed after three hours of incubation. Plin4 12mer could target LDs in yeast in exponential phase incubated with 2-DG (Fig. 8-6 B). Hence, this is a useful system for inducing LD formation and analyzing if Plin4 AH has any effect.

In order to analyze whether Plin4 AH had an effect on LD formation, we mixed yeast in exponential phase expressing either Plin4 12mer or empty GFP plasmid in a microfluidics chamber. This allowed us to follow the 2-DG induction of LDs over time simultaneously in the two strains, one of which was labelled with a blue dye. I did not observe any effect of Plin4 12mer expression on the LD content during the three hours time course (Fig. 8-6 C).

Another possibility for inducing LDs was to use the strain with *lro1Δ* and *are1Δ* mutations and *DGA1* and *ARE2* controlled by an inducible galactose promoter (Becuwe et al. 2018). This strain has inducible LDs because the expression of two enzymes, one for TAG and one for STE, are regulated by galactose and the other two enzymes for neutral lipids synthesis are deleted. Using this strain, we expressed Plin4 12mer-mCherry or the empty mCherry plasmid and compare the LD content. There are no big differences between the two conditions (Fig. 8-6 D). These results suggest that there is no observable effect of Plin4 12mer in new-formed LDs or in LD accumulation in yeast.

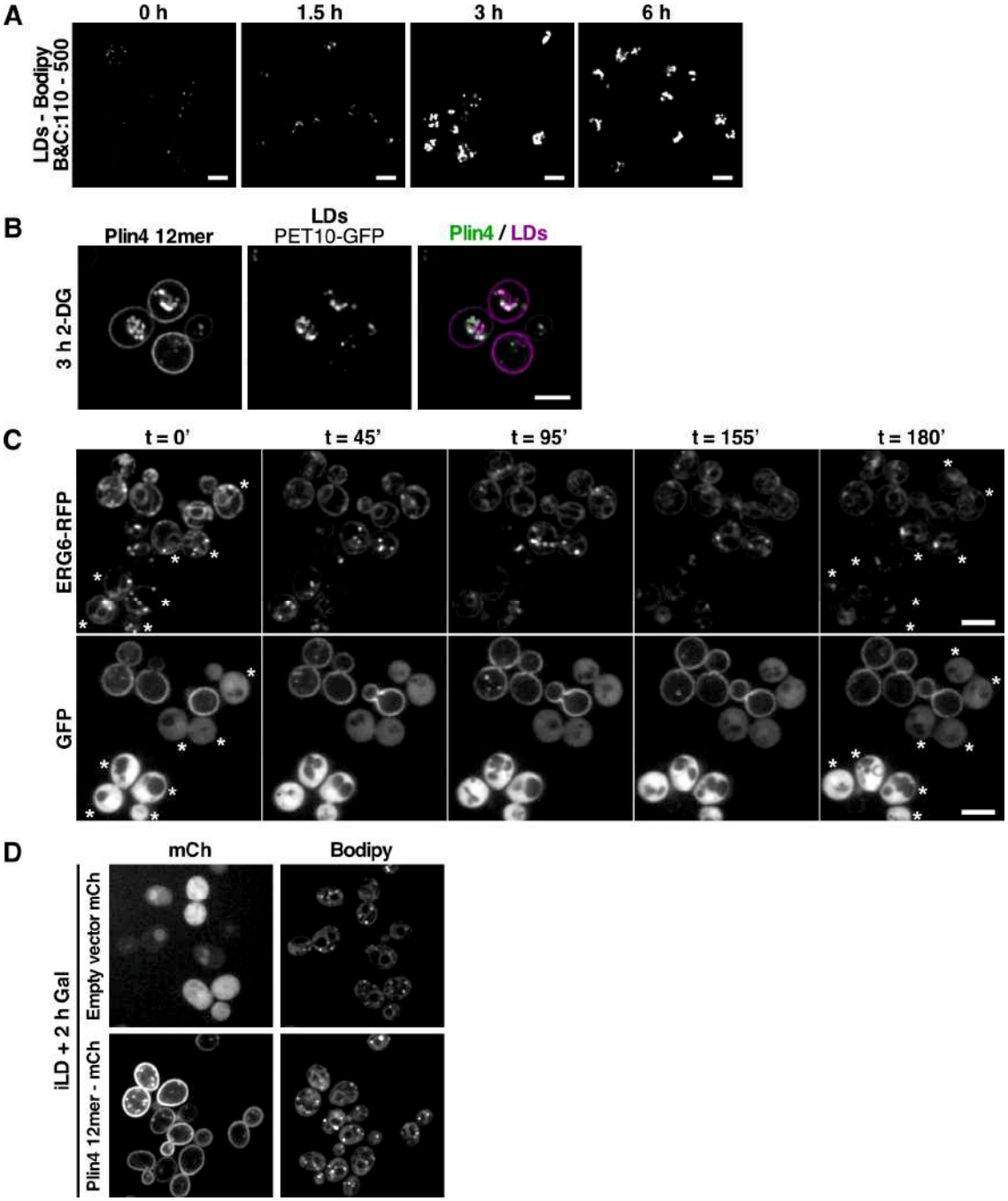

Fig. 8-6. Plin4 AH does not affect newly formed LDs in yeast. A. Induction of LDs in yeasts in exponential phase after 0 h, 1.5 h, 3 h and 6 h of 0.2% 2-Deoxyglucose (2-DG). Scale bars: 5 μm. **B**. Plin4 12-mer targets LDs in yeast in exponential phase after a 3h incubation with 0.2% 2-DG. **C**. ERG6-RFP yeast transformed either with Plin4 12-mer-GFP or the empty GFP vector followed by light imaging during LD induction. * marks yeast expressing the empty GFP vector. Scale bars: 5 μm. **D**. LD content in the iLD strain incubated for 2 h with galactose expressing either Plin4 12-mer-mCherry or the empty mCherry plasmid. Assay performed by Alenka Čopič.

CONCLUSION

Chapter 9: Conclusion and perspectives

How proteins interact with specific intracellular locations where they perform their function is an important question in cellular biology. In the case of the interaction of LDs and proteins, this is not elucidated. AHs are protein motifs that interact with lipid surfaces, including LDs (Giménez-Andrés et al. 2018). Plins are abundant LD proteins. Some Plins have well established functions regulating lipid metabolism in LDs (Sztalryd and Brasaemle 2017). Plin4 is the less studied member of this family. It contains a remarkably long AH, composed of highly homologous 33mer repeats.

First, we used the Plin4 AH as a model to study how AHs interact with LDs. We obtained the following results:

- Longer length of Plin4 AH targets better LDs.
- Higher hydrophobicity also improves LD binding. However, it also results in Plin4 interacting more strongly with other membranes.
- Modification of the charge to make it more positive or negative reduces LD targeting, but it can be compensated with more hydrophobicity.
- Plin4 AH is able to interact with neutral lipids directly *in vitro*, forming oil particles surrounded by Plin4 AH. These experiments suggest that Plin4 AH can replace PL monolayer on LDs. Supporting this model, in cells with PL depletion, which leads to large LDs, expression of Plin4 AH reduced LD size.

In order to assess the interaction of Plin4 AH with neutral lipids, I developed assays to evaluate the protein dynamics on oil droplets and the stability of the oil droplets formed *in vitro* using purified and fluorescently-labeled proteins. I observed the protein dynamics by observing the fluorescence recovery on the surface of oil droplets after photobleaching of fluorescent protein. Protein dynamics in real time during adsorption and desorption were evaluated with the microfluidics system developed in collaboration with Tadej Emeršič and Jure Derganc. To observe the stability of the oil particles formed, I used DLS

to follow the size of protein-oil droplets over time and evaluated of the aggregation of big particles with light microscopy. These techniques can be used in the future to characterize the interaction of other AHs with LDs.

My results are the following:

- The droplets formed by Plin4 AH and neutral lipids are very stable.
- Plin4 is remarkably immobile on the surface of these droplets.

Next, I compared Plin4 AH with the AHs of other Plins. I started by expressing Plin1, Plin2 and Plin3 in strains of budding yeast with different LD binding permissibility. I also purified Plin3 AH and tested its interaction with oil *in vitro*. I developed a fluorescent assay to observe the exchange of AHs on the surface of oil droplets. The results of these experiments are:

- Plin4 AH targets LDs the best because of its length. However, a shorter Plin4 AH fragment, similar in length to other Plin AHs, targets LDs to the same extent as Plin2 and Plin3 AH, consistent with their similar overall composition. All these AHs have a low hydrophobicity. Plin1 AH targets better LDs, in agreement with its increased hydrophobicity.
- In contrast, Plin1 AH and Plin3 AH are much more dynamic on the LD surface in yeast than Plin4 AH.
- Purified Plin3 AH can solubilize oil. However, the droplets formed by Plin3 AH are less stable than the ones formed with a Plin4 AH fragment of comparable length.
- Plin3 AH, but not a Plin4 AH fragment of a similar length, can be quickly replaced on the surface of oil droplets by a longer Plin4 AH fragment.

These results suggest that the differences between the behavior of Plin4 AH and other Plin AHs on LDs do not come only from differences in their length. We hypothesized that the aa sequence of Plin4 AH is important for its stability on the LD surface. The positions of polar and charged residues (lysine, glutamic acid, glutamine and asparagine) are highly conserved within Plin4 repeats. These residues would not be expected to directly interact with the LD surface.

- Conservative mutagenesis of polar and charged residues had a strong effect on Plin4 AH LD targeting.

- A Plin4 AH mutant with a redistribution of positive residues in its polar face had a reduced targeting to LDs, but still targeted the plasma membrane in yeast. When purified, this mutant was efficiently replaced on the oil droplet surface by wild type Plin4 AH of the same length.

I compared Plin4 AH sequences from different mammals. Within each orthologue sequence, Plin4 33mer repeats are highly conserved, including the positions of polar residues. However, the number of repeats varies between species. Specific residues in the polar face of Plin4 AH may promote self-stabilization through lateral interactions between folded Plin4 AH chains (Fig. 9-1).

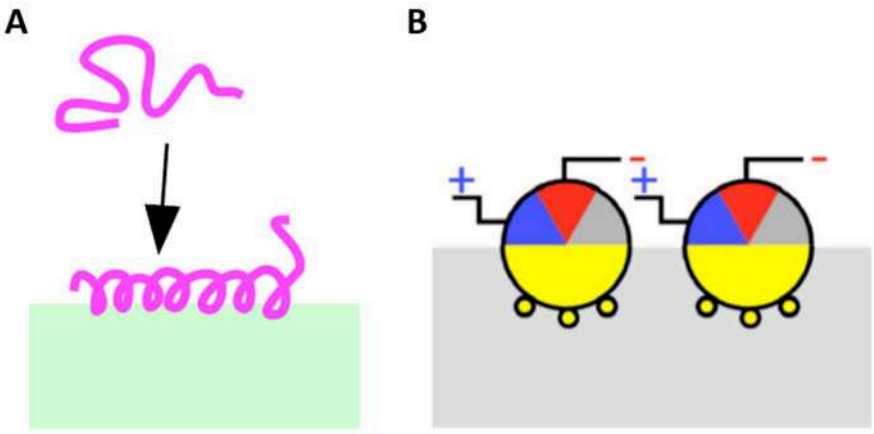

Fig. 9-1. Interaction of Plin4 AHs with LD surface. A. Plin4 AHs are unfolded in solution and folds upon the interaction with LD surface. This process is likely to happen also for other Plin AHs. **B.** Model of Plin4 AHs molecules interacting with between themselves on the LD surface.

Our model for the interaction of Plin AH with LDs is the following: Plin4 is unfolded in solution and acquires highly helical conformation upon interaction with a lipid surface (Fig. 9-1 A) (Chapter 6) (Čopič et al. 2018). This likely applies to other Plin AHs. In contrast to other Plin AHs, we propose that once Plin4 AH is folded on the LD surface, it laterally interacts with adjacent AHs via electrostatic interactions, forming an immobile protein layer on the LD surface (Fig. 9-1 B) (Chapter 7). These ordered interhelical interactions would explain the high stability of Plin4-covered lipid particles.

Similar interactions have been observed between AHs of ApoA-I, which wraps around small lipid particles forming high density lipoparticles (Bibow et al. 2017; Melchior et al. 2017). To

demonstrate the presence of these interactions in Plin4 coated oil droplets, techniques as protein cross-linking (Cornell 1989) or Förster resonance energy transfer assays could be used. Moreover, the structure of the protein on a lipid surface could be analyzed using cryo-electron microscopy (Sui et al. 2018).

Protein concentration would affect the formation of these interactions: a higher concentration of Plin4 molecules would result in a bigger possibility that these molecules interact between themselves. Therefore, increased Plin4 concentration would also mean a more stable interaction with LDs. This hypothesis could be checked in cells expressing Plin4 at different levels by following Plin4 dynamics on LDs. Moreover, it could also be tested *in vitro* by measuring the surface tension of oil with different concentrations of purified Plin4 AH using the oil droplet tensiometer (Small et al. 2009; Mitsche and Small 2013).

The C-terminal parts of Plin1, Plin2 and Plin3 may contribute to their targeting to LDs. The C-terminal domain of Plin1 reduced its dynamics on the LD surface in comparison with Plin2 and Plin3 (Ajjaji et al. 2019). In contrast, the C-terminal part of Plin4 did not localize to LDs in HeLa cells (Čopič et al. 2018), therefore the localization and dynamics of Plin4 may depend more strongly on its AH. This shows differences in the ways that Plins interact with LDs.

It would be interesting to study whether the protein layer formed by Plin4 AH can desorb from the surface of LDs during LD shrinkage. This aspect could be addressed by measuring the surface pressure during oil surface compression and expansion with an oil droplet tensiometer. The compression of the oil droplet surface will lead to a higher surface pressure if all the molecules of Plin4 AH remain stably bound to oil (Wang et al. 2006).

Plin4 AH has the capacity to coat LDs in cells preventing formation of LDs with increased size (Chapter 6) (Čopič et al. 2018). This observation and my results from *in vitro* experiments suggest that the function of Plin4 could be to substitute the PL monolayer and stabilize LDs under some conditions leading to PL depletion. LD coating by Plin4 would prevent LD fusion, maintaining a normal LD size. The 950 aa of Plin4 AH, when completely folded, would be able to substitute around 200 PLs of the LD monolayer when fully packed. In order to test this model in cells, Plin4 should be studied in the cell types where it is highly expressed, mainly white adipocytes during differentiation but also muscle cells. As Plin4 concentration could

affect the lateral interactions of Plin4 AH and its function, its endogenous concentration should be measured.

Recently, Plin4 AHs mutations have been linked with a rare autosomal dominant progressive myopathy. Individuals from a single family were found to have 40 repeats of the 33mer region of Plin4 instead of 29. Plin4 with this extended AH aggreged in skeletal muscle cells, where Plin4 is highly expressed (Ruggieri et al. 2020). The 16 mammalian species that we checked have very long Plin4 AHs. A longer Plin4 AH results in better targeting to LDs and a larger area of coating. However, higher length can also be dangerous due to aggregation, as this study suggests. We can study Plin4 aggregation *in vitro* by incubating at room temperature different lengths of the already purified constructs of Plin4 AH. Whether Plin4 AH has aggregated after a certain time could be examined with transmission electron microscopy. If Plin4 AH aggregates, further characterization would be possible by protease degradation or x-ray diffraction (Bousset et al. 2013).

It was suggested that Plin4 has a preference for STE-rich LDs, whereas an isoform of Plin1 has a preference for TAG-rich LDs in adrenocortical cells (Hsieh et al. 2012). In yeasts, we have shown that Plin4 AH is able to target both TAG-rich and STE-rich LDs. Further studies should address the selectivity of Plin AHs for different LDs and the role of their AH in this selectivity. For instance, AH selectivity could be checked *in vitro* using the droplet embedded vesicle system and light microscopy (Chorlay and Thiam 2020), or combining the techniques of Raman based spectroscopy and Bodipy based fluorophore probes.

A Plin4 knock-out mouse showed little phenotype. It had some reduction in storage of TAG in heart muscle and downregulation of Plin5 expression (Chen et al. 2013). However, the variability in number and composition of Plin4 33mer repeats in mammals, along with their high conservation within the same species, suggest an important role of Plin4 in mammalian evolution. We have shown that Plin4 binds directly to neutral lipids and stabilized them. Plin4 coats and reduces the size of LDs in cells lacking PLs. To understand physiological function of Plin4, it should be studied in cultured adipocytes.

MATERIALS AND METHODS

Chapter 10: Materials and methods

Yeast growth and media

Strains of the budding yeast *Saccharomyces cerevisiae* used in this work are listed in Table 9-1. Yeast media used were:

- Yeast extract, peptone, dextrose (YPD): 10 g/L yeast extract, 20 g/L peptone, 20 g/L glucose
- Synthetic complete medium lacking uracil (SC-Ura): 6.7 g/l yeast nitrogen base, aa supplement without uracil, 2% glucose.
- Oleic acid (OA) medium: 0.67% yeast nitrogen base without aa, 0.1 % yeast extract, 0.1 % (v/v) oleate, 0.25 % (v/v) Tween 40, aa supplement lacking uracil
- Raffinose medium: 6.7 g/l yeast nitrogen base, aa supplement without uracil, 2% raffinose

Yeast strains were grown in YPD and transformed by standard lithium acetate/polyethylene glycol procedure. Yeast cells expressing different AH constructs were grown in SC-Ura. LDs were induced by the following techniques:

- Yeast cells were grown to stationary phase in SC-Ura for 24 at 30°C
- 24 h in SC-Ura, followed by 24h incubation in OA medium
- 0.2 % 2-Deoxy glucose was added to a yeast liquid culture around 0.5 OD in SC-Ura and incubated for 3 h at 30 °C.
- iLD induction: yeasts were precultured in SC-URA then diluted overnight to 0.02 ODs in raffinose medium overnight until cultures reached 0.4-0.5 OD. Then, 2% galactose was added to the medium.

Yeast growth assays:

Wild-type, ΔSTE, ΔTAG or ΔLDs yeasts transformed either with pMGA4 (mCherry) or pMGA16 (Plin4 12mer-mCherry) were grown overnight in SC-URA to stationary phase. 10-fold serial dilutions were plated on SD-Ura agar plates.

Bacteria growth and media

Two strains of bacteria were used: XL-1 Blue used to amplify constructed plasmids and BL21 DE3 used for protein expression. Bacteria were grown overnight at 37 °C. For standard plasmid construction protocols the media used to grow bacteria was LB (10 g/L tryptone, 5 g/L yeast extract, 10 g/L NaCl) and for protein purification 2X-YT (16 g/L tryptone, 10 g/L of yeast extract, 5 g/L NaCl). Plasmid selection was done adding 100 μg/ml ampicillin to the media.

Sequence analysis

Sequences of human Plin4, Plin4 from other mammals and of human Plin1, Plin2, Plin3 and Plin5 were obtained from Uniprot. The 33mer repeats of Plin4 in various species and 11mer repeats of human Plins were identified using HHrepID tool from the MPI Bioinformatics Toolkit server (Biegert and Söding 2008; Zimmermann et al. 2018). With the identified region of repeats, repeats within species were aligned with themselves using T-coffee (Tommaso et al. 2011) and their conservation was represented using Weblogo (Crooks et al. 2004). The amphipathic character of these sequences was analyzed using HeliQuest (Gautier et al. 2008). Helical wheels were plotted as complete 3–11 helices; the presentation of helices was chosen such as to maximize their hydrophobic moment, as calculated by Heliquest, and inclusion of identified 11-aa repeats, excluding helix-breaking proline (Pace and Scholtz 1998) from the middle of the helices.

Plasmid DNA construction

All plasmids used in this study are listed in Table 9-2. DNAs encoding AHs of human Plin1, Plin2 and Plin3 were PCR-amplified from the corresponding cDNAs that had been cloned into pGREG576 plasmids (gift from R. Schneiter, U. of Fribourg) (Jacquier et al. 2013). DNA for Plin4 6mer and Plin4 8mer was amplified from plasmid pCLG26, and DNA for Plin4 4mer mutant 4T-S was amplified from plasmids pSB49 (Čopič et al., 2018). Plin4 4mer mutants (2D>E, 3K>3, NN, QN and QQ), and Plin4 12mer mutant csw 12mer were constructed using synthetic double-stranded DNA fragments. All 4mer mutants were exact 4× repeats of a 33-aa sequence, based on the parental sequence of human Plin4 fragment aa246-278. The protein sequence for csw 12mer was designed by manually adjusting 33-aa helical wheels of the parental Plin4 12mer sequence using HeliQuest to increase the symmetry of charged residue

distribution in the polar side of the helix while minimizing changes in the hydrophobic moment. DNA sequences were optimized for synthesis using the algorithm on the Eurofins website (https://www.eurofinsgenomics.eu). Table 4 lists all protein sequences used in this study.

For expression of proteins in *E. coli*, PCR-amplified DNA fragments were inserted into pET21b (Novagen) without adding a tag using *NheI* and *XhoI* restriction sites, which were introduced by PCR. For expression of Plin3 AH, an additional sequence 'MASC' was introduced upstream of the AH.

For expression of GFP fusion proteins in *S. cerevisiae*, PCR-amplified DNA fragments were inserted into pRS416-derived (URA3 and AmpR markers) CEN plasmid pRHT140 containing ADH1 promoter and GFP for C-terminal tagging (gift from S. Leon, IJM). For expression of mCherry fusion proteins, GFP-encoding fragment in this vector was replaced with mCherry using *KpnI* and *BamHI* restriction sites to generate plasmid pMGA4. All AH DNA fragments were cloned into these plasmids using *NheI* and *BamHI* restriction sites that were introduced by PCR. The sequence of the multiple cloning site introduces a linker peptide in the resulting fusion protein between the AH and GFP, 'PLDPPGLQEF', and linker peptide 'VKDPDIKLID' between the AH and mCherry.

Protein purification

All proteins were purified from *E. coli* without a tag. Plin4 12mer, Plin4 4mer, Plin4 4T-S and csw 12mer were purified following the same protocol. This protocol consists of a boiling step and cationic exchange chromatography (Čopič et al., 2018). In contrast, Plin3 AH has a net negative charge at neutral pH (pI = 4.65). Therefore, Plin3 AH purification protocol consists of a boiling step followed by anion exchange chromatography. *E. coli* cells BL21DE3 transformed with expression plasmids were grown in 2X-YT to OD ≈ 0.6 at 37°C from a liquid preculture and induced with 1 mM IPTG at 37 °C for 1h in the case of Plin3 AH, and for 3h in the case of the rest of constructs. Cells from 0.25 L cultures were collected by centrifugation and frozen. The bacterial pellets were thawed in lysis buffer (50 mM Tris-HCl pH 7.5, 150 mM NaCl, 1 mM DTT, supplemented with 0.1 mM PMSF, and complete protease inhibitor cocktail (Roche). Cells were broken by sonication. The lysate was centrifuged at 100,000 × g for 30 min at 4°C

in a 70.1Ti Rotor (40,000 rpm; Beckman). The supernatant in centrifuge tubes was immersed in boiling water (95°C) for 30 min. The resulting cloudy suspension was centrifuged at 100,000 × g for 15 min at 4°C to remove precipitated material. The supernatant was dialyzed against 20 mM Tris-HCl pH 7.5, 10 mM NaCl, 1 mM DTT (2 x 30 min using 1 L of buffer) at 4 °C using Spectra/Por membranes with a cut-off of 6000 Da (Spectrum labs) and then centrifuged again at 100,000 × g for 30 min at 4 °C. Plin4 12mer, Plin4 4mer, Plin4 4T-S and csw 12mer were then further purified in a single step by cation exchange chromatography on a 20 ml Hiprep S HP column (GE Healthcare). Plin3 AH was purified by anion exchange chromatography on a 20 ml Hiprep Q HP column (GE Healthcare). Constructs were eluted with a salt gradient from 10 mM to 400mM NaCl (3 column volumes) in 20 mM Tris-HCl pH 7.5, 1 mM DTT at a flow rate of 2 ml/min using an Akta purifier system (GE Healthcare), eluting at approximately 100 mM NaCl. After analysis of the chromatography fractions by protein electrophoresis, the protein pools were divided into small aliquots and stored at –80°C.

Protein electrophoresis and determination of protein concentration

Standard Glycine SDS-PAGE was used for the analysis of Plin4 12mer and csw 12mer (Mw ~ 40 kDa) using homemade 13% acrylamide bis-acrylamide gels. Tricine SDS-PAGE (Schägger and Jagow, 1987) was used for proteins with lower molecular weight, i.e. Plin4 4mer, Plin4 4T-S, or Plin3 AH (9 – 15 kDa). For that we either used TruPAGE commercial gels (Sigma) and homemade Tris-MOPS buffer (60 mM Trizma, 30 mM 4-Morpholinepropanesulfonic acid (MOPS), 0.1% w/v SDS) or, for better resolution, homemade 16.5% acrylamide-polyacrylamide (29:1) gels run with tricine buffer (100 mM Tris-HCl pH 8 – 8.5, 0.1 M Tricine, 0.1% SDS) in the cathode and 200 mM Tris HCl pH 8.9 in the anode chamber. Gels were rinsed in 7.5% acetic acid, stained with Sypro Orange (Life Technologies) and visualized with a MP imaging system (Bio-Rad) using the Alexa 488 settings. Because the AHs purified lack aromatic residues, preventing protein quantification by UV spectroscopy or by Coomassie Blue, protein concentration was routinely determined by densitometry of Sypro-Orange stained gels against a calibration curve with protein standards (Sigma) using ImageJ. Quantification by gel electrophoresis was verified by Ellman´s reaction method, which quantifies the cysteines concentration with Edman reagent (Sigma), after dialysis to remove DTT and with a standard curve of free cysteines. Relying on numerous cysteines in each construct (4 in Plin4 4mer, Plin4

12mer, 4T-S and csw 12mer, and 1 cysteine introduced by cloning in Plin3 AH) protein concentration can be obtained. This procedure was performed after protein dialysis to eliminate DTT.

Protein labelling with fluorescent probes

Purified AHs were covalently labeled via cysteines using Alexa C5 maleimide probes (either 488 or 568; Thermofisher). Plin4 12mer, Plin4 4mer and Plin4 4T-S and csw 12mer were labeled on endogenous cysteines present in their AHs; they all contain 4 cysteines in total. Plin3 AH is devoid of cysteines, therefore a single cysteine was introduced at its N-terminus. To remove DTT, 1 ml of protein solution at concentration 0.7 mg/ml (18 µM of Plin4 12mer and csw 12mer, 50 µM of Plin4 4mer and Plin4 4T-S) was exchanged into labelling buffer (20 mM Tris-HCl pH 7.5, 100 mM NaCl) using size exclusion NAP10 columns (GE Healthcare). Protein-containing fractions were identified by protein electrophoresis and pooled. Protein solutions were incubated for 5 minutes at 4 °C with Alexa C5 maleimide probes at an equimolar ratio to their total number of cysteines (1 ml reaction volume). The reactions were stopped by the addition of DTT to 10 mM final concentration and loaded on NAP10 columns to separate the labeled protein from the excess of fluorescent probe. Fractions were analyzed by protein electrophoresis. Fluorescence in the gel was directly visualized on ChemiDoc MP imaging system (Bio-Rad) either with Alexa 488 or Sypro Ruby (for Alexa 568) settings. Fractions with labeled protein were pooled, aliquoted and stored at -80°C. The same protocol was used for labelling of free cysteine, but without NAP10 purification steps.

We used FRAP assays on protein-oil emulsions (see below) with different ratios of labeled to unlabeled proteins to verify that the fluorescent label did not change the behavior of the protein. This was not the case for labeled Plin3 AH, thus we only used this protein in unlabeled form in our biochemical assays.

Preparation of protein-oil emulsions

Proteins were diluted to 0.5 mg/ml in freshly degassed HKM buffer (50 mM Hepes-KOH pH 7.2, 120 mM K-acetate, 1 mM $MgCl_2$) supplemented after degassing with 1 mM DTT. 190 µl of each solution were pipetted into a 600 µl glass tube, and a 10 µl drop of triolein (>99% purify, T7140 Sigma) was added to the top. In some cases, emulsions were prepared to have a final

volume of 100 µl and the drop of triolein was 5 µl. They were vortexed manually at a fixed angle of ~30° for three cycles of 30 s on 30 s off at 25 °C under argon atmosphere. Images of resulting emulsions were taken with a compact camera. For analysis by fluorescent microscopy, emulsions were prepared using a mixture of fluorescent and unlabeled protein at a mass ratio 1:20.

For the tests with varying the neutral lipids instead of triolein the neutral lipids used were: Cholesteryl oleate (C9253, Sigma), Glyceryl trilinoleate (T9517, Sigma), Glyceryl trinoneate (92909, Sigma). Cholesteryl oleate was solubilized with triolein (1:3, cholesteryl oleate: triolein) at 50 °C.

Dynamic Light Scattering (DLS)

Measurements of the mean hydrodynamic radius of the Plin4-oil droplets by DLS were performed on a sample taken from the middle of the tube after the vortexing reaction, avoiding any unreacted oil that remained at the top of the emulsion, at least 3 h after vortexing to prevent the interference of gas bubbles with the measurement. Subsequent samples at later time points were removed in the same manner without any additional mixing. Emulsion samples were diluted 100-fold in freshly degassed HKM buffer with 1mM DTT. Measurements were performed on a Zetasizer Nano ZS machine (Malvern) at 25°C, and data were processed using the CONTIN method.

Circular dichroism (CD)

The experiments were done on a Jasco J-815 spectrometer at room temperature with a quartz cell of 0.05 cm path length. Each spectrum is the average of several scans recorded from 195 to 260 nm with a bandwidth of 1 nm, a step size of 0.5 nm and a scan speed of 50 nm/min. Control spectra of buffer with or without liposomes were subtracted from the protein spectra. The buffer used was Tris 10 mM, pH 7.5, KCl 150 mM.

Trypsin protection assays

Plin4-oil emulsion was prepared using Plin4-12mer (1mg/ml) and triolein as described above. At time zero, 100 µl of this emulsion or of Plin4-12mer starting solution were mixed with 13

or 130 µg ml-1 trypsin (Sigma) solution. At the indicated times, 30 µl of samples were withdrawn and added 3 µl of 100 mM PMSF (Sigma) to stop the reactions, then stored on ice. Reactions were analyzed by SDS-PAGE and Sypro Orange staining.

Separation of Plin4-oil emulsion on sucrose gradients

Oil droplets in suspension are separated from the rest of the in vitro reaction by centrifugation because of their lower density. This also separates the protein interacting with the oil droplets from the unreacted protein in the solution, allowing their quantification. The protocol is as follows: Emulsions were prepared as specified in a final volume of 300 µl including 15 µl of triolein and 0.5 mg/ml of protein. Next, 240 µl of 60% w/v solution of sucrose in HKM buffer with 1 mM DTT was mixed with 240 µl of emulsion, avoiding any oil. 450 µl of this suspension was loaded on the bottom of a centrifuge tube and overlaid with a step sucrose gradient consisting of 300 µl 20%, 300 µl 10% and 100 µl 0% sucrose in HKM buffer with 1mM DTT. The samples were centrifuged at 50,000 rpm (214,000 × g) in a Beckman swing-out rotor (TLS 55) for 80 min at 8°C. Four fractions were carefully collected from the bottom with a Hamilton syringe, having the following volumes: 450 µl, 300 µl, 300 µl, and 100 µl, respectively. Equal volumes of all fractions were analyzed by protein electrophoresis.

Fluorescent microscopy

For imaging of purified protein-oil emulsions, emulsions prepared with fluorescent protein were gently mixed in the glass tube before 1.5 µl of emulsion was withdrawn with a long 200 µl tip and placed on untreated glass slides (Thermo Scientific). A coverslip was carefully placed on top without applying any pressure.

Yeast cells were harvested by centrifugation, washed, placed on a glass slide and covered with a coverslip. For some experiments, LDs were stained with 1 µg/ml Bodipy 493/503 (Life Technologies) or with Autodot blue dye (Clinisciences) diluted 1000 folds for 30 min at room temp, after which the cells were washed twice and imaged.

Images of emulsions and yeast were acquired at room temperature with an Axio Observer Z1 (Zeiss) microscope, equipped with an oil immersion plan-Apochromat 100x/1.4 objective, an sCMOS PRIME 95 (Photometrics) camera, and a spinning-disk confocal system CSU-X1

(Yokogawa) driven by MetaMorph software (Molecular Devices). GFP-tagged or Alex488-labeled proteins and mCherry-tagged or Alex568-labeled proteins were visualized with a GFP Filter 535AF45 and an RFP Filter 590DF35, respectively. When imaging emulsions, images were acquired in 10 to 15 z-sections of 0.2 µm were taken. For quantification of LD-to-PM signal ratio in yeast, we used an LSM 780 confocal microscope (Zeiss) with a x63/1.4 oil objective and a PMT GaAsP camera, driven by ZEN software. Images were processed with ImageJ and prepared for figures with Canvas Draw (canvas X).

Fluorescence recovery after photobleaching (FRAP)

FRAP assays *in vitro* were performed on freshly-prepared fluorescent emulsions with Alex488-labeled proteins on glass slides using the CSU-X1 spinning disc microscope and 100x objective, bleaching laser with a wavelength of 473 nm and iLas software controlled by Metamorph. Several circular areas of 25 x 25 pixels were bleached in each field (828 x 960 pixels), either on oil particles or in surrounding solution. The following FRAP time-course was used: 6 images pre-bleach, then bleach followed by 10 s of 1 image/s, 60 s of 1 image/10 s, and finally 600 s of 1 image/30 s (or until the loss of focus). Fluorescence of the bleached area at each time point was normalized to the average fluorescence before bleaching. Data was processed using Excel.

For FRAP assays in yeast cells, a circular area of 15 x 15 pixels in a cell expressing a GFP-fusion protein was bleached, either on the LDs or on the plasma membrane. 5 images were taken before bleaching, followed by a post-bleach time-course: 15 s of 1 image/s, 60 s of 1 image/5 s, and ~200 s of 1 image/20 s. Background fluorescence outside the cell was subtracted from the bleached area and the signal was normalized to the whole cell signal for each time-point. Data was processed with Excel and plotted using SigmaPlot (Systat Software).

Protein exchange assay on protein-oil emulsions

Emulsions were prepared as described using unlabeled protein at 0.5 mg/ml and checked by microscopy using CSU-X1 spinning disc microscope (time 0). Then, fluorescent Plin4 12mer-Alexa488 was gently added to the suspension to a final concentration of 0.025 mg/ml (20 : 1, unlabeled protein : labeled Plin4 12mer). Samples from the emulsions were withdrawn at indicated time-points without mixing and imaged on glass slides. The re-vortex sample was

prepared after 2h of incubation by withdrawing 20 μl of the emulsion and vortexing it in a fresh 600 μl glass tube in the same manner as for initial emulsion preparation. Samples were imaged in 10 z-sections of 0.5 μm in randomly-selected fields of 76 μm x 101 μm. The z-section containing the highest number of small droplets was selected for analysis.

Yeast imaging in microfluidics chamber with 2-deoxy glucose (2-DG)

Yeast were imaged in the Axio Observer Z1 microscopy using the microfluidic perfusion platform (ONIX) driven by the interface software ONIX-FG-SW (Millipore). ERG6-RFP yeast strain transformed with pRHT140 (expressing GFP) and stained with CMAC 1x for 10 min at room temperature and the same strain transformed with or pKE33 (expressing Plin4 12mer-GFP) were mixed at 1:1 ratio. The yeast mixture was injected into a YO4C microfluidics chamber with applying 3 psi for 8" twice. Cells were maintained in a uniform focal plane. Normal growth conditions were maintained by flowing cells with SD-URA + 0.2% 2-DG at 3 psi. Cells were imaged every 10 min over a total time of 180 min. Cells were imaged in 5 z-sections separated by 0.5 μm, afterwards manually selecting for the best focal plane, in order to correct for any focal drift during the experiment.

Image analysis

Images were analyzed using ImageJ/Fiji (Schindelin et al., 2012). To quantify the number of droplets in protein-oil emulsions, the number of particles in a randomly-selected area in a single z-section was counted using 'find maxima' in the fluorescent channel with noise tolerance set to 100. Larger clusters were counted manually. For quantification in the exchange assay, the noise tolerance was set to 150. To quantify the number of yeast cells with protein signal on LDs, cells were counted manually after applying the same brightness/contrast settings to all images. To quantify the ratio of LD to PM protein signal (mCherry fusions), Pet10-GFP LD marker was used to select the regions of interest (ROIs) corresponding to LDs and the total mCherry fluorescence in the ROIs was recorded. For the quantification of PM fluorescence, images were converted to binary to select the whole yeast perimeter. Them, a band of 5 pixels was applied to include all of PM signal. After background subtraction, the total LD signal per cell was divided by the total PM signal. LD size in yeast cells grown in oleic-acid medium was measured using the fluorescent protein. Isolated LDs were

fitted manually with a perfect circle and the size of each circular area was recorder. Data were analyzed in Excel and plotted with KaleidaGraph (Synergy software).

Table 9-1. Yeast strains used in this study.

Name	Genotype	Reference
BY4742	BY4742 MATα *his3Δ1 leu2Δ0 lys2Δ0 ura3Δ0*	Euroscarf
ERG6-RFP	BY4742 MATα *his3Δ1 leu2Δ0 lys2Δ0 ura3Δ0 ERG6::mRFP*	Jackson lab collection
PET10-GFP	BY4741 MATa *his3Δ1 leu2Δ0 met15Δ0 ura3Δ0 PET10::GFP::HisMX*	(Huh et al. 2003)
pet10Δ	BY4742 *his3Δ1 leu2Δ0 lys2Δ0 ura3Δ0 pet10Δ::KANMX4*	Euroscarf
ΔSTE	MATα *his3Δ1 leu2Δ0 lys2Δ0 ura3Δ0 are1Δ::KANMX are2Δ::KANMX*	Klaus Natter
ΔTAG	MATα *his3Δ1 leu2Δ0 lys2Δ0 ura3Δ0 dga1Δ::KANMX lro1Δ::KANMX*	Klaus Natter
ΔLDs	MATα *his3Δ1 leu2Δ0 lys2Δ0 ura3Δ0 dga1Δ::KANMX lro1Δ::KANMX are1Δ::KANMX are2Δ::KANMX*	Klaus Natter
iLD.	MATα *his3Δ1 leu2Δ0 lys2Δ0 ura3Δ0 GalP::DGA1 GalP::ARE2 lro1Δ::HPH are2Δ::NAT*	(Becuwe et al. 2018)

Table 9-2. Plasmids used in this study.

Name	Insert	Region (aa) (1)	Vector	Host	Source
pCLG03	Plin4 4mer	hPlin4 (aa246-377)	pET21b	*E. coli*	Čopič 2018
pKE23	Plin4 12mer	hPlin4 (aa510-905)	pET21b	*E. coli*	Čopič 2018
pMGA9	4T-S (4mer)	4x[246-278 M5t]	pET21b	*E. coli*	This study
pMGA19	Plin3 AH	hPlin3(aa113 – 205)	pET21b	*E. coli*	This study
pMGA1	Csw 12mer	Charge swap of hPlin4(aa510-905)	pET21b	*E. coli*	This study
pGFP-Plin1	Human Plin1	Full cDNA	pGREG576 (ADH1pr, GFP)	Yeast	Jacquier 2013
pGFP-Plin2	Human Plin2	Full cDNA	pGREG576 (ADH1pr, GFP)	Yeast	Jacquier 2013
pGFP-Plin3	Human Plin3	Full cDNA	pGREG576 (ADH1pr, GFP)	Yeast	Jacquier 2013
pRHT140	ADHpr-mcs-GFP		pRS416 (CEN-URA3)	Yeast	S. Leon
pMGA4	ADHpr-mcs-mCherry (swap of GFP for mCherry in pRHT140)		pRS416 (CEN-URA3)	Yeast	This study
pMGA10	Plin1 AH-GFP	hPlin1 (aa108-194)	pRHT140	Yeast	This study
pMGA5	Plin2 AH-GFP	hPlin2 (aa100-192)	pRHT140	Yeast	This study
pMGA7	Plin3 AH-GFP	hPlin3 (aa113-205)	pRHT140	Yeast	This study
pMGA28	Plin3(87-205)-GFP	hPlin3 (aa87-205)	pRHT140	Yeast	This study
pKE31	Plin4 4mer-GFP	hPlin4 (aa246-377)	pRHT140	Yeast	Čopič 2018
pKE33	Plin4 12mer-GFP	hPlin4 (aa510-905)	pRHT140	Yeast	Čopič 2018
pMGA16	Plin4 12mer-mCherry	hPlin4 (aa510-905)	pMGA4	Yeast	This study
pMGA30	Plin4 6mer-GFP	hPlin4 (aa246-433)	pRHT140	Yeast	This study
pMGA22	Plin4 8mer-GFP	hPlin4 (aa246-509)	pRHT140	Yeast	This study
pMGA34	P4M24bP	bPlin4 (aa558-953)	pMGA4	Yeast	This study
pMGA35	P4M25bT 6mer	1P>T bPlin4 (aa558-755)	pMGA4	Yeast	This study
pMGA36	P4M25bT 8mer	1P>T bPlin4 (aa558-821)	pMGA4	Yeast	This study
pMGA37	P4M25bT 12mer	1P>T bPlin4 (aa558-953)	pMGA4	Yeast	This study

(1) Position of aa in human Plins (hPlin) or bat Plin4 (bPlin4) sequences.

Table 9-3. Protein sequences expressed in this study.

Name	Construct	protein sequence
PLin4-4mer	Plin4[246-377]	MSKTVLTGTKDTVCSGVTGAMNVAKGTIQTGVDTSKTVLTGTKDTVCSGVTGAM NVAKGTIQTGVDTSKTVLTGTKDTVCSGVTGAMNVAKGTIQTGVDTTKTVLTGTKN TVCSGVTGAVNLAKEAIQGGLDT
PLin4-6mer	Plin4[246-443]	MSKTVLTGTKDTVCSGVTGAMNVAKGTIQTGVDTSKTVLTGTKDTVCSGVTGAM NVAKGTIQTGVDTSKTVLTGTKDTVCSGVTGAMNVAKGTIQTGVDTTKTVLTGTKN TVCSGVTGAVNLAKEAIQGGLDTTKSMVMGTKDTMSTGLTGAANVAKGAMQTGL NTTQNIATGTKDTVCSGVTGAMNLARGTIQTGVDT
Plin4-8mer	Plin4[246-509]	MSKTVLTGTKDTVCSGVTGAMNVAKGTIQTGVDTSKTVLTGTKDTVCSGVTGAM NVAKGTIQTGVDTSKTVLTGTKDTVCSGVTGAMNVAKGTIQTGVDTTKTVLTGTK NTVCSGVTGAVNLAKEAIQGGLDTTKSMVMGTKDTMSTGLTGAANVAKGAMQ TGLNTTQNIATGTKDTVCSGVTGAMNLARGTIQTGVDTTKIVLTGTKDTVCSGVT GAANVAKGAVQGGLDTTKSVLTGTKDAVSTGLTGAVNVAKGTVQTGVDTKD
Plin4-12mer	Plin4[510-905]	MTKTVLTGTKDTVCSGVTSAVNVAKGAVQGGLDTTKSVVIGTKDTMSTGLTGAA NVAKGAVQTGVDTAKTVLTGTKDTVTTGLVGAVNVAKGTVQTGMDTTKTVLTG TKDTIYSGVTSAVNVAKGAVQTGLKTTQNIATGTKNTFGSGVTSAVNVAKGAAQT GVDTAKTVLTGTKDTVTTGLMGAVNVAKGTVQTSVDTTKTVLTGTKDTVCSGVT GAANVAKGAIQGGLDTTKSVLTGTKDAVSTGLTGAVKLAKGTVQTGMDTTKTVL TGTKDAVCSGVTGAANVAKGAVQMGVDTAKTVLTGTKDTVCSGVTGAANVAK GAVQTGLKTTQNIATGTKNTLGSGVTGAAKVAKGAVQGGLDTTKSVLTGTKDAV STGLTGAVNLAKGTVQTGVDTKD
Plin4-4T-S	4xM5t	SKTVLTGSKDSVCSGVTGAMNVAKGSIQTGVDSSKTVLTGSKDSVCSGVTGAMN VAKGSIQTGVDSSKTVLTGSKDSVCSGVTGAMNVAKGSIQTGVDSSKTVLTGSKD SVCSGVTGAMNVAKGSIQTGVDS
csw-12mer (charge swap)	P4-M14kd	TKDKLTGTVTTVCNVVTSAGSVAKDLVQGGAGTTKSVVIGTTDKMSTGLTGAVN AAKGAVQTGTDVAKTVLTGTTDKVTTGLVGAVNVAKGTVQTGTDMTKTVLTGT TDKIYSGVTSAVNVAKGAVQTGTKLTGNIATQTKNTFSSGVTGAVNVATGAAQK GVDTAKTVLTGTTDKVTTGLMGAVNVAKGTVQTSTDVTKDKLTGTVTTVCNAV TGAGSVAKDLIQGGAGTTKSVLTGTADKVSTGLTGALKVAKGTVQTGTDMTKT VLTGTADKVCSGVTGAVNAAKGAVQMGTDVAKTVLTGTTDKVCSGVTGAVN AAKGAVQTGTKLTQNIATGTTNKLGSGVTGAVKAAKGAVQGGTDLTKSVLTGT ADKVSTGLTGALNVAKGTVQTGTDV
Plin1 AH	hPlin1 aa109-194	MPPEKIASELKDTISTRLRSARNSISVPIASTSDKVLGAALAGCELAWGVARDTAE FAANTRAGRLASGGADLALGSIEKVVEYLLPP
Plin2 AH	hPlin2 aa100-192	PSTQIVANAKGAVTGAKDAVTTTVTGAKDSVASTITGVMDKTKGAVTGSVEKTK SVVSGSINTVLGSRMMQLVSSGVENALTKSELLVEQYLP
Plin3 AH (1)	hPlin3 aa113-205	*masc*PTEKVLADTKELVSSKVSGAQEMVSSAKDTVATQLSEAVDATRGAVQSGV DKTKSVVTGGVQSVMGSRLGQMVLSGVDTVLGKSEEWADNHLP
Plin3(87-205)	hPlin3 aa87-205	PQIASASEYAHRGLDKLEENLPILQQPTEKVLADTKELVSSKVSGAQEMVSSAKD TVATQLSEAVDATRGAVQSGVDKTKSVVTGGVQSVMGSRLGQMVLSGVDTVL GKSEEWADNHLP
P4M24bP	*M. brandti*i Plin4 aa558-953	SKTILTGTKDTVSTGLPGAVGVAKSAVQTGMDTSKTILTGTKDTVSTGLPGAVGV AKSAVQTGMDTSKTILTGTKDTVSTGLPGAVGVAKSAVQTGMDTSKTILTGTKD TVSTGLPGAVGVAKSAVQTGMDTSKTILTGTKDTVSTGLPGAVGVAKSAVQTG MDTSKTILTGTKDTVSTGLPGAVGVAKSAVQTGMDTSKTILTGTKDTVSTGLPGA VGVAKSAVQTGMDTSKTILTGTKDTVSTGLPGAVGVAKSAVQTGMDTSKTILTG TKDTVSTGLPGAVGVAKSAVQTGMDTSKTILTGTKDTVSTGLPGAVGVAKSAVQ TGMDTSKTILTGTKDTVSTGLPGAVGVAKSAVQTGMDTSKTILTGTKDTVSTGLP GAVGVAKSAVQTGMDT

P4M25bT 12mer	P>T *M. brandtii* Plin4 aa558-953	SKTILTGTKDTVSTGLTGAVGVAKSAVQTGMDTSKTILTGTKDTVSTGLTGAVGVA KSAVQTGMDTSKTILTGTKDTVSTGLTGAVGVAKSAVQTGMDTSKTILTGTKDTV STGLTGAVGVAKSAVQTGMDTSKTILTGTKDTVSTGLTGAVGVAKSAVQTGMDT SKTILTGTKDTVSTGLTGAVGVAKSAVQTGMDTSKTILTGTKDTVSTGLTGAVGVA KSAVQTGMDTSKTILTGTKDTVSTGLTGAVGVAKSAVQTGMDTSKTILTGTKDTV STGLTGAVGVAKSAVQTGMDTSKTILTGTKDTVSTGLTGAVGVAKSAVQTGMDT SKTILTGTKDTVSTGLTGAVGVAKSAVQTGMDTSKTILTGTKDTVSTGLTGAVGVA KSAVQTGMDT

REFERENCES

Abell BM, Holbrook LA, Abenes M, Murphy DJ, Hills MJ, Moloney MM. Role of the proline knot motif in oleosin endoplasmic reticulum topology and oil body targeting. Plant Cell. 1997;9(8):1481–93.

Ajjaji D, Mbarek KB, Mimmack ML, England C, Herscovitz H, Dong L, et al. Dual binding motifs underpin the hierarchical association of perilipins1-3 with lipid droplets. Molecular biology of the cell. 2019;mbcE18080534.

Ali A, Mekhloufi G, Huang N, Agnely F. β-lactoglobulin stabilized nanemulsions—Formulation and process factors affecting droplet size and nanoemulsion stability. International Journal of Pharmaceutics. 2016 Mar 16;500(1–2):291–304.

Altmann R. Die elementaroganismen und ihre Beziehungen zu den Zellen. 1890.

Antonny B, Beraud-Dufour S, Chardin P, Chabre M. N-Terminal Hydrophobic Residues of the G-Protein ADP-Ribosylation Factor-1 Insert into Membrane Phospholipids upon GDP to GTP Exchange. Biochemistry. 1997;36(15):4675–84.

Athenstaedt K, Jolivet P, Boulard C, Zivy M, Negroni L, Nicaud J-M, et al. Lipid particle composition of the yeast Yarrowia lipolytica depends on the carbon source. PROTEOMICS. 2006 Mar;6(5):1450–9.

Bacle A, Gautier R, Jackson CL, Fuchs PFJ, Vanni S. Interdigitation between Triglycerides and Lipids Modulates Surface Properties of Lipid Droplets. Biophysj. 2017 Apr 11;112(7):1417–30.

Bartz R, Li W-H, Venables B, Zehmer JK, Roth MR, Welti R, et al. Lipidomics reveals that adiposomes store ether lipids and mediate phospholipid traffic. The Journal of Lipid Research. 2007 Mar 26;48(4):837–47.

Becuwe M, Bond LM, Mejhert N, Boland S, Elliott SD, Cicconet M, et al. FIT2 is a lipid phosphate phosphatase crucial for endoplasmic reticulum homeostasis. Biorxiv. 2018;291765.

Beller M, Bulankina AV, Hsiao H-H, Urlaub H, Jäckle H, Kühnlein RP. PERILIPIN-Dependent Control of Lipid Droplet Structure and Fat Storage in Drosophila. Cell Metabolism. 2010;12(5):521–32.

Benerito RR, Singleton WS, Feuge RO. Surface and Interfacial Tensions of Synthetic Glycerides of Known Composition and Configuration. The Journal of Physical Chemistrya. 1954 Oct;58(10):831–4.

Bersuker K, Olzmann JA. Establishing the lipid droplet proteome_ Mechanisms of lipid droplet protein targeting and degradation. BBA - Molecular and Cell Biology of Lipids. 2017 Oct 1;1862(Part B):1166–77.

Bersuker K, Peterson CWH, To M, Sahl SJ, Savikhin V, Grossman EA, et al. A Proximity Labeling Strategy Provides Insights into the Composition and Dynamics of Lipid Droplet Proteomes. Developmental Cell. 2017 Dec 19;1–24.

Bibow S, Polyhach Y, Eichmann C, Chi CN, Kowal J, Albiez S, et al. Solution structure of discoidal high-density lipoprotein particles with a shortened apolipoprotein A-I. Nat Struct Mol Biol. 2017;24(2):187–93.

Bickel PE, Tansey JT, Welte MA. PAT proteins, an ancient family of lipid droplet proteins that regulate cellular lipid stores. Biochim Biophys Acta. 2009;1791(6):419–40.

Biegert A, Söding J. De novo identification of highly diverged protein repeats by probabilistic consistency. Bioinformatics. 2008;24(6):807–14.

Bigay J, Casella J-F, Drin G, Mesmin B, Antonny B. ArfGAP1 responds to membrane curvature through the folding of a lipid packing sensor motif. The EMBO Journal. 2005 Jul 6;24(13):2244–53.

Bininda-Emonds ORP, Cardillo M, Jones KE, MacPhee RDE, Beck RMD, Grenyer R, et al. The delayed rise of present-day mammals. Nature. 2007;446(7135):507–12.

Blanchette-Mackie EJ, Dwyer NK, Barber T, Coxey RA, Takeda T, Rondinone CM, et al. Perilipin is located on the surface layer of intracellular lipid droplets in adipocytes. The Journal of Lipid Research. 1995;36(6):1211–26.

Bousset L, Pieri L, Ruiz-Arlandis G, Gath J, Jensen PH, Habenstein B, et al. Structural and functional characterization of two alpha-synuclein strains. Nat Commun. 2013;4(1):2575.

Brasaemle DL, Barber T, Wolins NE, Serrero G, Blanchette-Mackie EJ, Londos C. Adipose differentiation-related protein is an ubiquitously expressed lipid storage droplet-associated protein. J Lipid Res. 1997;38(11):2249–63.

Brasaemle DL, Dolios G, Shapiro L, Wang R. Proteomic analysis of proteins associated with lipid droplets of basal and lipolytically stimulated 3T3-L1 adipocytes. J Biological Chem. 2004;279(45):46835–42.

Brasaemle DL, Wolins NE. Isolation of Lipid Droplets from Cells by Density Gradient Centrifugation. Curr Protoc Cell Biology. 2016;72(1):3.15.1-3.15.13.

Bulankina AV, Deggerich A, Wenzel D, Mutenda K, Wittmann JG, Rudolph MG, et al. TIP47 functions in the biogenesis of lipid droplets. The Journal of Cell Biology. 2009;185(4):641–55.

Bussell R, Eliezer D. A Structural and Functional Role for 11-mer Repeats in α-Synuclein and Other Exchangeable Lipid Binding Proteins. J Mol Biol. 2003 Jun;329(4):763–78.

Cases S, Stone S, Zhou P, Yen E, Tow B, Lardizabal KD, et al. Cloning of DGAT2, a second mammalian diacylglycerol acyltransferase, and related family members. J Biol Chem. 2001;276(42):38870–6.

Chen HC, Farese RV. Determination of adipocyte size by computer image analysis. J Lipid Res. 2002;43(6):986–9.

Chen W, Chang B, Wu X, Li L, Sleeman M, Chan L. Inactivation of Plin4 downregulates Plin5 and reduces cardiac lipid accumulation in mice. AJP: Endocrinology and Metabolism. 2013;304(7):E770–9

Cheng C, Geng F, Cheng X, Guo D. Lipid metabolism reprogramming and its potential targets in cancer. Cancer Commun. 2018;38(1):27.

Chitraju C, Walther TC, Farese RV. The triglyceride synthesis enzymes DGAT1 and DGAT2 have distinct and overlapping functions in adipocytes. Journal of lipid research. 2019 ;jlr.M093112.

Chorlay A, Monticelli L, Ferreira JV, M'barek KB, Ajjaji D, Wang S, et al. Membrane Asymmetry Imposes Directionality on Lipid Droplet Emergence from the ER. Developmental Cell. 2019 May 17;1–26.

Chorlay A, Thiam A-R. An Asymmetry in Monolayer Tension Regulates Lipid Droplet Budding Direction. Biophysj. 2018 Feb 6;114(3):631–40.

Chorlay A, Thiam A-R. Neutral lipids regulate amphipathic helix affinity for model lipid droplets. The Journal of Cell Biology. 2020 Mar 10;219(4):703–21.

Choudhary V, Ojha N, Golden A, Prinz WA. A conserved family of proteins facilitates nascent lipid droplet budding from the ER. The Journal of Cell Biology. 2015 Oct 26;211(2):261–71.

Cohen B-C, Shamay A, Argov-Argaman N. Regulation of Lipid Droplet Size in Mammary Epithelial Cells by Remodeling of Membrane Lipid Composition—A Potential Mechanism. Plos One. 2015;10(3):e0121645.

Čopič A, Antoine-Bally S, Giménez-Andrés M, Garay CT, Antonny B, Manni MM, et al. A giant amphipathic helix from a perilipin that is adapted for coating lipid droplets. Nat Commun. 2018;9(1):1–16.

Cornell R. Chemical cross-linking reveals a dimeric structure for CTP:phosphocholine cytidylyltransferase. J Biological Chem. 1989;264(15):9077–82.

Cotte AK, Aires V, Fredon M, Limagne E, Derangère V, Thibaudin M, et al. Lysophosphatidylcholine acyltransferase 2-mediated lipid droplet production supports colorectal cancer chemoresistance. Nat Commun. 2018;9(1):1–16.

Crooks GE, Hon G, Chandonia J-M, Brenner SE. WebLogo: A Sequence Logo Generator. Genome Res. 2004;14(6):1188–90.

Czabany T, Athenstaedt K, Daum G. Synthesis, storage and degradation of neutral lipids in yeast. Biochimica et Biophysica Acta (BBA) - Molecular and Cell Biology of Lipids. 2007;1771(3):299–309.

Czabany T, Wagner A, Zweytick D, Lohner K, Leitner E, Ingolic E, et al. Structural and biochemical properties of lipid particles from the yeast Saccharomyces cerevisiae. Journal of Biological Chemistry. 2008 Jun 20;283(25):17065–74.

Das KMP, Wechselberger L, Liziczai M, Rodriguez MD la R, Grabner GF, Heier C, et al. Hypoxia-inducible lipid droplet-associated protein inhibits adipose triglyceride lipase. J Lipid Res. 2018;59(3):531–41.

Daubert TE, Danner RP. Physical and thermodynamic properties of pure chemicals data compilation. 1989.

Defenouillère Q, Verraes A, Laussel C, Friedrich A, Schacherer J, Léon S. The induction of HAD-like phosphatases by multiple signaling pathways confers resistance to the metabolic inhibitor 2-deoxyglucose. Sci Signal. 2019;12(597):eaaw8000.

Delacotte J, Gourier C, Pincet F. Interfacial pressure and phospholipid density at emulsion droplet interface using fluorescence microscopy. Colloids Surfaces B Biointerfaces. 2014;117:545–8.

Der-Sarkissian A, Jao CC, Chen J, Langen R. Structural Organization of α-Synuclein Fibrils Studied by Site-directed Spin Labeling. Journal of Biological Chemistry. 2003;278(39):37530–5.

Doucet CM, Esmery N, Saint-Jean M de, Antonny B. Membrane Curvature Sensing by Amphipathic Helices Is Modulated by the Surrounding Protein Backbone. PLOS ONE. 2015;10(9):e0137965-23.

Drin G, Antonny B. Amphipathic helices and membrane curvature. FEBS Letters. 2010;584(9):1840–7.

Drin G, Casella J-F, Gautier R, Boehmer T, Schwartz TU, Antonny B. A general amphipathic α-helical motif for sensing membrane curvature. Nature Structural & Molecular Biology. 2007;14(2):138–46.

Egan JJ, Greenberg AS, Chang MK, Wek SA, Moos MC, Londos C. Mechanism of hormone-stimulated lipolysis in adipocytes: translocation of hormone-sensitive lipase to the lipid storage droplet. Proc National Acad Sci. 1992;89(18):8537–41.

Eisenberg D, Weiss RM, Terwilliger TC. The helical hydrophobic moment: a measure of the amphiphilicity of a helix. Nature. 1982;299(5881):371–4.

Ejsing CS, Sampaio JL, Surendranath V, Duchoslav E, Ekroos K, Klemm RW, et al. Global analysis of the yeast lipidome by quantitative shotgun mass spectrometry. Proceedings of the National Academy of Sciences of the United States of America. 2009;106(7):2136–41.

Ellman GL. Tissue sulfhydryl groups. Arch Biochem Biophys. 1959;82(1):70–7.

Exner T, Romero-Brey I, Yifrach E, Rivera-Monroy J, Schrul B, Zouboulis CC, et al. An alternative membrane topology permits lipid droplet localization of peroxisomal fatty acyl-CoA reductase 1. Journal of Cell Science. 2019 Mar 18;132(6):jcs223016-15.

Fauchère JL, Pliska V. HYDROPHOBIC PARAMETERS PI OF AMINO-ACID SIDE CHAINS FROM THE PARTITIONING OF N-ACETYL-AMINO AMIDES. Eur J Med Chem. 1983;(18):369–75.

Fernández-Vidal M, Jayasinghe S, Ladokhin AS, White SH. Folding Amphipathic Helices Into Membranes: Amphiphilicity Trumps Hydrophobicity. Journal of Molecular Biology. 2007 Jul;370(3):459–70.

Fredrikson G, Strålfors P, Nilsson NO, Belfrage and P. Hormone-sensitive lipase of rat adipose tissue. Purification and some properties. J Biol Chem. 1981;(256):6311.

Fu D, Yu Y, Folick A, Currie E, Farese RV, Tsai T-H, et al. In Vivo Metabolic Fingerprinting of Neutral Lipids with Hyperspectral Stimulated Raman Scattering Microscopy. J Am Chem Soc. 2014;136(24):8820–8.

Gao Q, Binns DD, Kinch LN, Grishin NV, Ortiz N, Chen X, et al. Pet10p is a yeast perilipin that stabilizes lipid droplets and promotes their assembly. The Journal of Cell Biology. 2017a ;181:jcb.201610013-19.

Gao G, Chen F-J, Zhou L, Su L, Xu D, Xu L, et al. Control of lipid droplet fusion and growth by CIDE family proteins. BBA - Molecular and Cell Biology of Lipids. 2017b; Jul 19;1–0.

Garcia A, Sekowski A, Subramanian V, Brasaemle DL. The Central Domain Is Required to Target and Anchor Perilipin A to Lipid Droplets. J Biol Chem. 2002;278(1):625–35.

Gautier R, Douguet D, Antonny B, Drin G. HELIQUEST: a web server to screen sequences with specific helical properties. Bioinformatics. 2008;24(18):2101–2.

Giaever G, Nislow C. The yeast deletion collection: a decade of functional genomics. Genetics. 2014;197(2):451–65.

Giménez-Andrés M, Čopič A, Antonny B. The Many Faces of Amphipathic Helices. Biomol. 2018;8(3):45.

Gluchowski NL, Becuwe M, Walther TC, Farese RV. Lipid droplets and liver disease: from basic biology to clinical implications. Nature Publishing Group. 2017 Apr 21;14(6):343–55.

Golczak M, Kiser PD, Sears AE, Lodowski DT, Blaner WS, Palczewski K. Structural basis for the acyltransferase activity of lecithin:retinol acyltransferase-like proteins. Journal of Biological Chemistry. 2012 Jul;287(28):23790–807.

Goldstein JL, Dana SE, Brown MS. Esterification of Low Density Lipoprotein Cholesterol in Human Fibroblasts and Its Absence in Homozygous Familial Hypercholesterolemia. Proc National Acad Sci. 1974;71(11):4288–92.

Gong J, Sun Z, Wu L, Xu W, Schieber N, Xu D, et al. Fsp27 promotes lipid droplet growth by lipid exchange and transfer at lipid droplet contact sites. J Cell Biology. 2011;195(6):953–63.

Granneman JG, Kimler VA, Zhang H, Ye X, Luo X, Postlethwait JH, et al. Lipid droplet biology and evolution illuminated by the characterization of a novel perilipin in teleost fish. eLife. 2017;6:799.

Greenberg AS, Egan JJ, Wek SA, Garty NB, Blanchette-Mackie EJ, Londos C. Perilipin, a major hormonally regulated adipocyte-specific phosphoprotein associated with the periphery of lipid storage droplets. Journal of Biological Chemistry. 1991 Jun 15;266(17):11341–6.

Greenfield NJ. Using circular dichroism spectra to estimate protein secondary structure. Nat Protoc. 2006;1(6):2876–90.

Grillitsch K, Connerth M, Köfeler H, Arrey TN, Rietschel B, Wagner B, et al. Lipid particles/droplets of the yeast Saccharomyces cerevisiae revisited: Lipidome meets Proteome. Biochimica et Biophysica Acta (BBA) - Molecular and Cell Biology of Lipids. 2011;1811(12):1165–76.

Gross DA, Silver DL. Cytosolic lipid droplets: From mechanisms of fat storage to disease. Critical Reviews in Biochemistry and Molecular Biology. 2014;49(4):304–26.

Gross DA, Zhan C, Silver DL. Direct binding of triglyceride to fat storage-inducing transmembrane proteins 1 and 2 is important for lipid droplet formation. Proceedings of the National Academy of Sciences of the United States of America. 2011 Dec 6;108(49):19581–6.

Gross DN, Miyoshi H, Hosaka T, Zhang H-H, Pino EC, Souza S, et al. Dynamics of Lipid Droplet-Associated Proteins during Hormonally Stimulated Lipolysis in Engineered Adipocytes: Stabilization and Lipid Droplet Binding of Adipocyte Differentiation-Related Protein/Adipophilin. Mol Endocrinol. 2006;20(2):459–66.

Guo Y, Walther TC, Rao M, Stuurman N, Goshima G, Terayama K, et al. Functional genomic screen reveals genes involved in lipid-droplet formation and utilization. Nature. 2008 Apr 13;453(7195):657–61.

Haider A, Wei Y-C, Lim K, Barbosa AD, Liu C-H, Weber U, et al. PCYT1A Regulates Phosphatidylcholine Homeostasis from the Inner Nuclear Membrane in Response to Membrane Stored Curvature Elastic Stress. Developmental Cell. 2018 May 7;1–24.

Hansen JS, x000E9 SM, Jones HA, ransson OG x000F6, Lindkvist-Petersson K. Visualization of lipid directed dynamics of perilipin 1 in human primary adipocytes. Sci Rep. 2017;7(1):1–14.

Henne WM, Reese ML, Goodman JM. The assembly of lipid droplets and their roles in challenged cells. The EMBO Journal. 2018;e98947-14.

Herbert AP, Riesen M, Bloxam L, Kosmidou E, Wareing BM, Johnson JR, et al. NMR Structure of Hsp12, a Protein Induced by and Required for Dietary Restriction-Induced Lifespan Extension in Yeast. PLOS ONE. 2012;7(7):e41975-12.

Hickenbottom SJ, Kimmel AR, Londos C, Hurley JH. Structure of a Lipid Droplet Protein. Structure. 2004;12(7):1199–207.

Hofbauer HF, Gecht M, Fischer SC, Seybert A, Frangakis AS, Stelzer EHK, et al. The molecular recognition of phosphatidic acid by an amphipathic helix in Opi1. The Journal of Cell Biology. 2018;154(9):jcb.201802027-3126.

Hoffman R, Grabińska K, Guan Z, Sessa WC, Neiman AM. Long-Chain Polyprenols Promote Spore Wall Formation in Saccharomyces cerevisiae. Genetics. 2017;genetics.300322.2017.

Holm C, Østerlund T, Laurell H, Contreras JA. M OLECULAR M ECHANISMS R EGULATING H ORMONE -S ENSITIVE L IPASE A ND L IPOLYSIS. Annu Rev Nutr. 2000;20(1):365–93.

Hsieh K, Lee YK, Londos C, Raaka BM, Dalen KT, Kimmel AR. Perilipin family members preferentially sequester to either triacylglycerol-specific or cholesteryl-ester-specific intracellular lipid storage droplets. Journal of Cell Science. 2012 Oct 27;125(17):4067–76.

Huh W-K, Falvo JV, Gerke LC, Carroll AS, Howson RW, Weissman JS, et al. Global analysis of protein localization in budding yeast. Nature. 2003;425(6959):686–91.

Jackson CL. Lipid droplet biogenesis. Current Opinion in Cell Biology. 2019;59:88–96.

Jacquier N, Choudhary V, Mari M, Toulmay A, Reggiori F, Schneiter R. Lipid droplets are functionally connected to the endoplasmic reticulum in Saccharomyces cerevisiae. Journal of Cell Science. 2011 Jun 27;124(14):2424–37.

Jacquier N, Mishra S, Choudhary V, Schneiter R. Expression of oleosin and perilipins in yeast promotes formation of lipid droplets from the endoplasmic reticulum. Journal of Cell Science. 2013;126(22):5198–209.

Jao CC, Hegde BG, Chen J, Haworth IS, Langen R. Structure of membrane-bound alpha-synuclein from site-directed spin labeling and computational refinement. Proceedings of the National Academy of Sciences of the United States of America. 2008 Dec 16;105(50):19666–71.

Kassan A, Herms A, Fernández-Vidal A, Bosch M, Schieber NL, Reddy BJN, et al. Acyl-CoA synthetase 3 promotes lipid droplet biogenesis in ER microdomains. The Journal of Cell Biology. 2013 Dec 23;203(6):985–1001.

Kaushik S, Cuervo AM. Degradation of lipid droplet-associated proteins by chaperone-mediated autophagy facilitates lipolysis. Nature Cell Biology. 2015 May 11;17(6):759–70.

Kimmel AR, Brasaemle DL, McAndrews-Hill M, Sztalryd C, Londos C. Adoption of PERILIPIN as a unifying nomenclature for the mammalian PAT-family of intracellular lipid storage droplet proteins. The Journal of Lipid Research. 2010;51(3):468–71.

Kimmel AR, Sztalryd C. The Perilipins: Major Cytosolic Lipid Droplet–Associated Proteins and Their Roles in Cellular Lipid Storage, Mobilization, and Systemic Homeostasis. Annual Review of Nutrition. 2016;36(1):471–509.

Klose C, Surma MA, Gerl MJ, Meyenhofer F, Shevchenko A, Simons K. Flexibility of a Eukaryotic Lipidome – Insights from Yeast Lipidomics. PLOS ONE. 2012;7(4):e35063-11.

Klug L, Daum G. Yeast lipid metabolism at a glance. FEMS Yeast Research. 2014;14(3):369–88.

Köffel R, Tiwari R, Falquet L, Schneiter R. The Saccharomyces cerevisiae YLL012/YEH1, YLR020/YEH2, and TGL1 Genes Encode a Novel Family of Membrane-Anchored Lipases That Are Required for Steryl Ester Hydrolysis. Mol Cell Biol. 2005;25(5):1655–68.

Koizume S, Miyagi Y. Lipid Droplets: A Key Cellular Organelle Associated with Cancer Cell Survival under Normoxia and Hypoxia. International Journal of Molecular Sciences. 2016;17(9):1430–23.

Kory N, Farese RV., Walther TC. Targeting Fat: Mechanisms of Protein Localization to Lipid Droplets. Trends in Cell Biology. 2016 Mar 16;26(7):1–12.

Kory N, Thiam A-R, Farese RV, Walther TC. Protein Crowding Is a Determinant of Lipid Droplet Protein Composition. Developmental Cell. 2015;34(3):351–63.

Krahmer N, Farese RV, Walther TC. Balancing the fat: lipid droplets and human disease. EMBO Molecular Medicine. 2013;5(7):973–83.

Krahmer N, Guo Y, Wilfling F, Hilger M, Lingrell S, Heger K, et al. Phosphatidylcholine Synthesis for Lipid Droplet Expansion Is Mediated by Localized Activation of CTP:Phosphocholine Cytidylyltransferase. Cell Metabolism. 2011 Oct 5;14(4):504–15.

Kuerschner L, Moessinger C, Thiele C. Imaging of Lipid Biosynthesis: How a Neutral Lipid Enters Lipid Droplets. Traffic. 2008;9(3):338–52.

Kulminskaya N, Oberer M. Protein-protein interactions regulate the activity of Adipose Triglyceride Lipase in intracellular lipolysis. Biochimie. 2019;1–7.

Laforest S, Labrecque J, Michaud A, Cianflone K, Tchernof A. Adipocyte size as a determinant of metabolic disease and adipose tissue dysfunction. Crit Rev Cl Lab Sci. 2015;52(6):301–13.

Lardizabal KD, Metz JG, Sakamoto T, Hutton WC, Pollard MR, Lassner MW. Purification of a jojoba embryo wax synthase, cloning of its cDNA, and production of high levels of wax in seeds of transgenic arabidopsis. Plant Physiology. 2000 Mar;122(3):645–55.

Li Z, Thiel K, Thul PJ, Beller M, Kühnlein RP, Welte MA. Lipid Droplets Control the Maternal Histone Supply of Drosophila Embryos. Curr Biol. 2012;22(22):2104–13.

Listenberger LL, Ostermeyer-Fay AG, Goldberg EB, Brown WJ, Brown DA. Adipocyte differentiation-related protein reduces the lipid droplet association of adipose triglyceride lipase and slows triacylglycerol turnover. J Lipid Res. 2007;48(12):2751–61.

Liu Q, Luo Q, Halim A, Song G. Targeting lipid metabolism of cancer cells: A promising therapeutic strategy for cancer. Cancer Letters. 2017;401:39–45.

Loewen CJR, Gaspar ML, Jesch SA, Delon C, Ktistakis NT, Henry SA, et al. Phospholipid metabolism regulated by a transcription factor sensing phosphatidic acid. Science. 2004;304(5677):1644–7.

Lu X, Gruia-Gray J, Copeland NG, Gilbert DJ, Jenkins NA, Londos C, et al. The murine perilipin gene: the lipid droplet-associated perilipins derive from tissue-specific, mRNA splice variants and define a gene family of ancient origin. Mamm Genome. 2001;12(9):741–9.

Luo J, Yang H, Song B-L. Mechanisms and regulation of cholesterol homeostasis. Nature Reviews Molecular Cell Biology. 2019;44:1–21.

M'barek KB, Ajjaji D, Chorlay A, Vanni S, Forêt L, Thiam AR. ER Membrane Phospholipids and Surface Tension Control Cellular Lipid Droplet Formation. Dev Cell. 2017 May 30;41(6):591-604.e7.

Mahamid J, Tegunov D, Maiser A, Arnold J, Leonhardt H, Plitzko JM, et al. Liquid-crystalline phase transitions in lipid droplets are related to cellular states and specific organelle association. Proceedings of the National Academy of Sciences of the United States of America. 2019 Aug 2;1862:201903642.

Massey JB, Bick DH, Pownall HJ. Spontaneous transfer of monoacyl amphiphiles between lipid and protein surfaces. Biophys J. 1997;72(4):1732–43.

McClements DJ, Gumus CE. Natural emulsifiers — Biosurfactants, phospholipids, biopolymers, and colloidal particles: Molecular and physicochemical basis of functional performance. Advances in Colloid and Interface Science. 2016 May 12;234:1–24.

McManaman JL, Zabaronick W, Schaack J, Orlicky DJ. Lipid droplet targeting domains of adipophilin. The Journal of Lipid Research. 2003;44(4):668–73.

Melchior JT, Walker RG, Cooke AL, Morris J, Castleberry M, Thompson TB, et al. A consensus model of human apolipoprotein A-I in its monomeric and lipid-free state. Nat Struct Mol Biol. 2017;24(12):1093–9.

Meyers NL, Larsson M, Olivecrona G, Small DM. A Pressure-dependent Model for the Regulation of Lipoprotein Lipase by Apolipoprotein C-II. The Journal of biological chemistry. 2015 Jul 17;290(29):18029–44.

Mirheydari M, Mann EK, Kooijman EE. Interaction of a model apolipoprotein, apoLp-III, with an oil-phospholipid interface. BBA - Biomembranes. 2017 Nov 22;1860(2):396–406.

Mitsche MA, Packer LE, Brown JW, Jiang ZG, Small DM, McKnight CJ. Surface tensiometry of apolipoprotein B domains at lipid interfaces suggests a new model for the initial steps in triglyceride-rich lipoprotein assembly. The Journal of biological chemistry. 2014 Mar 28;289(13):9000–12.

Mitsche MA, Small DM. C-Terminus of Apolipoprotein A-I Removes Phospholipids from a Triolein/ Phospholipids/Water Interface, but the N-Terminus Does Not: A Possible Mechanism for Nascent HDL Assembly. Biophysj. 2011 Jul 20;101(2):353–61.

Mitsche MA, Small DM. Surface pressure-dependent conformation change of apolipoprotein-derived amphipathic α-helices. The Journal of Lipid Research. 2013;54(6):1578–88.

Mitsche MA, Wang L, Small DM. Adsorption of Egg Phosphatidylcholine to an Air/Water and Triolein/Water Bubble Interface: Use of the 2-Dimensional Phase Rule To Estimate the Surface Composition of a Phospholipid/Triolein/Water Surface as a Function of Surface Pressure. J Phys Chem B. 2010;114(9):3276–84.

Mishra S, Schneiter R. Expression of perilipin 5 promotes lipid droplet formation in yeast. Commun Integr Biology. 2015;8(6):e1071728.

Miura S, Gan J-W, Brzostowski J, Parisi MJ, Schultz CJ, Londos C, et al. Functional Conservation for Lipid Storage Droplet Association among Perilipin, ADRP, and TIP47 (PAT)-related Proteins in Mammals, Drosophila , and Dictyostelium. J Biol Chem. 2002;277(35):32253–7.

Moessinger C, Kuerschner L, Spandl J, Shevchenko A, Thiele C. Human lysophosphatidylcholine acyltransferases 1 and 2 are located in lipid droplets where they catalyze the formation of phosphatidylcholine. J Biological Chem. 2011;286(24):21330–9.

Molenaar MR, Wassenaar TA, Yadav KK, Toulmay A, Mari MC, Caillon L, et al. Lecithin:Retinol Acyl Transferase (LRAT) induces the formation of lipid droplets. 2019 Aug 13;1862:176–38.

Murphy DJ. The dynamic roles of intracellular lipid droplets: from archaea to mammals. Protoplasma. 2011;249(3):541–85.

Nakagawa H, Hayata Y, Kawamura S, Yamada T, Fujiwara N, Koike K. Lipid Metabolic Reprogramming in Hepatocellular Carcinoma. Cancers. 2018;10(11):447–14.

Nakamura N, Fujimoto T. Adipose differentiation-related protein has two independent domains for targeting to lipid droplets. Biochemical and Biophysical Research Communications. 2003;306(2):333–8.

Nevin CS, Althouse PM, Triebold HO. Surface tension determinations of some saturated fat acid methyl esters. J Am Oil Chem Soc. 1951;28(8):325–7.

Olzmann JA, Carvalho P. Dynamics and functions of lipid droplets. Nature Publishing Group. 2018 Dec 5;1–19.

Orlicky DJ, DeGala G, Greenwood C, Bales ES, Russell TD, McManaman JL. Multiple functions encoded by the N-terminal PAT domain of adipophilin. Journal of Cell Science. 2008;121(17):2921–9.

Pace CN, Scholtz JM. A Helix Propensity Scale Based on Experimental Studies of Peptides and Proteins. Biophys J. 1998 Jul 1;75(1):422–7.

Pan L, Segrest JP. Computational studies of plasma lipoprotein lipids. Biochimica et Biophysica Acta (BBA) - Biomembranes. 2016 Oct 1;1858(10):2401–20.

Parker ML, Murphy GJ. Oleosomes in flag leaves of wheat; their distribution, composition and fate during senesence and rust-infection. Planta. 1981 May;152(1):36–43.

Pataki CI, Rodrigues J, Zhang L, Qian J, Efron B, Hastie T, et al. Proteomic analysis of monolayer-integrated proteins on lipid droplets identifies amphipathic interfacial α-helical membrane anchors. Proceedings of the National Academy of Sciences. 2018;128:201807981–9.

Paul A, Wang Y, Brännmark C, Kumar S, Bonn M, Parekh SH. Quantitative mapping of triacylglycerol chain length and saturation using broadband CARS microscopy. Biophys J. 2019;116(12):2346–55.

Payne F, Lim K, Girousse A, Brown RJ, Kory N, Robbins A, et al. Mutations disrupting the Kennedy phosphatidylcholine pathway in humans with congenital lipodystrophy and fatty liver disease. Proceedings of the National Academy of Sciences. 2014 Jun 17;111(24):8901–6.

Penno A, Hackenbroich G, Thiele C. Phospholipids and lipid droplets. Biochimica et Biophysica Acta (BBA) - Molecular and Cell Biology of Lipids. 2013 Mar;1831(3):589–94.

Pranke IM, Morello V, Bigay J, Gibson K, Verbavatz J-M, Antonny B, et al. α-Synuclein and ALPS motifs are membrane curvature sensors whose contrasting chemistry mediates selective vesicle binding. The Journal of Cell Biology. 2011;194(1):89–103.

Prévost C, Sharp ME, Kory N, Lin Q, Voth GA, Farese RV, et al. Mechanism and Determinants of Amphipathic Helix- Containing Protein Targeting to Lipid Droplets. Developmental Cell. 2018 Jan 8;44(1):73-86.e4.

Puri V, Ranjit S, Konda S, Nicoloro SMC, Straubhaar J, Chawla A, et al. Cidea is associated with lipid droplets and insulin sensitivity in humans. Proceedings of the National Academy of Sciences of the United States of America. 2008 Jun 3;105(22):7833–8.

Rey J, Deville J, Chabbert M. Structural determinants stabilizing helical distortions related to proline. Journal of Structural Biology. 2010 Sep 1;171(3):266–76.

Robenek H, Hofnagel O, Buers I, Robenek MJ, Troyer D, Severs NJ. Adipophilin-enriched domains in the ER membrane are sites of lipid droplet biogenesis. Journal of Cell Science. 2006;119(20):4215–24.

Rodriguez MA de la R, Kersten S. Regulation of lipid droplet-associated proteins by peroxisome proliferator-activated receptors. BBA - Molecular and Cell Biology of Lipids. 2017;1–0.

Rowe ER, Mimmack ML, Barbosa AD, Haider A, Isaac I, Ouberai MM, et al. Conserved Amphipathic Helices Mediate Lipid Droplet Targeting of Perilipins 1–3. Journal of Biological Chemistry. 2016;291(13):6664–78.

Ruggiano A, Mora G, Buxó L, Carvalho P. Spatial control of lipid droplet proteins by the ERAD ubiquitin ligase Doa10. The EMBO Journal. 2016;35(15):1644–55.

Ruggieri A, Naumenko S, Smith MA, Iannibelli E, Blasevich F, Bragato C, et al. Multiomic elucidation of a coding 99-mer repeat-expansion skeletal muscle disease. Acta Neuropathol. 2020;1–5.

Ruggles KV, Turkish A, Sturley SL. Making, Baking, and Breaking: the Synthesis, Storage, and Hydrolysis of Neutral Lipids. Annu Rev Nutr. 2013;33(1):413–51.

Rutkowski JM, Stern JH, Scherer PE. The cell biology of fat expansion. J Cell Biology. 2015;208(5):501–12.

Rydén M, Arner P. Cardiovascular risk score is linked to subcutaneous adipocyte size and lipid metabolism. Journal of Internal Medicine. 2017;282(3):220–8.

Salo VT, Li S, Vihinen H, Vuori MH, Szkalisity A, Horvath P, et al. Seipin Facilitates Triglyceride Flow to Lipid Droplet and Counteracts Droplet Ripening via Endoplasmic Reticulum Contact. Developmental Cell. 2019 Jun 7;1–26.

Sandager L, Gustavsson MH, Ståhl U, Dahlqvist A, Wiberg E, Banas A, et al. Storage Lipid Synthesis Is Non-essential in Yeast. Journal of Biological Chemistry. 2002;277(8):6478–82.

Scherer PE, Bickel PE, Kotler M, Lodish HF. Cloning of cell-specific secreted and surface proteins by subtractive antibody screening. Nature biotechnology. 1998;16(6):581–6.

Schott MB, Weller SG, Schulze RJ, Krueger EW, Drizyte-Miller K, Casey CA, et al. Lipid droplet size directs lipolysis and lipophagy catabolism in hepatocytes. The Journal of Cell Biology. 2019 Aug 7;38:jcb.201803153-16.

Schulze A, Harris AL. How cancer metabolism is tuned for proliferation and vulnerable to disruption. Nature. 2012;491(7424):364–73.

Schulze RJ, Sathyanarayan A, Mashek DG. Breaking fat_ The regulation and mechanisms of lipophagy. BBA - Molecular and Cell Biology of Lipids. 2017 Jun 30;1–0.

Segrest JP, Jackson RL, Morrisett JD, Gotto AM. A molecular theory of lipid-protein interactions in the plasma lipoproteins. FEBS Letters. 1974 Jan 15;38(3):247–58.

Segrest JP, Jones MK, Klon AE, Sheldahl CJ, Hellinger M, Loof HD, et al. A detailed molecular belt model for apolipoprotein A-I in discoidal high density lipoprotein. Journal of Biological Chemistry. 1999;274(45):31755–8.

Senkal CE, Salama MF, Snider AJ, Allopenna JJ, Rana NA, Koller A, et al. Ceramide Is Metabolized to Acylceramide and Stored in Lipid Droplets. Cell Metabolism. 2017 Mar 7;25(3):686–97.

Sherman F. Getting started with yeast. Methods in enzymology. 2002;350:3–41.

Sirwi A, Hussain MM. Lipid transfer proteins in the assembly of apoB-containing lipoproteins. J Lipid Res. 2018;59(7):1094–102.

Small DM, Wang L, Mitsche MA. The adsorption of biological peptides and proteins at the oil/water interface. A potentially important but largely unexplored field. Journal of Lipid Research. 2008 Dec 19;50(Supplement):S329–34.

Soni KG, Mardones GA, Sougrat R, Smirnova E, Jackson CL, Bonifacino JS. Coatomer-dependent protein delivery to lipid droplets. Journal of Cell Science. 2009 May 20;122(11):1834–41.

Sorger D, Athenstaedt K, Hrastnik C, Daum G. A Yeast Strain Lacking Lipid Particles Bears a Defect in Ergosterol Formation. J Biol Chem. 2004;279(30):31190–6.

Sorger D, Daum G. Synthesis of Triacylglycerols by the Acyl-Coenzyme A:Diacyl-Glycerol Acyltransferase Dga1p in Lipid Particles of the Yeast Saccharomyces cerevisiae. J Bacteriol. 2002;184(2):519–24.

Spanova M, Czabany T, Zellnig G, Leitner E, Hapala I, Daum G. Effect of Lipid Particle Biogenesis on the Subcellular Distribution of Squalene in the Yeast Saccharomyces cerevisiae. Journal of Biological Chemistry. 2010 Feb 19;285(9):6127–33.

Stauffer CE. The Measurement of Surface Tension by the Pendant Drop Technique. J Phys Chem. 1965;69(6):1933–8.

Stenkula KG, Erlanson-Albertsson C. Adipose cell size: importance in health and disease. American Journal of Physiology-Regulatory, Integrative and Comparative Physiology. 2018;315(2):R284–95.

Stetefeld J, McKenna SA, Patel TR. Dynamic light scattering: a practical guide and applications in biomedical sciences. Biophysical Rev. 2016;8(4):409–27.

Stone SJ, Levin MC, Farese RV. Membrane Topology and Identification of Key Functional Amino Acid Residues of Murine Acyl-CoA:Diacylglycerol Acyltransferase-2. J Biol Chem. 2006;281(52):40273–82.

Strandberg E, Grau-Campistany A, Wadhwani P, Bürck J, Rabanal F, Ulrich AS. Helix Fraying and Lipid-Dependent Structure of a Short Amphipathic Membrane-Bound Peptide Revealed by Solid-State NMR. J Phys Chem B. 2018 Jun 1;122(23):6236–50.

Straub BK, Stoeffel P, Heid H, Zimbelmann R, Schirmacher P. Differential pattern of lipid droplet-associated proteins and de novo perilipin expression in hepatocyte steatogenesis. Hepatology Baltim Md. 2008;47(6):1936–46.

Sui X, Arlt H, Brock KP, Lai ZW, DiMaio F, Marks DS, et al. Cryo–electron microscopy structure of the lipid droplet–formation protein seipin. The Journal of Cell Biology. 2018 Oct 16;jcb.201809067-12.

Sun Z, Gong J, Wu L, Li P. Imaging lipid droplet fusion and growth. Methods Cell Biol. 2013;116:253–68.

Suzuki M, Shinohara Y, Ohsaki Y, Fujimoto T. Lipid droplets: size matters. Microscopy. 2011;60(suppl 1):S101–16.

Sztalryd C, Brasaemle DL. The perilipin family of lipid droplet proteins_ Gatekeepers of intracellular lipolysis. BBA - Molecular and Cell Biology of Lipids. 2017;1862(Part B):1221–32.

Sztalryd C, Xu G, Dorward H, Tansey JT, Contreras JA, Kimmel AR, et al. Perilipin A is essential for the translocation of hormone-sensitive lipase during lipolytic activation. J Cell Biology. 2003;161(6):1093–103.

Tabibiazar M, Davaran S, Hashemi M, Homayonirad A, Rasoulzadeh F, Hamishehkar H, et al. Design and fabrication of a food-grade albumin-stabilized nanoemulsion. Food hydrocolloids. 2015 Feb 1;44(C):220–8.

Targett-Adams P, Chambers D, Gledhill S, Hope RG, Coy JF, Girod A, et al. Live Cell Analysis and Targeting of the Lipid Droplet-binding Adipocyte Differentiation-related Protein. Journal of Biological Chemistry. 2003;278(18):15998–6007.

Tauchi-Sato K, Ozeki S, Houjou T, Taguchi R, Fujimoto T. The Surface of Lipid Droplets Is a Phospholipid Monolayer with a Unique Fatty Acid Composition. Journal of Biological Chemistry. 2002 Nov 15;277(46):44507–12.

Thiam A-R, Antonny B, Wang J, Delacotte J, Wilfling F, Walther TC, et al. COPI buds 60-nm lipid droplets from reconstituted water-phospholipid-triacylglyceride interfaces, suggesting a tension clamp function. Proceedings of the National Academy of Sciences of the United States of America. 2013a Aug 13;110(33):13244–9.

Thiam A-R, Farese RV, Walther TC. The biophysics and cell biology of lipid droplets. Nature Publishing Group. 2013b Nov 13;14(12):775–86.

Thiam A-R, Forêt L. The physics of lipid droplet nucleation, growth and budding. BBA - Molecular and Cell Biology of Lipids. 2016 Aug 1;1861(Part A):715–22.

Tommaso PD, Moretti S, Xenarios I, Orobitg M, Montanyola A, Chang J-M, et al. T-Coffee: a web server for the multiple sequence alignment of protein and RNA sequences using structural information and homology extension. Nucleic Acids Res. 2011;39(suppl):W13–7.

Vigouroux C, Caron-Debarle M, Dour CL, Magré J, Capeau J. Molecular mechanisms of human lipodystrophies: From adipocyte lipid droplet to oxidative stress and lipotoxicity. International Journal of Biochemistry and Cell Biology. 2011;43(6):862–76.

Voynova NS, Vionnet C, Ejsing CS, Conzelmann A. A novel pathway of ceramide metabolism in Saccharomyces cerevisiae. Biochemical Journal. 2012 Sep 12;447(1):103–14.

Walther TC, Chung J, Farese RV. Lipid Droplet Biogenesis. Annual Review of Cell and Developmental Biology. 2017 Oct 6;33(1):491–510.

Walther TC, Farese RV. Lipid droplets and cellular lipid metabolism. Annu Rev Biochem. 2012 Jul 7;81(1):687–714.

Wang C-W. Lipid droplet dynamics in budding yeast. Cellular and Molecular Life Sciences. 2015a;72(14):2677–95.

Wang W, Wei S, Li L, Su X, Du C, Li F, et al. Proteomic analysis of murine testes lipid droplets. Sci Rep. 2015b;5(1):12070.

Wang H, Becuwe M, Housden BE, Chitraju C, Porras AJ, Graham MM, et al. Seipin is required for converting nascent to mature lipid droplets. eLife. 2016;5:440.

Wang H, Bell M, Sreenivasan U, Sreenevasan U, Hu H, Liu J, et al. Unique regulation of adipose triglyceride lipase (ATGL) by perilipin 5, a lipid droplet-associated protein. The Journal of biological chemistry. 2011a;286(18):15707–15.

Wang H, Sreenivasan U, Sreenevasan U, Hu H, Saladino A, Polster BM, et al. Perilipin 5, a lipid droplet-associated protein, provides physical and metabolic linkage to mitochondria. J Lipid Res. 2011b;52(12):2159–68.

Wang L, Walsh MT, Small DM. Apolipoprotein B is conformationally flexible but anchored at a triolein/water interface: A possible model for lipoprotein surfaces. Proc National Acad Sci. 2006;103(18):6871–6.

Wang S, Idrissi F-Z, Hermansson M, Grippa A, Ejsing CS, Carvalho P. Seipin and the membrane-shaping protein Pex30 cooperate in organelle budding from the endoplasmic reticulum. Nature Communications. 2018;9(1):1–12.

Wang Y-J, Bian Y, Luo J, Lu M, Xiong Y, Guo S-Y, et al. Cholesterol and fatty acids regulate cysteine ubiquitylation of ACAT2 through competitive oxidation. Nat Cell Biol. 2017;19(7):808–19.

Wilfling F, Thiam A-R, Olarte M-J, Wang J, Beck R, Gould TJ, et al. Arf1/COPI machinery acts directly on lipid droplets and enables their connection to the ER for protein targeting. eLife. 2014 Feb 4;3:604–20.

Wilfling F, Wang H, Haas JT, Krahmer N, Gould TJ, Uchida A, et al. Triacylglycerol Synthesis Enzymes Mediate Lipid Droplet Growth by Relocalizing from the ER to Lipid Droplets. Developmental Cell. 2013 Feb 25;24(4):384–99.

Wolins NE, Brasaemle DL, Bickel PE. A proposed model of fat packaging by exchangeable lipid droplet proteins. FEBS Letters. 2006a;580(23):5484–91.

Wolins NE, Quaynor BK, Skinner JR, Tzekov A, Croce MA, Gropler MC, et al. OXPAT/PAT-1 Is a PPAR-Induced Lipid Droplet Protein That Promotes Fatty Acid Utilization. Diabetes. 2006b;55(12):3418–28.

Wolins NE, Rubin B, Brasaemle DL. TIP47 associates with lipid droplets. J Biological Chem. 2000;276(7):5101–8.

Wolins NE, Skinner JR, Schoenfish MJ, Tzekov A, Bensch KG, Bickel PE. Adipocyte Protein S3-12 Coats Nascent Lipid Droplets. Journal of Biological Chemistry. 2003;278(39):37713–21.

Wurie HR, Buckett L, Zammit VA. Diacylglycerol acyltransferase 2 acts upstream of diacylglycerol acyltransferase 1 and utilizes nascent diglycerides and de novo synthesized fatty acids in HepG2 cells. Febs J. 2012;279(17):3033–47.

Xu G, Sztalryd C, Londos C. Degradation of perilipin is mediated through ubiquitination-proteasome pathway. Biochimica Et Biophysica Acta Bba - Mol Cell Biology Lipids. 2006;1761(1):83–90.

Yeung A, Dabros T, Masliyah J, Czarnecki J. Micropipette: a new technique in emulsion research. Colloids Surfaces Physicochem Eng Aspects. 2000;174(1–2):169–81.

Yeung T, Gilbert GE, Shi J, Silvius J, Kapus A, Grinstein S. Membrane phosphatidylserine regulates surface charge and protein localization. Science. 2008;319(5860):210–3.

Yu J, Li P. The size matters: regulation of lipid storage by lipid droplet dynamics. Sci China Life Sci. 2017;60(1):46–56.

Yu J, Zhang L, Li Y, Zhu X, Xu S, Zhou X-M, et al. The Adrenal Lipid Droplet is a New Site for Steroid Hormone Metabolism. PROTEOMICS. 2018 Dec 5;18(23):1800136–12.

Zechner R, Madeo F, Kratky D. Cytosolic lipolysis and lipophagy: two sides of the same coin. Nat Rev Mol Cell Bio. 2017;18(11):671–84.

Zechner R, Zimmermann R, Eichmann TO, Kohlwein SD, Haemmerle G, Lass A, et al. FAT SIGNALS - Lipases and Lipolysis in Lipid Metabolism and Signaling. Cell Metabolism. 2012 Mar 7;15(3):279–91.

Zhang P, Meng L, Song L, Du J, Du S, Cui W, et al. Roles of Perilipins in Diseases and Cancers. Current Genomics. 2018;19(4):247–57.

Zimmermann L, Stephens A, Nam S-Z, Rau D, Kübler J, Lozajic M, et al. A Completely Reimplemented MPI Bioinformatics Toolkit with a New HHpred Server at its Core. J Mol Biol. 2018;430(15):2237–43.

Zimmermann R, Strauss JG, Haemmerle G, Schoiswohl G, Birner-Gruenberger R, Riederer M, et al. Fat Mobilization in Adipose Tissue Is Promoted by Adipose Triglyceride Lipase. Science. 2004;306(5700):1383–6.

Zweytick D, Leitner E, Kohlwein SD, Yu C, Rothblatt J, Daum G. Contribution of Are1p and Are2p to steryl ester synthesis in the yeast Saccharomyces cerevisiae: Are1p and Are2p of the yeast Saccharomyces cerevisiae. Eur J Biochem. 2000;267(4):1075–82.

ANNEXES

biomolecules

MDPI

Review

The Many Faces of Amphipathic Helices

Manuel Giménez-Andrés [1,2], Alenka Čopič [1,*] and Bruno Antonny [3,*]

1 Institut Jacques Monod, CNRS, UMR 7592, Université Paris Diderot, Sorbonne Paris Cité, 75013 Paris, France; manuel.gimenezandres@ijm.fr
2 Université Paris-Sud, Université Paris-Saclay, 91405 Orsay, France
3 Université Côte d'Azur, CNRS, IPMC, 06560 Valbonne, France
* Correspondence: alenka.copic@ijm.fr (A.Č.); antonny@ipmc.cnrs.fr (B.A.); Tel.: +33-1-57-27-80-06 (A.Č.); +33-4-93-95-77-75 (B.A.)

Received: 30 May 2018; Accepted: 2 July 2018; Published: 5 July 2018

Abstract: Amphipathic helices (AHs), a secondary feature found in many proteins, are defined by their structure and by the segregation of hydrophobic and polar residues between two faces of the helix. This segregation allows AHs to adsorb at polar–apolar interfaces such as the lipid surfaces of cellular organelles. Using various examples, we discuss here how variations within this general scheme impart membrane-interacting AHs with different interfacial properties. Among the key parameters are: (i) the size of hydrophobic residues and their density per helical turn; (ii) the nature, the charge, and the distribution of polar residues; and (iii) the length of the AH. Depending on how these parameters are tuned, AHs can deform lipid bilayers, sense membrane curvature, recognize specific lipids, coat lipid droplets, or protect membranes from stress. Via these diverse mechanisms, AHs play important roles in many cellular processes.

Keywords: amphipathic helix; membrane deformation; membrane curvature sensor; ALPS motif; phosphatidic acid; lipid packing defect; perilipin; LEA protein; membrane targeting; desiccation

1. Introduction

Amphipathic helices (AHs) are protein sequences that fold into a helical structure upon contact with a polar/non-polar interface. They can be found in many stably folded proteins. However, in this review we will focus solely on AHs that fold in contact with the surface of a bilayer-bound organelle or a lipid droplet inside the cell [1,2]. In such sequences, hydrophobic amino-acids (aa) are regularly distributed every N + 3 and/or N + 4 positions with polar residues in between, thereby allowing the helix to present two faces with opposite chemical features: a hydrophobic face and a polar face. Owing to this segregation, the helix lays down parallel to the membrane interface and anchors the protein in a reversible manner.

Since the development of pioneering studies on amphipathic helical regions in apolipoproteins and secreted antimicrobial peptides [2–4], the field of AHs has flourished, with the discovery that many eukaryotic, viral, or bacterial proteins contain AHs which contribute to intracellular membrane targeting, sometimes in combination with other modes of protein–membrane interaction [2,5]. Furthermore, studies have revealed that many AHs act not only as membrane anchors but also fulfill other functions owing to their extended contact with membrane interfaces. These include sensing membrane curvature and the level of lipid unsaturation [6], remodeling membranes into tubular or spherical intermediates [7,8], or acting as a shield to protect membranes or lipid droplets [9,10].

In this review, we use a few examples of membrane-adsorbing AHs to illustrate how variations in length and amino-acid sequence (Figure 1) provide AHs with different interfacial properties and, thereby, different cellular functions (Figure 2). This is because the repertoire of hydrophobic and polar

residues is vast enough to allow the synthesis of helices that, apart from their amphipathic character, differ considerably in their possible interfacial interactions. To facilitate their comparison, the AHs are represented with a normalized scheme that aims to highlight their distinguishing features (Figure 1). However, it should be noted that neither the structure of these AHs nor their position at the lipid interface is known in most cases. Thus, these drawings should be taken as working models, not as definitive pictures.

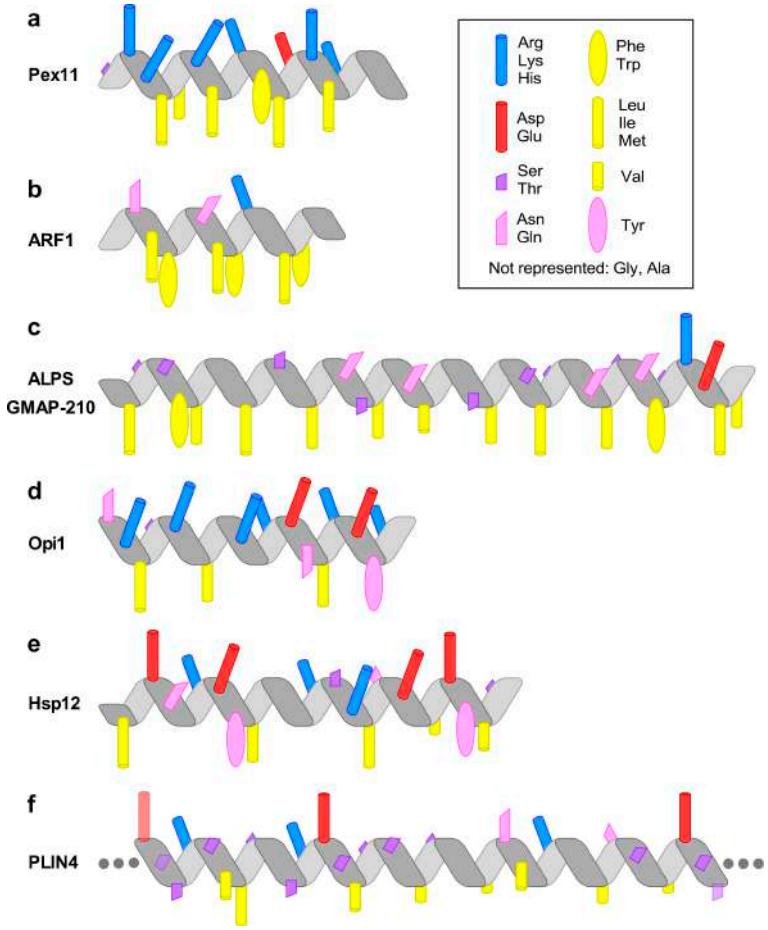

Figure 1. The chemical diversity of amphipathic helices (AHs). The diagrams highlight the most prominent chemical features of the AHs discussed in the text. (**a**) The AH of Pex11 has a highly basic polar face and a prominent hydrophobic face (amino-acids (aa) 66–83 of *Penicillium chrysogenum* Pex11). (**b**) The AH of the small G protein ARF1 contains two bulky hydrophobic residues per helical turn (aa 2–14, human protein). (**c**) The amphipathic lipid packing sensor (ALPS) motif of the golgin GMAP-210 contains one bulky hydrophobic residue per helical turn and is rich in Ser, Thr, and Gly in its polar face (aa 1–38, human protein). (**d**) The AH of Opi1 contains basic residues in its polar face, which have been proposed to bind preferentially to the negatively charged phosphatidic acid (PA) (aa 111–128, *Saccharomyces cerevisiae* protein). (**e**) The four AHs of heat-shock protein-12 (Hsp12) contain both positively and negatively charged residues. The positively charged residues form two wings at the polar/non-polar interface, whereas the negatively charged residues are concentrated in the center of the polar face. The longest helix, helix 4 (aa 74–97 in the *S. cerevisiae* protein), is shown. (**f**) Perilipin 4 (PLIN4) contains a giant and highly repetitive AH of about 1000 aa. The drawing schematizes the chemistry of a single human 33-mer repeat. Large hydrophobic residues are absent from this AH. Instead, the hydrophobic face is rich in Ala, Val, and Thr residues. The polar face contains both positively and negatively charged residues, with the positive charge concentrated on one side of the AH.

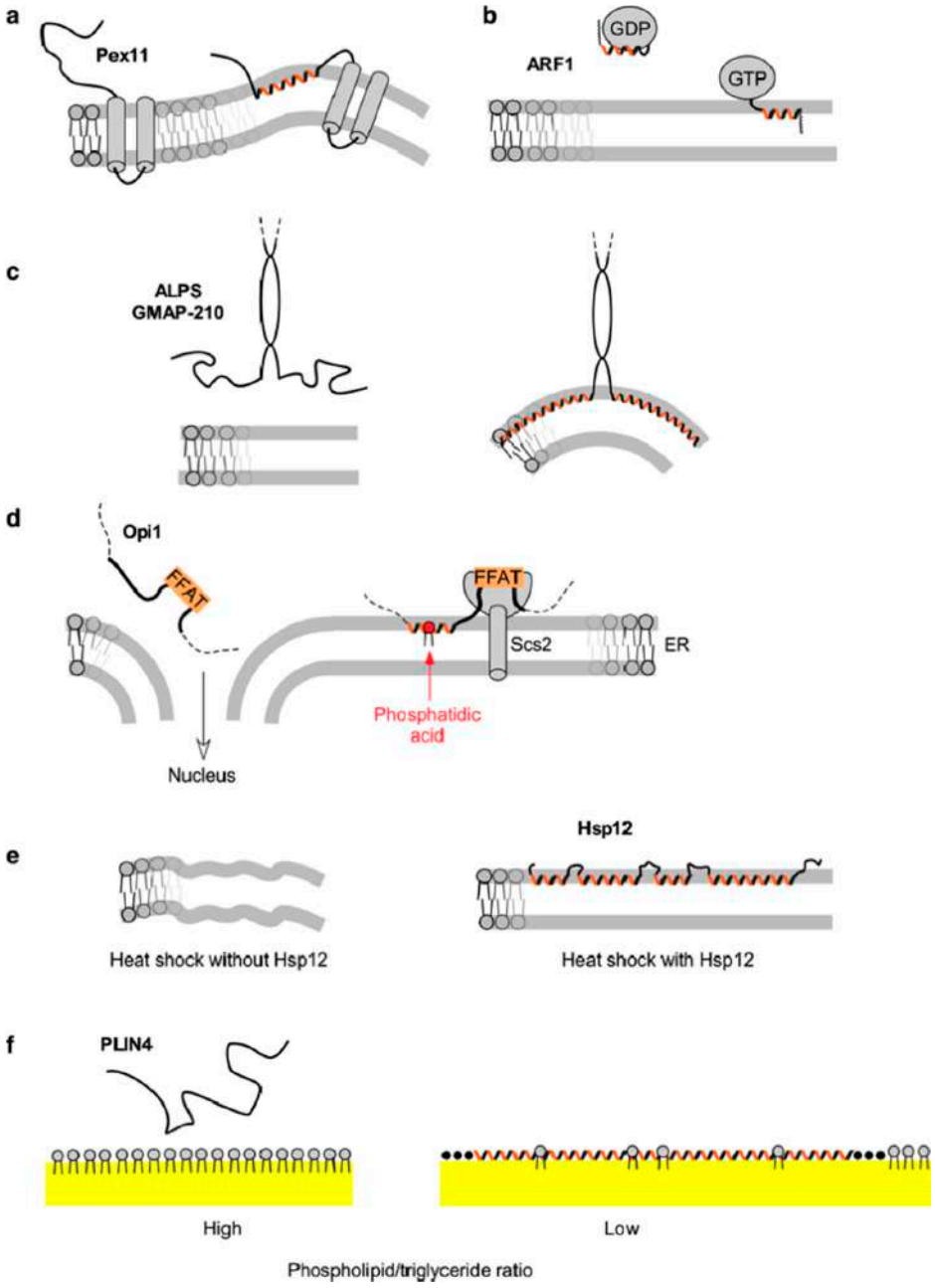

Figure 2. Functional diversity of AHs. This figure illustrates the cellular roles of the AHs shown in Figure 1. (**a**) Membrane deformation induced by the AH of the peroxisomal membrane protein Pex11. (**b**) Guanosine diphosphate/guanosine triphosphate (GDP/GTP) exchange in ARF1 controls the exposure of its AH and thereby the translocation of this small G protein to lipid membranes. (**c**) The ALPS motif of the golgin GMAP-210 captures small vesicles on the basis of their high curvature. (**d**) The yeast transcriptional repressor Opi1 is retained at the endoplasmic reticulum (ER) membrane through its dual interaction with PA and the ER receptor Scs2 (member of the VAP protein family), via an AH and a FFAT motif, respectively. When the amount of PA decreases, Opi1 is released from the ER and is translocated to the nucleus where it represses genes involved in lipid synthesis. (**e**) The adsorption of the large AH region of the heat shock protein Hsp12 has a protective effect on the plasma membrane by adjusting its physical properties. (**f**) The giant AH of PLIN4 coats lipid droplets under conditions of insufficient phospholipids by directly substituting the phospholipid monolayer.

2. Predictions and Experimental Approaches to Study Amphipathic Helices

The analysis of AHs is facilitated by bioinformatics tools such as Heliquest [11] which project any amino-acid sequence onto a helical wheel and calculate various parameters such as AH hydrophobicity, charge, and hydrophobic moment (an index of the amphipathic character of the putative helix). Note that some AHs slightly depart from the archetypal α-helical structure, which contains 3.6 aa per turn. These so-called 3–11 helices contain 3.67 aa/turn (giving an integer number of 11 aa for three turns) and are generally associated with extended sequences made of repetitions of 11, 22, or 33 aa present in apolipoproteins [4], synucleins [12], and perilipins, respectively [10].

Even though the bioinformatics approach is helpful in order to identify, characterize, and mutagenize some putative AHs, it does not provide proof of AH formation. Furthermore, the AH structure requires an appropriate but poorly defined amino-acid sequence interacting with a hydrophobic interface. Many membrane-interacting AH sequences have a low probability of α-helical formation and are in fact intrinsically unstructured in solution owing to an abundance of Gly, which increases conformational freedom. Only when facing an appropriate interface do they adsorb and fold into a helix [1,2].

The structures of membrane-binding AHs are generally less well-established than those of helices in stably-folded protein domains because of the difficulty in crystallizing proteins in an interfacial environment. However, a combination of site-directed mutagenesis and spectroscopic and biochemical methods can give reasonable clues about the relevance of a predicted AH (for a typical example, see [13]). Among these methods are: (i) liposome–protein binding assays, in which the fraction of bound protein is recovered by flotation or sedimentation; (ii) circular dichroism (CD) spectroscopy to assess the ability of the sequence of interest to fold into a helical structure; and (iii) various fluorescence methods to probe the environment of selected intrinsic residues (e.g., tryptophan) or extrinsic probes such as 7-nitrobenz-2-oxa-1,3-diazol-4-yl (NBD). Binding assays at the level of single liposomes represent a more sophisticated type of analysis [14].

Deeper structural analysis of AHs is sometimes performed but requires more advanced approaches. Various nuclear magnetic resonance (NMR) methods allow for the visualization of the structure and aa environment of AHs in membrane mimetic systems such as bicelles, which are discoidal lipid bilayer patches [15], or, more classically, in detergent (e.g., sodium dodecyl sulfate—SDS) micelles [16]. However, the small size of micelles can lead to helix breakage (discussed in [17]). X-ray diffraction in the presence of model bilayer membranes gives information about the time averaged density of AH atoms across the bilayer normal [18]. In the case of the apolipoprotein A-I, this method indicates that the axis of the helix is positioned at the level of the glycerol atoms, almost exactly between the polar and non-polar region of the bilayer, whereas large hydrophobic residues insert as far as the middle of the lipid acyl chains. Finally, in site-directed spin labeling, selected aa along the sequence are mutated into Cys, which are then labelled with spin probes to give information about the position of aa relative to the membrane surface by electron paramagnetic resonance spectroscopy [9,17]. A most spectacular example is the structural characterization of α-synuclein, in which aa from positions 25 to 90 was sequentially labeled, leading to a high-resolution reconstruction of a continuous helix that extends parallel to a phospholipid membrane with a 3–11 helical periodicity [17].

These various biophysical methods give details about the depth of insertion of the AH into the membrane, which can be decisive for understanding its impact on membrane organization (e.g., curvature) [16–18]. However, one difficulty in structural studies is finding a model membrane system that is simple enough to be compatible with physical measurements, and yet similar enough to an authentic membrane. Due to their small size and highly charged surface, SDS micelles can lead to artefactual protein conformations (as discussed in [17]). As illustrated by the few examples discussed below, much information stems from experiments on liposomes of defined size and lipid composition; however, inappropriate liposome composition or concentration can likewise produce experimental artefacts.

Molecular dynamics simulations can give some plausible mechanisms for how the AH sequence adsorbs and folds at an interface. In the few examples that have been studied so far, a few hydrophobic residues start inserting into the membrane in a random manner, followed by a gradual increase in AH folding and by the coalescence of the cavities hosting the hydrophobic residues [19–21]. Therefore, the final footprint of the helix in the membrane is much larger than the lipid packing defects initially present at the interface. However, AH folding at membrane interfaces is a slow process at the scale of molecular dynamics and has been poorly characterized so far.

3. Pex11 and Membrane Deformation

Pex11 is a conserved peroxisomal protein whose expression level modulates the number of peroxisomes in a cell [22]. It induces tubulation of peroxisomal membranes, which is followed by a fission step performed by the dynamin-related GTPase Dnm1 [23]. Pex11 contains an AH in its N-terminal part, followed by two predicted transmembrane helices (Figures 1a and 2a). The AH has a well-developed hydrophobic face and a polar face rich in positively charged aa (Figure 1a). In vitro, it binds significantly better to liposomes containing negatively charged lipids that mimic the peroxisomal membrane as compared to neutral phosphatidylcholine (PC) liposomes [24]. Mutational analysis indicates that both hydrophobic and electrostatic interactions contribute to this binding. Amphipathic helices peptides from diverse yeast species as well as from the human Pex11 orthologue induce strong tubulation of negatively charged liposomes [24]. Similarly, tubulation of peroxisomes in the yeast *Hansenula polymorpha* lacking Dnm1 depends on Pex11 AH [24], and there is a similar requirement for Pex11β in human cells [25]. However, in addition to the amphipathic character of Pex11 AH, oligomerization may also contribute to its tubulation activity [25–27].

There are many proteins that shape membranes by a mechanism similar to that described for Pex11. In general, their AH is relatively short, has a strong hydrophobic moment, and acts in concert with other structural elements that position the helix close to the membrane surface. The large GTPase atlastin, which mediates endoplasmic reticulum (ER) membrane fusion, contains two transmembrane segments flanked by the GTPase domain and by an AH on the N-terminal and C-terminal ends, respectively. The AH hydrophobic face is rich in aromatic aa, whereas the polar face contains three basic and three acidic residues, with a resulting high hydrophobic moment [28]. This AH participates in ER membrane fusion by destabilizing the lipid bilayer. Although the mechanism is still uncertain, it was proposed that the AH insertion causes the displacement of the negatively charged phospholipid heads, leading to exposure of their hydrocarbon chains and bilayer destabilization. Facilitation of fusion also occurs when the AH is separated from the rest of atlastin, but in that case a 50-fold higher AH concentration is required, highlighting the advantage of having the AH within the same protein chain [28].

A recent publication demonstrates that a similar mechanism is involved in mitochondrial fusion, specifically the fusion of outer mitochondrial membranes that is mediated by mitofusins, large GTPases similar to atlastin [29]. Like in the case of atlastin, mitofusin-mediated mitochondrial fusion requires a conserved AH adjacent to the transmembrane domains that dock mitofusin in the mitochondrial membrane. This AH is similar in character to that of atlastin, although it contains even higher amounts of charged residues and no aromatic residues. Notably, it lacks any Gly residues and accordingly is quite helical even in the absence of membranes. The authors propose that, like in atlastin, this AH acts to destabilize the mitochondrial bilayer. Interestingly, a chimeric mitofusin containing the transmembrane domains of atlastin is targeted to the ER instead of the mitochondria and can at least partially restore the ER morphology in yeast lacking the atlastin orthologue [30]. This group identified another AH on the other side of the mitofusin transmembrane domains, but the role of this segment is less clear. Given the rather different lipid compositions of ER and mitochondrial membranes, it will be interesting to see to what extent the functions of these two large GTPases, and in particular their AHs, overlap.

Endocytosis is one of the best characterized mechanisms of membrane deformation in vivo and in vitro. Central to membrane deformation in endocytosis are BAR domain-containing proteins, which through their banana shape and positively concave face interact electrostatically with the lipid bilayer and deform it. Some of these BAR domains are flanked by AHs. Amphipathic helices are also present in other endocytic proteins such as epsin. The relative contribution of BAR domains and AHs in membrane binding, deformation, and fission is a matter of debate [7,8,31,32]. More recently, protein crowding has been evoked as another mechanism of membrane deformation [33,34]. In the crowding regime, an AH may act as a membrane anchor but is not required for destabilizing the bilayer; for example, Stachowiak et al. demonstrated that an epsin mutant whose AH was replaced by a His-tag was also sufficient to deform liposomes [33]. Careful work will be needed to determine how these different effects combine in the complex cellular environment.

4. ARF1—A Small Amphipathic Helix Regulated by a GDP/GTP Switch

The small G protein ARF1 is involved in intracellular vesicle trafficking [35]. It is myristoylated on its N-terminal Gly, followed by a small AH of 14 a.a. The hydrophobic face of the AH is highly developed, with one pair of strong hydrophobic residues per turn (Leu–Phe or Ile–Phe) (Figure 1b). When ARF1 is in the guanosine diphosphate (GDP) state, the AH is folded, with the hydrophobic residues pointing towards the protein core. Upon activation by a nucleotide exchange factor, which promotes the replacement of GDP by guanosine triphosphate (GTP), the AH can no longer interact with the protein core and instead extends on membrane surface [15]. Thus, GDP/GTP exchange controls ARF1 interaction with lipid membranes (Figure 2b). The interaction of ARF1–GTP with model membranes is very strong, with a spontaneous dissociation rate in the order of minutes. When hydrophobic residues of the AH are mutated to Ala, the membrane interaction of ARF1–GTP is reduced [34]. Importantly, ARF1–GTP can bind to most interfaces including lipid bilayers of different curvature and lipid composition (saturated/unsaturated, charged/neutral) as well as to lipid droplets covered by phospholipids, but not to liquid-ordered domains [36–39]. In the cell, ARF1 localization is therefore controlled by the distribution of exchange factors, among which many reside at the Golgi [35].

The coupling between GDP/GTP switch and AH exposure allows ARF1 to control the membrane recruitment of numerous effectors [35]. In some cases, this process is followed by membrane deformation. Thus, ARF1 and cognate proteins such as SAR1 drive the recruitment of protein coats, which polymerize into a spherical shell to promote vesicle formation. The high surface density of the AHs of ARF1/SAR1 under coat formation contributes, in combination with other factors (i.e., coat structure and protein crowding), to membrane shaping [40–46].

5. The Amphipathic Lipid Packing Sensor Motif: Amphipathic Helices with Sparse Hydrophobic Residues to Sense Membrane Curvature

Amphipathic lipid packing sensors (ALPS) are AHs characterized by a polar face made of small polar residues, notably Ser, Thr, and Gly (Figure 1c). Furthermore, due to a lack of charged residues in the polar face, electrostatic interactions do not participate in the interaction of ALPS motifs with membranes. Instead, membrane adsorption is driven by the hydrophobic effect. Amphipathic lipid packing sensor motifs are very sensitive to both lipid unsaturation and membrane curvature, and therefore bind poorly to most membranes, except those containing a high amount of monounsaturated lipids (e.g., C16:0–C18:1–PC) and a high curvature (radius < 50 nm) [47,48] (Figure 2c). Several mutagenesis studies indicate that the atypical amino-acid composition of ALPS motifs is critical for their dual sensitivity. Thus, mutating an ALPS motif with two Lys close to the polar/non-polar interface causes a loss in the specificity for curved membranes due to electrostatic interactions [6].

A more recent study suggests that another key factor for membrane curvature sensing lies in the sparse distribution of the large hydrophobic residues in the AH [49]. In contrast to the AH of ARF1, which contains two hydrophobic residues per turn, the ALPS motif of the Golgi tether

GMAP-210 (Golgi-microtubule-associated protein 210) contains one hydrophobic residues per turn (Figure 1b,c). Condensing the ALPS motif of GMAP-210 to pair up its hydrophobic residues makes the resulting AH more promiscuous: in vitro, it binds to liposomes regardless of their curvature; in the cell, it can no longer specifically recognize small vesicles over flat organelle surfaces, in particular lipid droplets [49]. The AH of GMAP-210 is therefore optimized for trapping small neutral vesicles that transport proteins between the ER and the Golgi apparatus. This selectivity can be demonstrated by introducing synthetic vesicles into living cells: these vesicles accumulate around the Golgi as a function of their physico-chemical properties in a GMAP-210-dependant manner, or can be even targeted to the mitochondria using a mitochondrially-targeted GMAP-210 construct [49].

6. Specific Recognition of Lipids by Amphipathic Helices: Opi1 and Other Examples

By being embedded at the interface between the polar and non-polar regions of membranes, AHs necessarily contact many lipids. The question then arises as to whether AH insertion is solely driven by bulk membrane properties (notably lipid packing defects and electrostatics) or whether specific interactions with defined lipid species also contribute to AH binding.

The binding of the yeast transcriptional repressor Opi1 to the ER membrane depends on phosphatidic acid (PA) and on the interaction of Opi1 with the ER protein Scs2, member of the VAP protein family [50,51] (Figures 1d and 2d). In the absence of PA, Opi1 translocates to the nucleus where it represses several genes involved in membrane lipid biogenesis [50,52]. Opi1 senses PA with an AH that has a positively charged polar face rich in Lys [53] (Figure 1d). Depending on its membrane environment, PA displays one or two negative charges [54]. To determine if the binding of Opi1 AH to membranes is driven by electrostatics or by stereospecific interactions, its membrane affinity was tested on liposomes containing increasing concentrations of PA or phosphatidylserine (PS), for example 20% PA or 40% PS to maintain a similar net charge. Interestingly, Opi1 AH interacted more strongly with the PA-containing liposomes, suggesting a stereospecific interaction with PA [53] (Figure 1d).

Using molecular dynamic simulations, Hofbauer et al. identified two motifs that contributed to the preference of the Opi1 AH for PA versus other negatively charged lipids [53]: one composed of three Lys and the second of Lys-Arg-Lys. Each motif forms a three-finger grip that is able to accommodate the small polar head of PA but not the larger polar head of PS. When all Lys are mutated to Arg, the AH can no longer distinguish between PA and PS.

The AH of the yeast protein Spo20 is also sensitive to PA levels. It has a polar face very rich in basic residues, including three His, displaying a chemistry that is strikingly different from that of Opi1 AH [55]. Whereas Spo20 AH was suggested to specifically recognize PA in membranes, careful in vivo and in vitro analysis revealed that this AH is primarily sensitive to lipid charge, independent of the exact nature of the anionic lipids present [56]. Indeed, once the differences in charge of PA and other negative lipids are corrected, the affinity of Spo20 AH for PA, PS, or phosphatydilinositol 4 phosphate-containing liposomes is remarkably similar [56]. Therefore, the use of Spo20 as a reporter for the quantity of PA in membranes should be taken with caution (for further reading on PA sensing, see [57]). In the future, an artificial helix with several (Lys)3 and Lys–Arg–Lys motifs, inspired by the Opi1 AH, could be developed to a get a more specific fluorescent reporter for PA in cellular membranes.

Cholesterol represents a very different kind of membrane lipid, but one whose concentration in cellular membranes highly varies and is carefully regulated. It can specifically interact with membrane proteins to regulate their function by filling a selective cholesterol-binding pocket [58], but it is less clear whether an AH could specifically contact a cholesterol molecule embedded in a bilayer. Chua et al. recently proposed an intriguing hypothesis for squalene monooxygenase (SM), an enzyme in the biosynthetic pathway of cholesterol located at the ER [59]. In the presence of excess cholesterol, SM is degraded. A small AH of 12 aa is present in the SM sequence, containing several large hydrophobic residues and a poorly developed polar face. A combination of mutagenesis data, molecular dynamics simulations, and CD measurements suggests a feedback model, whereby the AH is embedded in the ER membrane at low cholesterol but becomes displaced and unfolds in the cytosol

when cholesterol concentration increases. The authors propose that the AH displacement is caused by the membrane becoming thicker and more condensed due to cholesterol increase, with cholesterol therefore indirectly but specifically regulating AH binding. Together with an upstream disordered region, the unfolded AH then signals through the ubiquitination-proteasome system, inducing SM degradation [59]. However, the mechanism by which the AH of SM senses cholesterol levels awaits further investigation.

In plants, the 140K replication protein of the turnip yellow mosaic virus precisely targets the outer chloroplast membrane during viral replication. The 140K replication protein contains two short AHs, separated by a short loop. Both AHs have a high hydrophobic moment due to a well-developed hydrophobic face containing two aromatic residues, and a polar face that is positively charged. The two AHs have been shown to specifically target the outer chloroplast membrane in vivo [60]. This targeting can occur even when one or the other AH is mutated, suggesting that the two AHs may be at least partially redundant for targeting. Because the outer membrane of the chloroplast contains unique lipids, notably sulfolipids and mono- and di-galactosyldiacylglycerol, further investigations are now needed to assess whether specific interactions may exist between these AHs and these unique lipids, or whether the lipids impart particular bulk properties on the outer chloroplast membrane.

7. Amphipathic Helices that Respond to Environmental Changes: Small Heat-Shock Protein Hsp12

Whereas membranes of warm-blooded animals generally do not experience large fluctuations in physical environmental conditions, membranes of microorganisms and plants have to be able to adapt to changes in temperature and humidity. This can happen through changes in membrane lipid composition or accumulation of dissacharides, notably trehalose. Recent work suggests that binding of peripheral proteins may be another important way of changing membrane physical properties by which a variety of cells cope with a varying environment. An interesting example is the small heat shock protein Hsp12 in yeast, which rescues cell growth under various stress conditions by stabilizing the plasma membrane [9]. Like many other heat shock proteins, Hsp12 is present in cells at a low copy number under standard growth conditions but can be induced more than 100-fold by harsh conditions. However, Hsp12 does not appear to interact with other proteins, and is in fact disordered in solution. Instead, it can bind directly to the plasma membrane via four independently-folding non-interacting AHs that represent the majority of its 109 aa sequence, and its binding was shown to increase the stability of model membranes [9,16] (Figures 1e and 2e).

Expression of intrinsically disordered proteins, many of which have been demonstrated to fold into AHs in contact with membranes, is in fact emerging as a widespread mechanism of coping with fluctuations in physical environmental conditions. Late embryogenesis abundant (LEA) proteins represent a large group with members identified in plants and also in some invertebrate animals [61]. Among these, members of the dehydrin family are particularly interesting: these are modular proteins with a very particular amino-acid composition that protect plants against drought and cold. Several of them have been shown to contain a series of short but strong AHs that fold on synthetic membranes, for example dehydrin K2 from *Vitis riparia* (frost grape) [62]. This protein can protect liposomes against fusion during freeze-thaw cycles and can lower membrane phase transition temperature. Another member of the family, Lti30, is found in *Arabidopsis*. The presence of short lipid-induced AHs in Lti30 has been confirmed by NMR, and this protein also reduced lipid phase transition of model membranes [63,64]. Also in *Arabidopsis*, cold-regulated (COR) proteins target and stabilize mitochondrial or chloroplast membranes, possibly via poorly-hydrophobic AH sequences [65,66]. Striking examples from the animal kingdom are LEA proteins from the brine shrimp *Artemia franciscana*, which contain long predicted AHs of more than 100 aa and protect liposomes against desiccation, especially in combination with trehalose [67]. Finally, a number of disordered proteins have been identified in the unicellular tardigrades, which can survive several years of desiccation but produce no or very little trehalose [68].

Much work is still needed to understand how these fascinating proteins modulate membrane properties, leading to possibly very important technological applications.

8. Amphipathic Helices Acting as Coats: The (Curious) Case of Perilipin 4

Perilipins are a family of proteins that reversibly associate with lipid droplets and mediate in the regulation of these intracellular organelles [69]. Lipid droplets are unusual in that they contain a hydrophobic core of neutral lipids and a monolayer of phospholipids and proteins [70]. All mammalian perilipins contain a predicted AH region that contributes to their lipid droplet localization [71–73]. This region is by far the longest in perilipin-4: the human sequence suggests a continuous AH of more than 950 aa, which, when folded, would measure about 140 nm. Indeed, a purified peptide of 660 aa is unfolded in solution but adopts a highly helical conformation in the presence of a lipid surface [10]. The AH belongs to the family of helices 3–11 and is composed of 33 aa repeats that are remarkable in their degree of conservation and in their lack of large hydrophobic residues (Figure 1f). The low hydrophobicity combined with the high length of this AH is essential for its specificity for lipid droplets in cells. Accordingly, the AH interacts very weakly with bilayer liposomes, but can directly bind to neutral lipids and act as a replacement for the phospholipid monolayer both in vitro and in cells [10] (Figure 2f). Thus, perilipin-4 AH appears optimized for coating lipid droplets and could be important for their stabilization, for example during adipocyte differentiation. A striking feature of this AH is also the distribution of charged residues in the polar face of the AH; their asymmetric organization is not optimal for interacting with a charged lipid surface, but they may instead be mediating lateral inter-helical interactions that would stabilize the protein coat [10] (Figure 1f).

Although perilipins have often been described as lipid droplet coats, it is currently not known whether other members of the family can act in a manner similar to perilipin-4. Interestingly, perilipins share some structural homology with the apolipoproteins [74], whose AHs also interact with neutral lipids to form small lipoprotein particles [75,76]. Conversely, what makes the oil–water interface adapt to some AHs is not well understood, although molecular dynamics simulations indicate a large increase in lipid packing defects under conditions of low phospholipid density [77].

9. Conclusions

Except for their amphipathic character, the various AHs that are presented here are very different in their composition (length, amino-acid sequence) and in their surface-binding properties (Figures 1 and 2). Two most contrasting examples are the ARF1 AH and the PLIN4 AH, which differ in all parameters: their length (12 vs. 950 aa), their hydrophobic residues (Leu, Phe vs. Ala, Val, Thr), and their polar residues (uncharged vs. charged) (compare Figure 1b,f). These differences translate into strikingly different binding properties: ARF–GTP binds to most lipid membranes, whereas Plin4 is specific for the lipid droplet surface [10,36,37]. Similarly, the ALPS motif and the AH of α-synuclein display contrasting chemistries and have been shown to recognize different transport vesicles [78]. In most cases, however, we still miss an atomic description of the interaction between an AH and its preferred lipid surface.

However, factors other than the AH–lipid surface interaction can also play a decisive role in regulating AH targeting or function. The presence of transmembrane regions in Pex11 and atlastin or mitofusin necessarily impose their subcellular localization, making the AH a domain important for membrane shaping, but not for targeting. In α-synuclein, the highly acidic region downstream of the AH region exacerbates the sensitivity of the AH to physical membrane parameters [79]. Furthermore, the properties of α-synuclein in vivo are also linked to its interactions with other proteins and to its tendency to self-aggregate into fibrils, a process that is exacerbated by pathological mutations [80]. A different type of example is CTP:phosphocholine cytidylyltransferase (CCTα), which contains one of the most studied AHs so far, but whose exact place of function in the cell has been highly debated [81]. A recent study indicates that, in vivo, this protein resides almost exclusively in the nucleus, suggesting

that the inner membrane of the nuclear envelope is the only membrane that CCTα actually senses under most physiological contexts [82]. Lastly, a full understanding of not only giant AHs such as PLIN4, but also apolipoproteins and Hsp12, which necessarily cover very large surfaces, requires a better evaluation of their overall conformation (straight vs. kinked), of their potential intra- and intermolecular interactions, and of their ability to cope with the very crowded environment on the surface of cellular organelles.

Author Contributions: M.G.A., A.C., and B.A. wrote the paper. M.G.A. prepared the figures.

Funding: This research was funded by the French National Research Agency (ANR), grant LDsurfDynamics (ANR-13-BSV2-0013), "Fondation pour la Recherche Médicale", grant number DEQ20150934717, and the European Research Council (ERC Advanced Grant 268 888). A.C. was supported by a Marie Curie career integration grant (631997). M.G.A. is supported by a PhD fellowship from the French "Ministère de l'Education National, de l'Enseignement Supérieur de la Recherche".

Acknowledgments: We thank Romain Gautier for his help with the bioinformatics analysis of AHs and Cathy Jackson for support.

Conflicts of Interest: The authors declare no conflict of interest.

References

1. Cornell, R.B.; Taneva, S.G. Amphipathic helices as mediators of the membrane interaction of amphitropic proteins, and as modulators of bilayer physical properties. *Curr. Protein Pept. Sci.* **2006**, *7*, 539–552. [CrossRef] [PubMed]
2. Drin, G.; Antonny, B. Amphipathic helices and membrane curvature. *FEBS Lett.* **2010**, *584*, 1840–1847. [CrossRef] [PubMed]
3. Segrest, J.P.; Jackson, R.L.; Morrisett, J.D.; Gotto, A.M. A molecular theory of lipid–protein interactions in the plasma lipoproteins. *FEBS Lett.* **1974**, *38*, 247–258. [CrossRef]
4. Segrest, J.P.; Jones, M.K.; De Loof, H.; Brouillette, C.G.; Venkatachalapathi, Y.V.; Anantharamaiah, G.M. The amphipathic helix in the exchangeable apolipoproteins: A review of secondary structure and function. *J. Lipid Res.* **1992**, *33*, 141–166. [PubMed]
5. Cornell, R.B.; Ridgway, N.D. CTP:phosphocholine cytidylyltransferase: Function, regulation, and structure of an amphitropic enzyme required for membrane biogenesis. *Prog. Lipid Res.* **2015**, *59*, 147–171. [CrossRef] [PubMed]
6. Drin, G.; Casella, J.F.; Gautier, R.; Boehmer, T.; Schwartz, T.U.; Antonny, B. A general amphipathic α-helical motif for sensing membrane curvature. *Nat. Struct. Mol. Biol.* **2007**, *14*, 138–146. [CrossRef] [PubMed]
7. Gallop, J.L.; Jao, C.C.; Kent, H.M.; Butler, P.J.G.; Evans, P.R.; Langen, R.; McMahon, H.T. Mechanism of endophilin N-BAR domain-mediated membrane curvature. *EMBO J.* **2006**, *25*, 2898–2910. [CrossRef] [PubMed]
8. Masuda, M.; Takeda, S.; Sone, M.; Ohki, T.; Mori, H.; Kamioka, Y.; Mochizuki, N. Endophilin BAR domain drives membrane curvature by two newly identified structure-based mechanisms. *EMBO J.* **2006**, *25*, 2889–2897. [CrossRef] [PubMed]
9. Welker, S.; Rudolph, B.; Frenzel, E.; Hagn, F.; Liebisch, G.; Schmitz, G.; Scheuring, J.; Kerth, A.; Blume, A.; Weinkauf, S.; et al. Hsp12 is an intrinsically unstructured stress protein that folds upon membrane association and modulates membrane function. *Mol. Cell* **2010**, *39*, 507–520. [CrossRef] [PubMed]
10. Čopič, A.; Antoine-Bally, S.; Giménez-Andrés, M.; La Torre Garay, C.; Antonny, B.; Manni, M.M.; Pagnotta, S.; Guihot, J.; Jackson, C.L. A giant amphipathic helix from a perilipin that is adapted for coating lipid droplets. *Nat. Commun.* **2018**, *9*, 1332. [CrossRef] [PubMed]
11. Gautier, R.; Douguet, D.; Antonny, B.; Drin, G. HELIQUEST: A web server to screen sequences with specific α-helical properties. *Bioinformatics* **2008**, *24*, 2101–2102. [CrossRef] [PubMed]
12. Burré, J.; Sharma, M.; Südhof, T.C. α-Synuclein assembles into higher-order multimers upon membrane binding to promote SNARE complex formation. *Proc. Natl. Acad. Sci. USA* **2014**, *111*, E4274–E4283. [CrossRef] [PubMed]

13. Mesmin, B.; Drin, G.; Levi, S.; Rawet, M.; Cassel, D.; Bigay, J.; Antonny, B. Two lipid-packing sensor motifs contribute to the sensitivity of ArfGAP1 to membrane curvature. *Biochemistry* **2007**, *46*, 1779–1790. [CrossRef] [PubMed]
14. Jensen, M.B.; Bhatia, V.K.; Jao, C.C.; Rasmussen, J.E.; Pedersen, S.L.; Jensen, K.J.; Langen, R.; Stamou, D. Membrane curvature sensing by amphipathic helices: A single liposome study using α-synuclein and annexin B12. *J. Biol. Chem.* **2011**, *286*, 42603–42614. [CrossRef] [PubMed]
15. Liu, Y.; Kahn, R.A.; Prestegard, J.H. Dynamic structure of membrane-anchored Arf·GTP. *Nat. Struct. Mol. Biol.* **2010**, *17*, 876–881. [CrossRef] [PubMed]
16. Herbert, A.P.; Riesen, M.; Bloxam, L.; Kosmidou, E.; Wareing, B.M.; Johnson, J.R.; Phelan, M.M.; Pennington, S.R.; Lian, L.Y.; Morgan, A. NMR structure of Hsp12, a protein induced by and required for dietary restriction-induced lifespan extension in yeast. *PLoS ONE* **2012**, *7*, e41975. [CrossRef] [PubMed]
17. Jao, C.C.; Hegde, B.G.; Chen, J.; Haworth, I.S.; Langen, R. Structure of membrane-bound α-synuclein from site-directed spin labeling and computational refinement. *Proc. Natl. Acad. Sci. USA* **2008**, *105*, 19666–19671. [CrossRef] [PubMed]
18. Hristova, K.; Wimley, W.C.; Mishra, V.K.; Anantharamiah, G.M.; Segrest, J.P.; White, S.H. An amphipathic α-helix at a membrane interface: A structural study using a novel X-ray diffraction method. *J. Mol. Biol.* **1999**, *290*, 99–117. [CrossRef] [PubMed]
19. Vanni, S.; Vamparys, L.; Gautier, R.; Drin, G.; Etchebest, C.; Fuchs, P.F.J.; Antonny, B. Amphipathic lipid packing sensor motifs: Probing bilayer defects with hydrophobic residues. *Biophys. J.* **2013**, *104*, 575–584. [CrossRef] [PubMed]
20. Cui, H.; Lyman, E.; Voth, G.A. Mechanism of membrane curvature sensing by amphipathic helix containing proteins. *Biophys. J.* **2011**, *100*, 1271–1279. [CrossRef] [PubMed]
21. Prévost, C.; Sharp, M.E.; Kory, N.; Lin, Q.; Voth, G.A.; Farese, R.V., Jr.; Walther, T.C. Mechanism and determinants of amphipathic helix-containing protein targeting to lipid droplets. *Dev. Cell* **2018**, *44*, 73–86. [CrossRef] [PubMed]
22. Fagarasanu, A.; Fagarasanu, M.; Rachubinski, R.A. Maintaining peroxisome populations: A story of division and inheritance. *Annu. Rev. Cell Dev. Biol.* **2007**, *23*, 321–344. [CrossRef] [PubMed]
23. Smith, J.J.; Aitchison, J.D. Peroxisomes take shape. *Nat. Rev. Mol. Cell Biol.* **2013**, *14*, 803–817. [CrossRef] [PubMed]
24. Opaliński, Ł.; Kiel, J.A.K.W.; Williams, C.; Veenhuis, M.; van der Klei, I.J. Membrane curvature during peroxisome fission requires Pex11. *EMBO J.* **2011**, *30*, 5–16. [CrossRef] [PubMed]
25. Yoshida, Y.; Niwa, H.; Honsho, M.; Itoyama, A.; Fujiki, Y. Pex11p mediates peroxisomal proliferation by promoting deformation of the lipid membrane. *Biol. Open* **2015**, *4*, 710–721. [CrossRef] [PubMed]
26. Marshall, P.A. Redox-sensitive homodimerization of Pex11p: A proposed mechanism to regulate peroxisomal division. *J. Cell Biol.* **1996**, *135*, 123–137. [CrossRef] [PubMed]
27. Su, J.; Thomas, A.S.; Grabietz, T.; Landgraf, C.; Volkmer, R.; Marrink, S.J.; Williams, C.; Melo, M.N. The N-terminal amphipathic helix of Pex11p self-interacts to induce membrane remodelling during peroxisome fission. *Biochim. Biophys. Acta* **2018**, *1860*, 1292–1300. [CrossRef] [PubMed]
28. Liu, T.Y.; Bian, X.; Sun, S.; Hu, X.; Klemm, R.W.; Prinz, W.A.; Rapoport, T.A.; Hu, J. Lipid interaction of the C-terminus and association of the transmembrane segments facilitate atlastin-mediated homotypic endoplasmic reticulum fusion. *Proc. Natl. Acad. Sci. USA* **2012**, *109*, E2146–E2154. [CrossRef] [PubMed]
29. Daste, F.; Sauvanet, C.; Bavdek, A.; Baye, J.; Pierre, F.; Le Borgne, R.; David, C.; Rojo, M.; Fuchs, P.; Tareste, D. The heptad repeat domain 1 of Mitofusin has membrane destabilization function in mitochondrial fusion. *EMBO Rep.* **2018**, *19*, E43637. [CrossRef] [PubMed]
30. Huang, X.; Zhou, X.; Hu, X.; Joshi, A.S.; Guo, X.; Zhu, Y.; Chen, Q.; Prinz, W.A.; Hu, J. Sequences flanking the transmembrane segments facilitate mitochondrial localization and membrane fusion by mitofusin. *Proc. Natl. Acad. Sci. USA* **2017**, *114*, E9863–E9872. [CrossRef] [PubMed]
31. Ambroso, M.R.; Hegde, B.G.; Langen, R. Endophilin A1 induces different membrane shapes using a conformational switch that is regulated by phosphorylation. *Proc. Natl. Acad. Sci. USA* **2014**, *111*, 6982–6987. [CrossRef] [PubMed]
32. Boucrot, E.; Pick, A.; Çamdere, G.; Liska, N.; Evergren, E.; McMahon, H.T.; Kozlov, M.M. Membrane fission is promoted by insertion of amphipathic helices and is restricted by crescent BAR domains. *Cell* **2012**, *149*, 124–136. [CrossRef] [PubMed]

33. Stachowiak, J.C.; Schmid, E.M.; Ryan, C.J.; Ann, H.S.; Sasaki, D.Y.; Sherman, M.B.; Geissler, P.L.; Fletcher, D.A.; Hayden, C.C. Membrane bending by protein-protein crowding. *Nat. Cell Biol.* **2012**, *14*, 944–949. [CrossRef] [PubMed]
34. Chen, Z.; Zhu, C.; Kuo, C.J.; Robustelli, J.; Baumgart, T. The N-terminal amphipathic helix of endophilin does not contribute to its molecular curvature generation capacity. *J. Am. Chem. Soc.* **2016**, *138*, 14616–14622. [CrossRef] [PubMed]
35. Donaldson, J.G.; Jackson, C.L. ARF family G-proteins and their regulators: Roles in membrane transport, development and disease. *Nat. Rev. Mol. Cell Biol.* **2011**, *12*, 362–375. [CrossRef] [PubMed]
36. Antonny, B.; Beraud-Dufour, S.; Chardin, P.; Chabre, M. N-terminal hydrophobic residues of the G-protein ADP-ribosylation factor-1 insert into membrane phospholipids upon GDP to GTP exchange. *Biochemistry* **1997**, *36*, 4675–4684. [CrossRef] [PubMed]
37. Thiam, A.R.; Antonny, B.; Wang, J.; Delacotte, J.; Wilfling, F.; Walther, T.C.; Beck, R.; Rothman, J.E.; Pincet, F. COPI buds 60-nm lipid droplets from reconstituted water–phospholipid–triacylglyceride interfaces, suggesting a tension clamp function. *Proc. Natl. Acad. Sci. USA* **2013**, *110*, 13244–13249. [CrossRef] [PubMed]
38. Manneville, J.-B.; Casella, J.F.; Ambroggio, E.E.; Gounon, P.; Bertherat, J.; Bassereau, P.; Cartaud, J.; Antonny, B.; Goud, B. COPI coat assembly occurs on liquid-disordered domains and the associated membrane deformations are limited by membrane tension. *Proc. Natl. Acad. Sci. USA* **2008**, *105*, 16946–16951. [CrossRef] [PubMed]
39. Wilfling, F.; Thiam, A.R.; Olarte, M.-J.; Wang, J.; Beck, R.; Gould, T.J.; Allgeyer, E.S.; Pincet, F.; Bewersdorf, J.; Farese, R.V.; et al. Arf1/COPI machinery acts directly on lipid droplets and enables their connection to the ER for protein targeting. *eLife* **2014**, *3*, e01607. [CrossRef] [PubMed]
40. Bacia, K.; Futai, E.; Prinz, S.; Meister, A.; Daum, S.; Glatte, D.; Briggs, J.A.G.; Schekman, R. Multibudded tubules formed by COPII on artificial liposomes. *Sci. Rep.* **2011**, *1*, 17. [CrossRef] [PubMed]
41. Lee, M.C.S.; Orci, L.; Hamamoto, S.; Futai, E.; Ravazzola, M.; Schekman, R. Sar1p N-terminal helix initiates membrane curvature and completes the fission of a COPII vesicle. *Cell* **2005**, *122*, 605–617. [CrossRef] [PubMed]
42. Krauss, M.; Jia, J.Y.; Roux, A.; Beck, R.; Wieland, F.T.; De Camilli, P.; Haucke, V. Arf1-GTP-induced tubule formation suggests a function of Arf family proteins in curvature acquisition at sites of vesicle budding. *J. Biol. Chem.* **2008**, *283*, 27717–27723. [CrossRef] [PubMed]
43. Bielli, A.; Haney, C.J.; Gabreski, G.; Watkins, S.C.; Bannykh, S.I.; Aridor, M. Regulation of Sar1 NH_2 terminus by GTP binding and hydrolysis promotes membrane deformation to control COPII vesicle fission. *J. Cell Biol.* **2005**, *171*, 919–924. [CrossRef] [PubMed]
44. Manni, M.M.; Derganc, J.; Čopič, A. Crowd-sourcing of membrane fission: How crowding of non-specialized membrane-bound proteins contributes to cellular membrane fission. *BioEssays* **2017**, *39*, 1700117:1–1700117:7. [CrossRef] [PubMed]
45. Beck, R.; Sun, Z.; Adolf, F.; Rutz, C.; Bassler, J.; Wild, K.; Sinning, I.; Hurt, E.; Brügger, B.; Béthune, J.; et al. Membrane curvature induced by Arf1-GTP is essential for vesicle formation. *Proc. Natl. Acad. Sci. USA* **2008**, *105*, 11731–11736. [CrossRef] [PubMed]
46. Snead, W.T.; Hayden, C.C.; Gadok, A.K.; Zhao, C.; Lafer, E.M.; Rangamani, P.; Stachowiak, J.C. Membrane fission by protein crowding. *Proc. Natl. Acad. Sci. USA* **2017**, *114*, E3258–E3267. [CrossRef] [PubMed]
47. Bigay, J.; Casella, J.F.; Drin, G.; Mesmin, B.; Antonny, B. ArfGAP1 responds to membrane curvature through the folding of a lipid packing sensor motif. *EMBO J.* **2005**, *24*, 2244–2253. [CrossRef] [PubMed]
48. Ho, R.; Stroupe, C. The HOPS/Class C VPS complex tethers high-curvature membranes via a direct protein–membrane interaction. *Traffic* **2016**, *17*, 1078–1090. [CrossRef] [PubMed]
49. Magdeleine, M.; Gautier, R.; Gounon, P.; Barelli, H.; Vanni, S.; Antonny, B. A filter at the entrance of the Golgi that selects vesicles according to size and bulk lipid composition. *eLife* **2016**, *5*, 292. [CrossRef] [PubMed]
50. Loewen, C.J.R.; Gaspar, M.L.; Jesch, S.A.; Delon, C.; Ktistakis, N.T.; Henry, S.A.; Levine, T.P. Phospholipid metabolism regulated by a transcription factor sensing phosphatidic acid. *Science* **2004**, *304*, 1644–1647. [CrossRef] [PubMed]
51. Gaspar, M.L.; Chang, Y.F.; Jesch, S.A.; Aregullin, M.; Henry, S.A. Interaction between repressor Opi1p and ER membrane protein Scs2p facilitates transit of phosphatidic acid from the ER to mitochondria and is essential for INO1 gene expression in the presence of choline. *J. Biol. Chem.* **2017**, *292*, 18713–18728. [CrossRef] [PubMed]

52. Carman, G.M.; Henry, S.A. Phosphatidic acid plays a central role in the transcriptional regulation of glycerophospholipid synthesis in *Saccharomyces cerevisiae*. *J. Biol. Chem.* **2007**, *282*, 37293–37297. [CrossRef] [PubMed]
53. Hofbauer, H.F.; Gecht, M.; Fischer, S.; Seybert, A.; Frangakis, A.S.; Stelzer, E.; Covino, R.; Hummer, G.; Ernst, R. The molecular recognition of phosphatidic acid by an amphipathic helix in Opi1. *J. Cell Biol.* **2018**. [CrossRef] [PubMed]
54. Kooijman, E.E.; Carter, K.M.; van Laar, E.G.; Chupin, V.; Burger, K.N.J.; de Kruijff, B. What makes the bioactive lipids phosphatidic acid and lysophosphatidic acid so special? *Biochemistry* **2005**, *44*, 17007–17015. [CrossRef] [PubMed]
55. Nakanishi, H.; de los Santos, P.; Neiman, A.M. Positive and negative regulation of a SNARE protein by control of intracellular localization. *Mol. Biol. Cell* **2004**, *15*, 1802–1815. [CrossRef] [PubMed]
56. Horchani, H.; de Saint-Jean, M.; Barelli, H.; Antonny, B. Interaction of the Spo20 membrane-sensor motif with phosphatidic acid and other anionic lipids, and influence of the membrane environment. *PLoS ONE* **2014**, *9*, e113484. [CrossRef] [PubMed]
57. Tanguy, E.; Kassas, N.; Vitale, N. Protein–phospholipid interaction motifs: A focus on phosphatidic acid. *Biomolecules* **2018**, *8*, 20. [CrossRef] [PubMed]
58. Luchetti, G.; Sircar, R.; Kong, J.H.; Nachtergaele, S.; Sagner, A.; Byrne, E.F.; Covey, D.F.; Siebold, C.; Rohatgi, R. Cholesterol activates the G-protein coupled receptor smoothened to promote Hedgehog signaling. *eLife* **2016**, *5*, 1055. [CrossRef] [PubMed]
59. Chua, N.K.; Howe, V.; Jatana, N.; Thukral, L.; Brown, A.J. A conserved degron containing an amphipathic helix regulates the cholesterol-mediated turnover of human squalene monooxygenase, a rate-limiting enzyme in cholesterol synthesis. *J. Biol. Chem.* **2017**, *292*, 19959–19973. [CrossRef] [PubMed]
60. Moriceau, L.; Jomat, L.; Bressanelli, S.; Alcaide-Loridan, C.; Jupin, I. Identification and molecular characterization of the chloroplast targeting domain of turnip yellow mosaic virus replication proteins. *Front. Plant Sci.* **2017**, *8*, 2138. [CrossRef] [PubMed]
61. Boothby, T.C.; Pielak, G.J. Intrinsically disordered proteins and desiccation tolerance. *BioEssays* **2017**, *39*, 1700119:1–1700119:4. [CrossRef] [PubMed]
62. Clarke, M.W.; Boddington, K.F.; Warnica, J.M.; Atkinson, J.; McKenna, S.; Madge, J.; Barker, C.H.; Graether, S.P. Structural and functional insights into the cryoprotection of membranes by the intrinsically disordered dehydrins. *J. Biol. Chem.* **2015**, *290*, 26900–26913. [CrossRef] [PubMed]
63. Eriksson, S.K.; Kutzer, M.; Procek, J.; Gröbner, G.; Harryson, P. Tunable membrane binding of the intrinsically disordered dehydrin Lti30, a cold-induced plant stress protein. *Plant Cell* **2011**, *23*, 2391–2404. [CrossRef] [PubMed]
64. Eriksson, S.; Eremina, N.; Barth, A.; Danielsson, J.; Harryson, P. Membrane-induced folding of the plant stress dehydrin Lti30. *Plant Physiol.* **2016**, *171*, 932–943. [PubMed]
65. Thalhammer, A.; Bryant, G.; Sulpice, R.; Hincha, D.K. Disordered cold regulated15 proteins protect chloroplast membranes during freezing through binding and folding, but do not stabilize chloroplast enzymes in vivo. *Plant Physiol.* **2014**, *166*, 190–201. [CrossRef] [PubMed]
66. Thalhammer, A.; Hundertmark, M.; Popova, A.V.; Seckler, R.; Hincha, D.K. Interaction of two intrinsically disordered plant stress proteins (COR15A and COR15B) with lipid membranes in the dry state. *Biochim. Biophys. Acta* **2010**, *1798*, 1812–1820. [CrossRef] [PubMed]
67. Moore, D.S.; Hansen, R.; Hand, S.C. Liposomes with diverse compositions are protected during desiccation by LEA proteins from *Artemia franciscana* and trehalose. *Biochim. Biophys. Acta* **2016**, *1858*, 104–115. [CrossRef] [PubMed]
68. Boothby, T.C.; Tapia, H.; Brozena, A.H.; Piszkiewicz, S.; Smith, A.E.; Giovannini, I.; Rebecchi, L.; Pielak, G.J.; Koshland, D.; Goldstein, B. Tardigrades use intrinsically disordered proteins to survive desiccation. *Mol. Cell* **2017**, *65*, 975–984. [CrossRef] [PubMed]
69. Sztalryd, C.; Brasaemle, D.L. The perilipin family of lipid droplet proteins: Gatekeepers of intracellular lipolysis. *Biochim. Biophys. Acta* **2017**, *1862*, 1221–1232. [CrossRef] [PubMed]
70. Thiam, A.R.; Farese, R.V.; Walther, T.C. The biophysics and cell biology of lipid droplets. *Nat. Rev. Mol. Cell Biol.* **2013**, *14*, 775–786. [CrossRef] [PubMed]

71. Rowe, E.R.; Mimmack, M.L.; Barbosa, A.D.; Haider, A.; Isaac, I.; Ouberai, M.M.; Thiam, A.R.; Patel, S.; Saudek, V.; Siniossoglou, S.; et al. Conserved amphipathic helices mediate lipid droplet targeting of perilipins 1–3. *J. Biol. Chem.* **2016**, *291*, 6664–6678. [CrossRef] [PubMed]
72. Bulankina, A.V.; Deggerich, A.; Wenzel, D.; Mutenda, K.; Wittmann, J.G.; Rudolph, M.G.; Burger, K.N.J.; Höning, S. TIP47 functions in the biogenesis of lipid droplets. *J. Cell Biol.* **2009**, *185*, 641–655. [CrossRef] [PubMed]
73. Bussell, R.; Eliezer, D. A Structural and functional role for 11-mer repeats in α-synuclein and other exchangeable lipid binding proteins. *J. Mol. Biol.* **2003**, *329*, 763–778. [CrossRef]
74. Hickenbottom, S.J.; Kimmel, A.R.; Londos, C.; Hurley, J.H. Structure of a lipid droplet protein. *Structure* **2004**, *12*, 1199–1207. [CrossRef] [PubMed]
75. Mirheydari, M.; Mann, E.K.; Kooijman, E.E. Interaction of a model apolipoprotein, apoLp-III, with an oil–phospholipid interface. *Biochim. Biophys. Acta* **2018**, *1860*, 396–406. [CrossRef] [PubMed]
76. Pan, L.; Segrest, J.P. Computational studies of plasma lipoprotein lipids. *Biochim. Biophys. Acta* **2016**, *1858*, 2401–2420. [CrossRef] [PubMed]
77. Bacle, A.; Gautier, R.; Jackson, C.L.; Fuchs, P.F.J.; Vanni, S. Interdigitation between triglycerides and lipids modulates surface properties of lipid droplets. *Biophys. J.* **2017**, *112*, 1417–1430. [CrossRef] [PubMed]
78. Pranke, I.M.; Morello, V.; Bigay, J.; Gibson, K.; Verbavatz, J.M.; Antonny, B.; Jackson, C.L. α-Synuclein and ALPS motifs are membrane curvature sensors whose contrasting chemistry mediates selective vesicle binding. *J. Cell Biol.* **2011**, *194*, 89–103. [CrossRef] [PubMed]
79. Chong, S.S.Y.; Taneva, S.G.; Lee, J.M.C.; Cornell, R.B. The curvature sensitivity of a membrane-binding amphipathic helix can be modulated by the charge on a flanking region. *Biochemistry* **2014**, *53*, 450–461. [CrossRef] [PubMed]
80. Bendor, J.T.; Logan, T.P.; Edwards, R.H. The function of α-synuclein. *Neuron* **2013**, *79*, 1044–1066. [CrossRef] [PubMed]
81. Cornell, R.B. Membrane lipid compositional sensing by the inducible amphipathic helix of CCT. *Biochim. Biophys. Acta* **2015**, *1861*, 847–861. [CrossRef] [PubMed]
82. Haider, A.; Wei, Y.C.; Lim, K.; Barbosa, A.D.; Liu, C.H.; Weber, U.; Mlodzik, M.; Oras, K.; Collier, S.; Hussain, M.M.; et al. PCYT1A regulates phosphatidylcholine homeostasis from the inner nuclear membrane in response to membrane stored curvature elastic stress. *Dev. Cell* **2018**, *45*, 481–495. [CrossRef] [PubMed]

nature COMMUNICATIONS

ARTICLE

DOI: 10.1038/s41467-018-03717-8 OPEN

A giant amphipathic helix from a perilipin that is adapted for coating lipid droplets

Alenka Čopič[1], Sandra Antoine-Bally[1], Manuel Giménez-Andrés[1,2], César La Torre Garay[1], Bruno Antonny[3], Marco M. Manni[3], Sophie Pagnotta[3], Jeanne Guihot[1] & Catherine L. Jackson[1]

How proteins are targeted to lipid droplets (LDs) and distinguish the LD surface from the surfaces of other organelles is poorly understood, but many contain predicted amphipathic helices (AHs) that are involved in targeting. We have focused on human perilipin 4 (Plin4), which contains an AH that is exceptional in terms of length and repetitiveness. Using model cellular systems, we show that AH length, hydrophobicity, and charge are important for AH targeting to LDs and that these properties can compensate for one another, albeit at a loss of targeting specificity. Using synthetic lipids, we show that purified Plin4 AH binds poorly to lipid bilayers but strongly interacts with pure triglycerides, acting as a coat and forming small oil droplets. Because Plin4 overexpression alleviates LD instability under conditions where their coverage by phospholipids is limiting, we propose that the Plin4 AH replaces the LD lipid monolayer, for example during LD growth.

[1] Institut Jacques Monod, CNRS, UMR 7592, Université Paris Diderot, Sorbonne Paris Cité, 75013 Paris, France. [2] Université Paris-Sud, Université Paris-Saclay, 91405 Orsay, France. [3] Université Côte d'Azur, CNRS, IPMC, 06560 Valbonne, France. These authors contributed equally: Sandra Antoine-Bally, Manuel Giménez-Andrés, César La Torre Garay. Correspondence and requests for materials should be addressed to A.Č. (email: alenka.copic@ijm.fr)

Lipid droplets are ubiquitous cellular organelles that serve as the primary depot for energy and lipid storage in eukaryotic cells. As such, they play an important role in the maintenance of cellular homeostasis and their malfunction is associated with numerous diseases, from obesity and diabetes to cancer and neurodegenerative diseases[1–3]. How proteins that mediate LD function (for example enzymes and regulators of lipid metabolism) are selectively targeted to the surface of this organelle is poorly understood[4].

LDs are composed of a neutral lipid core, consisting primarily of triglycerides and sterol esters, which is covered by a monolayer of phospholipids and other amphiphilic lipids, and by proteins[4,5]. Unlike the two leaflets of a bilayer, which are physically coupled, this monolayer can be stretched infinitely, resulting in an increasing surface tension. LDs with high surface tension are unstable and tend to fuse; LD fusion appears to be one mechanism by which cells can cope with an imbalance in synthesis of neutral lipids and phospholipids[6–8]. LD size appears regulated and is highly variable between different cells, ranging from 100 nm to 100 µm, with mature adipocytes often containing only one large LD[4,9]. On the other side of the size spectrum are the small lipoprotein particles, which, like LDs, are adapted for harboring neutral lipids, but are secreted from cells or form extracellularly[10].

Numerous LD proteins contain regions that are predicted to form amphipathic helices (AHs), and it has been shown in many cases that these regions are important for LD targeting[6,11–13]. AHs are also involved in targeting of proteins to other cellular organelles. They have been shown to specifically recognize different features of lipid bilayers, such as surface charge, packing of acyl chains, and membrane curvature[14–17]. Lipid packing and membrane curvature promote AH recruitment through creation of lipid packing defects, which have been analyzed extensively in bilayer membranes[18–20]. It is not clear which parameters are important for AH binding to the LD surface[21]. A recent in silico analysis suggests that whereas an LD phospholipid monolayer at zero surface tension does not behave very differently from a bilayer, lipid packing defects increase non-linearly with increasing surface tension of the monolayer[22]. This result could explain why under some experimental conditions, AHs have been observed to bind to LDs rather non-discriminately[23–25]. Finally, recruitment of proteins to the LD surface also appears sensitive to protein crowding[26,27].

We aim to understand to what extent AHs can be selective for the LD surface and what parameters are important for this selectivity. The AHs that have been shown to localize to LDs appear highly diverse, precluding any speculation about AH localization based on sequence comparisons[6,11,13,23,25,28]. We have instead focused on one particular AH present in the mammalian LD protein perilipin 4 (Plin4). Plin4 is related in its sequence to the other mammalian perilipins (Plin1–5), which all localize to LDs and interact with lipid enzymes and other regulators of LD metabolism[29]. The carboxy-terminal portions of perilipins are predicted to fold into a four-helix bundle, which has been crystalized in Plin3[30], whereas in their amino terminal/central region they all contain an 11-mer repeat sequence[31]. These 11-mer repeat regions have been shown to mediate LD localization of Plin1–3 and can form an AH[11,13]. Interestingly, these features are also present in apolipoproteins, which form small lipoprotein particles, but it is not clear whether the two protein families are evolutionarily related[30–32]. Plin4 is the least explored of all perilipins; it is highly expressed in adipocytes, where it may associate preferentially with small LDs, but it is absent from most other tissues and its physiological role is not clear[33–36]. However, the 11-mer repeat sequence of Plin4 is exceptional in terms of its length and repetitiveness (Fig. 1).

We now show that the Plin4 11-mer repeat region localizes to LDs in different cellular models and can directly interact with neutral lipids in vitro. The properties of this giant AH have allowed us to manipulate it in a modular manner to dissect the parameters that control its localization in cells. We show that the length, hydrophobicity, and charge of the AH all contribute to its LD localization and that these properties can to some extent compensate for one another. Finally, we show that overexpression of the Plin4 AH can rescue an LD size defect associated with cellular depletion of phosphatidylcholine (PC)[6,7], suggesting that the ability of this AH to interact with neutral lipids may be important for its in vivo function.

Results

Plin4 contains a giant AH that localizes to LDs. The length of the predicted AH in Plin4 surpasses that of other known AHs involved in organelle targeting by an order of magnitude (Fig. 1a and Table 1). The defining feature of this region is the presence of 11-mer repeats; if folded, these repeats could adopt a slightly extended version of an α-helix termed a 3–11 helix (Fig. 1b). This type of helix has been well characterized in apolipoproteins and in α-synuclein, where the folding is dependent on contact with lipids[31,37,38]. Furthermore, the repeats in Plin4 are extremely well conserved at the level of 33-mer (3×11-mer): 29 tandem 33-mer repeats can be identified in the human Plin4 sequence, entirely without deletions or insertions between them (Fig. 1c, d). These striking properties make Plin4 an ideal model to study the parameters that govern AH targeting to LDs.

In contrast to its exceptional length and monotonous composition, the Plin4 AH is weak in its amphipathic character when compared to other well-studied AHs (Table 1 and Supplementary Fig. 1). For our analysis of Plin4 AH targeting in cells, we chose the most conserved central portion of the predicted AH sequence, where the small differences between the 33-mer repeats can be considered negligible (Fig. 1 and Supplementary Fig. 1b). We expressed different fragments of the protein as fluorescent protein fusions in HeLa cells, which do not express endogenous Plin4 (Fig. 1d, e)[39]. Whereas a peptide comprising 66 amino acids of the Plin4 AH, i.e., two 33-mers, was completely cytosolic, increasing the length to 4×33-mer repeats (132 aa) or 8×33-mers resulted in a fraction of LDs that were positive for Plin4. Further extending the length of the AH to 20×33-mer repeats (660 aa) led to its localization to all LDs (Fig. 1e, f). The size and number of LDs in cells was not significantly affected by the expression of these constructs (Supplementary Fig. 2a). In all cases, an appreciable amount of cytosolic signal could also be observed, independent of the amount of LDs in cells (cells were either grown in standard medium or supplemented with oleic acid to induce LD accumulation, Supplementary Fig. 2b). In contrast to the AH region, the C-terminus of Plin4 containing the predicted 4-helix bundle was completely cytosolic (Supplementary Fig. 2c). The experiments presented so far were performed on fixed cells, and we found that fixation itself augmented Plin4 AH targeting to LDs, presumably by stabilizing the protein on LDs. However, a similar trend of improved LD targeting with increasing length of constructs could be observed in live cells (Supplementary Fig. 2d).

We confirmed the LD surface targeting of the Plin4 AH by expressing it in budding yeast, which contain proteins that are distantly related to human perilipins[27,40]. Similar to HeLa cells, a robust LD signal could be observed with Plin4-12mer, whereas Plin4-4mer remained largely cytosolic (Fig. 1g). The fact that the same sequence is targeted to LDs in such evolutionarily distant organisms speaks to the universal nature of AH–LD interactions, as previously shown[13,40]. In addition, the Plin4-12mer was also

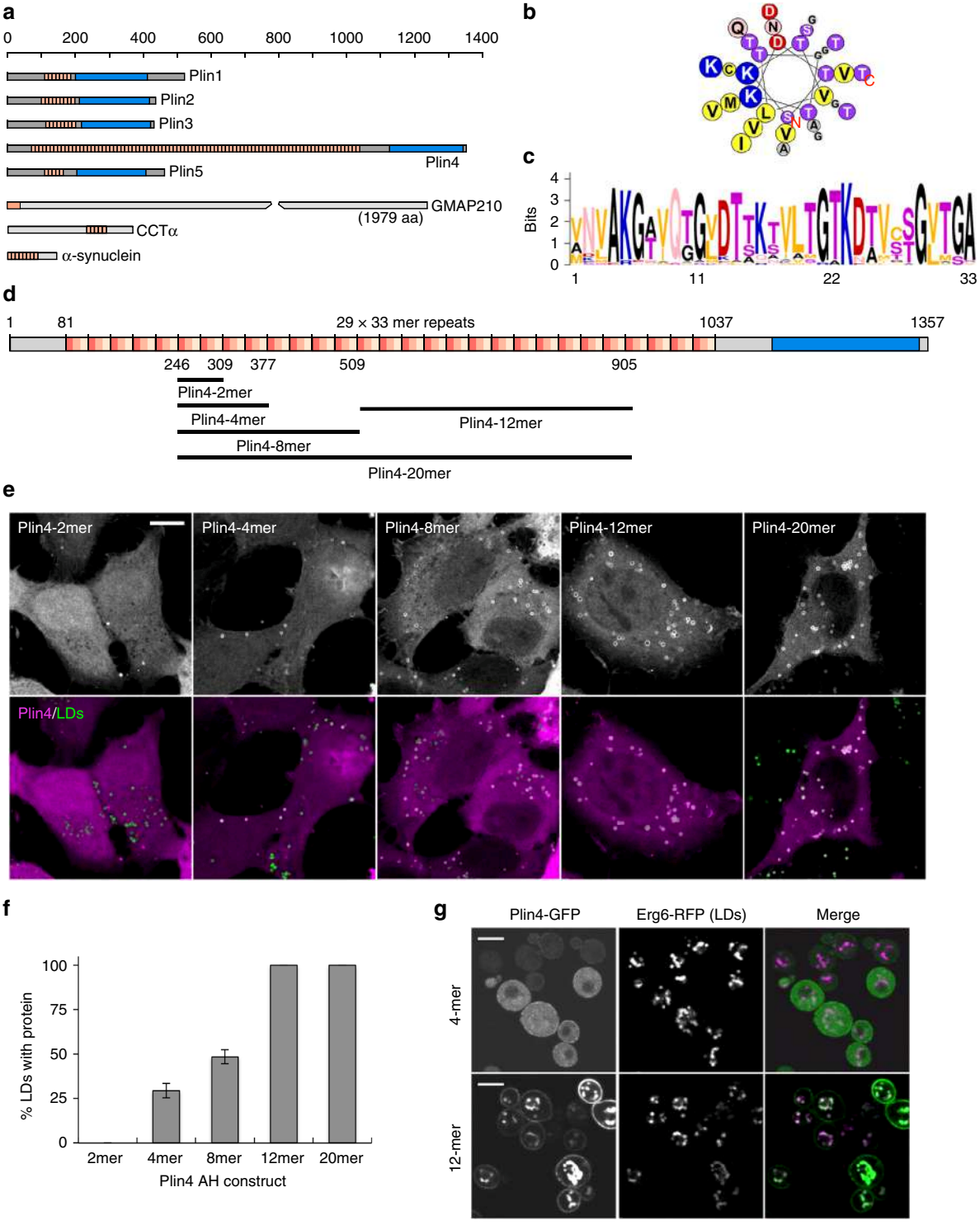

Fig. 1 Plin4 contains a very long AH that localizes to LDs. **a** Schematic diagrams of human proteins with long AH regions (pink). In the proteins of the perilipin family (Plin1–5), CTP:Phosphocholine Cytidylyltransferase α (CCTα) and α-synuclein, in which the AH region contains 11-mer repeats, the corresponding bars are segmented to indicate the approximate repeat number. In Plin4, these repeats are remarkably conserved at the level of 33-mers. All perilipins also contain a predicted 4-helix bundle (blue), which has been crystalized in Plin3. **b** Helical wheel plot of one 33-mer repeat from Plin4, plotted as a 3–11 helix[71]. **c** Weblogo generated from an alignment of 29 33-mer repeats from human Plin4 sequence[72]. **d** Schematic representation of human Plin4. Position and length of different Plin4 constructs is also shown. **e** Localization of Plin4-AH-mCherry constructs of different length in HeLa cells (upper panels). Lower panels show colocalization of Plin4-AH (magenta) and LDs stained with Bodipy (green). Scale bar: 10 μm. **f** Quantification of the mean fraction of LDs stained with Plin4-AH per cell in HeLa cells. 40–60 cells in two independent experiments were quantified for each construct. Error bars depict s.e.m. from one experiment (the range between the two experiments is smaller than this error bar). **g** Localization of Plin4-4mer and Plin4-12mer GFP fusions in yeast. Lipid droplets are marked with Erg6-RFP. Scale bar: 5 μm

Table 1 Comparison of properties of different AHs

AH	Position[a]	Length[b]	Hydr. mom[c]	Fract of residues[d]			Lipid-binding properties	Ref
				Hdr	LH	Ch		
Hel 13-5	n.a.[e]	18	0.69	0.72	0.06	0.28	Tubulates liposomes	73
GMAP210	1–38 (1979)	38	0.48	0.37	0.05	0.05	Golgi vesicles/abundant packing defects	14, 25
Nup133	247–267 (1156)	21	0.44	0.38	0.05	0.10	Nuclear pore membrane	67
CIDEA	163–180 (219)	18	0.53	0.5	0.11	0.17	LDs[f]	28
CCTα	236–294 (368)	59	0.48*	0.32	0.10	0.49	Nuclear envelope/ER and LDs/ liposomes	6, 16, 64
Apolipoprotein-AI	74–267 (267)	186 (7 P)[g]	0.39*	0.40	0.065	0.35	Lipoprotein particles	48
α-Synuclein	1–89 (144)	89	0.30*	0.47	0.02	0.24	Synaptic vesicles/neg. charged small liposomes	44
Plin3	114–204 (434)	90	0.35*	0.37	0.01	0.23	LDs and cytosol	11
Plin4	70–1037 (1357)	968	(0.257)*	0.35	0.002	0.15	This study	

[a] Numbers give the first and last amino acid in the protein sequence, with the total length of each protein given in brackets
[b] Length is based on structural data, when available, and visual inspection using Heliquest[71]. Prolines are considered as helix breakers
[c] Hydrophobic moment is calculated using Heliquest[74]. The AHs that contain 11-mer repeats are plotted as 3–11 helices. For longer AHs (*), the mean of hydrophobic moments of consecutive helices is given (see Supplementary Fig. 1 for details)
[d] Fraction of different amino acids in the AH sequence: Hdr, all hydrophobic (A, I, L, M, V, F, W, Y); LH, large hydrophobic (aromatic) (F, W, Y); Ch, charged=acidic (D, E) and basic (K, R)
[e] This is an artificial AH
[f] This AH has only been tested as a fusion with other parts of the protein, therefore its specificity for LDs is not known
[g] The helix is broken by seven prolines, which induce a kink; ten separate helices in the structure (Supplementary Fig. 1)

detected at the periphery of yeast cells. This is in accordance with the net positive charge of this amphipathic sequence (Fig. 1b), which could be interacting electrostatically with the negatively charged plasma membrane[41,42]. A fluorescent signal could also sometimes be observed at the periphery of HeLa cells, but due to cell shape and a large pool of cytoplasmic protein, this signal was difficult to quantify. Endogenous Plin4 has been detected at the cell periphery in adipocytes, in addition to its localization to LDs[33,35,43]. Furthermore, the Plin4 AH is related in its chemistry to the AH of α-synuclein, a protein enriched in presynaptic termini and on negatively charged vesicles[44] (Supplementary Fig. 1). Interestingly, α-synuclein has also been observed on LDs when expressed heterologously[44,45], and the closely-related γ-synuclein localizes to LDs in adipocytes, where it affects lipid metabolism[46]. An α-synuclein AH construct containing 85 amino acids localizes to LDs slightly better than Plin-4mer (Supplementary Fig. 2e, f), consistent with the higher hydrophobic moment of the α-synuclein AH (Table 1).

Overall, our analysis indicates a correlation between the targeting of the Plin4 AH to LDs and its length: longer constructs interact better owing to a more extensive interaction surface. A relatively long Plin4 sequence (>66 aa) is required for targeting to LDs, indicating that the elementary 33-mer repeat of Plin4 is a selective but intrinsically weak determinant for LD targeting. In this respect, we note that the Plin4 33-mer repeat displays the smallest hydrophobicity and hydrophobic moment among all AHs known to interact with lipid surfaces (Table 1)[47].

The Plin4 AH is intrinsically unfolded in solution. Membrane-interacting AHs are often unfolded in solution, adopting a helical structure only upon contact with membranes, as exemplified by the AH of α-synuclein[38]. Alternatively, the AH may be folded into a different structure in the soluble form of its parent protein, as is for example the case for CTP:Phosphocholine Cytidylyltransferase α (CCTα) and Arf1[16,37,48,49]. To study the biochemical properties of the different Plin4 AH fragments, we expressed and purified them from *Escherichia coli*, following the procedure that was used for purification of α-synuclein[50]. The Plin4 4mer, 12mer, and 20mer in bacterial lysates were resistant to boiling, and they could subsequently be purified from the remaining contaminants by anion-exchange chromatography (Supplementary Fig. 3a, b). All constructs eluted from the column at the same salt concentration, as expected considering their similar sequences.

We used size exclusion chromatography to characterize the hydrodynamic properties of the three Plin4 constructs. They migrated on the column at the same elution volume as well-folded protein standards with a twofold higher MW (Fig. 2a, b). Because such an increase in apparent MW (i.e., Stokes radius) is observed for many proteins upon denaturation[51], this result suggests that all Plin4 constructs are intrinsically unfolded. The lack of secondary structure was confirmed by circular dichroism (CD) spectroscopy (Fig. 2c). However, Plin4 fragments adopted a highly helical conformation when incubated in 50% trifluoroethanol solution. These experiments indicate that Plin4 contains a giant repetitive region that is intrinsically unfolded but has the potential to fold into a helix much longer than any other previously described AH (Table 1).

Plin4 AH targeting to LDs is controlled by hydrophobicity. The amino acid composition of the Plin4 AH region is very particular: the segment containing close to 1000 aa is almost devoid of aromatic residues (accounting for only 0.6% of all residues in the human Plin4 AH sequence, about 20 times less than is the vertebrate average), whereas some amino acids, in particular threonine, glycine, and valine, are highly enriched (Supplementary Table 1)[52]. These features contribute to the low hydrophobicity and low-hydrophobic moment of the predicted AH (Table 1).

Given the importance of Plin4 AH length for LD targeting, we surmise that its binding to LDs is mediated by multiple weak interactions over an extended binding surface. To probe the nature of these interactions, we devised a mutagenesis strategy whereby subtle mutations were repeated along the helix. As the starting point, we used the Plin4-4mer, whose length is just above the threshold for LD binding and thus the targeting of this helix may be sensitive to even small perturbations. All mutants were expressed in HeLa cells as mCherry fusions in the same manner as the wild-type form. The LD targeting phenotypes of the different constructs did not depend on their expression levels.

We mutated threonine residues in the non-polar face of the helix into the structurally similar but more hydrophobic valine (Fig. 3a and Supplementary Table 2). A single threonine to valine

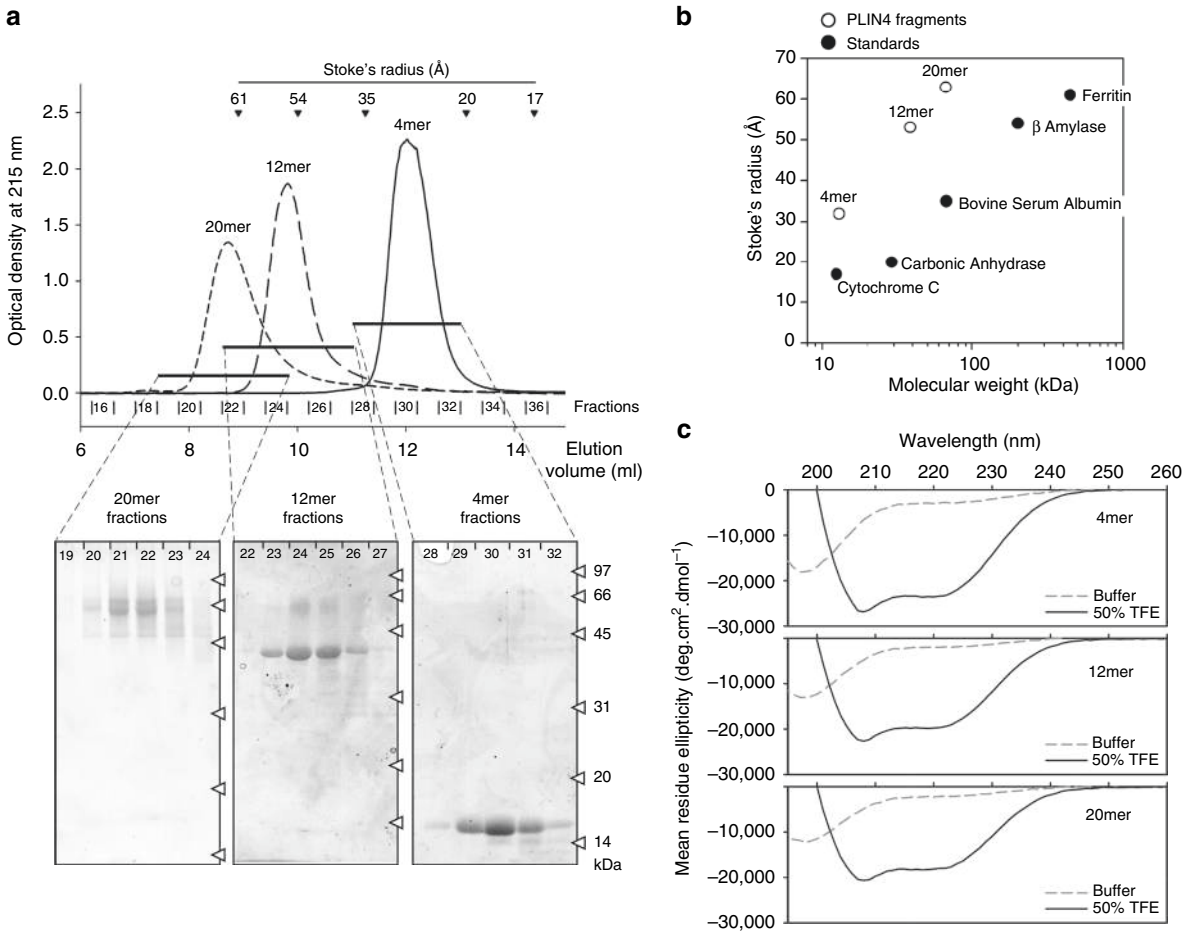

Fig. 2 Hydrodynamic and secondary structure analysis of Plin4 AH fragments. **a** Elution profiles of the 4mer, 12mer, and 20mer fragments of Plin4 on a Superose 12 column. The black arrowheads indicate the elution volumes of protein standards of defined Stoke's radii, which were used to calibrate the column. The indicated fractions were analyzed by SDS-PAGE with Sypro Orange staining. The white arrowheads indicate the migration of molecular weight (MW) standards on the gels. **b** Plot of the apparent Stoke's radius vs MW for Plin4-4mer, 12mer, and 20mer (white circles) and protein standards (black circles) as determined from the chromatograms shown in **a**. The Stoke's radius of the Plin4 fragments is about twofold higher than that of folded proteins of similar MW. **c** CD analysis of the Plin4 fragments. The spectra were acquired either in buffer (dashed gray lines) or in an equal volume of buffer and trifluoroethanol (black lines). PLIN4 concentration: 4mer, 19 μM; 8mer, 7.5 μM; 20mer, 4 μM

substitution in each of the 33-mers (1T→V mutant) resulted in a marked improvement in LD localization, as now all LDs in transfected cells became positive for mutated Plin4 AH. The same was true for 2T→V and 3T→V mutations, and even for the only slightly more hydrophobic 3T→A construct (Fig. 3b, c). The T→V mutants could also be observed on LDs in live cells (Supplementary Fig. 4a). In contrast, a less hydrophobic 4T→S mutant with the same number of hydroxylated residues was completely cytosolic under all experimental conditions (Fig. 3b, c).

Concomitant with an increase in their affinity for LDs, the hydrophobic mutants became more promiscuous for binding to other cellular membranes. First, unlike the wild-type Plin4-4mer, more hydrophobic mutants did not stain the nucleus, suggesting that the non-LD localized Plin4 pool has shifted from soluble to membrane-bound (Fig. 3b, d). Note that the Plin4-4mer fused to mCherry is small enough to freely diffuse from the cytosol to the nucleus. Second, a strong reticular signal was observed in cells that highly expressed the 3T→V mutant, whereas in low-expressing cells the signal was much brighter on LDs than in the cytoplasm, suggesting that this AH saturates the LDs before invading other membranes (Fig. 3e). Note that the degree of AH localization to LDs was independent of protein expression levels. Finally, the 3T→V mutant colocalized well with the endoplasmic reticulum (ER) marker Sec61b, in contrast to the wild-type Plin4-4mer (Supplementary Fig. 4b). We conclude that the low hydrophobicity of the Plin4 AH permits a reversible interaction with LDs over a long interaction surface while minimizing the AH binding to other cellular membranes.

Charge of the Plin4 AH affects its targeting. We next analyzed the polar face of the predicted Plin4 AH, which is equally striking in composition. Almost systematically, each 33-mer repeat contains three positively and two negatively charged amino acids. We reversed the net charge of the AH from +1 to −1 by mutating 2 lysines per 33-mer to glutamine, again aiming to minimize other changes to helical properties (Fig. 4a and Supplementary Table 2). Despite being more hydrophobic, the 2K→Q–mCherry fusion became cytosolic and absent from all LDs (Fig. 4b, c). However, its targeting to LDs could be rescued by a further increase in hydrophobicity via the addition of the previously tested 2T→V substitution, showing that the helix is still functional. These results suggest that, whereas net positive charge of the AH is advantageous for LD targeting, it is not essential: a negatively charged AH can also localize to the LD surface, excluding a large contribution from electrostatic interactions and consistent with

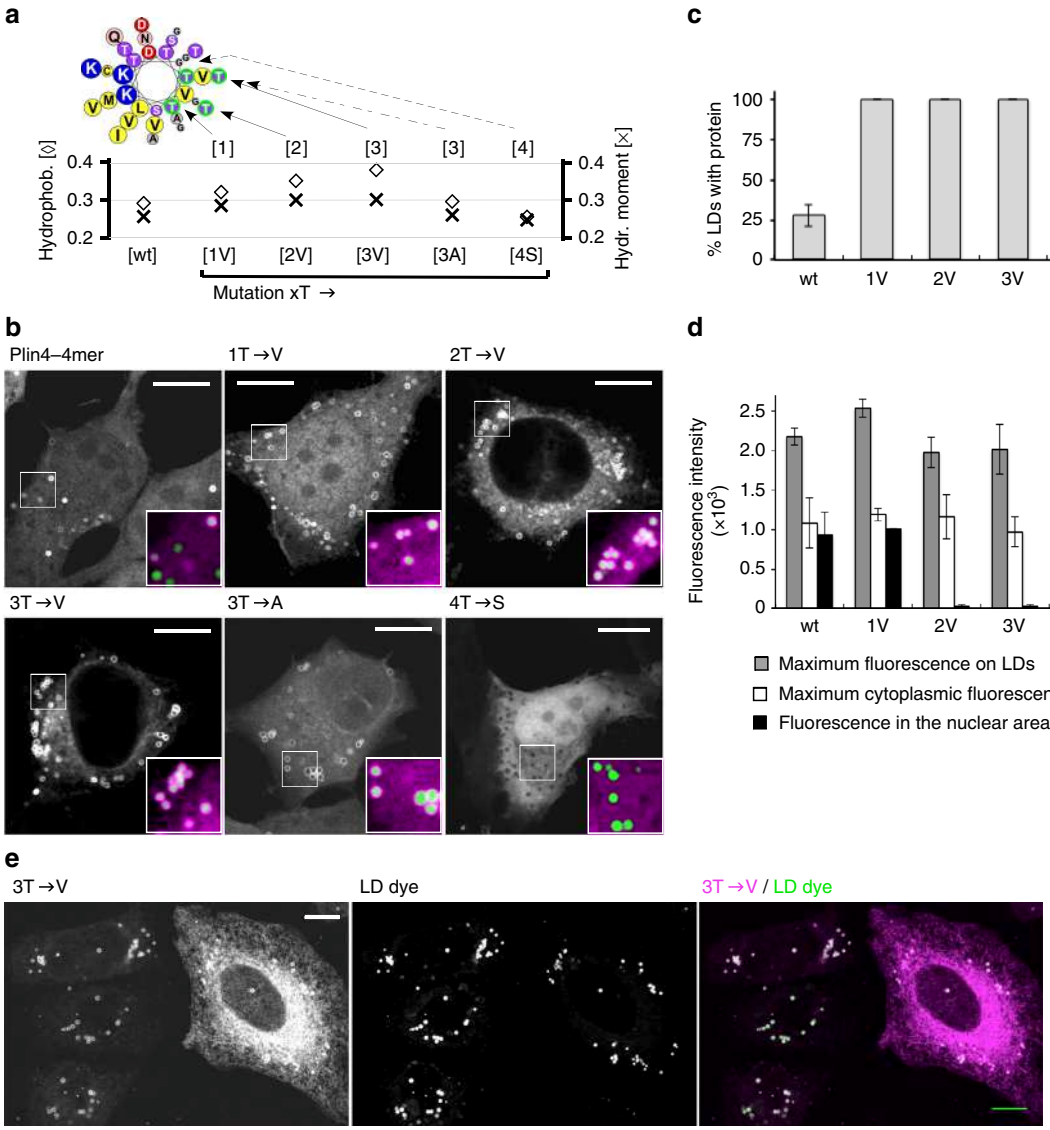

Fig. 3 Influence of AH hydrophobicity on the selective targeting of Plin4 to LDs. **a** Helical wheel depicting cumulative mutations in the hydrophobic face of a Plin4 33-mer. The plot shows the hydrophobicity and hydrophobic moment of each mutant as calculated using Heliquest[71]. **b**–**d** Analysis of the mutants in the context of the Plin4-4mer in HeLa cells described in **a**. For example, the 2T→V mutant corresponds to a construct containing four identical 33mer repeats with two threonine to valine substitutions per repeat. All constructs were expressed as mCherry fusions. **b** Representative examples with large image showing mCherry staining and insets showing merge between the mCherry signal and the LD dye Bodipy. **c** Fraction of LDs per cell positive for the indicated Plin4 construct. **d** Quantification of maximum fluorescence on LDs, maximum fluorescence in the cytoplasm (excluding LDs), and mean fluorescence in the nuclear area for each Plin4 construct. 30–40 cells per experiment were quantified for each construct, and the error bars depict the range of means between two independent experiments. **e** At higher expression level, the 2T→V (not shown) and 3T→V mutants strongly stain the ER network in addition to LDs. In contrast, LD staining is similar between cells with different level of Plin4 expression. Scale bar: 10 μm

lipidomic analysis of LDs[53]. When we expressed the 2K→Q, 2T→V mutant in budding yeast, it could likewise be observed on LDs (Fig. 4d). In contrast, the 2K→Q mutation largely prevented localization of the AH to the negatively charged plasma membrane, where electrostatic interactions are important for protein targeting.

We then constructed an inverse type of mutant, 2D→N, in which we mutated all acidic residues to glutamine (Fig. 4a). As this mutant is more positively charged, it should bind better to negatively charged surfaces[14–16]. Strikingly, we observed a decrease in LD localization, which could be rescued by the 2T→V substitutions (Fig. 4b, c), suggesting that acidic residues also contribute to LD-Plin4 association.

If electrostatic interactions between the Plin4 AH and the lipid surface of LDs are not essential, why are charged residues so conserved throughout the AH sequence? We have noted that charge is always distributed asymmetrically in the polar face of the Plin4 helix, with lysines clustering on one side. This organization is unusual and is not optimal for interaction between lysines and a lipid surface[14,54]. We reorganized the charged residues in the Plin4 AH to make them more symmetrically distributed while maintaining the same amino acid composition and minimizing the change in hydrophobic moment (Fig. 4b). The resulting 'charge-swap' mutant could not be detected on LDs when expressed in HeLa cells. As with the previous charge mutants, the LD-targeting of the charge-swap AH could be rescued by the 2T→V substitution (Fig. 4d). Based

on these observations, we hypothesize that charged residues in Plin4 could be mediating inter-helical interactions to stabilize the AHs on the LD surface, making recruitment of this AH cooperative. Cooperative binding is consistent with our observation that even for helices that are recruited relatively poorly to LDs, the maximum intensity of fluorescent signal on LDs is similar to that of the more hydrophobic AHs of the same length (Fig. 3b, d).

Overall, the mutational analysis of the polar face of the Plin4 AH indicates that the targeting of Plin4 to LDs strongly departs

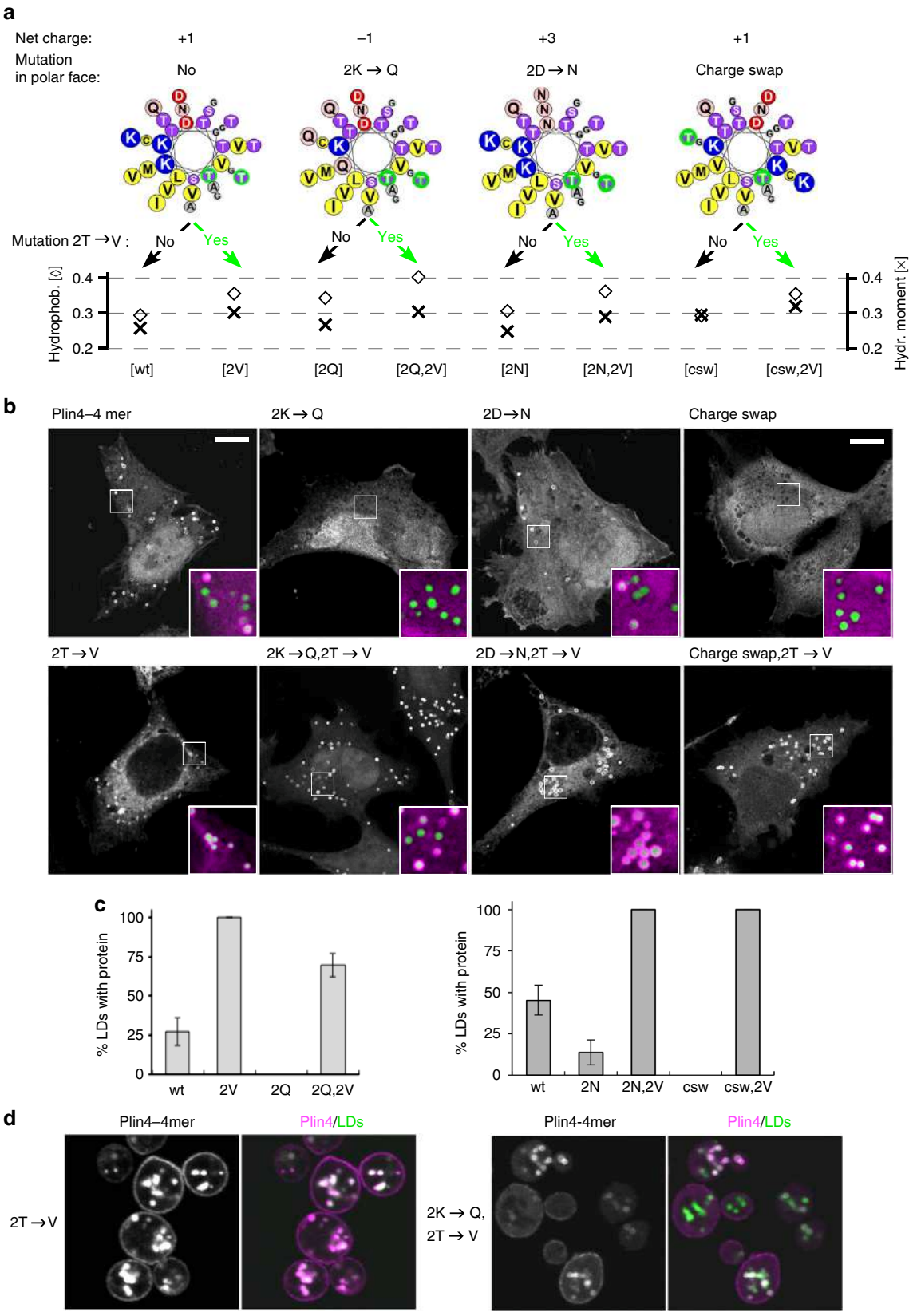

from the mechanism by which many AHs interact with bilayers. In general, positively charged residues electrostatically interact with negatively charged phospholipids. In Plin4, instead, both positively and negatively charged residues contribute to LD targeting and this contribution requires these residues to be properly distributed.

Purified Plin4 AH interacts poorly with bilayer membranes. We used purified Plin4 AH constructs to dissect how they interact with artificial lipid surfaces. Proteins were labeled with NBD or Alexa fluorescent probes via cysteine residues that are present in the Plin4 AH sequence (Fig. 5a, Supplementary Fig. 3c). NBD fluorescence increases in a non-polar environment, allowing quantitative measurement of membrane association.

We performed binding experiments with liposomes of defined size and composition, and varied two parameters that influence the recruitment of many AHs to bilayers: membrane electrostatics and lipid packing (Fig. 5b–e)[14,17,18]. For electrostatics, we replaced PC with phosphatidylserine (PS). For lipid packing, we modulated the amount of lipid packing defects (i.e., exposure of non-polar hydrocarbons) in three different ways. First, we increased lipid unsaturation by replacing saturated-monounsaturated (C16:0-C18:1) phospholipids with their dioleyl equivalents (18:1-C18:1). Second, we increased membrane curvature by decreasing the pore size of the filters used for liposome extrusion. Third, we included the unusual methyl-branched diphytanoyl phospholipids. These lipids, which are not present in eukaryotic cells, have been recently shown to strongly promote α-synuclein adsorption to liposomes by inducing a more drastic increase in lipid packing defects than curvature or lipid mono-unsaturation[55]. In all cases, NBD-labeled proteins were incubated with liposomes at a low protein-to-lipid ratio to minimize crowding effects. For comparison, we used α-synuclein, whose association with bilayers has been studied extensively[17,38,44].

For most liposomes tested, the NBD fluorescence of wild-type Plin4-4mer remained close to that observed in solution suggesting very weak membrane adsorption. These included liposomes with a high content of dioleoyl lipids, negatively charged liposomes, and small liposomes (Fig. 5b–e, black symbols). Furthermore, Plin4 AH was not recruited to liposomes containing an increasing concentration of dioleoyl-glycerol (DOG) (Fig. 5f). DOG was shown to promote Plin3 localization to the ER or to ER-associated LDs[56,57]. The only exception was liposomes containing diphytanoyl phospholipids, for which we observed a dramatic increase in the fluorescence of NBD-Plin4-4mer (Fig. 5b). Flotation experiments indicated total binding of all NBD constructs to 100% diphytanoyl-PS liposomes, thus we used these liposomes to calibrate the fluorescence signal and determine the percentage of protein recruitment under all conditions. In contrast to wild-type Plin4-4mer, the 2T→V mutant displayed a marked increase in fluorescence in the presence of liposomes, and its fluorescence was further augmented by increasing charge or amount of membrane packing defects (Fig. 5b–e, green symbols). α-synuclein, behaved as was previously shown[17]: it interacted with charged and highly curved liposomes, but displayed no binding to neutral liposomes regardless of their degree of unsaturation (Fig. 5b–e, blue symbols).

All Plin4-AH wild-type constructs interacted with diphytanoyl liposomes and their binding affinity increased with AH length, similar to the effect on LD targeting in cells (Figs. 5g and 1). Finally, we used diphytanoyl liposomes to test whether the Plin4 repetitive sequence can fold into a helix in contact with a lipid surface. The addition of such liposomes to the Plin4 peptide induced a large CD peak at 220 nm, indicative of very high α-helical content (≈70%, Fig. 5h). The result shown was achieved with the Plin4-20mer peptide that contains 660 amino acids, which is far longer than other α-helices with a similarly characteristic CD signature.

In conclusion, purified Plin4 AH interacts poorly with most bilayers, but small and repetitive modifications in its amino acid composition can dramatically improve membrane binding in a non-selective manner, as demonstrated by the slightly more hydrophobic 2T→V mutant. In contrast, α-synuclein displays selectivity for bilayers combining curvature and electrostatics (Fig. 5c–e)[17]. The amino acid composition of Plin4 AH therefore seems tuned to exclude most lipid bilayers, which fits well with the low staining of membrane-bound organelles in vivo. However, this lack of avidity for lipid bilayers does not explain why Plin4 selectively adsorbs to lipid droplets.

Plin4 can bind directly to neutral lipids. Given our observations that Plin4 AH selectively binds to LDs in cells and to diphytanoyl liposomes in vitro, we considered possible similarities between these structures. Due to the presence of methyl side chains, diphytanoyl phospholipids form a very poorly packed bilayer with a high degree of exposure of acyl chain carbons (i.e., lipid packing defects)[55]. An in silico analysis demonstrates a sharp increase in lipid packing defects on the phospholipid monolayer of a model LD under conditions of increased surface tension (i.e., an increase in neutral core to surface phospholipid ratio)[22]. Furthermore, increased surface tension promotes α-synuclein binding to inverted LDs in vitro[23]. At the extreme end, an LD completely devoid of a phospholipid monolayer (consisting of only neutral lipids) can be imagined as a lipid surface with infinite packing defects (acyl chain carbons exposed over the whole surface). We therefore asked if the Plin4-AH is capable of interacting with neutral lipids in the absence of any phospholipids.

We mixed a drop of a triglyceride, triolein, with purified Plin4-12mer at increasing protein concentrations, up to a protein-to-lipid molar ratio 1:2000, although there is some uncertainty in protein concentration (Methods). After vigorous vortexing, the suspensions became turbid, suggesting that the oil was emulsified into smaller droplets (Fig. 6a). Vortexing did not affect the properties of the Plin4 AH (Supplementary Fig. 5a, b). Electron microscopy of the Plin4-triolein emulsion revealed numerous spherical droplets with a diameter of 50 to 250 nm (Fig. 6b, Supplementary Fig. 5c). Dynamic light scattering measurements confirmed the presence of particles in the same size range (Fig. 6c,

Fig. 4 Influence of AH charge on the selective targeting of Plin4 to LDs. **a** Helical wheels depicting the mutations that were introduced into Plin4 33mer. In this series, charged residues in the polar face were mutated, and the hydrophobic face was either kept intact or modified with the previously characterized 2T→V mutation (Fig. 3). Charge-swap mutant is abbreviated as 'csw'. The plot shows the hydrophobicity and hydrophobic moment of each mutant as calculated using Heliquest[71]. **b** Representative images of the mutants expressed as mCherry fusions in HeLa cells LDs were stained with Bodipy. All mutants were prepared as identical 4-mer repeats. Scale bar: 10 μm. **c** Quantification of HeLa images, showing % of LDs per cell positive for the indicated Plin4 construct. 30–40 cells per experiment were quantified for each construct and the error bars depict the range of means between two independent experiments. Two sets of mutants were analyzed at different times in the project and are therefore presented on separate plots. **d** Representative images of the mutants expressed as GFP fusions in budding yeast. LDs were marked with Erg6-RFP. For consistency, the colors of the yeast images are inverted. Scale bar: 5 μm

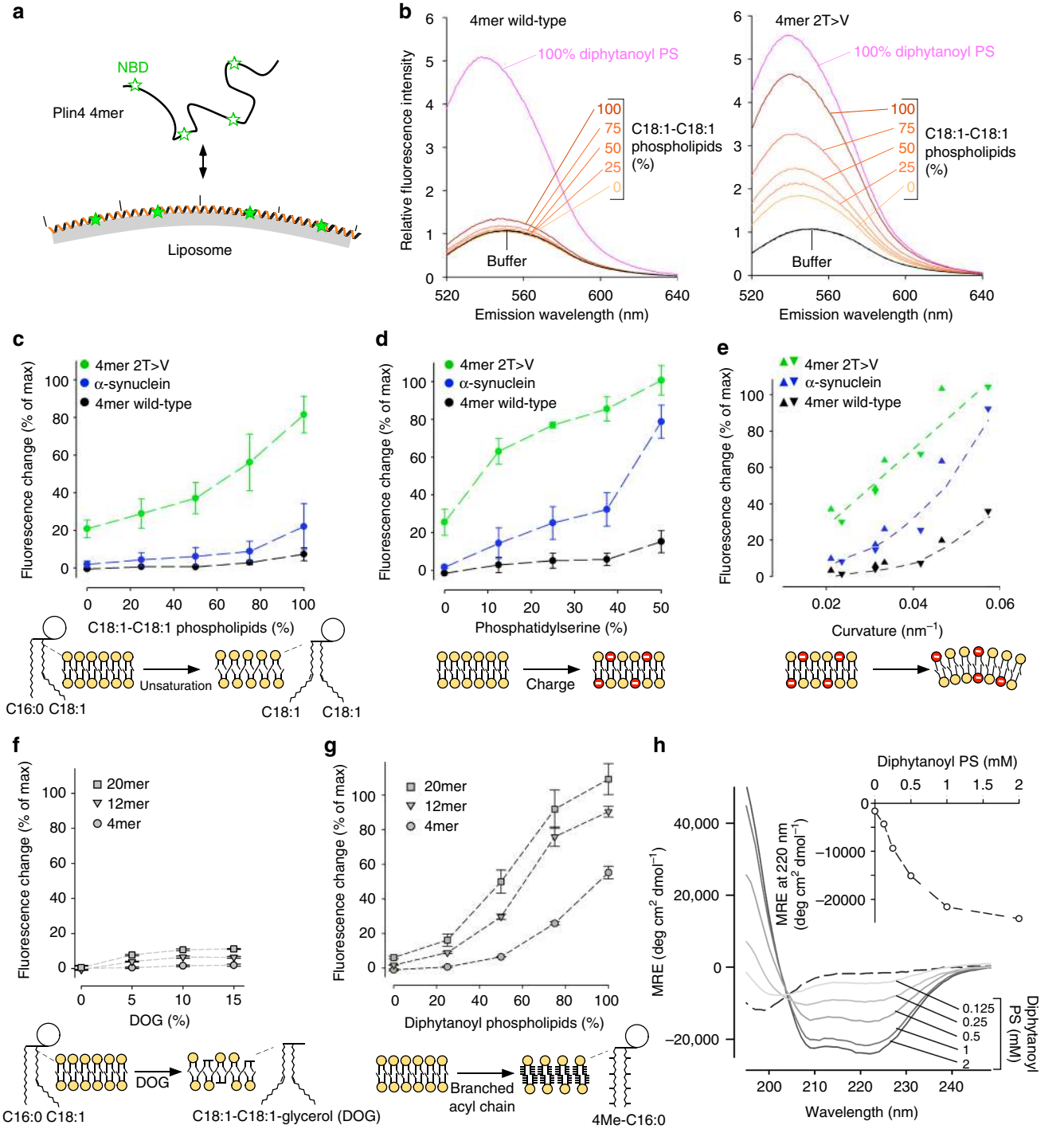

Fig. 5 Plin4 AH is not adapted to classical phospholipid bilayers. **a** Principle of the assay. Plin4 fragments labeled with NBD were mixed with liposomes and their membrane association was determined by measuring the increase in NBD fluorescence. **b** Typical measurements. NBD-Plin4-4mer or the 2T→V mutant were mixed with liposomes containing PC, phosphatidylethanolamine (PE), and cholesterol (50/17/33 mol%). The acyl chains of PC and PE varied from C16:0-C18:1 to C18:1-C18:1 as indicated. The spectra in solution or with diphytanoyl-PS liposomes are also shown. These spectra were used to calculate % binding for each construct (Methods). **c**–**f** Effect of phospholipid unsaturation, PS, membrane curvature, and DOG on liposome binding of the indicated constructs as determined from experiments similar to **b**. The liposome composition (mol%) was: **c** PC (50), PE (17) and cholesterol (33) with an increasing fraction of C18:1-C18:1 at the expense of C16:0-C18:1 phospholipids; **d** C16:0-C18:1-PE (17), cholesterol (33) and an increasing fraction of C16:0-C18:1-PS (0 to 50) at the expense of C16:0-C18:1-PC (50–0); **e** C16:0-C18:1-PC (30), C16:0-C18:1-PS (20) C16:0-C18:1-PE (17) and cholesterol (33). The liposomes were extruded with polycarbonate filters of decreasing pore radius and the liposome radius was determined by dynamic light scattering; **f** C16:0-C18:1-PE (17), cholesterol (33) and an increasing fraction of DOG (0 to 15) at the expense of C16:0-C18:1-PC (50 to 35). **g** Influence of AH length on binding to diphytanoyl lipids. Liposomes contained PC (50), PE (17), and cholesterol (33) with an increasing fraction of diphytanoyl at the expense of C16:0-C18:1 phospholipids. **h** CD spectra of Plin4-20mer in solution or with increasing amounts of diphytanoyl-PS liposomes. Inset: titration of the CD signal at at 222 nm as a function of liposome concentration. Data shown in **c**, **d**, and **g** are means ± s.e.m. from three independent experiments; **e**–**f** show the results of two independent experiments

d). Particle size did not change with the length of the Plin4 AH (Supplementary Fig. 5d). We also prepared a Plin4-oil emulsion using fluorescently labeled Plin4 and visualized it using a spinning disc microscope. Whereas most particles were below the resolution of the microscope, we could visualize larger oil droplets, which were uniformly coated with fluorescent protein (Fig. 6e).

Many protein emulsifiers interact with neutral lipids by essentially denaturing[58,59]. In contrast, apolipoproteins have been shown to interact with neutral lipids via AHs or β-sheets[10]. Given the uniform fluorescent signal of Plin4 that we observe around oil droplets, we hypothesize that Plin4 also folds into a secondary structure in contact with oil, possibly an α-helix. Due to high light scattering of the emulsion, we could not test this directly by CD spectroscopy. Instead, we tested if Plin4 displayed any resistance to proteolysis upon triolein binding, which can be an indication of folding[60]. We observed that Plin4 in oil emulsion was more resistant to trypsin than Plin4 in solution (Fig. 6f), suggesting an increase in secondary structure. We note that in the Plin4 emulsion, the majority of the protein (≥90%) was not bound to

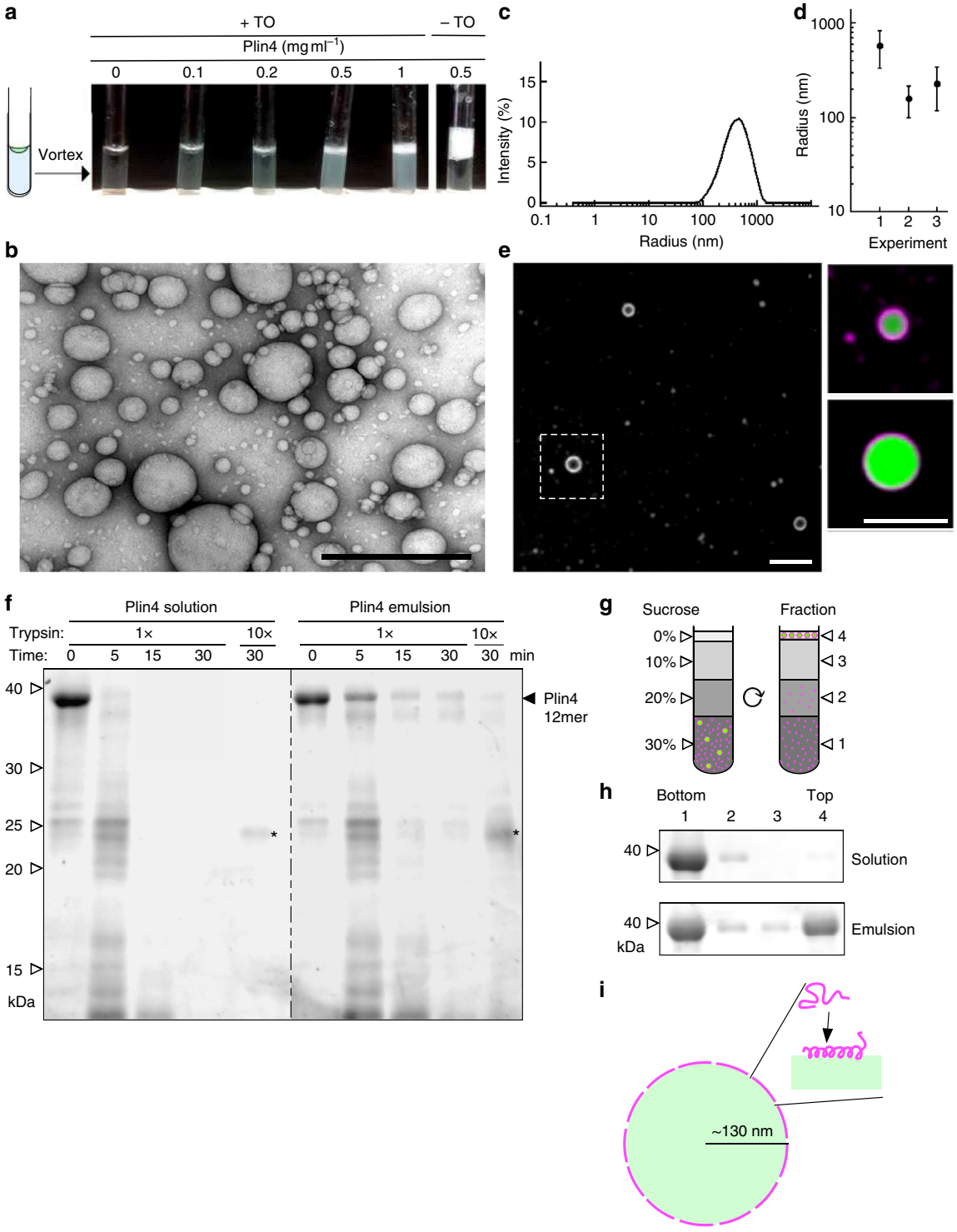

oil, as estimated by flotation of the emulsion through a sucrose gradient (Fig. 6g, h). Therefore, our trypsin assay under-estimates the increase in protease-resistance of Plin4 on oil.

Assuming that Plin4 adopts a perfectly helical conformation in contact with oil, one Plin4-12mer molecule would cover the area of ~60 nm^2[38,61]. Further assuming that all triolein in the emulsion experiment (10 µl) was consumed into oil droplets of 200 nm in diameter, this would give us 3×10^{11} oil droplets with a total surface area of 1.5×10^{17} nm^2 (this is an approximation, as we can also see larger drops of oil in the fluorescent-labeled emulsion). If we consider that 10% of Plin4 molecules used in the experiment (=1 nmol) are coating the oil, this gives a total Plin4 helical area of 3.6×10^{16} nm^2, in the same range as the estimated oil surface area (Fig. 6i; see Supplementary Note 1 for details).

Plin4 AH expression can rescue the PC depletion phenotype. The ability of Plin4-AH to directly coat pure triolein suggests that Plin4 could have a protective effect on LDs in cells, notably under conditions where phospholipids are limiting. To test this hypothesis, we turned to Drosophila Schneider 2 (S2) cells, which have been used extensively to study factors that influence LD homeostasis[6,7,62], and where LD production can be strongly induced by exogenous addition of fatty acids (Fig. 7a). We expressed Plin4-12mer in S2 cells as a GFP fusion from an inducible promoter. In the absence of oleic acid, where LDs were largely absent, only soluble signal of Plin4-12mer-GFP was observed in these cells. Upon oleic acid treatment, we observed strong localization of Plin4-AH on LDs (Fig. 7a). Full-length Plin4-12mer is efficiently expressed in S2 cells under all growth conditions (Fig. 7b).

CTP:Phosphocholine Cytidylyltransferase 1 (CCT1), a homolog of human CCTα, catalyzes the rate limiting reaction in the synthesis of PC and has been shown to be particularly important for maintaining stable LDs in S2 cells. When CCT1 is depleted, insufficient PC production leads to a large increase in the size of LDs, decreasing their net surface to volume ratio[6], (Fig. 7c, Supplementary Fig. 6a). We hypothesized that due to the ability of the Plin4 AH to directly coat neutral lipids, its expression under these conditions should decrease the size of LDs. Indeed, the CCT1 depleted cells that were expressing Plin4-12mer-GFP had significantly smaller LDs than non-expressing cells in the same population (Fig. 7c, d). Plin4 expression also led to a small but reproducible decrease in the size of LDs in control cells (Fig. 7c, d; Supplementary Fig. 6b, c). Based on these observations, we conclude that in a cellular context, Plin4-AH can replace the PL monolayer of LDs insufficiently covered with PLs and stabilize them.

Discussion

We have analyzed the mode of binding of a highly unusual AH, present in the human protein Plin4, to LDs. This AH is exceptional in terms of its length and the repetitiveness of its primary sequence. We demonstrate that the Plin4 AH is exquisitely tuned for binding to LDs and not to bilayer membranes and that this interaction is promoted by depletion of PC from cells, in agreement with the strong interaction of this helix with neutral lipids in vitro. Altogether, these observations suggest that Plin4 acts as a reversible coat that contacts directly the LD core, substituting for phospholipids. By varying the properties of this exceptional AH one at a time, we demonstrate that different AH parameters contribute to specificity and strength of LD binding: length, hydrophobicity, charge and charge distribution. Whereas these properties can to some extent substitute for one another, this may be at the expense of LD selectivity.

Lipid-interacting AHs generally adopt their helical structure when in contact with a lipid surface, whereas in their soluble form they are either unfolded or folded within the soluble conformation of the host protein[16,44,47]. We have demonstrated that the Plin4 AH is unfolded in solution and that it folds into a super long helix in the presence of diphytanoyl liposomes. We show that there is a clear correlation between the Plin4 AH length and its targeting to LDs and to synthetic liposomes (Fig. 1 and Fig. 5). This fits with the "Velcro model", which postulates that the combined effect of low-affinity interactions, repeated over an extended binding surface, leads to the stabilization of the bound AH[15]. Although this model is very intuitive, the previous experimental evidence was less direct or based on small changes in length[10,17,25,63].

A diverse array of AHs has been implicated in LD targeting, and many of them can also bind to lipid bilayers (Table 1). Both α-synuclein, a synaptic vesicle protein, and the nucleo-ER localized enzyme CCTα can be observed on LDs[6,45,64]. Furthermore, the small GTPase Arf1 and the GTP exchange factor GBF1 utilize AHs to target Golgi membranes and also LDs[12,23,62,65]. Interactions of these proteins with LDs are physiologically relevant, as they have reported roles in LD function, with the exception of α-synuclein (but its close homolog γ-synuclein has a function in adipocyte metabolism[46]).

Comparing the AHs that localize to LDs suggests that the LD surface can accommodate a wide range of different AH chemistries. Caution is warranted, as adjacent peptide sequences can influence binding preferences of an AH[66,67]. In contrast, the length and the homogenous nature of the Plin4 AH have allowed us to evaluate the influence of different AH parameters on LD targeting in a context-independent manner. LD targeting is permitted by the weakest AH character, exemplified by the wild-type Plin4 AH sequence (Table 1). This suggest that the LD surface is very permissive for AH binding, in accordance with in silico analysis demonstrating that this surface is abundant in lipid packing defects, which promote AH adsorption[22]. Because packing defects increase with decreasing density of surface phospholipids, conditions that decrease monolayer density may

Fig. 6 Plin4 interacts directly with neutral lipids in vitro forming oil droplets. **a** Images of tubes in which a drop of triolein (10 µl) was vigorously mixed with a solution (190 µl) of increasing concentration of Plin4-12mer. **b** Representative image of the Plin4-oil emulsion by negative staining electron microscopy. Scale bar: 0.5 µm. **c**, **d** Dynamic light scattering measurement of the size distribution of an aliquot withdrawn from the middle of the oil emulsion obtained with 0.5 mg ml^{-1} Plin4-12mer, and comparison between three independent experiments, with dots representing peak maxima and vertical bars representing polydispersity. **e** Plin4-oil emulsion was visualized by confocal fluorescence microscopy. Unlabeled Plin4-12mer (0.3 mg ml^{-1}) was mixed Plin4-12mer-Alexa568 at a ratio 20:1 (magenta), and oil was stained with Bodipy (green). Left panel shows Plin4 and right panels show zoom-ins of merged images. Scale bars: 5 µm. **f** Plin4 in the oil emulsion is protected from degradation by trypsin. Plin4-12mer (1 mg ml^{-1}) was incubated in buffer only or vortexed with triolein as in **a**, then digested with 13 µg ml^{-1} (×1) or 130 µg ml^{-1} (×10) trypsin for the amount of time indicated. Samples were analyzed by SDS-PAGE with Sypro Orange staining. Five times less sample was loaded in the 0 min controls than in the other lanes. White arrowheads indicate the migration of molecular weight standards. Asterisks indicate the trypsin band. **g**, **h** Plin4-12mer (1 mg ml^{-1}) before (solution) or after (emulsion) the reaction depicted in (**a**) was mixed with sucrose and loaded on the bottom of a sucrose gradient. After centrifugation, four fractions were collected from the bottom and equal volumes were analyzed by SDS-PAGE with Sypro Orange staining. See Supplementary Fig. 7 for uncropped gels in **f**–**h**. **i** Model of a Plin4-12mer-covered oil droplet, drawn to scale. Calculation (see main text) suggests complete coverage of the oil surface by Plin4 AH

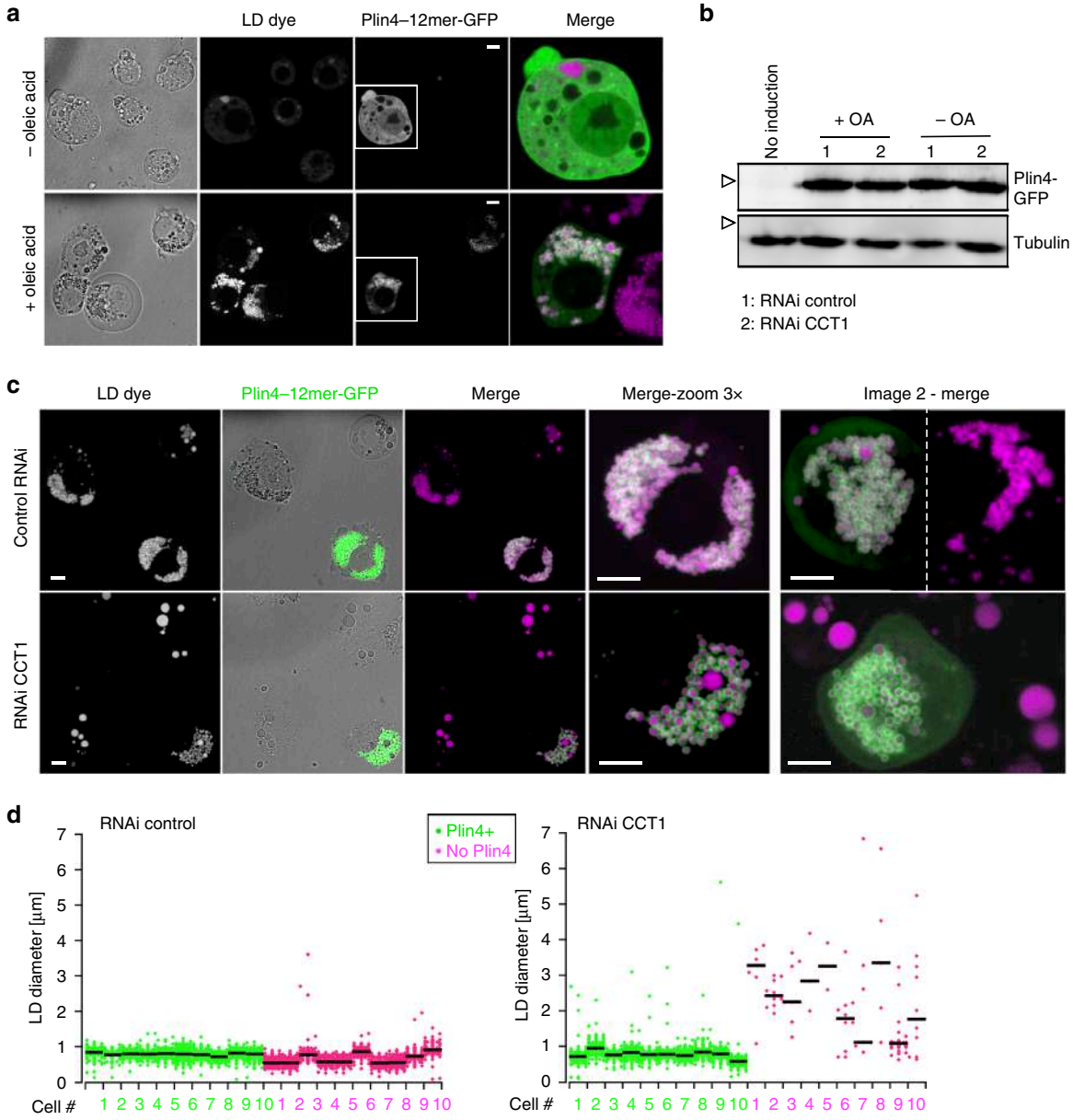

Fig. 7 Plin4 AH expression in Drosophila S2 cells rescues the defect in LD size due to PC depletion. **a** Plin4-12mer-GFP localizes to LDs. Expression was induced with copper for 48 h. For the last 24 h, cells were either supplemented with oleic acid to induce LDs (+OA) or were kept in normal growth medium (−OA). LDs were stained with Autodot dye. Images were obtained with a spinning disc microscope and are presented as projected z-stacks. The merged images show a ×3 zoom of the area marked in the Plin4 images with LDs in magenta and Plin4 in green. Scale bar: 5 µm. **b** Western blot analysis of Plin4-12mer-GFP expression in non-induced cells (no copper addition, lane 1), or in copper-induced cells (lanes 2–5) that were subjected to the indicated treatments. Plin4-12mer levels were not affected by oleic acid treatment or by RNAi against CCT1 (**c**). Tubulin was used as loading control (uncropped membranes in Supplementary Fig. 7). White arrowheads indicate the migration of 70 kDa and 55 kDa molecular weight standards, respectively. **c**, **d** Cells were treated with RNAi against CCT1 to deplete PC or with control RNAi, followed by Plin4-12mer-GFP induction and oleic acid treatment; **c** images show a comparison of LD size between Plin4-transfected and non-transfected cells in the same field, with enlarged images of the merged channels; **d** graphs show quantification of LD size in individual cells in a representative of three experiments (shown in Supplementary Fig. 6b, c), with bars depicting median values

further promote AH binding, as has been observed[23,24]. The "sticky" nature of the LD surface is also in agreement with findings that LDs can act as sinks for various non-LD proteins to prevent their accumulation in the cytosol[3]. The fact that AHs can easily target LDs suggests that mechanisms that prevent their localization to LDs play a significant role, for example competition between proteins for a limited LD surface[26].

We show that the Plin4 AH can directly coat neutral lipids to make small oil droplets in the absence of any other emulsifier. Perilipins are often described as LD coat proteins, however, this activity remains poorly characterized[21,27,68]. Various proteins can function as emulsifiers and are in fact widely used for various applications[58]. Many soluble globular proteins bind irreversibly to oils, essentially undergoing denaturation. In contrast, apolipoprotein B, which directly interacts with neutral lipids in low density lipoprotein particles, forms a series of AHs that reversibly bind to lipids in vitro[59].

With its exceptional length, we estimate that one full-length human Plin4 AH of 950 amino acids can replace around 250 phospholipids in a packed monolayer, and could form a surface

that is similarly smooth. The sequence of Plin4 AH, with its high repetitiveness, low hydrophobicity and particular charge organization, may be exquisitely adapted to forming a homogeneous coat whose recruitment to LDs is highly reversible. It is interesting to note a parallel with the structure of synthetic peptoid nanosheets that assemble on an oil–water interface and are stabilized by side-side electrostatic interactions[69]. Further studies will be needed to understand the structural organization of the Plin4 coat.

If Plin4 AH can directly interact with neutral lipids in vitro, what is the situation in cells? Branched diphytanoyl phospholipids also promote binding of Plin4 AH to liposomes, suggesting that the presence of polar lipids does not preclude binding. Instead, the Plin4 AH seems to bind to any surface with a very high density of packing defects, for example an LD with increased surface tension. Although Plin4 is highly expressed in adipocytes, and its unusual structure suggests a specialized function, little is known about the physiological role of this protein[29]. Our data suggest that Plin4 may be optimized for coating and thereby stabilizing LDs under conditions of limiting phospholipids. Interestingly, Plin4 has been observed to preferentially localize to small LDs in differentiating adipocytes[33,34], suggesting a function in regulating LD surface to volume ratio. In addition, it has been shown to display a preference for LDs with a particular neutral lipid composition[43]. Further studies are needed to analyze the properties and dynamic behavior of this protein coat in vitro and in cells. The AH of Plin4 is about 10 times longer than the longest predicted AH region in other human perilipins, in which the repeats are less conserved and sometimes broken up by deletions or insertions. However, compared to AHs found in other proteins, these AH regions are all still very long, and it will be interesting to explore to what extent our findings on Plin4 AH apply to perilipins in general.

Finally, we note that a study published while this paper was under review also concludes that the LD surface can interact with AHs of widely different chemistries[70]. However, the authors suggest that one requirement for LD binding is the presence of large hydrophobic residues in the AH, which is at odds with our results based on Plin4. Because our study indicates that increasing the size of hydrophobic residues promotes a general increase in the binding of AHs to both LDs and bilayer membranes, such a mechanism probably applies to proteins like Arf that have a short AH and act on both LDs and on bilayer-bound organelles[62,65]. For proteins like perilipins, AH length and electrostatic interactions compensate for the lack of large hydrophobic residues and lead to a more selective mode of LD binding.

Methods

Sequence analysis. Sequences of AHs were identified and plotted using Heliquest[71]. Heliquest was also used to calculate their hydrophobicity and hydrophobic moment. For longer AHs containing more than 3 helical turns, hydrophobic moment was calculated as the average of values for individual helices, as shown in figures, normalizing for the length of AHs. The amino acid conservation of the 33 amino acid repeats of Plin4 was analyzed using Weblogo[72].

Plasmid DNA construction. All human Plin4 expression plasmids used in this study (Supplementary Table 3) were constructed using synthetic double-stranded DNA fragments. Due to the highly repetitive nature of the Plin4 AH region, DNA sequences were optimized for synthesis using the algorithm on the Eurofins website (https://www.eurofinsgenomics.eu). Plin4-4mer, Plin4-8mer, and Plin4-12mer–mCherry fusion plasmids for expression in HeLa cells were generated by cloning synthetic genes (Supplementary Table 4) into the pmCherry-N1 expression plasmid (Clontech) using XhoI and BamHI restriction sites. Note that we define a 1mer unit as 33 amino acids of the Plin4 AH sequence. Plin4-2mer was generated by PCR-amplification of the first 67 codons of Plin4-4mer and XhoI-BamHI into pmCherry-N1. Plin4-20mer was generated by assembling synthetic genes for Plin4-8mer and Plin4-12mer into pmCherry-N1 using GeneArt Assembly kit (Life Technologies), without introducing any additional nucleotides between the DNA sequences encoding the two Plin4 fragments. The C-terminal region of Plin4, encoding amino acids 1060-1356 of mouse Plin4, was PCR-amplified from vector pKTD-16A (gift from Knut Dalen, University of Oslo) and cloned XhoI-BamHI into vectors pmCherry-N1 and pEGFP-N1. Plin4 mutants were generated using synthetic genes whose sequences were optimized for DNA synthesis. All 4mer mutants were exact 4× repeats of a 33 amino acid sequence, based on the parental sequence of human Plin4 fragment aa246-278 (Supplementary Table 4). All mutant synthetic genes were cloned BamH1-XhoI into pmCherry-N1.

For expression of Plin4 constructs in *Saccharomyces cerevisiae*, the pRS416-derived CEN plasmid pRHT140 (gift from Sebastien Leon, IJM, Paris) containing ADH1promotor and GFP expression tag for C-terminal tagging, was mutated by site-directed mutagenesis to introduce an Nhe1 restriction site and correct the reading frame, generating pKE28. DNA sequences encoding various Plin4 fragments were then subcloned by restriction and ligation from pmCherry-N1 plasmids using HindIII and NheI restriction sites. For expression of Plin4 constructs in *E. coli* without any tag, various Plin4 fragments were PCR-amplified to introduce NheI and XhoI restriction sites and ligated into pET21b (Novagen), resulting in the elimination of the T7 and His tags from the vector. The only exception was plasmid pKE25 for expression of Plin4-20mer, which was generated by restriction and ligation of the Plin4-20mer DNA fragment from the pmCherry plasmid pCLG70 using NheI and BamHI restriction sites. For this purpose, pET21b was mutagenized by site-directed mutagenesis to include 3 stop codons after the BamHI restriction site in the vector, resulting in pET21b-3stop. For expression of Plin4-12mer in Drosophila S2 cells, Puro-pMTWG vector was generated by digestion of pAWG destination vector (the Drosophila GatewayTM Vector Collection) by EcoRV and BglII enzymes to excise the actin promoter. Puromycin resistance gene and metallothionein promoter were obtained by PCR from pMT-Puro vector (Riken, ref. RDB08532), and subsequently inserted by In-Fusion reaction (Clontech) into the destination vector. Primers used are TCATTTTTCCAGATCTCGGTACCCGATCCAGACATGATAAG (Fw); TAGACAGGCCTCGATATCCCTTTAGTTGCACTGAGATGATTC (Rv). DNA for Plin4-12mer was PCR-amplified and cloned into this vector using the Gateway LR reaction technology (Life Technologies).

Yeast growth and media. Yeast strains used were BY4742 *MATα his3Δ1 leu2Δ0 lys2Δ0 ura3Δ0*, or into BY4742 *ERG6::mRFP::KanMX6*. Yeast cells were grown in yeast extract/peptone/glucose (YPD) rich medium, or in synthetic complete (SC) medium containing 2% glucose. Yeast was transformed by standard lithium acetate/polyethylene glycol procedure. For observation of LDs, liquid cell cultures were inoculated from a single colony and grown for 24 h at 30 °C in SC-Ura with 2% glucose to maintain plasmid selection.

Cell culture and transfection. HeLa cells were grown in Dulbecco's modified Eagle's medium (DMEM) supplemented with 4.5 g l^{-1} glucose (Life technologies), 10% fetal bovine serum (FBS, Life technology) and 1% Penicillin/Streptomycin antibiotics (Life technologies). For protein expression, subconfluent cells were transfected with Lipofectamine 2000 (Invitrogen) in Optimem medium (Life technologies) for 6 h, followed by 16 h in standard growth medium or standard growth medium containing 250 µM oleic acid (Sigma) in complex with fatty-acid free BSA (Sigma).

Drosophila S2 cells (ThermoFisher) were cultured in Schneider's Drosophila medium (Invitrogen) supplemented with 10% FBS and 1% Penicillin/Streptomycin at 25 °C. For generating stably-transfected cells, cells were incubated with plasmid DNA and TransIT-Insect Reagent (Mirus), followed by selection with 2 µg ml^{-1} puromycin (Life technologies) for 2 weeks. Protein expression from the metal-inducible promoter was induced for 48 h with the addition of 100 µM Cu-sulfate to the medium. Lipid droplets were induced with 1 mM oleic acid-BSA complex for 24 h.

RNAi depletion. RNAi depletion against CCT1 in stably-transfected S2 cells was performed as described[6], using the same primer sequences to generate 580 bp dsRNA (Fwd, ACATCTATGCTCCTCTCAAGG C; Rev, CTCTGCA-GACTCTGGTAACTGC). For RNAi control experiment, we used dsRNA against luciferase (Fwd, AAATCATTCCGGATACTGCG; Rev, CTCTCTGAT-TAACGCCCAGC). The dsRNA fragments were generated with T7 RiboMAX™ Express RNAi System (Promega) using two separate PCR reactions with a single T7 promoter (sequence TAATACGACTCACTATAGG appended to 5' ends of primers). 2×10^6 cells were incubated with 30 µg of dsRNA for 30 min in serum-free medium, followed by the addition of complete medium. Cells were incubated for 3 days. Protein expression was induced with Cu-sulfate for the last 2 days, and LDs were induced with 1 mM oleic acid during the final day of the experiment. To verify the depletion of CCT1, total RNA was prepared using the NucleoSpin RNA kit (Macherey-Nagel), and quantiTect Reverse Transcription kit (Qiagen) was used to synthesize complementary DNA. Quantitative real-time PCR was performed in triplicates using Light Cycler 480 SYBER Green I Master Kit (Roche) with primers for CCT1 (Fwd, GGAAGCGGACCTACGAGATA; Rev, GTGCCCTGATCCT-GAACTT), and for GAPDH as control (Fwd, ATGAAGGTGGTCTCCAACGC; Rev, TCATCAGACCCTCGACGA).

Western blot analysis. Total cell lysates from S2 cells were obtained by incubating harvested cells in ice-cold lysis buffer (300 mM NaCl, 100 mM Tris-HCl pH 8, 2% NP-40, 1% deoxycholate, 0.2% SDS, 10 mM EDTA, 'Complete mix' protease inhibitors from Roche), followed by centrifugation and denaturation in Laemmli buffer at 95 °C for 5 min. Proteins were separated on 13% SDS-PAGE gel and transferred to a nitrocellulose membrane (GE Healthcare). Rabbit polyclonal αGFP antibody (Invitrogen, A11122, 1:2000 dilution) was used for detection of Plin4-12mer-GFP, followed by HRP-conjugated secondary antibody. Mouse monoclonal α-tubulin (Sigma T9026, 1:4000 dilution) was used for loading control. ECL Western Blotting kit (GE Healthcare) was used for detection, and images were obtained using Fujifilm LAS3000.

Fluorescent microscopy. Transfected HeLa cells were fixed with 3.2% paraformaldehyde (Sigma) in PBS for 30 min at room temperature. After washing three times with PBS, cells were stained with Bodipy 493/503 (Life Technologies) at 1 µg ml^{-1} for 30 min at room temperature and washed three times with PBS. Cells were mounted on coverslips with Prolong (Life technologies). Images were acquired with a TCS SP5 confocal microscope (Leica) using a ×63/1.4 oil immersion objective driven by LAS AF Lite software. Alternatively, images were acquired with an LSM780 confocal microscope (Zeiss) using a ×63/1.4 oil immersion objective and a PMT GaAsP camera, driven by ZEN software. Mid-focal plane images were selected and they were processed with ImageJ and with Canvas Draw software. Figures were compiled in Canvas Draw.

Yeast cells were grown to post-diauxic shift (24 h) in selective media and imaged directly on glass slides. Images were acquired at room temperature with a DMI8 (Leica) microscope, equipped with an oil immersion plan apochromat 100 objective NA 1.4, an sCMOS Orca-Flash 4 V2+ camera (Hamamatsu), and a spinning-disk confocal system CSU-W1 (Yokogawa - Andor) driven by MetaMorph software. 5 z-sections separated by 0.5 µm were acquired. For quantification of plasma membrane and LD signal in yeast, images were acquired with LSM780 confocal microscope as described above. To visualize LDs and stably-transfected proteins in Drosophila S2 cells, cells were stained with Autodot autophagy visualization dye (Clinisciences) for 1 h and washed two times with PBS, after which they were resuspended in fresh growth medium and imaged directly on untreated glass slides using the CSU-W1 spinning-disk set-up described above. For 3D-reconstitutions of S2 cells, between 16 and 25 z-sections separated by 0.2 µm were acquired for each image.

Image analysis. Images of HeLa and yeast cells were analyzed using ImageJ. To determine the fraction of LDs in HeLa cells that were positive for transfected fluorescent protein, a single z-section that contained the most LDs in a cell was first selected. All LDs in the selected cell section were identified in the green (Bodipy dye) channel using the 'Analyze particle' plug-in. The total area of LD fluorescent signal in the cell was also measured, and the average size of LDs was determined by dividing these two values. LDs positive for fluorescent protein were then identified by determining a threshold value for the red fluorescent signal (mCherry-protein fusion), ×1.4 above average cellular fluorescence, and counting all LDs with fluorescence above this threshold. This number was divided by the total LD number to calculate the fraction of LDs in one cell section positive for protein. To determine the maximum intensity of fluorescent protein signal on LDs, five brightest LDs per cell were selected manually and the maximum fluorescent signal was determined from a line-based profile using the 'Find peaks' plug-in. The average of these five maxima was taken as the maximum LD fluorescence intensity. Similarly, the maximum cytoplasmic fluorescence was determined from the five maxima of line-based profiles going from the nucleus to the cell exterior, with lines drawn manually and not crossing any LDs. The average protein fluorescence in the nuclear area was determined by placing three squares in the nucleus of each cell and calculating their average fluorescence. Data was processed in Microsoft Excel.

To determine the diameter of LDs in Drosophila S2 cells, 3D-representations of S2 cells were generated from z-stacks and LDs were identified using spot detection with Imaris image analysis software (Bitplane, Oxford). Diameters of all spheres representing single LDs were recorded. LDs that were very close together and could not be identified by the software as individual spheres were manually eliminated. Therefore, the total number of LDs identified in each cell is lower than the actual number. LDs in all isolated cells transfected and non-transfected in a selected image were quantified. Data were processed in Excel and in KaleidaGraph.

Protein purification. Purification and labeling of full-length α-synuclein were as previously described[17]. The protocol for purifying the various Plin4 constructs was adapted from that used for α-synuclein[50], and included two steps: boiling to precipitate most proteins except Plin4, which is heat resistant, followed by ion exchange chromatography. In contrast to α-synuclein, Plin4-AH has a net positive charge at neutral pH (pI = 9.56 for the amphipathic region [95–985]). Therefore, Plin4 fragments were purified by cation chromatography. *E. coli* cells BL21DE3 transformed with expression plasmids were grown to O.D. ≈0.6 and induced with 1 mM IPTG for 3–4 h at 37 °C. Cells from 0.25 to 0.5 l cultures were collected by centrifugation and frozen. The bacterial pellet was thawed in 25 mM Tris, pH 7.5, 120 mM NaCl, supplemented with 1 mM DTT, 0.1 mM PMSF, and other protease inhibitors (Roche complete cocktail, phosphoramidon, pepstatin, bestatin). Cells were broken by three passages in a french press or by sonication. The lysate was centrifuged at 100,000 × *g* for 30 min at 4 °C in a TI45 rotor (Beckman). The supernatant in centrifuge tubes was immersed in boiling water for 30 min. The resulting cloudy suspension was centrifuged at 100,000 × *g* for 15 min at 4 °C to remove precipitated material. The supernatant was dialyzed against 25 mM Tris, pH 7.5, 10 mM NaCl, 1 mM DTT for 2 h in a cold room using Spectra/Por membranes with a cut off of 6000 Da (Spectrum labs) and then centrifuged again at 100,000 × *g* for 20 min at 4 °C. For chromatography, the final supernatant was loaded onto a Source S column (7.5 ml; GE Healthcare) and submitted to a salt gradient from 1 mM to 400 mM NaCl (8 column volumes) at a flow rate of 4 ml min^{-1} using an Akta purifier system (GE Healthcare). All Plin4 constructs (4mer, 12mer, 20mer, 4mer 2T→V mutants), eluted at approximately 100 mM NaCl. Alternatively, the purification was performed using a 1 ml hand-driven column (HiTrap, GE Healthcare) using a step salt gradient. After SDS-PAGE analysis of the chromatography fractions, the protein pool was divided in small aliquots, flash frozen in liquid nitrogen and stored at −80 °C. Of note, the lack of aromatic residues in Plin4-AH prevents the determination of its concentration by UV spectroscopy or by Coomassie Blue-based assays (e.g. Bradford). As a first estimation, we loaded the various Plin4 aliquots on SDS-PAGE along with BSA standards and stained the gel with Sypro Orange (Life Technologies), which interacts with SDS. This procedure gave a typical Plin4 concentration in the range of 1–2 mg ml^{-1}, except in the case of the 2T→V mutant, where the purification yield was lower (concentration ≈0.3 mg ml^{-1}). We also used a more accurate protocol of determining the protein concentration through cysteine quantification with the Edman reagent (Sigma), relying on numerous cysteines in Plin4-4mer, 12mer and 20mer constructs (4, 4, and 10, respectively). This procedure was performed after protein dialysis to eliminate DTT and gave a 2.5 higher concentration of protein for the wild-type constructs (in the range of 3.5 mg ml^{-1}).

Analytical gel filtration. Plin4-4mer, 12mer and 20mer were analyzed by gel filtration on a Superose-12 column (10×300 mm, GE Healthcare). Proteins were injected at a starting concentration and volume of 3.5 mg ml^{-1} and 100 µl. Elution was performed at room temperature in 25 mM Tris, pH 7.7, 125 mM NaCl, 0.5 mM DTT at a flow rate of 0.5 ml min^{-1}. Absorbance was continuously measured at 215 nm. Fractions were collected and analyzed by SDS-PAGE using Sypro Orange staining. To calibrate the column, the following standards were used: cytochrome C (MW: 12.4 kDa, Stoke's radius: 17 Å), Anhydrase Carbonic (29 kDa, 20 Å), Bovine Serum Albumin (67 kDa, 35 Å), ß amylase (200 kDa, 54 Å) and Ferritin (443 kDa, 61 Å).

Circular dichroism. The experiments were done on a Jasco J-815 spectrometer at room temperature with a quartz cell of 0.05 cm path length. Each spectrum is the average of several scans recorded from 200 to 260 nm with a bandwidth of 1 nm, a step size of 0.5 nm and a scan speed of 50 nm min^{-1}. Control spectra of buffer with or without liposomes were subtracted from the protein spectra. The buffer used was Tris 10 mM, pH 7.5, KCl 150 mM.

Protein labeling with fluorescent probes. Purified Plin4 constructs were labeled with fluorescent probes via endogenous cysteines. For NBD (nitrobenzoxadiazole) labeling, 1 ml of Plin4-4mer, 12mer, 20mer, or 2T→V 4mer mutant was dialyzed on a NAP10 column in Hepes 50 mM K-Acetate 120 mM, pH 7.4 (HK buffer) to remove DTT. The protein fraction was then incubated for 5 min at room temperature with 8–20 mol excess of NBD-iodoacetamide (Life Technologies), corresponding to a 2 mol excess over cysteines. After the addition of 2–5 mM DTT to stop the reaction, the mixture was loaded again onto a NAP10 column to separate the labeled protein from the excess of probe. The fractions were analyzed by SDS-PAGE and UV-visible chromatography. For labeling with Alexa C5 maleimide probes (Life Technologies), we used a similar protocol except that the probe was incubated with the protein at 1:1 ratio for 5 min at 4 °C before the addition of DTT to stop the reaction.

NBD fluorescence assay for liposome binding. Dry films containing the desired amount of phospholipids and cholesterol were prepared from stock solutions of lipids in chloroform (Avanti Polar Lipids) using a rotary evaporator. The film was resuspended in 50 mM Hepes, pH 7.2, 120 mM K-acetate at a concentration of 2 mM phospholipids. After five cycle of freezing in liquid nitrogen and thawing in a water bath at 30 °C, the resulting multi-lamellar liposome suspension was extruded through polycarbonate filters. Filters with a pore size of 100 nm were used for all experiments except when studying the effect of membrane curvature. In this case, the liposome suspension was sequentially extruded through 200, 100, 50, and 30 nm pore size filters, or sonicated with a titanium probe to get the smallest liposomes. The size distribution of the liposomes was determined by dynamic light scattering using a Dynapro apparatus.

Fluorescence emission spectra upon excitation at 505 nm were recorded in a Jasco RF-8300 apparatus. The sample (600 µl) was prepared in a cylindrical quartz cuvette containing liposomes (150 µM lipids) in HK buffer supplemented with 1 mM $MgCl_2$ and 1 mM DTT. The solution was stirred with a magnetic bar and the temperature of the cuvette holder was set at 37 °C. After acquiring a blank spectrum, the protein was added and a second spectrum was determined and corrected for the blank. The Plin4 4mer, 12mer, and 20mer constructs were used at 120, 40, and 24 nM, respectively, in order to have the same concentration of amino

acids (≈15 μM) and thus the same amino acid/phospholipid ratio (≈1:10) in all experiments. The fraction of liposome bound protein was defined as $(F-F_{sol})/(F_{max}-F_{sol})$, where F is the actual fluorescence level at 540 nm, and F_{sol} and F_{max} are the fluorescence levels of the NBD-labeled construct in buffer and in the presence of diphytanoyl-PS liposomes, respectively. Flotation experiments in the presence of diphytanoyl-PS liposomes indicated that all Plin4 constructs as well as α-synuclein were completely bound to these liposomes.

Preparation and analysis of protein-oil emulsions. Dilutions of purified Plin4-12mer (up to 1 mg ml^{-1}, or 25 μM) were prepared in HK buffer supplemented with 1 mM $MgCl_2$ and 1 mM DTT. 190 μl of each solution was pipetted into a 600 μl glass tube, and a 10 μl drop of triolein (Sigma) was added to the top. They were vortexed for three cycles of 30 s on 30 s off at 25 °C under argon atmosphere. Images of resulting emulsions were taken with a phone camera. Measurements of the mean hydrodynamic radius of the Plin4-oil droplets by dynamic light scattering were performed on a sample taken from the middle of the tube, avoiding any unreacted oil that remained at the top of the emulsion, at least 3 h after vortexing to prevent the interference of gas bubbles with the measurement. Measurements were performed on a Zetasizer nano ZS machine (Malvern) at 25 °C, and data were processed using the CONTIN method.

For analysis by electron microscopy, samples of emulsion were deposited on glow discharge carbon-coated grids and negatively stained with 1% uranyl acetate. They were observed with a JEOL 1400 transmission electron microscope using a Morada Olympus CCD camera.

For analysis by fluorescent microscopy, emulsions were prepared as described, except that Plin4-12mer was mixed with Alexa-568-labeled Plin4-12mer at a ratio 20:1, and then mixed with triolein containing 2 μg ml^{-1} Bodipy 493/503. Fluorescent oil droplets were visualized directly on untreated glass coverslips with the spinning-disk confocal system. 10 to 15 z-sections of 0.2 μm were acquired in order to visualize both small and large droplets.

Separation of Plin4-oil emulsion on sucrose gradients. The Plin4-oil emulsion was prepared as above using 1 mg ml^{-1} Plin4-12mer. Next, 60% w/v solution of sucrose in HK buffer supplemented with 1 mM $MgCl_2$ and 1 mM DTT was added to the emulsion, to obtain a final sucrose concentration of 30%. 450 μl of the resulting suspension was loaded on the bottom of a centrifuge tube and overlaid with a step sucrose gradient consisting of 300 μl 20% w/v sucrose, 300 μl 10% w/v sucrose, and finally with 100 μl of buffer alone. The samples were centrifuged at 50000 rpm (214,000 × *g*) in a Beckman swing-out rotor (TLS 55) for 80 min at 8 °C. Four fractions were carefully collected from the bottom with a Hamilton syringe, having the following volumes: 450 μl, 300 μl, 320 μl, and 80 μl, respectively. Equal volumes of all fractions were analyzed by SDS-PAGE and proteins were stained with Sypro Orange (Life Technologies). The gels were imaged with a FUJI LAS-3000 fluorescence imaging system.

Trypsin protection assays. Plin4-oil emulsion was prepared using Plin4-12mer (1 mg ml^{-1}) and triolein as described above. At time zero, 100 μl of this emulsion or of Plin4-12mer starting solution were mixed with 13 or 130 μg ml^{-1} trypsin (Sigma) solution. At the indicated times, 30 μl of samples were withdrawn and added 3 μl of 100 mM PMSF (Sigma) to stop the reactions, then stored on ice. Reactions were analyzed by SDS-PAGE and Sypro Orange staining.

Data availability. All plasmids, DNA sequences and bacterial or yeast strains used in this study are available upon request (see Supplementary Tables 3 and 4). All relevant data are available from the authors.

Received: 14 July 2017 Accepted: 5 March 2018
Published online: 06 April 2018

References

1. Krahmer, N., Farese, R. V. Jr & Walther, T. C. Balancing the fat: lipid droplets and human disease. *EMBO Mol. Med.* **5**, 973–983 (2013).
2. Pol, A., Gross, S. P. & Parton, R. G. Biogenesis of the multifunctional lipid droplet: lipids, proteins, and sites. *J. Cell. Biol.* **204**, 635–646 (2014).
3. Welte, M. A. Expanding roles for lipid droplets. *Curr. Biol.* **25**, R470–R481 (2015).
4. Thiam, A. R., Farese, R. V. Jr & Walther, T. C. The biophysics and cell biology of lipid droplets. *Nat. Rev. Mol. Cell Biol.* **14**, 775–786 (2013).
5. Wang, C.-W. Lipid droplet dynamics in budding yeast. *Cell Mol. Life. Sci.* **72**, 2677–2695 (2015).
6. Krahmer, N. et al. Phosphatidylcholine synthesis for lipid droplet expansion is mediated by localized activation of CTP:Phosphocholine Cytidylyltransferase. *Cell. Metab.* **14**, 504–515 (2011).
7. Guo, Y. et al. Functional genomic screen reveals genes involved in lipid-droplet formation and utilization. *Nature* **453**, 657–661 (2008).
8. Fei, W. et al. A role for phosphatidic acid in the formation of 'supersized' lipid droplets. *PLoS Genet.* **7**, e1002201 (2011).
9. Thiam, A. R. & Beller, M. The why, when and how of lipid droplet diversity. *J. Cell Sci.* **130**, 315–324 (2017).
10. Pan, L. & Segrest, J. P. Computational studies of plasma lipoprotein lipids. *Biochim. Biophys. Acta* **1858**, 2401–2420 (2016).
11. Bulankina, A. V. et al. TIP47 functions in the biogenesis of lipid droplets. *J. Cell Biol.* **185**, 641–655 (2009).
12. Bouvet, S., Golinelli-Cohen, M.-P., Contremoulins, V. & Jackson, C. L. Targeting of the Arf-GEF GBF1 to lipid droplets and Golgi membranes. *J. Cell Sci.* **126**, 4794–4805 (2013).
13. Rowe, E. R. et al. Conserved amphipathic helices mediate lipid droplet targeting of perilipins 1–3. *J. Biol. Chem.* **291**, 6664–6678 (2016).
14. Drin, G. et al. A general amphipathic α-helical motif for sensing membrane curvature. *Nat. Struct. Mol. Biol.* **14**, 138–146 (2007).
15. Antonny, B. Mechanisms of membrane curvature sensing. *Annu. Rev. Biochem.* **80**, 101–123 (2011).
16. Cornell, R. B. Membrane lipid compositional sensing by the inducible amphipathic helix of CCT. *BBA - Mol. Biochim. Biophys. Acta* **1861**, 847–861 (2016).
17. Pranke, I. M. et al. α-Synuclein and ALPS motifs are membrane curvature sensors whose contrasting chemistry mediates selective vesicle binding. *J. Cell Biol.* **194**, 89–103 (2011).
18. Vanni, S., Hirose, H., Barelli, H., Gautier, R. & Antonny, B. A sub-nanometre view of how membrane curvature and composition modulate lipid packing and protein recruitment. *Nat. Commun.* **5**, 1–10 (2014).
19. Vanni, S. et al. Amphipathic lipid packing sensor motifs: probing bilayer defects with hydrophobic residues. *Biophys. J.* **104**, 575–584 (2013).
20. Cui, H., Lyman, E. & Voth, G. A. Mechanism of membrane curvature sensing by amphipathic helix containing proteins. *Biophys. J.* **100**, 1271–1279 (2011).
21. Mirheydari, M. et al. Insertion of perilipin 3 into a glycero(phospho)lipid monolayer depends on lipid headgroup and acyl chain species. *J. Lipid Res.* **57**, 1465–1476 (2016).
22. Bacle, A., Gautier, R., Jackson, C. L., Fuchs, P. F. J. & Vanni, S. Interdigitation between triglycerides and lipids modulates surface properties of lipid droplets. *Biophys. J.* **112**, 1417–1430 (2017).
23. Thiam, A. R. et al. COPI buds 60-nm lipid droplets from reconstituted water-phospholipid-triacylglyceride interfaces, suggesting a tension clamp function. *Proc. Natl Acad. Sci. USA* **110**, 13244–13249 (2013).
24. Grippa, A. et al. The seipin complex Fld1/Ldb16 stabilizes ER-lipid droplet contact sites. *J. Cell. Biol.* **211**, 829–844 (2015).
25. Magdeleine, M. et al. A filter at the entrance of the Golgi that selects vesicles according to size and bulk lipid composition. *eLife* **5**, e16988 (2016).
26. Kory, N., Thiam, A. R., Farese, R. V. Jr & Walther, T. C. Protein crowding is a determinant of lipid droplet protein composition. *Dev. Cell* **34**, 351–363 (2015).
27. Gao, Q. et al. Pet10p is a yeast perilipin that stabilizes lipid droplets and promotes their assembly. *J. Cell Biol.* **216**, 3199–3217 (2017).
28. Barneda, D. et al. The brown adipocyte protein CIDEA promotes lipid droplet fusion via a phosphatidic acid-binding amphipathic helix. *eLife* **4**, e07485 (2015).
29. Kimmel, A. R. & Sztalryd, C. The perilipins: major cytosolic lipid droplet–associated proteins and their roles in cellular lipid storage, mobilization, and systemic homeostasis. *Annu. Rev. Nutr.* **36**, 471–509 (2016).
30. Hickenbottom, S. J., Kimmel, A. R., Londos, C. & Hurley, J. H. Structure of a lipid droplet protein; the PAT family member TIP47. *Structure* **12**, 1199–1207 (2004).
31. Bussell, R. Jr & Eliezer, D. A structural and functional role for 11-mer repeats in α-synuclein and other exchangeable lipid binding proteins. *J. Mol. Biol.* **329**, 763–778 (2003).
32. Segrest, J. P. et al. The amphipathic helix in the exchangeable apolipoproteins: a review of secondary structure and function. *J. Lipid Res.* **33**, 141–166 (1992).
33. Wolins, N. E. Adipocyte protein S3-12 coats nascent lipid droplets. *J. Biol. Chem.* **278**, 37713–37721 (2003).
34. Wolins, N. E. S3-12, adipophilin, and TIP47 package lipid in adipocytes. *J. Biol. Chem.* **280**, 19146–19155 (2005).
35. Scherer, P. E., Bickel, P. E., Kotler, M. & Lodish, H. F. Cloning of cell-specific secreted and surface proteins by subtractive antibody screening. *Nat. Biotechnol.* **16**, 581–586 (1998).
36. Chen, W. et al. Inactivation of Plin4 downregulates Plin5 and reduces cardiac lipid accumulation in mice. *Am. J. Physiol. Endocrinol. Metab.* **304**, E770–E779 (2013).
37. Ajees, A. A., Anantharamaiah, G. M., Mishra, V. K., Hussain, M. M. & Murthy, H. M. K. Crystal structure of human apolipoprotein A-I: insights into its protective effect against cardiovascular diseases. *Proc. Natl Acad. Sci. USA* **103**, 2126–2131 (2006).
38. Jao, C. C., Hegde, B. G., Chen, J., Haworth, I. S. & Langen, R. Structure of membrane-bound alpha-synuclein from site-directed spin labeling and computational refinement. *Proc. Natl Acad. Sci. USA* **105**, 19666–19671 (2008).

39. Hein, M. Y. et al. A human interactome in three quantitative dimensions organized by stoichiometries and abundances. *Cell* **163**, 712–723 (2015).
40. Jacquier, N., Mishra, S., Choudhary, V. & Schneiter, R. Expression of oleosin and perilipins in yeast promotes formation of lipid droplets from the endoplasmic reticulum. *J. Cell Sci.* **126**, 5198–5209 (2013).
41. Yeung, T. et al. Membrane phosphatidylserine regulates surface charge and protein localization. *Science* **319**, 210–213 (2008).
42. Simon, M. L. A. et al. A PtdIns(4)P-driven electrostatic field controls cell membrane identity and signalling in plants. *Nat. Plants* **2**, 16089–35 (2016).
43. Hsieh, K. et al. Perilipin family members preferentially sequester to either triacylglycerol-specific or cholesteryl-ester-specific intracellular lipid storage droplets. *J. Cell Sci.* **125**, 4067–4076 (2012).
44. Bendor, J. T., Logan, T. P. & Edwards, R. H. The Function of α-Synuclein. *Neuron* **79**, 1044–1066 (2013).
45. Cole, N. B. et al. Lipid droplet binding and oligomerization properties of the Parkinson's disease protein alpha-synuclein. *J. Biol. Chem.* **277**, 6344–6352 (2002).
46. Millership, S. et al. Increased lipolysis and altered lipid homeostasis protect γ-synuclein-null mutant mice from diet-induced obesity. *Proc. Natl Acad. Sci. USA* **109**, 20943–20948 (2012).
47. Drin, G. & Antonny, B. Amphipathic helices and membrane curvature. *FEBS Lett.* **584**, 1840–1847 (2010).
48. Borhani, D. W., Rogers, D. P., Engler, J. A. & Brouillette, C. G. Crystal structure of truncated human apolipoprotein A-I suggests a lipid-bound conformation. *Proc. Natl Acad. Sci. USA* **94**, 12291–12296 (1997).
49. Liu, Y., Kahn, R. A. & Prestegard, J. H. Dynamic structure of membrane-anchored Arf*GTP. *Nat. Struct. Mol. Biol.* **17**, 876–881 (2010).
50. Der-Sarkissian, A., Jao, C. C., Chen, J. & Langen, R. Structural organization of alpha-synuclein fibrils studied by site-directed spin labeling. *J. Biol. Chem.* **278**, 37530–37535 (2003).
51. Dutta, S. & Bhattacharyya, D. Size of unfolded and dissociated subunits versus that of native multimeric proteins. *J. Biol. Phys.* **27**, 59–71 (2001).
52. Creighton, T. E. *Proteins* (Freeman & Co, New York, 1993).
53. Bartz, R. et al. Lipidomics reveals that adiposomes store ether lipids and mediate phospholipid traffic. *J. Lipid Res.* **48**, 837–847 (2007).
54. Mishra, V. K., Palgunachari, M. N., Segrest, J. P. & Anantharamaiah, G. M. Interactions of synthetic peptide analogs of the class A amphipathic helix with lipids. Evidence for the snorkel hypothesis. *J. Biol. Chem.* **269**, 7185–7191 (1994).
55. Garten, M. et al. Methyl-branched lipids promote the membrane adsorption of alpha-synuclein by enhancing shallow lipid-packing defects. *Phys. Chem. Chem. Phys.* **17**, 15589–15597 (2015).
56. Skinner, J. R. et al. Diacylglycerol enrichment of endoplasmic reticulum or lipid droplets recruits perilipin 3/TIP47 during lipid storage and mobilization. *J. Biol. Chem.* **284**, 30941–30948 (2009).
57. Ben M'barek, K. et al. ER membrane phospholipids and surface tension control cellular lipid droplet formation. *Dev. Cell.* **41**, 591–604 (2017).
58. McClements, D. J. & Gumus, C. E. Natural emulsifiers — Biosurfactants, phospholipids, biopolymers, and colloidal particles: Molecular and physicochemical basis of functional performance. *Adv. Colloid Interface Sci.* **234**, 3–26 (2016).
59. Small, D. M., Wang, L. & Mitsche, M. A. The adsorption of biological peptides and proteins at the oil/water interface. A potentially important but largely unexplored field. *J. Lipid Res.* **50**, S329–S334 (2009).
60. Bigay, J., Casella, J.-F., Drin, G., Mesmin, B. & Antonny, B. ArfGAP1 responds to membrane curvature through the folding of a lipid packing sensor motif. *Embo. J.* **24**, 2244–2253 (2005).
61. Hristova, K. et al. An amphipathic alpha-helix at a membrane interface: a structural study using a novel X-ray diffraction method. *J. Mol. Biol.* **290**, 99–117 (1999).
62. Wilfling, F. et al. Arf1/COPI machinery acts directly on lipid droplets and enables their connection to the ER for protein targeting. *eLife* **3**, e01607 (2014).
63. Mishra, V. K. et al. Studies of synthetic peptides of human apolipoprotein A-I containing tandem amphipathic alpha-helixes. *Biochemistry* **37**, 10313–10324 (1998).
64. Payne, F. et al. Mutations disrupting the Kennedy phosphatidylcholine pathway in humans with congenital lipodystrophy and fatty liver disease. *Proc. Natl. Acad. Sci. USA* **111**, 8901–8906 (2014).
65. Soni, K. G. et al. Coatomer-dependent protein delivery to lipid droplets. *J. Cell. Sci.* **122**, 1834–1841 (2009).
66. Chong, S. S. Y., Taneva, S. G., Lee, J. M. C. & Cornell, R. B. The curvature sensitivity of a membrane-binding amphipathic helix can be modulated by the charge on a flanking region. *Biochemistry* **53**, 450–461 (2014).
67. Doucet, C. M., Esmery, N., de Saint-Jean, M. & Antonny, B. Membrane curvature sensing by amphipathic helices is modulated by the surrounding protein backbone. *PLoS ONE* **10**, e0137965–23 (2015).
68. Sletten, A., Seline, A., Rudd, A., Logsdon, M. & Listenberger, L. L. Surface features of the lipid droplet mediate perilipin 2 localization. *Biochem. Biophys. Res. Commun.* **452**, 422–427 (2014).
69. Robertson, E. J. et al. Assembly and molecular order of two-dimensional peptoid nanosheets through the oil–water interface. *Proc. Natl Acad. Sci. USA* **111**, 13284–13289 (2014).
70. Prévost, C. et al. Mechanism and determinants of amphipathic helix-containing protein targeting to lipid droplets. *Dev. Cell.* **44**, 73–86 (2018).
71. Gautier, R., Douguet, D., Antonny, B. & Drin, G. HELIQUEST: a web server to screen sequences with specific alpha-helical properties. *Bioinformatics* **24**, 2101–2102 (2008).
72. Crooks, G. E., Hon, G., Chandonia, J.-M. & Brenner, S. E. WebLogo: a sequence logo generator. *Genome Res.* **14**, 1188–1190 (2004).
73. Lee, S. et al. De novo-designed peptide transforms Golgi-specific lipids into Golgi-like nanotubules. *J. Biol. Chem.* **276**, 41224–41228 (2001).
74. White, S. H. & Wimley, W. C. Hydrophobic interactions of peptides with membrane interfaces. *Biochim. Biophys. Acta* **1376**, 339–352 (1998).

Acknowledgements

We thank Karine Eudes and Joel Polidori for technical support, Romain Gautier for help with bioinformatic analyses, the ImagoSeine facility at the Institut Jacques Monod, member of IBiSA and the France-BioImaging (ANR-10-INBS-04) infrastructure, and in particular Xavier Baudin and Vincent Contremoulins for help with imaging and image analysis, Florent Carn for assistance with dynamic light scattering, Sebastien Léon for yeast plasmids and reagents, and Jean-Marc Verbavatz, Veronique Albanèse, Luc Bousset, Yvon Jaillais and members of our labs for comments and discussions. This work was supported by the French National Research Agency (ANR), grant LDsurfDynamics (ANR-13-BSV2-0013) to C.J. and B.A., "Fondation pour la Recherche Médicale", grant number DEQ20150934717 to C.J. and A.C., Marie Curie career integration grant (631997) to A.C., PhD fellowship from the French "Ministère de l'Education National, de l'Enseignement Supérieur de la Recherche" to M.G.-A., and postdoctoral fellowship from the Basque Foundation for Science (Ikerbasque) to M.M.

Author contributions

A.C. designed and supervised research. A.C., S.A.-B., M.G.-A., and C.L.T.G. performed the cell biology experiments. M.G.-A., M.M.M., A.C., and B.A. performed the in vitro experiments. S.P. and B.A. performed electron microscopy. A.C., C.L.T.G., S.A.-B., M.G.-A., M.M., and B.A. analyzed data. J.G. contributed unpublished reagents. B.A. and C.L.J. participated in the initiation of the project and assisted with the manuscript. A.C. wrote the manuscript.

Additional information

Supplementary Information accompanies this paper at https://doi.org/10.1038/s41467-018-03717-8.

Competing interests: The authors declare no competing interests.

Résumé en français

Gouttelettes lipidiques

Les organismes ont besoin de stocker de l'énergie afin de survivre dans les conditions fluctuantes de leur environnement. L'énergie peut être stockée dans des molécules riches en énergie. Les triacylglycérides (TAG) sont des molécules très réduites disponibles pour l'oxydation. Les TAG sont une sorte de lipides neutres. Les lipides neutres sont des lipides qui n'ont pas de groupes chargés et polaires. Pour cette raison, ces molécules son très hydrophobes et sont immiscibles dans l'eau. Les TAG et d'autres lipides neutres, comme les esters de stérol (STE), sont stockés dans des gouttelettes lipidiques (LDs). Les LDs sont des organites intracellulaires. Ses principales fonctions sont de stocker et de fournir de l'énergie et des composés membranaires en fonction de l'état métabolique de la cellule. Les LDs ont une structure sphérique. Au centre de la sphère, on trouve les lipides neutres comme les TAG et les STE. À leur surface, les LD possèdent une monocouche de phospholipides et de protéines associées.

D'un point de vue physique, les LD peuvent être considérées comme la phase dispersée d'une émulsion huile dans l'eau. La phase continue est le cytosol des cellules. L'absence d'interactions cohésives entre les deux composants de l'émulsion génère une tension de surface. Les agents de surface, ou surfactants, sont des molécules amphipathiques qui se situent à l'interphase et réduisent la tension de surface, produisant une émulsion plus stable. Les LD contiennent de nombreux tensioactifs à leur surface : divers types de phospholipides, protéines, des acides gras ou du diacylglycérol. Lorsque les concentrations de tensioactifs dans la surface lipidique neutre sont faibles, l'émulsion sera thermodynamiquement instable car il y a beaucoup de surface hydrophobe exposée à l'environnement aqueux du cytoplasme. Lorsque cela se produit, les LD sont fusionnés pour devenir plus stables.

Ciblage des protéines aux les gouttelettes de lipides

Les protéines présentes sur les LDs servent de médiateurs à leur métabolisme et à leurs fonctions. Les protéines peuvent interagir avec la surface des LD par les motifs suivants:

- Hélices amphipathiques (AHs) : s'agit des structures protéiques secondaires d'hélice ou les acides aminés (aa) sont séparés en deux faces distinctes : une hydrophobe et une polaire. Les protéines contenant des AHs ciblent des LD depuis le cytoplasme (Annexé I, Giménez-Andrés et al. 2018).
- Épingles à cheveux hydrophobes : des aa hydrophobes sont insérés dans la monocouche des phospholipides et sont flanqués des régions polaires exposées au cytosol. Ces protéines se transloquent depuis le réticulum endoplasmique vers les LDs.
- Modifications des lipides. Les conjugaisons lipidiques telles que la palmitylation, la prénylation ou la myristoylation peuvent servir de médiateurs pour le ciblage des membranes, ainsi que pour cibler des LDs.
- Association périphérique via une autre protéine. Ce sont des protéines qui se localisent aux LD en interagissant avec les protéines déjà présentes dans les LD.

Périlipines

Les périlipines (Plins) sont une famille de protéines qui ciblent et régulent des LD de manière non enzymatique. Certaines d'entre elles jouent un rôle clé dans la régulation de la lipolyse. Plin1 est bien caractérisé comme inhibiteur ou promoteur de la lipolyse en fonction de son état de phosphorylation dans les adipocytes. Cinq Plins ont été identifiées chez les mammifères.

Les Plins sont composées de trois régions principales : la région PAT, la région 11-mer et la région C-terminale (Fig. 11-1). La région de 11-mer cible des LD de la périlipine 1 (Plin1), la périlipine 2 (Plin2) et la périlipine 3 (Plin3). Il est prévu que cette région devrait former une hélice 3-11, trois tours chaque onze aa. Par leur séquence d'aa, l'hélice serait un AH. Il convient de remarquer que la séquence 11-mer de la périlipine 4 (Plin4) est exceptionnelle en termes de longueur et de répétitivité au niveau de trois répétitions de 11-mers, qui font une 33-mer. La Plin4 humain a environ 950 aa d'AH prédit, soit 10 fois plus que les autres Plins.

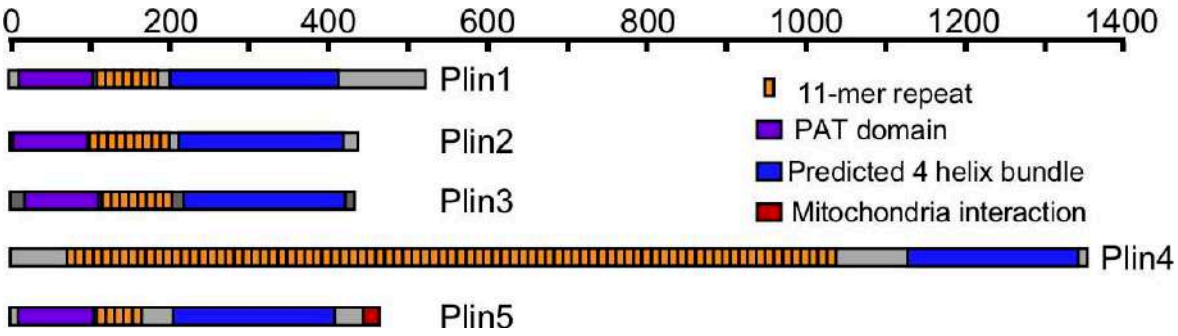

Fig. 11-1. Résumé des séquences de Plins. Les répétitions 11-mer sont marquées en orange, la partie C-terminale en bleu, le domaine PAT en violet et en rouge les aa pour l'interaction avec les mitochondries.

La Plin 1 est exprimé dans les adipocytes, alors que Plin2 et Plin3 ont une expression plus omniprésente. Plin4 s'exprime principalement dans les adipocytes, mais aussi dans les cellules squelettiques du cœur et muscle. La périlipine 5 est exprimée dans les tissus hautement oxydatifs. Une expérience d'immunofluorescence montre que la Plin3 et la Plin4 sont localisés sur les petites LD des adipocytes 3T3-L1 en culture. La Plin2 est lié aux LD intermédiaires, tandis que la Plin1 est présent à la surface des grosses LD.

Les LDs et les maladies

Le stockage excessif ou insuffisant des lipides est associé à de nombreux états pathologiques. Parmi celles-ci, on peut citer l'obésité, les maladies hépatiques grasses, l'insulinorésistance, l'athérosclérose, les maladies infectieuses, le développement du cancer et les maladies neurodégénératives. L'excès d'accumulation de graisse dans le tissu adipeux peut être obtenu soit par l'augmentation de la masse des adipocytes, l'hypertrophie ; soit par leur nombre, l'hyperplasie. Les adipocytes hypertrophiques ont une fonction cellulaire altérée, ce qui entraîne une inflammation et une réponse hormonale altérée. La taille des adipocytes a été proposée comme un biomarqueur potentiel pour les altérations et les maladies cardiométaboliques.

Une faible vascularisation des tissus tumoraux entraîne des conditions défavorables telles que le stress oxydatif et le manque de nutriments. Pour survivre, les cellules cancéreuses doivent s'adapter en reprogrammant leur métabolisme. Les voies métaboliques des lipides sont fortement affectées par cette reprogrammation. Par

exemple, les cellules cancéreuses présentent une augmentation de l'absorption et de la production des lipides et obtiennent plus d'énergie de l'oxydation des acides gras.

Objectifs du doctorat

La manière dont les protéines interagissent avec des emplacements intracellulaires spécifiques où elles exercent leur fonction est une question importante en biologie cellulaire. Dans le cas de l'interaction entre les LD et les protéines, cette question reste méconnue.

L'objectif de mon doctorat est de comprendre comment l'AH de Plin4 et les AHs d'autres Plins interagissent avec les LDs. Pour y parvenir, j'ai utilisé des systèmes biochimiquement reconstitués avec des protéines purifiées et des lipides neutres, et la levure bourgeonnante *Saccharomyces cerevisiae* comme cellule modèle.

Résultats

Tout d'abord, nous avons utilisé l'AH de Plin4 comme modèle pour étudier comment les AHs interagissent avec les LDs. Nous avons obtenu les résultats suivants (Chapitre 6, Annexé II) :

- Une plus grande longueur de l'AH de Plin4 permet de mieux cibler des LDs.
- Une hydrophobicité plus élevée améliore également la liaison des LDs. Cependant, il en résulte également que Plin4 interagit plus fortement avec d'autres membranes, le rendant moins spécifique pour les LDs.
- La modification de la charge pour la rendre plus positive ou négative réduit le ciblage des LDs, mais elle peut être compensée par une plus grande hydrophobicité.
- L'AH de Plin4 est capable d'interagir avec des lipides neutres directement in vitro, en formant des particules d'huile entourées de L'AH de Plin4 (Fig. 11-2). Ces expériences suggèrent que l'AH de Plin4 peut remplacer la monocouche des phospholipides sur les LDs. Dans cellules appauvri en phospholipides les LDs ont une taille plus grande. L'expression de l'AH de Plin4 réduit la taille des LDs dans ces cellules, en soutenant le modèle.

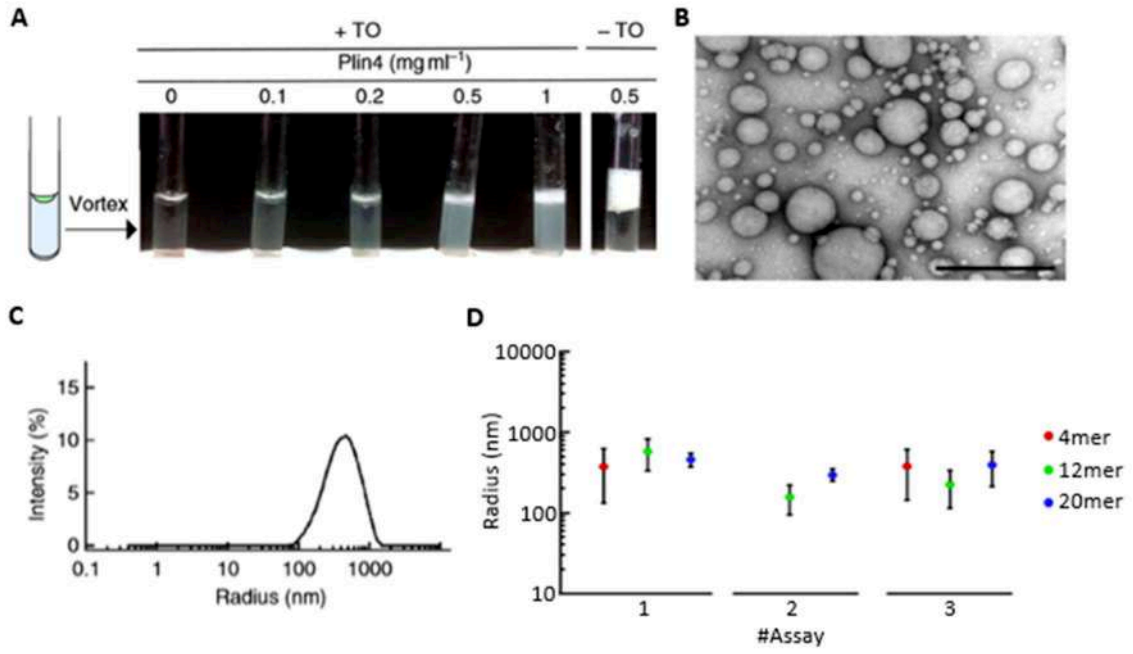

Fig. 11-2. Plin4 interagit directement avec les lipides neutres in vitro, formant des gouttelettes d'huile. A. Images des tubes dans lesquels une goutte de trioléine (10 µl) a été vigoureusement mélangée avec une solution de concentration croissante de Plin4 12-mer (190 µl). **B.** Image représentative de l'émulsion d'huile de Plin4 par microscopie électronique à coloration négative. Barre d'échelle : 0,5 µm. Réalisé par Sophia Pagnotta, service de microscopie électronique Université Côte d'Azur, CNRS, IPMC. **C.** Distribution de taille obtenue par la technique de diffusion dynamique de la lumière d'une aliquote prélevée au milieu de l'émulsion d'huile obtenue avec 0,5 mg/ml Plin4 12-mer. **D.** Comparaison de la distribution des gouttelettes entre des Plin4 avec différentes longueurs de les AHs : Plin4 4-mer, Plin4 12-mer et Plin4 20-mer. Trois expériences indépendantes sont présentées. Les points représentent les pics des maxima et les barres verticales représentent la polydispersité.

Afin d'évaluer l'interaction de l'AH de Plin4 avec les lipides neutres, j'ai développé des essais pour évaluer la dynamique des protéines sur les gouttelettes d'huile et la stabilité des gouttelettes d'huile formées *in vitro* en utilisant des protéines purifiées et marquées par fluorescence. J'ai observé la dynamique des protéines en observant la récupération de la fluorescence à la surface des gouttelettes d'huile après le photoblanchiment de la protéine fluorescente. La dynamique des protéines en temps réel pendant l'adsorption et la désorption a été évaluée avec le système de micro fluidique développé en collaboration avec Tadej Emeršič et Jure Derganc. Pour observer la stabilité des particules d'huile formées, j'ai utilisé la technique de diffusion dynamique de la lumière pour suivre la taille des gouttelettes d'huile-protéine dans le temps et évalué

l'agrégation des grosses particules avec la microscopie optique. Ces techniques pourront être utilisées à l'avenir pour caractériser l'interaction d'autres AH avec les LDs.

Mes résultats sont les suivants (Chapitre 7) :

- Les gouttelettes formées par l'AH de Plin4 et les lipides neutres sont très stables.
- Plin4 est remarquablement immobile à la surface de ces gouttelettes.

Ensuite, j'ai comparé l'AH de Plin4 avec les AH d'autres Plins. J'ai commencé par exprimer la Plin1, la Plin2 et la Plin3 dans des souches de levure bourgeonnante ayant des permissibilités différentes pour l'interaction avec des LDs. J'ai également purifié l'AH de la Plin3 et j'ai testé son interaction avec l'huile in vitro. J'ai développé un test fluorescent pour observer l'échange des AHs à la surface des gouttelettes d'huile. Les résultats de ces expériences sont les suivants (Chapitre 7) :

- L'AH de Plin4 cible mieux les LDs que les outres Plins en raison de sa longueur. Cependant, un fragment plus court de l'AH de Plin4, de longueur similaire aux autres AHs des Plins, cible des LDs dans la même mesure que Plin2 et Plin3 AH, ce qui correspond à leur composition globale similaire. Tous ces AHs ont une faible hydrophobicité. L'AH de la Plin1 cible les LDs mieux, en accord avec son hydrophobicité augmenté.
- En revanche, l'AH de la Plin1 et l'AH de la Plin3 sont beaucoup plus dynamiques à la surface des LD dans la levure que l'AH de Plin4.
- L'AH de la Plin3 purifié peut solubiliser l'huile. Cependant, les gouttelettes formées par elle sont moins stables que celles formées avec un fragment de l'AH de Plin4 de longueur comparable.
- L'AH de la Plin3, mais pas un fragment de l'AH de Plin4 de longueur similaire (Plin4 4mer), peut être rapidement remplacé à la surface des gouttelettes d'huile par un fragment de l'AH de Plin4 plus long (Plin4 12mer) (Fig. 11-3).

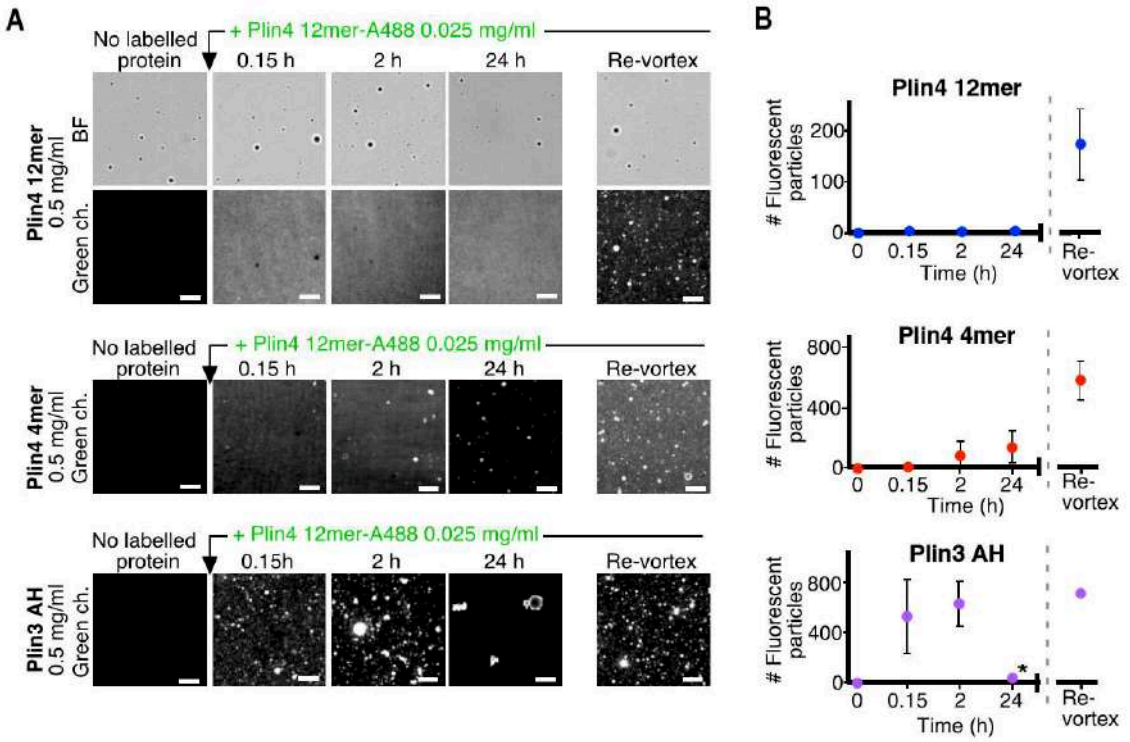

Fig. 11-3. Test d'échange protéique dans les émulsions des Plin4 et Plin3. A. Images des émulsions par microscopie optique en champ clair (BF) et fluorescence aux moments indiqués avant et après l'addition de Plin4 12mer marqué par fluorescence. Re-vortex est la condition avec une incorporation maximale de Plin4 12mer marqué. Barres d'échelle : 5 µm. **B.** Quantification des expériences indiquées en A. Le nombre de particules fluorescentes (moyenne ± écart type) a été déterminé à partir de quatre champs séparés dans la même expérience. Les graphiques sont représentatifs d'au moins deux expériences indépendantes. Les astérisques indiquent un regroupement de particules.

Ces résultats suggèrent que les différences entre le comportement de l'AH de Plin4 et d'autres AHs des Plins sur les LDs ne proviennent pas seulement des différences de longueur. Nous avons émis l'hypothèse que la séquence aa de l'AH de Plin4 est importante pour sa stabilité à la surface des LDs. Les positions des résidus polaires et chargés (lysine, acide glutamique, glutamine et asparagine) sont fortement conservées dans les répétitions de l'AH de Plin4. Ces résidus ne devraient pas interagir directement avec la surface des LDs. Les résultats de ces expériences sont les suivants (Chapitre 7) :

- La mutagenèse des résidus polaires et chargés a un fort effet sur le ciblage des LDs de l'AH de Plin4.
- Un mutant de l'AH de Plin4 avec une redistribution des résidus positifs dans sa face polaire a eu un ciblage réduit aux LDs, mais a toujours ciblé la membrane

plasmique dans la levure. Une fois purifié, ce mutant a été efficacement remplacé à la surface des gouttelettes d'huile par le type sauvage l'AH de Plin4 de même longueur.

J'ai comparé les séquences de l'AH de Plin4 de différents mammifères. Dans chaque séquence orthologue, les répétitions de Plin4 33-mer sont très bien conservées, y compris les positions des résidus polaires. Cependant, le nombre de répétitions varie selon les espèces. Des résidus spécifiques dans la face polaire de l'AH de Plin4 peuvent favoriser l'auto stabilisation par des interactions latérales entre les chaînes de l'AH de Plin4 repliées (**Fig. 11-4**).

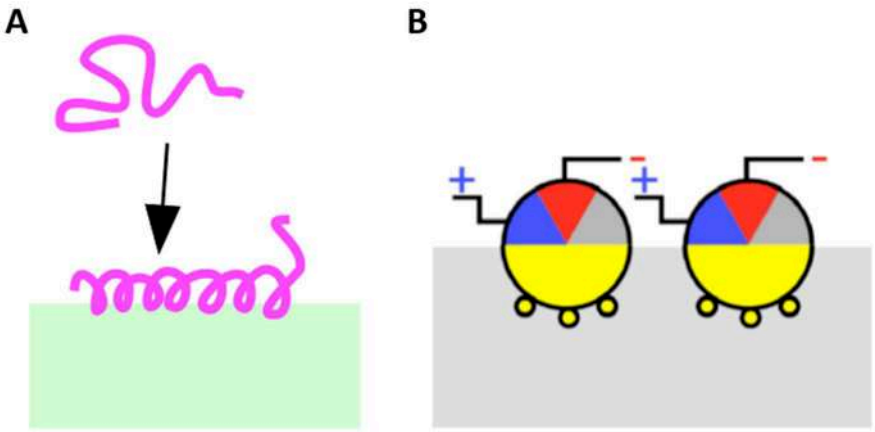

Fig. 11-4. Interaction de l'AH de Plin4 avec la surface des LDs. A. L'AH de Plin4 est dépliés en solution et se plie lors de l'interaction avec la surface des LDs. Ce processus est susceptible de se produire également pour d'autres AHs des Plins. **B.** Modèle des molécules de l'AH de Plin4 interagissant entre elles sur la surface des LDs.

Notre modèle pour l'interaction des AHs des Plins avec les LDs est le suivant : Plin4 est déplié en solution et acquiert une conformation fortement hélicoïdale lors de l'interaction avec une surface lipidique (**Fig. 11-4 A**) (Chapitre 6) (Čopič et al. 2018). Cela s'applique probablement à d'autres AH des Plins. Contrairement aux autres AHs des Plins, nous proposons qu'une fois que l'AH de Plin4 est repliée sur la surface des LDs, elle interagit latéralement avec les AHs adjacents par des interactions électrostatiques, formant une manteau protéique immobile sur la surface de la LD (**Fig. 11-4 B**) (Chapitre 7). Ces interactions entre les hélices expliqueraient la grande stabilité des particules lipidiques recouvertes par Plin4. Des interactions similaires ont été observées entre les

AH de l'apolipoprotéine A-I, qui s'enroule autour de petites particules lipidiques formant des lipoparticles de haute densité.

Une souris knock-out du Plin4 a montré un phénotype faible. Il y avait une certaine réduction du stockage de TAG dans le muscle cardiaque et une baisse de l'expression de la périlipine 5. Cependant, la variabilité du nombre et de la composition des répétitions de Plin4 33mer chez les mammifères, ainsi que leur forte conservation au sein d'une même espèce, suggèrent un rôle important de Plin4 dans l'évolution des mammifères. Nous avons montré que Plin4 se lie directement aux lipides neutres et les stabilise. Plin4 enrobe et réduit la taille des LDs dans les cellules dépourvues des phospholipides. Pour comprendre la fonction physiologique de Plin4, il faut l'étudier dans des adipocytes en culture.

université PARIS-SACLAY

ECOLE DOCTORALE N°577
Structure et dynamique des systèmes vivants (SDSV)

Titre : Interaction des hélices amphipathiques des périlipines avec des gouttelettes lipidiques

Mots clés : Hélice amphipathique, gouttelettes lipidiques, stockage des lipides, interaction protéines – lipides
périlipine, interface huile-eau

Résumé : Les gouttelettes lipidiques (LDs) sont des réservoirs d'énergie et des compartiments membranaires. Elles sont composées d'un noyau des lipides neutres et d'une monocouche de phospholipides associées à des protéines. Les hélices amphipathiques (AHs), sont des structures protéiques secondaires qui interagissent avec les membranes des organelles. La manière dont les AHs interagissent avec la surface des LDs reste largement méconnue. Les périlipines sont une famille de protéines abondantes dans les LDs. Elles utilisent les AHs pour cibler les LDs. Certains de leurs membres ont des fonctions bien définies comme régulateurs du métabolisme lipidique, en particulier dans les adipocytes, où ils sont fortement exprimés. La périlipine 4 (Plin4) humaine contient une longue AH de près de 1000 acides aminés, composée de répétitions de 33 acides aminés. Son AH est 10 fois plus longue que les AHs des autres périlipines. Dans ce travail, j'ai utilisé des systèmes biochimiquement reconstitués avec des protéines purifiées et des lipides neutres, et la levure bourgeonnante *Saccharomyces cerevisiae* comme cellule modèle pour étudier comment les AHs de Plin4 et d'autres périlipines interagissent avec les LDs. L'AH de Plin4 est dépliée en solution et se replie en une hélice au contact d'une surface lipidique. Nous avons observé qu'avec sa faible hydrophobicité et sa grande longueur, cette AH est adaptée pour interagir avec les LDs sur une grande surface. Elle peut remplacer la fonction des phospholipides à la surface des LDs. Lorsque l'AH de Plin4 purifiée est mélangée avec de l'huile, elle forme des gouttelettes d'huile extrêmement stables. En utilisant la microscopie à fluorescence et des expériences de photoblanchiment, j'ai montré que l'AH de Plin4 formait une couche très immobile sur ces gouttelettes, à la fois in vitro et dans les cellules de levure. Ce n'était pas le cas pour les AHs d'autres périlipines, qui se liaient aux LDs de manière dynamique et étaient rapidement échangées avec l'AH de Plin4 à la surface des gouttelettes d'huile, même lorsque leurs longueurs étaient similaires. Les AHs des périlipines ont également une composition en acides aminés similaire. Compte tenu de ces résultats, je fais donc l'hypothèse qu'une distribution précise des résidus polaires et chargés dans le côté polaire de l'AH de Plin4 est importante pour sa stabilité sur les LDs. L'AH de Plin4 pourrait être stabilisée à la surface des LDs par des interactions électrostatiques entre molécules adjacentes, agissant comme un manteau pour LDs. Cette propriété est probablement importante pour la fonction de Plin4 dans le tissu adipeux. Il est intéressant de noter que mon analyse des séquences de Plin4 AH de différents mammifères montre une variabilité de leur longueur, mais une conservation élevée entre les répétitions dans chaque espèce, en faveur de l'hypothèse selon laquelle l'organisation précise de l'AH de Plin4 est importante pour sa fonction.

Title : Interaction of perilipin amphipathic helices with lipid droplets

Key words : Amphipathic helix, lipid droplet, lipid storage, protein-lipid interaction, perilipin, oil-water interface

Abstract : Lipid droplets (LDs) are reservoirs of energy and membrane compounds. They are composed of a core of neutral lipids and a monolayer of phospholipids with associated proteins. Amphipathic helices (AHs), are secondary protein structures that interact with organelle membranes. How AHs interact with the surface of LDs is poorly understood. Perilipins are a family of abundant LD proteins that use AHs for targeting LDs. Some of their members have well known functions as regulators of lipid metabolism, especially in adipocytes, where they are highly expressed. Human perilipin 4 (Plin4) contains a very long AH of almost 1000 amino acids, which is very repetitive, composed of repeats of 33 amino acids. Its AH is 10 times longer than the AHs of other perilipins. In this work, I used biochemically reconstituted systems with purified proteins and neutral lipids, and the budding yeast *Saccharomyces cerevisiae* as a model cell to study how the AHs of Plin4 and of other perilipins interact with LDs. Plin4 AH is unfolded in solution and folds into a helix in contact with a lipid surface. We show that with its low hydrophobicity and high length, this AH is adapted for interacting with LDs over a large surface. It can replace phospholipids on the LD surface. When purified Plin4 AH is mixed with oil, it forms extremely stable oil droplets. Using fluorescent microscopy and photobleaching experiments, I showed that Plin4 AH formed a highly immobile coat on these droplets. Similarly, Plin4 AH was highly immobile when bound to LDs in yeast. This was not the case for the AHs of other perilipins, which bound to LDs in a dynamic manner and were rapidly exchanged with Plin4 AH on the surface of oil droplets, even when their lengths were similar. These AHs also share a similar amino acid composition. We hypothesize that precise distribution of polar and charged residues in the polar side of Plin4 AH is important for its stability on LDs. We propose that Plin4 AH is stabilized on the surface of LDs through electrostatic interactions between adjacent molecules, acting like an LD coat. This property is likely important for the function of Plin4 in adipocyte tissue. Interestingly, my analysis of Plin4 AH sequences from different mammals shows a variability in their length, but a high conservation between the repeats in each species, supporting the conclusion that the precise organization of Plin4 AH is important for its function.

Université Paris-Saclay
Espace Technologique / Immeuble Discovery
Route de l'Orme aux Merisiers RD 128 / 91190 Saint-Aubin, France